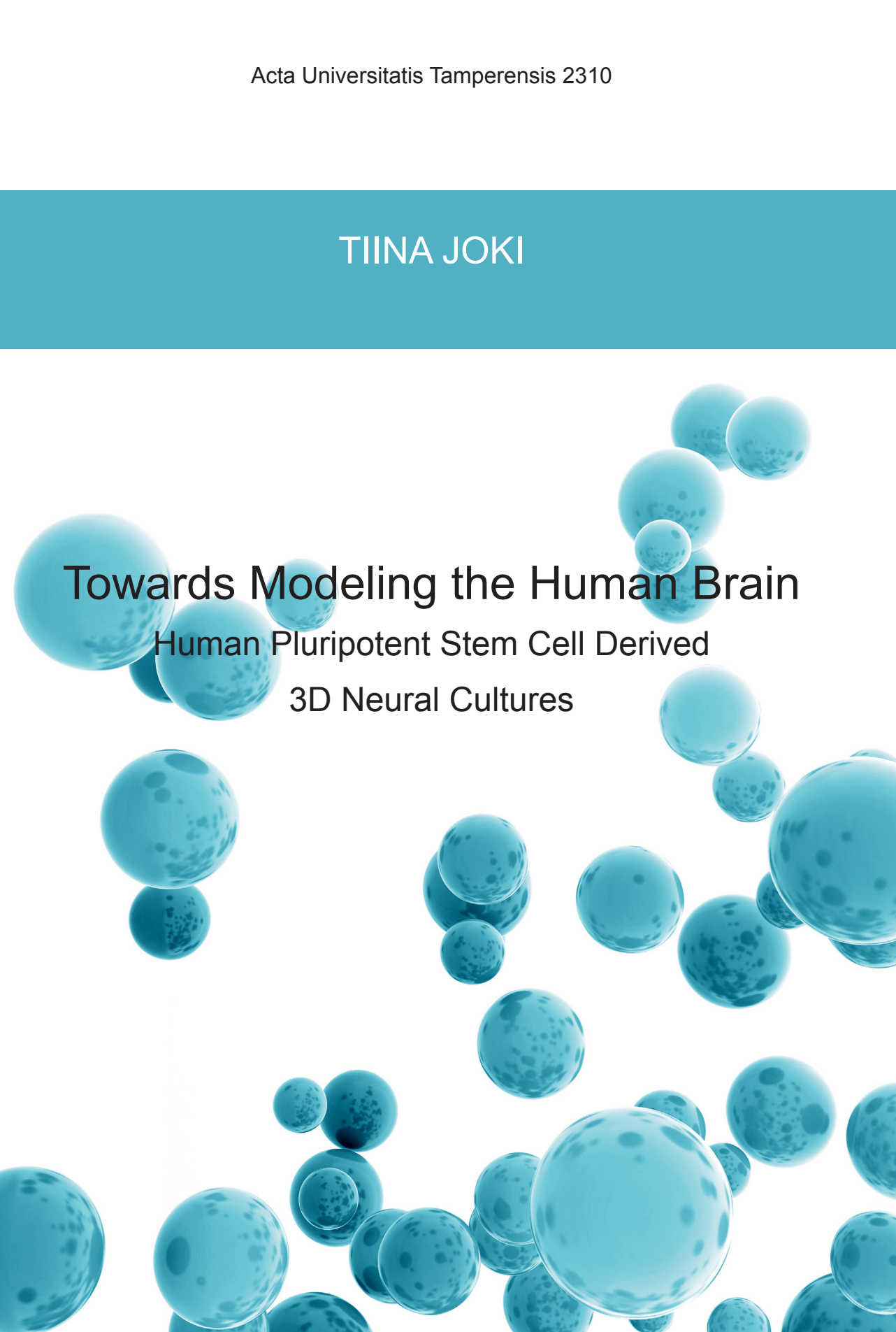


TIINA JOKI



# Towards Modeling the Human Brain

Human Pluripotent Stem Cell Derived  
3D Neural Cultures



TIINA JOKI

## Towards Modeling the Human Brain

Human Pluripotent Stem Cell Derived  
3D Neural Cultures



ACADEMIC DISSERTATION

To be presented, with the permission of  
the Faculty Council of the Faculty of Medicine and Life Sciences  
of the University of Tampere,  
for public discussion in the Jarmo Visakorpi auditorium  
of the Arvo building, Arvo Ylpön katu 34, Tampere,  
on 27 October 2017, at 12 o'clock.

UNIVERSITY OF TAMPERE

TIINA JOKI

Towards Modeling the Human Brain

Human Pluripotent Stem Cell Derived  
3D Neural Cultures

*Acta Universitatis Tamperensis 2310*  
*Tampere University Press*  
*Tampere 2017*

## ACADEMIC DISSERTATION

University of Tampere, Faculty of Medicine and Life Sciences  
Finland

*Supervised by*

Docent Susanna Narkilahti  
University of Tampere  
Finland  
PhD Mervi Ristola  
University of Tampere  
Finland  
PhD Laura Ylä-Outinen  
University of Tampere  
Finland

*Reviewed by*

Docent Varpu Marjomäki  
University of Jyväskylä  
Finland  
Associate Professor Ana Paula Pêgo  
University of Porto  
Portugal

The originality of this thesis has been checked using the Turnitin OriginalityCheck service in accordance with the quality management system of the University of Tampere.

Copyright ©2017 Tampere University Press and the author

Cover design by  
Mikko Reinikka

Acta Universitatis Tamperensis 2310  
ISBN 978-952-03-0529-1 (print)  
ISSN-L 1455-1616  
ISSN 1455-1616

Acta Electronica Universitatis Tamperensis 1814  
ISBN 978-952-03-0530-7 (pdf)  
ISSN 1456-954X  
<http://tampub.uta.fi>

Suomen Yliopistopaino Oy – Juvenes Print  
Tampere 2017



```
01100101 01100001 01110100
01110011 01101100 01100101 01100101 01110000
01110011 01100011 01101001 01100101 01101110 01100011 01100101
01110010 01100101 01110000 01100101 01100001 01110100
```

# ABSTRACT

**Background:** This thesis focuses on *in vitro* tissue engineering (TE) applications for the central nervous system (CNS). TE is a multidisciplinary research field that aims at healing human tissues by developing novel engineered biological constructs. Typically, these constructs are composed of cells in a 3D biomaterial scaffold. One promising research platform for neural TE is the use of human stem cell-derived neural cells, combined with a 3D scaffold, as a simplified model system for CNS – an *in vitro* neural model. The commonly used scaffold materials are brain extracellular matrix (ECM)-mimicking hydrogels or rigid microscale 3D matrices that support cell growth.

The main aim of this work was to create a 3D neural culturing setup that could serve as a brain tissue model in the future.

**Materials and Methods:** In this thesis, human pluripotent stem cell-derived neural cells were used. The neural cell cultures were visualized with fluorescent labeling, either using cell-accumulating probes or immunocytochemical labeling. Electrical neuronal network functionality was measured using a microelectrode array (MEA) platform. The hydrogels utilized were PuraMatrix®, a synthetic self-assembling hydrogel, and a natural polysaccharide gellan gum hydrogel crosslinked with spermidine (SPD). In this thesis, hydrogels were studied using three culturing methods:

- 1) Direct gelation of the hydrogel on top of the pre-cultured cell monolayer (2D);
- 2) Cells cultured on top of the hydrogel surface (2D);
- 3) Encapsulated cells cultured within the hydrogel (3D).

Rigid tubular microtower scaffolds were polymerized using 2 photon-direct laser writing (2PP-DLW) from a polymer-ceramic hybrid material,Ormocomp.

**Results:** Fluorescent probes were found to be suitable for tracking human neural cells for up to four weeks in culture. Co-cultures from two pre-labeled neural populations formed a homogenous neural network in 2D culture, and the electrical

neuronal network activity of these co-cultures was similar to that of the control cultures. Both of the studied hydrogel materials were optimized for human neural cell culturing by testing different hydrogel compositions. Interestingly, sparse hydrogels with low PuraMatrix® dilutions were best for neuronal cells, whereas stiff composition of gellan gum hydrogel supported neural networks better than the softer compositions. Neural networks cultured within the PuraMatrix® hydrogel were also shown to have spontaneous electrical activity. Maturation of neuronal activity was slow in the 3D setup; however, on the other hand, morphological inspection showed *in vivo*-mimicking complexity in the cell morphology. Rigid microtower scaffolds were found to be effective for supporting 3D neural network formation around the scaffold. These neural networks were stable for up to four weeks in culture, even though a slight decrease in cell number was seen at the four-week time point.

**Conclusions:** Both of the studied scaffold types, hydrogels and rigid scaffolds, were suitable as a supporting matrix for the formation of 3D neural networks. Large neural networks randomly formed inside hydrogels and were anisotropic, whereas the networks formed around microtowers were smaller, but more easily controlled with the microtower design. All of the studied scaffold materials have potential in *in vitro* neural applications, but they are applicable to different study questions.

# TIIVISTELMÄ

**Johdanto:** Kudosteknologia on monitieteellinen tutkimusala, jonka pitkän linjan tavoitteena on tuottaa uusia hoitomuotoja sairauksien hoitoon. Kudosteknologiassa yhdistetään biologiaa insinööritieteisiin ja pyritään laboratorio-oloissa luomaan keinotekoisia kudoksenomaisia viljelmiä, joissa soluja kasvatetaan biomateriaalitukirakenteessa. Tämä väitöskirja keskittyy ihmisen keskushermoston kudosteknologiaan sovelluksiin. Keskushermosto, kuten muutkin kudokset, koostuu solujen lisäksi soluväliaineesta. Keskushermoston soluväliaine on erittäin pehmeä, mutta elastinen rakenne, joka koostuu nanokokoisista säikeistä. Biomateriaalit, joita käytetään viljelmän tukena voivat jäljitellä kohdekudoksen ominaisuuksia tai toimia mekaanisena tukena solujen kasvulle. Tämän väitöskirjan tavoitteena oli luoda 3D-ympäristö, jota voidaan käyttää solumallin pohjana.

**Materiaalit ja menetelmät:** Tässä väitöskirjatyössä käytettiin ihmisen erittäin monikykyisistä kantasoluista erilaistettuja hermosoluja. 3D-soluviljelyyn tukirakenteina käytettiin joko synteettistä PuraMatrix®-hydrogeeliä tai gellan gum - polysakkaridipohjaista hydrogeeliä. Solujen vastetta hydrogeeleihin tutkittiin kolmella erilaisella tutkimusasetelmalla: 1) viljelemällä soluja hydrogeelin alla, jolloin hydrogeeli geeliytettiin suoraan soluviljelmän päälle, 2) viljelemällä soluja esigeeliytetyn hydrogeelipinnan päällä tai 3) viljelemällä soluja sekoitettuna hydrogeeliin. Hydrogeelien lisäksi kolmiulotteisia hermoverkkoja kasvatettiin käyttämällä tukimateriaalina sylinterimäisiä polymeerikomposiitti mikrorakenteita – mikrotorneja. Solujen kasvua tarkasteltiin fluoresoivien leimojen avulla. Tässä väitöskirjatyössä on käytetty sekä yleisiä kaikkiin soluihin sitoutuvia leimoja että vasta-ainetunnistuksen avulla vain kohdeproteiiniinsa sitoutuvia leimoja. Lisäksi hermosoluviljelmien sähköistä aktiivisuutta tutkittiin mikroelektrodihilaan (microelectrode array, MEA) perustuvalla menetelmällä.

**Tulokset:** Eläviin soluihin sitoutuvat fluoresoivat merkkiaineet osoittautuivat hyväksi tutkimusmenetelmäksi. Menetelmän avulla nähtiin, että kahdesta eri viljelmästä peräisin olevat hermosolut pystyivät muodostamaan yhtenäisen hermoverkon, kun ne yhdistettiin samaan viljelmään. Tämän löydöksen



soveltaminen jatkossa voi auttaa tutkimuksissa, joissa pyritään selvittämään solusiiirrehoidoissa tarvittavaa hermoverkkojen yhteensulautumista.

PuraMatrix®-hydrogeelin sisällä viljellyt hermosolut kypsyivät muodoltaan monimuotoisiksi sekä niiden sähköinen signaalointi oli hermosoluille tyypillistä. Löydösten valossa PuraMatrix® materiaalina vaikuttaa soveltuvan hyvin hermosolujen viljelyalustaksi. Hermosoluille parhaimmat geelipitoisuudet muodostivat hyvin löyhän geelin, minkä johdosta näytteiden valmistus ja käsittely oli haastavaa. Tämä seikka huonontaa PuraMatrix®-hydrogeelin käytettävyyttä hermokudosmallin tukimateriaalina, vaikka muutoin tulokset ovat erittäin lupaavia.

Gellan gum -pohjaisia geelejä apuna käyttäen tutkittiin tukimateriaalin jäykkyyden vaikutusta hermosolujen kasvuun ja yritettiin kartoittaa soluviljelyssä käytettävälle tukimateriaalin ihanteellisia ominaisuuksia. Jäykkyydeltään aivoja vastaava materiaali ei kuitenkaan osoittautunut solukokeissa parhaimmaksi. Tämän perusteella todettiin, että jäykkyyden lisäksi monet muut materiaalin ominaisuudet vaikuttavat solujen kasvuun. Parhaat tulokset saatiin gellan gum -hydrogeelillä, johon oli sekoitettu soluväliaineen proteiinia, laminiinia, lisäämään materiaalin bioaktiivisuutta.

Hydrogeelien lisäksi sylinterimäiset polymeerikomposiittimikrotornit osoittautuivat erinomaisiksi alustoiksi pienten kolmiulotteisten hermoverkkojen viljelemiseen. Hermoverkkojen muodostuminen mikrotornien ympärille tapahtui toistettavasti ja hermoverkot noudattelivat mikrotornin rakennetta. Tämä työ tukee ajatusta, jonka mukaan kovista materiaaleista valmistettu tukirakenne on hyvä vaihtoehto laboratoriomallin pohjaksi.

**Johtopäätökset:** Väitöskirjatyön pohjalta voidaan todeta, että ihmisen hermosoluille ihanteellisen tukimateriaalin mekaanisten tai kemiallisten ominaisuuksien kartoittaminen ei ole yksioikoista. Monet tutkimukset keskittyvät tuottamaan monikäyttöisiä materiaaleja keskushermoston sovelluksiin. Tämä on haastavaa, sillä erilaisiin koeasetelmiin tarvitaan hyvin erilaisia ominaisuuksia. Tämän työn pohjalta herääkin kysymys siitä, olisiko parempi keskittyä materiaalin yleisen optimoinnin sijasta optimoimaan sen käyttöä soluviljelyalustana valikoiduissa sovelluksissa. Tämä tarkoittaisi materiaalin valitsemista tutkimuskysymyksen mukaan niin, että materiaalin ominaisuudet tukevat parhaalla mahdollisella tavalla tutkimuksen kohteena olevan ilmiön havaitsemista.



# CONTENTS

|                                                                                   |    |
|-----------------------------------------------------------------------------------|----|
| Abstract.....                                                                     | 4  |
| Tiivistelmä .....                                                                 | 6  |
| List of abbreviations .....                                                       | 13 |
| List of original publications .....                                               | 17 |
| 1 Introduction.....                                                               | 19 |
| 2 Review of literature.....                                                       | 21 |
| 2.1 Stem cells and neural differentiation <i>in vitro</i> .....                   | 21 |
| 2.1.1 Pluripotent stem cells.....                                                 | 21 |
| 2.1.2 Neural differentiation <i>in vitro</i> .....                                | 22 |
| 2.2 Neural Stem Cell-based <i>in vitro</i> models.....                            | 24 |
| 2.3 Biomaterials in neural TE .....                                               | 27 |
| 2.3.1 Hydrogels .....                                                             | 28 |
| 2.3.2 Solid materials .....                                                       | 30 |
| 2.4 Important aspects of scaffold design .....                                    | 30 |
| 2.4.1 Brain extracellular matrix as inspiration for scaffolds .....               | 30 |
| 2.4.2 Different scales of the 3D biomaterial scaffolds .....                      | 31 |
| 2.4.3 Mechanical, physical and chemical properties of scaffold.....               | 32 |
| 2.4.4 Designing scaffolds for <i>in vitro</i> and <i>in vivo</i> neural TE .....  | 34 |
| 3 Aims of the study.....                                                          | 35 |
| 4 Materials and methods.....                                                      | 37 |
| 4.1 Cell culture (Studies I, II, III and IV).....                                 | 37 |
| 4.1.1 Stem cell lines.....                                                        | 37 |
| 4.1.2 Derivation of neural cultures.....                                          | 37 |
| 4.1.3 Quality control and ethical permission (Studies I, II, III<br>and IV) ..... | 39 |
| 4.2 Hydrogels (Studies II and III) .....                                          | 39 |

|       |                                                                                                    |    |
|-------|----------------------------------------------------------------------------------------------------|----|
| 4.2.1 | Hydrogel components and gelation .....                                                             | 40 |
| 4.2.2 | Mechanical testing.....                                                                            | 41 |
| 4.3   | Rigid tubular microstructures (Study IV).....                                                      | 42 |
| 4.4   | Fluorescent labeling and imaging.....                                                              | 43 |
| 4.4.1 | Cell viability analysis (Studies I, II, III and IV).....                                           | 43 |
| 4.4.2 | Live cell-accumulating fluorescent labels, DiD and CT<br>(Study I).....                            | 44 |
| 4.4.3 | Immunocytochemistry (Studies I, II, III and IV).....                                               | 44 |
| 4.4.4 | Wide field imaging and image processing (Studies I, II,<br>III and IV) .....                       | 48 |
| 4.4.5 | Confocal imaging and image processing (Studies I, II, III<br>and IV) .....                         | 48 |
| 4.5   | Sample preparation for SEM and imaging (Study IV).....                                             | 49 |
| 4.6   | Microelectrode array (MEA), (Studies I, and II) .....                                              | 49 |
| 4.7   | Statistical analysis (Studies I, II, III and IV).....                                              | 50 |
| 5     | Results .....                                                                                      | 51 |
| 5.1   | Fluorescent probes as a live cell visualization tool (Study I).....                                | 51 |
| 5.2   | Analyzing neuronal growth on top of the hydrogels (Studies II and<br>III) .....                    | 53 |
| 5.3   | Neuronal cells under, on top of, or encapsulated within the hydrogel<br>(Studies II and III) ..... | 55 |
| 5.4   | Spontaneous electrical neuronal network activity (Studies I and II).....                           | 57 |
| 5.5   | Microtowers as structural 3D cell culture matrix (Study IV).....                                   | 59 |
| 5.5.1 | Cell distribution in microtowers (Study IV) .....                                                  | 59 |
| 6     | Discussion.....                                                                                    | 63 |
| 6.1   | Fluorescent cell-accumulating labels .....                                                         | 63 |
| 6.1.1 | Method optimization as essential part of experimental<br>design.....                               | 63 |
| 6.2   | 3D cultures, repeatability and variability.....                                                    | 64 |
| 6.2.1 | PuraMatrix® is promising material for studying neuronal<br>electrical activity in 3D.....          | 65 |
| 6.2.2 | Neurons in gellan gum-based hydrogels benefit from<br>laminin.....                                 | 66 |
| 6.2.3 | Rigid microtower scaffold supports formation of restricted<br>and repeatable 3D culture .....      | 66 |
| 6.3   | Neural network formation and response to the mechanical<br>properties of the scaffold.....         | 67 |

|       |                                                                         |    |
|-------|-------------------------------------------------------------------------|----|
| 6.3.1 | Neurons prefer a sparse PuraMatrix® hydrogel.....                       | 68 |
| 6.3.2 | Neural cells prefer a stiff gellan gum hydrogel .....                   | 68 |
| 6.4   | Future perspectives: How to build a perfect model?.....                 | 69 |
| 6.4.1 | A relevant cell source for brain tissue models.....                     | 69 |
| 6.4.2 | Choosing an optimal biomaterial as a scaffold for a 3D<br>culture ..... | 71 |
|       | Conclusions.....                                                        | 75 |
|       | Acknowledgements.....                                                   | 76 |
|       | References .....                                                        | 79 |



# LIST OF ABBREVIATIONS

|                  |                                                                                |
|------------------|--------------------------------------------------------------------------------|
| AL               | Alginate                                                                       |
| aSC              | Adult stem cell                                                                |
| A116             | Human induced pluripotent stem cell line                                       |
| BBB              | Blood-brain barrier                                                            |
| BDNF             | Brain-derived neurotrophic factor                                              |
| bFGF             | Basic fibroblast growth factor (also known as FGF2 or FGF- $\beta$ )           |
| BSA              | Bovine serum albumin                                                           |
| B27 <sup>™</sup> | Cell culture supplement                                                        |
| b-Tub            | $\beta$ -tubulin isotype III                                                   |
| CNS              | Central nervous system                                                         |
| CT               | Cell-Tracker Green CMFDA                                                       |
| DAPI             | 4',6-diamidino-2-phenylindole                                                  |
| DiD              | Carbocyanine 1,1-dioctadecyl-3,3,3,3-tetramethylindodicarbocyanine perchlorate |
| DMEM/F12         | Dulbecco's Modified Eagle's Medium: Nutrient Mixture F-12                      |
| EB               | Embryoid body                                                                  |
| ECM              | Extracellular matrix                                                           |
| EEG              | Electroencephalography                                                         |
| EGF              | Epidermal growth factor                                                        |
| GFAP             | Glial fibrillary acidic protein                                                |
| HA               | Hyaluronic acid                                                                |
| (h)ESC           | (Human) embryonic stem cell                                                    |

|         |                                                                 |
|---------|-----------------------------------------------------------------|
| HEL24.3 | Human induced pluripotent stem cell line                        |
| HFF     | Human foreskin fibroblast                                       |
| (h)NPC  | (Human) neural precursor cell                                   |
| (h)PSC  | (Human) pluripotent stem cell                                   |
| H(n)    | Human stem cell lines (H1, H7, H9, H13, H14)                    |
| IKVAV   | Cell adhesion peptide, amino acid sequence: Ile-Lys-Val-Ala-Val |
| IPN     | Interpenetrating polymer network                                |
| iPSC    | Induced pluripotent stem cell                                   |
| MAP-2   | Microtubule associated protein 2                                |
| MEA     | Microelectrode array                                            |
| MCS     | Multichannel systems                                            |
| MEF     | Mouse embryonic fibroblast                                      |
| NF 200  | Neurofilament 200                                               |
| (1)NDM  | Neural differentiation media, (1) containing FGF                |
| NDS     | Normal donkey serum                                             |
| NPC     | Neural precursor cell                                           |
| N2      | Cell culture supplement                                         |
| ON      | Overnight                                                       |
| PA      | Peptide amphiphiles                                             |
| DPBS    | Dulbecco's Phosphate-Buffered Saline                            |
| PB      | Phosphate buffer without saline                                 |
| PEG     | Poly(ethylene glycol)                                           |
| PEO     | Poly(ethylene oxide) refers also to PEG                         |
| pHEMA   | Poly(2-hydroxyethyl methacrylate)                               |
| PLA     | Poly(lactic acid)                                               |
| PLGA    | Poly(lactic-co-glycolic acid)                                   |



|              |                                                                                          |
|--------------|------------------------------------------------------------------------------------------|
| POE          | Poly(oxyethylene) refers also to PEG                                                     |
| PSC          | Pluripotent stem cell                                                                    |
| PVA          | Poly(vinyl alcohol)                                                                      |
| pHEMA        | Poly(2-hydroxy ethyl methacrylate)                                                       |
| RADA-16      | Synthetic peptide (PuraMatrix®)                                                          |
| Regea xx/xxx | Human embryonic stem cell lines (Regea 06/040, Regea 08/056, Regea 08/023, Regea 11/013) |
| RGD          | Cell adhesion peptide, amino acid sequence: Arg-Gly-Asp                                  |
| RM           | Regenerative medicine                                                                    |
| RT           | Room temperature                                                                         |
| SMAD         | Small Mothers Against Decapentaplegic –Protein family                                    |
| SPD          | Spermidine                                                                               |
| SAP          | Self-assembly peptide                                                                    |
| SCP          | Self-complementary peptide                                                               |
| TE           | Tissue engineering                                                                       |
| UH           | University of Helsinki                                                                   |
| UTA          | University of Tampere                                                                    |
| UTA.04511.WT | Human induced pluripotent stem cell line                                                 |
| YIGSR        | Cell adhesion peptide, amino acid sequence: Tyr-Ile-Gly-Ser-Arg                          |
| 2D           | Two-dimensional                                                                          |
| 3D           | Three-dimensional                                                                        |
| 2PP-DLW      | Two-photon-direct laser writing                                                          |



# LIST OF ORIGINAL PUBLICATIONS

This thesis is based on the following original publications, which are referred to in the text using the following Roman numerals (I–IV):

I Mäkinen M.\*, **Joki T.\***, Ylä-Outinen L., Skottman H., Narkilahti S., Äänismaa R. (2013), “Fluorescent probes as a tool for cell population tracking in spontaneously active neural networks derived from human pluripotent stem cells.” *J Neurosci Methods*. 2013 Apr 30;215(1):88–96. DOI: 10.1016/j.jneumeth.2013.02.019.

II Ylä-Outinen L., **Joki T.**, Varjola M., Skottman H., Narkilahti S. (2014), “Three dimensional growth matrix for human embryonic stem cell-derived neuronal cells.” *J Tissue Eng Regen Med*. 2014 Mar;8(3):186–94. DOI: 10.1002/term.1512.

III Koivisto J.\*, **Joki T.\***, Parraga J. Pääkkönen R., Ylä-Outinen L., Salonen L., Jönkkari I., Peltola M., Ihalainen T., Narkilahti S.\*\*, Kellomäki, M.\*\* (2017), “Bioamine-crosslinked gellan gum hydrogel for neural tissue engineering.” *Biomed Mater.*, 2017 Mar 24;12(2):025014. DOI: 10.1088/1748-605X/aa62b0

IV Turunen S.\*, **Joki T.\***, Hiltunen M., Ihalainen T., Narkilahti S.\*\*, Kellomäki M.\*\* (2017), ”Direct Laser Writing of Tubular Microtowers for 3D Culture of Human Pluripotent Stem Cell-Derived Neuronal Cells.” *ACS Appl Mater Interfaces*. 2017 9(31):25717–25730 DOI: 10.1021/acsami.7b05536

\* and \*\* Authors contributed equally

II Publication has been previously included in the doctoral dissertation, “Functionality of Human Stem Cell-Derived Neuronal Networks - Biomimetic Environment and Characterization” by Laura Ylä-Outinen, University of Tampere, 2012.

The original communications included in this dissertation are reproduced with the permission of the copyright holders.



# 1 INTRODUCTION

Tissue engineering (TE) and regenerative medicine (RM) are multidisciplinary fields of biotechnology that combine engineering and life sciences. They both aim at developing engineered biological constructs for restoring, maintaining, or improving the functionality of diseased or damaged human tissues. Sometimes the terms “tissue engineering” and “regenerative medicine” are used synonymously, but they can also be divided by their different areas of application. One classification is that TE aims to reproduce artificial tissue *in vitro*, while RM aims to repair tissue *in vivo*. This *in vitro* artificial tissue can also be called a cell-based *in vitro* model, which means that it is a platform for studying biological phenomena in a controlled, simplified environment. The research performed with these models can focus on developmental studies or on solving a clinical problem in human patients. Therefore, the final aims for developing TE *in vitro* tissue models include advanced therapies, *in vitro* diagnostics, preclinical tests for transplantation and a reduction in animal experiments. The current trend in these *in vitro* tissue models is towards organotypic 3D cultures. In this thesis, the main focus is to develop an *in vitro* neural model based on biomaterial scaffolds and human pluripotent stem cell-derived neural cells.

The human brain has unique processing power among animals, and the biological reasons behind this power are still not fully understood. From a TE point of view, the central nervous system (CNS) is a very interesting and promising target for new therapies, as its defects are difficult to treat with traditional methods. This is partially due to the poor inbuilt regeneration capacity of human CNS, and this lack of spontaneous regeneration causes many medical challenges. The current care guidelines are mainly targeted at alleviating symptoms; cures for the underlying dysfunctions in CNS are only available in rare cases. Both new knowledge on the disease mechanisms and new treatment strategies are needed.



## 2 REVIEW OF LITERATURE

The focus of this thesis is the development of stem cell-based neural *in vitro* models. This literature review will describe different *in vitro* models and their key features, including 1) stem cells and neural differentiation, 2) biomaterial scaffolds and 3) aspects of scaffold design.

### 2.1 Stem cells and neural differentiation *in vitro*

Stem cells have long been regarded as a potential cell source for TE applications since they offer an unlimited source of differentiated target cell types (Kim and Evans 2005, Avasthi *et al.* 2008). All stem cells possess the ability to both self-renew and differentiate. Stem cells can be classified according to their differentiation potential: totipotent, pluripotent, or multipotent. Totipotent stem cells are the only cell type that have the ability to form a new individual. The fertilized egg and cells in the first divisions of an early embryo are the only cells with totipotent differentiation capacity. After these developmental stages, the differentiation capacity of stem cells decreases. When the embryo develops into a blastocyst, the cells in the inner cell mass become pluripotent, having the capacity to differentiate into all tissues except the extra embryonic tissue (placenta). Later in development, the differentiation capacity further narrows and the cells become multipotent stem cells. Multipotent stem cells are tissue-specific and have a restricted capacity to differentiate into the cell types present in their tissues of origin (Avasthi *et al.* 2008). In many human tissues, a small number of cells remain in a multipotent state throughout adulthood and are responsible for wound or bone healing, for example. These stem cells are also called adult stem cells (aSC), and they can be found, for example, in bone marrow or in adipose tissue (Qian *et al.* 2010).

#### 2.1.1 Pluripotent stem cells

Embryonic stem cells (ESCs) are undifferentiated pluripotent cells derived from the inner cell mass of the blastocyst; they can be maintained and multiplied in a

laboratory and can be grown as a stable cell line (Tabar and Studer 2014). The stem cell line derivation from the inner cell mass is shown in Figure 1. Before ESCs, the first pluripotent cells that were found and cultured *in vitro* were from mouse teratocarcinoma, which is a malignant teratoma (Evans 2011). These stem cells were abnormal, malignant cells, but they enabled the experimental setups and methodological development that finally led to the derivation of native pluripotent stem cells (PSCs) from embryos (Evans 2011). The first human ESC lines (H1, H7, H9, H13, H14) were derived in 1998 by Thomson and co-workers (Thomson 1998), and these lines are still used today. The H9 line in particular is widely used in neural studies (Guo *et al.* 2013, Marx 2016). In 2006, a novel type of pluripotent stem cells, induced pluripotent stem cells (iPSCs), was created from somatic human cells, even though the principles behind the method had been studied much earlier (Gurdon 1962, Takahashi and Yamanaka 2006). These artificial stem cells are somatic cells that are reprogrammed into a stem cell-like state using genetic modifications (Figure 1). iPSC technology enables the generation of patient-specific cell lines for studying genetic diseases and developing personalized medicine in the future (Carlson *et al.* 2016)

### 2.1.2 Neural differentiation *in vitro*

Human PSC differentiation *in vitro* is based on signals given to the cell, or an artificial stem cell niche, to guide differentiation into the target cell type (Walters and Gentleman 2015, Clevers 2016). The protocols for deriving neural cells from hPSCs can be roughly divided into two stages (Figure 1). In stage 1, called neural differentiation or neural induction, the hPSCs are directed towards neural fate to create neural precursor cells (NPCs). In stage 2, called neural maturation, the NPCs are further matured into neurons and/or glial cells. The most commonly used neural differentiation methods are based on two strategies (Fisher 1997, Dhara and Stice 2008):

- A) Basic fibroblast growth factor (abbreviated here as bFGF, but also known as FGF2 or FGF- $\beta$ ) and epidermal growth factor (EGF) based pathways;
- B) Dual Small Mothers Against Decapentaplegic (SMAD) inhibition-based pathways.

EGF/FGF-based methods are widely used with slightly different variations (Carpenter *et al.* 2001, Dhara and Stice 2008, Lappalainen *et al.* 2010). The dual SMAD method was published in 2009 by Chambers and co-workers, and it has been



widely used since (Chambers *et al.* 2009, Shi *et al.* 2012). Both of these methods can have suspension or adherent culturing steps in variable order. Suspension culturing can be performed at the beginning of the differentiation as free-floating embryonic bodies (EBs) in a stem cell medium (Dhara and Stice 2008) or in a medium that directs cells to neural fate as free-floating neurospheres (Lappalainen *et al.* 2010). Adherent culturing steps can be used at the beginning of the differentiation, when stem cells are directed toward neural fate (Chambers *et al.* 2009). In addition, adherent cultures can be utilized as a purification step to collect neural rosettes (Malchenko *et al.* 2014). Many protocols have final neural maturation steps in adherent culture (Dhara and Stice 2008).

In addition to hPSC-derived neural cells, other techniques to obtain human neural cultures have been studied. One example of a recent hot topic method is transdifferentiation, or so-called lineage reprogramming. In older literature, transdifferentiation, for example, referred to growth factor-based methods where adipose-derived stem cells were differentiated into neuron-like cells (Safford and Rice 2005, Qian *et al.* 2010). More commonly, transdifferentiation refers to a recent transcription factor-based technique where adult somatic cells, such as skin fibroblasts, can be directly converted into other somatic cell types, such as neural cells, without the pluripotent step (Jopling *et al.* 2011). So far, neurons have been successfully created using transcription factors from human glial cells (Gascón *et al.* 2016), pericytes (Heinrich *et al.* 2015) and skin fibroblasts (Victor *et al.* 2014, Koch 2015).

All of the abovementioned techniques and innovations have enabled the routine use of human neural cells in the laboratory. In addition, after the deluge of stem cell lineages, stem cells and *in vitro*-derived neurons are thought to have four main application areas:

1. A tool to study development (*in vitro* models)
2. A tool to study diseases (*in vitro* models)
3. A tool for testing new drugs or the toxicity of compounds (*in vitro* models)
4. A tool to replace damaged cells or support endogenous regeneration (*in vivo*)

The use of neural cells *in vitro* to study development, diseases, drugs or toxicology will be further discussed in the following chapters.

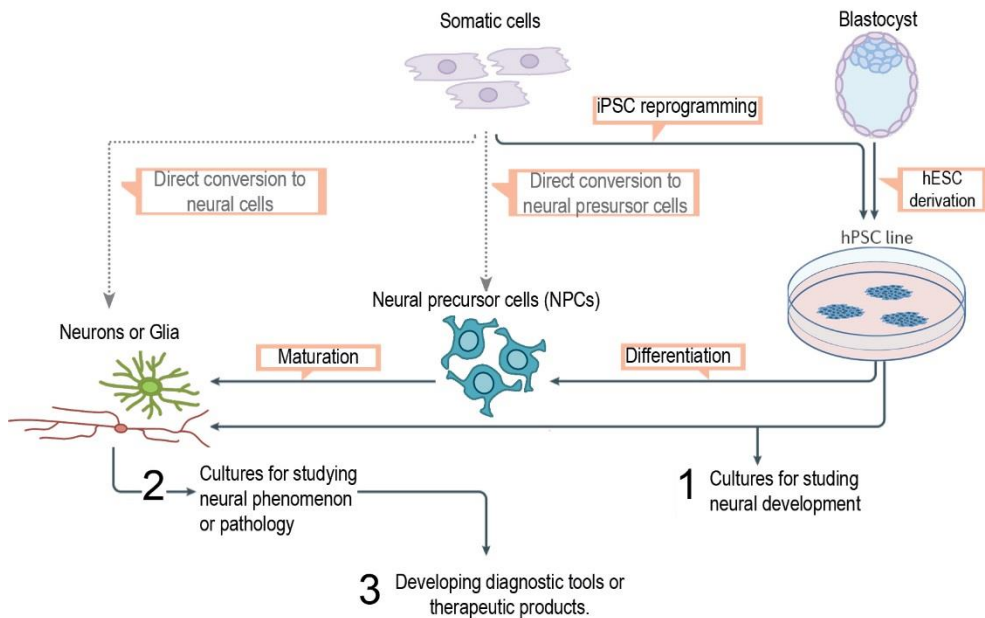


Figure 1. Common strategies to derive neural cultures for research and how these cultures can be utilized. Neural cells can be obtained by differentiation from pluripotent stem cell (hPSC) lines using either induced pluripotent stem cells (iPSCs) or embryonic stem cells (ESCs). Patient-specific iPSC lines can be created from somatic cells by genetic modification. Usually, patient lines are created by first making an iPSC line, which can be differentiated. It is also possible to use transdifferentiation, where somatic cells are directly converted into specific cell types or tissue-specific precursor cells. Neural differentiation for PSCs has two stages: initial differentiation into neural precursor cells (NPCs) and then maturation into neurons or glial cells. Established, matured neural cultures can be used for basic research in 1) neural development, 2) neural biology or more applied research, and 3) drug screening or the modeling of diseases. iPSC induced pluripotent stem cell, hESC human embryonic stem cell, hPSC human pluripotent stem cell, NPC neural precursor cell. Image modified from (Mertens *et al.* 2016).

## 2.2 Neural Stem Cell-based *in vitro* models

A cell-based *in vitro* neural model is a cell culture in a laboratory that can be used to study the biology of health or disease at the level of a single cell or cell population or at a subcellular level (Lancaster *et al.* 2013, Choi *et al.* 2014, Frega *et al.* 2015). Compared to patients or animal models, these cell-based neural *in vitro* models are always simplified study platforms. Thus, they fail to reproduce the whole complexity of organs and organisms, but they offer an ethical, controlled and cost-effective environment to perform experiments (Astashkina *et al.* 2012, Kelava and Lancaster 2016).

In principle, the neural *in vitro* models can be divided into two categories, either planar 2D cultures, i.e., “the conventional way,” or 3D cultures, i.e., “the modern way” (Sanyal 2014, Ravi *et al.* 2015). The simplest models contain only one cell type in 2D culture, whereas the more complex models contain several neural cell types in tissue-mimicking organotypic 3D culture (Kelava and Lancaster 2016). In the following sections, different types of *in vitro* neural models are described.

**Neural 2D culture** is the simplest and oldest neural *in vitro* model. These cultures are usually composed of a monolayer of dissociated cells on a rigid protein-coated surface. Usually, these cultures have only one cell type and a low amount of tissue-like complexity. These 2D cultures are relatively easy to handle, and a huge amount of literature is available describing the protocols for neural cultures (Dhara and Stice 2008, Marx 2016). Also, analyzing the results from 2D cultures, especially monolayer cultures, is relatively straightforward, even automatic, and the results can be compared to a large number of published studies (Dragunow 2008, Smith *et al.* 2013). These 2D *in vitro* neural models can be used to study many cell properties, such as morphological changes in neural cells caused by chemical insult (Harrill *et al.* 2010), or diseases, such as RETT syndrome (Williams *et al.* 2014). The parameters used to measure neuronal morphology include neurite outgrowth: number of neurites, length of neurites or amount of branching in neurites (Harrill *et al.* 2010). Functional *in vitro* neural models include neural 2D cultures on top of small electrodes in a microelectrode array (MEA; can also be referred to as a multielectrode array), which can be used to monitor neuronal network development or network responses to different compounds, such as drugs or toxicants (Johnstone *et al.* 2010). MEA measures the sum of electrical signaling in neuronal networks and MEA technology has similar features to electroencephalography (EEG) measurements in patients (Schevon *et al.* 2012). Neuro-developmental 2D models with anatomical correspondence include neural rosettes, which are cell clusters mimicking neural tube formation during early CNS development (Malchenko *et al.* 2014).

**Transwell culture** is a co-culture method combining elements of 2D and 3D culture. It is a cell culture insert-based system that has a porous membrane between two cell populations. The cell populations can be cultured without physical contact, with one on the insert part (on top of the membrane) and the other on the bottom of the cell culture well. Other approach is to culture the cells with a possibility of physical contact through the pores of the membrane on the upper and lower surfaces

of the membrane. This setup is ideal for co-cultures and for studying interactions between cell types, either via soluble factors or via cell-cell contacts (Sanyal 2014). Transwell systems are widely used in blood-brain barrier (BBB) *in vitro* models that are co-cultures of different cell populations associated with the BBB, including astrocytes and brain microvascular endothelial cells (Eugenin *et al.* 2011, Lippmann *et al.* 2012).

**Cell aggregate-based 3D *in vitro* models (spheroids and organoids)** are progenitor cell cultures where the cells differentiate into cell types found in the target tissue and self-organize to form structures that mimic the anatomical features of the target organ (Lancaster and Knoblich 2014). Cell aggregates called brain spheroids are neurosphere-like cultures that may contain several neural cell types, but usually lack large anatomical features (Nat *et al.* 2007, Paşca *et al.* 2015, Kelava and Lancaster 2016). Aggregates called organoids are more matured, larger and have macroscopic anatomical features, such as a fluid-filled cavity in the middle (Lancaster *et al.* 2013). Based on the cell population, neural organoids are further classified into whole-brain organoids (including different brain regions, Lancaster *et al.* 2013) or region-specific organoids, such as cortical organoids (Kadoshima *et al.* 2013). Many spheroid or organoid protocols include the use of Matrigel or corresponding ECM extract as a coating (Tieng *et al.* 2014), a supportive 3D matrix (Lancaster *et al.* 2013), or a supplement in the medium (Kadoshima *et al.* 2013). ECM extracts are thought to have a beneficial effect on organoid self-orientation (Kelava and Lancaster 2016).

**Scaffold-based neural 3D *in vitro* models** are 3D cell cultures where cells are cultured on a physically supportive biomaterial, or a scaffold. This *in vitro* neural scaffold can be a soft brain ECM-mimicking hydrogel formed via traditional *in situ* crosslinking (Saul and Williams 2013, Broguiere *et al.* 2016) or 3D printing (Lozano *et al.* 2015). Also, the scaffold can be a rigid infrastructure for cells to grow on, e.g., fibers (Carlson *et al.* 2016) or beads (Pautot *et al.* 2008).

Recently, researchers have realized that monolayer cultures on a rigid surface might lead to biased conclusions because the cells adapt to the unnatural 2D environment (Sanyal 2014, Frega *et al.* 2015). Thus, for cells, 2D culture is a very simplified environment that fails to offer tissue contacts, such as cell-cell and cell-ECM contacts (Baker and Chen 2012). These contacts are linked to the cell's cytoskeleton (Figure 2) and many signaling routes, thus having a huge effect on cell behavior (Doyle and

Yamada 2016). Not only the number but also the localization of cell attachment sides is important because cell attachment sites determine cell polarization by modulating the cytoskeleton (Harunaga and Yamada 2011).

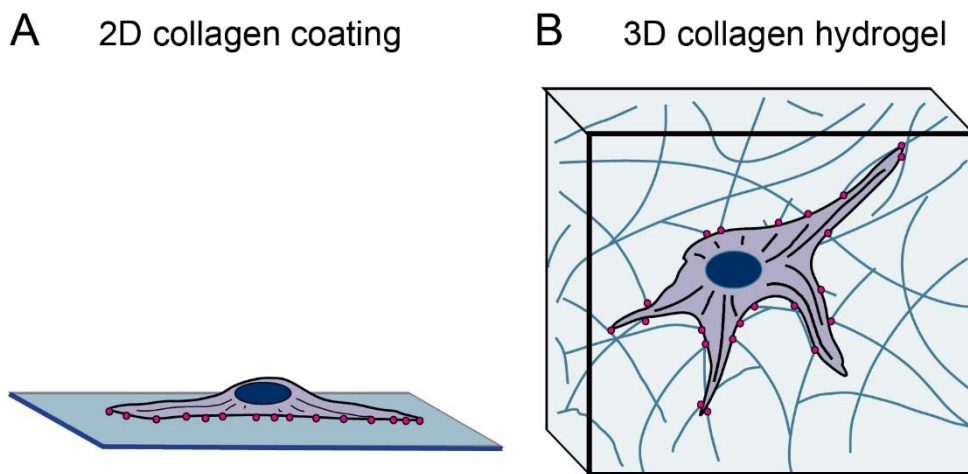


Figure 2. A schematic figure of the differences in cell adhesion and polarization between 2D and 3D culturing environments. Cell culture-based models can be built using either simplified planar 2D models or more tissue-mimicking 3D structures. In a 2D culture, cells become polarized due to the different stimuli on the cell culture medium side and the cell culture well side (A). In a 3D culture, cells are surrounded by an ECM-like matrix and the different kinds of stimuli are more evenly distributed around the cells (B). Cell adhesion is illustrated as red dots. Figure modified from (Baker and Chen 2012).

In summary, the current trend in models is clearly towards 3D models, either as organoids (Lancaster and Knoblich 2014, Clevers 2016, Kelava and Lancaster 2016) or as 3D neural networks utilizing biomaterial scaffolds (East *et al.* 2012, Lozano *et al.* 2015). These 3D models are usually based on biomaterial scaffolds and, in the future, biomaterials may have a more important role in the design of *in vitro* neural models.

### 2.3 Biomaterials in neural TE

Biomaterials play a very important role in TE, as they serve as one of the basic components of TE products. These products are cell transplants and *in vitro* models which can consist of cells, scaffold and growth factors (Chan and Leong 2008).

Biomaterials can be considered as an artificial ECM (Subramanian *et al.* 2009). Like native ECM in a tissue, the biomaterial scaffold offers cells an infrastructure to grow *in vitro* (Di Cio and Gautrot 2016). In neural TE, the scaffold is usually either a soft hydrogel or solid porous matrix, e.g., micro fibrous (Subramanian *et al.* 2009).

### 2.3.1 Hydrogels

Hydrogels are 3D crosslinked networks formed from polymers. Hydrogels with a high water content, as high as over 99 wt% water and less than 1 wt% polymer, are potential for neural TE applications due to ECM like properties (Appel *et al.* 2012, Dai and Huang 2013). The stiffness of hydrogel materials varies from less than 0.1 kPa (very soft gel, such as a viscous fluid) to approximately 500 kPa (hard gel, like silicone) (Tsou *et al.* 2016). Hydrogels used for neural TE commonly have stiffness less than 10 kPa (Aurand *et al.* 2012). It could be said that a soft tissue ECM also meets the criteria of a hydrogel (Bidarra *et al.* 2014). For this reason, hydrogels are considered potential materials for soft tissue applications. Hydrogel properties, such as elasticity and stiffness, can be tailored to be very similar to the soft tissue ECM (Brandl *et al.* 2007). Many hydrogel materials have good biocompatibility and mild crosslinking conditions, which are needed in TE applications (Aurand *et al.* 2012).

Hydrogels can be classified in many ways, and division according to their origin, i.e., either natural or synthetic, is only one possibility. In this thesis, hydrogels are examined based on origin from a practical point of view in scaffold design.

The **natural materials** used as hydrogels for neural TE are mainly proteins and polysaccharides or composites made from these two materials. Natural polymers have similarities to native ECMs (Cyphert *et al.* 2015) and thus have good bioactivity (Tsou *et al.* 2016). Their main disadvantage is fast degradation (Tsou *et al.* 2016).

- The protein-based hydrogels used for neural applications are collagen, gelatin, fibrin, silk, and rich ECM extracts, such as Matrigel™ or other similar products, reviewed by LaPlaca *et al.* (2010).
- The polysaccharide-based hydrogels used for neural applications are hyaluronic acid (HA), agarose, dextran, alginate (AL), cellulose, gellan gum, and chitosan (Nisbet *et al.* 2007, Suri and Schmidt 2010, Zhu and Marchant 2011, Lozano *et al.* 2015, Palazzolo *et al.* 2015).

- The protein/polysaccharide hybrid hydrogels used for neural applications include collagen/HA, laminin/cellulose, gelatin/chitosan, and fibrin/alginate (Zhu & Marchant 2011).

**Synthetic materials** are engineered artificial molecules. Traditionally, the widely used synthetic materials include poly(ethylene glycol) (PEG, also called poly(oxyethylene) (POE) or poly(ethylene oxide) (PEO)), poly(vinyl alcohol) (PVA), and poly(2-hydroxy ethyl methacrylate) (pHEMA). These three materials all are biologically inert, but they can provide structural support for cells (Zhu and Marchant 2011, Gu *et al.* 2014). Another group of synthetic materials is self-assembly peptide (SAP) hydrogels, which, unlike those mentioned above, are not inert (Zhu and Marchant 2011). Some natural ECM components, such as collagen, can be used as a SAP-like material, but usually the term SAP is used for synthetic materials.

There are two major SAP types:

- 1) Peptide amphiphiles (PAs), such as tenascin-C mimetic PA, (Berns *et al.* 2016)
- 2) Self-complementary peptides (SCPs), such as PuraMatrix® (Zhao *et al.* 2005)

PuraMatrix® consists of short oligomers (RADA-16, Arg-Ala-Asp-Ala repetition sequences) and is thus classified as a SCP. These alternating amino acids, which have hydrophilic side chains (arginine and aspartate) and hydrophobic side chains (alanine), trigger self-assembly into a  $\beta$ -sheet structure upon exposure to physiological ionic strength (Zhao *et al.* 2005). Commonly, SAPs have very good biocompatibility due to the nanofibrous structure that mimics the fibrous proteins in native ECM (Truong *et al.* 2011).

Hydrogels can also be composites of several materials and can form an interpenetrating polymer network (IPN) of two or more components. However, these kinds of complex materials are not widely used in the neural TE field (Suri and Schmidt 2010, Matricardi *et al.* 2013, Zhang *et al.* 2016).

### 2.3.2 Solid materials

In addition to hydrogels, solid materials are also used as neural scaffolds. These scaffolds include synthetic biodegradable polymers, such as poly(lactic-co-glycolic acid) (PLGA) (Lee *et al.* 2010), poly( $\epsilon$ -caprolactone) (PCL) (Sharifi *et al.* 2016) and poly(lactic acid) (PLA) (Melissinaki *et al.* 2011). These materials can be fabricated into various scaffolds at differing scales, such as nano- or microfiber scaffolds with electrospinning (Han and Cheung 2011), micro-lined scaffolds (Weng *et al.* 2015) with 2 photon-direct laser writing (2PP-DLW) or solid porous scaffolds by salt leaching (Murphy *et al.* 2017).

Other materials that have been studied in the neural field but are not widely used include conducting polymers, such as poly(pyrrole) or poly(aniline) (Subramanian *et al.* 2009), and synthetic non-degradable polymers, such as silicone (Lee *et al.* 2010), graphene (Li *et al.* 2013), silica (Pautot *et al.* 2008) and carbon nanotubes (Bokara *et al.* 2013).

## 2.4 Important aspects of scaffold design

### 2.4.1 Brain extracellular matrix as inspiration for scaffolds

The main cellular components of the brain are neurons and glial cells (astrocytes, oligodendrocytes, ependymal cells, and microglia). In addition to cells, brain tissue is composed of ECM, which constitutes quite a large amount of the brain, i.e., 10–20 vol% in adults (Lau *et al.* 2013). The ECM is a dynamic structure that is continuously modulated by cells. Cell-ECM contacts form via transmembrane proteins on the cell surface. These proteins recognize and bind to EMC molecules, thus linking the cell cytoskeleton to the ECM and anchoring the cell to its surroundings. These linkage sites are called local focal adhesion sites (Stevens 2005).

ECM is commonly divided into two types: 1) pericellular matrices (like basement membranes), which are situated directly around the cells; and 2) interstitial matrices, which fill the spaces between the cells in the tissue. The brain is a special case, and its ECM is classified into three different types, which each have their own molecular compositions:



1) Basal lamina (basement membrane, pericellular matrix). The basement membrane is a thin, sheet-like layer that is rich in collagen, laminin-nidogen complexes (also known as entactin), and fibronectin.

2) Perineuronal nets (pericellular matrix). Perineuronal nets form from a dense mesh-like layer with a large amount of chondroitin sulfate proteoglycans and HA.

3) The ECM of the parenchyma (interstitial matrix). The ECM of the parenchyma is a HA- and proteoglycan-rich area with only low amounts of fibrous proteins, such as collagen, and cell adhesion proteins, such as laminin and fibronectin (Lau *et al.* 2013).

The structure of these ECM types provides the inspiration for artificial ECM engineering in biomaterial science. Many widely used cell adhesion sequences are inspired by these molecules, such as the most commonly used RGD-peptide (amino acid sequence: arginine–glycine–aspartic acid), which is present in many ECM molecules, such as fibronectin, laminin, vitronectin, and collagen (Drury and Mooney 2003). Other widely used peptides are YIGSR (tyrosine–isoleucine–glycine–serine–arginine) and IKVAV (isoleucine–lysine–valine–alanine–valine), which are both from laminin (Loo *et al.* 2015).

## 2.4.2 Different scales of the 3D biomaterial scaffolds

For different study questions and different researchers, the definition of 3D cell culture is different. One of the definitions of a 3D environment is the macroscopic dimensions of the scaffold. A macroscopically flat scaffold that has thickness over 10 times the diameter of the cell appears as 3D to the cells (LaPlaca *et al.* 2010). Such scaffolds, which have macroscopically low height, are relatively easy to analyze, but are too small for some applications. A controversial opinion about 3D culture is using scaffolds that are on the mm scale (Pautot *et al.* 2008).

Most studied scaffolds are macroscopically 3D, but also the nano- and microscales of the scaffold are extremely important to the cells. 3D scaffolds with features considerably larger than ECM fibers might appear to the cells as 2D surfaces (Figure 3A, B), whereas nanofibrous materials mimic ECM (Figure 3C). Some examples of scaffolds that are macroscopically 3D matrices, but might be more surface-like for the cells are beads (Pautot *et al.* 2008), microporous ceramics (Heinrich *et al.* 2007) or micron-scale fibers (Lee *et al.* 2010, Yla-Outinen *et al.* 2010, Sharifi *et al.* 2016). Despite the fact that the scaffold is a 3D block, it appears to the cells as a 2D solid

substance with cavities or curved surfaces (Figure 3). In fibrous scaffolds, the scale and fiber diameter (Figure 3B,C) determine how cells attach to the fibers (Stevens 2005). Microfiber scaffolds (Figure 3B) are typically made from synthetic polymers with a fiber diameter of  $\sim 10\text{--}50\ \mu\text{m}$  and a pore size of  $\sim 10\text{--}200\ \mu\text{m}$  (Zhang *et al.* 2005), such as the PCL fiber scaffold for neural TE with fiber diameters of 2.6 to 36.5  $\mu\text{m}$  (Sharifi *et al.* 2016). Because the pores of the scaffold are considerably larger than the cells and the fibers are on the same scale as the cells (typical diameter of a cell  $\sim 5\text{--}30\ \mu\text{m}$ ), the material fails to mimic ECM structure (Zhang *et al.* 2005). The ECM in the native tissue has a nanofibrous nature with a fiber diameter on the submicron scale, i.e., from 10 to 300 nm (Stevens 2005), which is considerably smaller in scale than the micro-size materials. Hydrogels are one example of nanofibrous materials that form ECM-mimicking scaffolds. The synthetic self-assembly peptide PuraMatrix<sup>®</sup> is one typical example of such a material (Zhao *et al.* 2005, Loo *et al.* 2012).

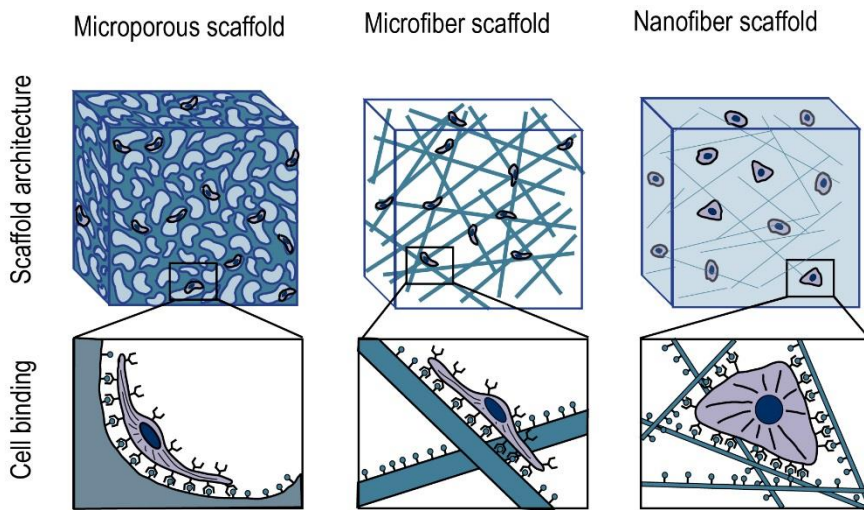


Figure 3. Different scales commonly used in scaffold materials. Microporous scaffolds are dense materials with large openings (A). Microfiber scaffolds are fibrous with a fiber diameter measured in microns (B). Nanofiber scaffolds are natural ECM-like materials with a fiber diameter measured in nanometers (C). Figure modified from (Stevens 2005). Mechanical, physical and chemical properties of scaffold

**The mechanical, physical and chemical** properties of the hydrogel are all important to the cells, but the mechanical properties are more commonly studied than the other two (Engler *et al.* 2006, Saha *et al.* 2008).

**Mechanical properties** are measured using the shear modulus, Young's modulus, and compressive modulus, which all measure the elastic properties of solid materials as defined by Hooke's law (Aurand *et al.* 2012). The modulus is calculated from the linear area of the stress/strain curve (Figure 4A). In the literature, stiffness and elasticity are the parameters that are most often used to determine the mechanical properties of soft tissues or scaffold materials, but comparing the exact values between studies is challenging. The terminology is not standardized, and it might lead to misinterpretations. Additionally, differences in measurement setups and analysis methods cause variations in the findings (Morris *et al.* 2012, Oyen 2014). In general, the stiffness (Young's modulus) measures the lowest amount of force that will break the material. A stiff material bears more force without breaking compared to a soft material. The elasticity or strength of the material is measured with a modulus called the elastic modulus or tensile modulus. The elastic modulus is also sometimes referred as Young's modulus, but it is different from Young's modulus for stiffness. The elasticity/strength is the amount of force that a material can withstand and still recover its original shape (sample does not break/no permanent damage). An elastic material can recover from higher forces, whereas a rigid material breaks. Mechanically, brain tissue is soft but elastic, and its elasticity or softness is considered to be in the range of 0.1–1 kPa (Engler *et al.* 2006). However, higher values have also been measured (Budday *et al.* 2015).

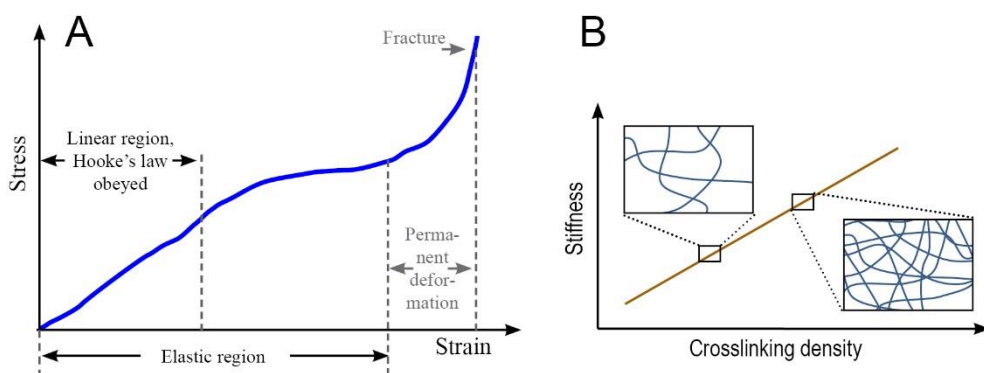


Figure 4. The mechanical properties of hydrogels are calculated from the linear part of the elastic region of in the stress-strain curve using Hooke's law (A). The effect of increasing the crosslinking density (x-axis) in the hydrogel to the hydrogel stiffness (Z-axis), and a visualization of the changes in hydrogel structure (small images, B). Figures modified from <http://cnx.org/> (A) and (Kloxin et al. 2010)(B).

The **physical properties** of the scaffold that have an effect on the cell growth are mesh size and porosity (Aurand *et al.* 2012, Saul and Williams 2013). Sometimes the terms “porosity” and “mesh size” are confused with one another. Usually, pores are considered to be large openings in the hydrogel structure with a diameter measured on a micron scale, usually from 3 to 600  $\mu\text{m}$  (Tsou *et al.* 2016). Mesh size is the distance between crosslinks (Figure 4B) and is measured in angstroms ( $\text{\AA}$ ), varying usually from 10 to 150  $\text{\AA}$  (Aurand *et al.* 2012). Both the pore size and mesh size affect scaffold properties, such as stiffness and nutrient flow (Yoo *et al.* 2011, Aurand *et al.* 2012). Of these two, cell migration is mainly affected by porosity, as cells need physical space for migration (Appel *et al.* 2012). For CNS, TE *in vitro* scaffolds with interconnected pores larger than 40  $\mu\text{m}$  have enhanced cell migration, whereas pores larger than 100  $\mu\text{m}$  might be needed *in vivo* for successful vascularization and tissue integration (Li *et al.* 2012).

**Chemical factors** that are important to the cell response include non-toxicity, pH, material surface characteristics, such as wettability or hydrophilicity, and material charge density (Subramanian *et al.* 2009).

### 2.4.3 Designing scaffolds for *in vitro* and *in vivo* neural TE

There are many general requirements that each scaffold material needs to meet, starting from general biocompatibility (Gu *et al.* 2014). In neuronal scaffolds, more specific requirements include the ability to support neuronal cell growth and normal functionality (Pautot *et al.* 2008). Material demands differ in *in vivo* and *in vitro* applications (Aurand *et al.* 2012). In *in vivo* applications, the materials are acting as a delivery vehicle for drugs, growth factors, or cells to the defected area, as well as acting as physical support that fills the defect cavity (Kretlow *et al.* 2007). In contrast, the main purpose of the material *in vitro* is to aid in reproducing the complexity of *in vivo* neural networks, both anatomically and functionally (Pautot *et al.* 2008, Limongi *et al.* 2013, Frega *et al.* 2015). In other words, biomaterials are used as a tool to make better *in vitro* neural models.

### 3 AIMS OF THE STUDY

The aim of this thesis was to create a 3D neural culturing setup that could be used as an *in vitro* neural tissue model in the future. The specific focus was to characterize both the materials and their effect on neural cell growth. The more specific aims for each study are listed below:

- I To optimize a fluorescent cell population tracking tool for long-term follow-up studies to be utilized in biomaterial studies or studies on the interactions between two different cell populations.
- II To study the suitability of PuraMatrix® as a structural scaffold for stem cell-derived neural cells and to show the maturation of human neuronal cells in a 3D environment.
- III To find the mechanical properties of hydrogels that could be used to predict biomaterial suitability of a neural scaffold *in vitro*.
- IV To study the suitability of cylindrical structures as an alternative 3D matrix for long-term neuronal cultures.



## 4 MATERIALS AND METHODS

### 4.1 Cell culture (Studies I, II, III and IV)

#### 4.1.1 Stem cell lines

The cells used in this thesis were human neural cells differentiated from hPSC-lines. Both hESC and iPSC lines were used (cell lines listed in Table 1). Derivation and characterization of the cell lines was previously described for hESC lines (Skottman 2010). Maintenance of the hPSC lines was performed as described earlier (Rajala *et al.* 2007, 2010).

**Table 1** Stem cell lines used in this thesis.

| Cell line    | Type (method)       | Feeder cells | Derivation | Study          | Publication                   |
|--------------|---------------------|--------------|------------|----------------|-------------------------------|
| Regea 06/040 | hESC                | hFF          | UTA*       | I, II          | (Rajala <i>et al.</i> 2010)   |
| Regea 08/056 | hESC                | hFF          | UTA*       | I              | (Skottman 2010)               |
| Regea 08/023 | hESC                | hFF          | UTA*       | I, II, III, IV | (Skottman 2010)               |
| Regea 11/013 | hESC                | hFF          | UTA*       | III            | (Sorkio <i>et al.</i> 2015)   |
| UTA.04511.WT | iPSC (retrovirus)   | MEF/hFF      | UTA**      | III            | (Ojala <i>et al.</i> 2016)    |
| Hel24.3      | iPSC (Sendai virus) | hFF          | UH***      | III            | (Trokovic <i>et al.</i> 2015) |
| A116         | iPSC (Sendai virus) | hFF          | UH***      | III            | (Toivonen <i>et al.</i> 2013) |

**hESC** human embryonic stem cell, **iPSC** induced pluripotent stem cell, **hFF** human foreskin fibroblast, **MEF** mouse embryonic fibroblast, **UTA** University of Tampere, **UH** University of Helsinki, \*derivation Adj. Prof. Heli Skottman (UTA), \*\*derivation Prof. Katriina Aalto-Setälä (UTA), \*\*\* A kind gift from Prof. Timo Otonkoski (UH).

#### 4.1.2 Derivation of neural cultures

The neural differentiation of hPSCs was performed using a bFGF-based neurosphere method, as published earlier (Lappalainen *et al.* 2010). This method contains a neural differentiation phase as freely floating neurospheres in suspension culture,

followed by growth factor withdrawal-induced neural maturation as an adherent culture. The experimental setup is briefly shown in Figure 5.

**Neural differentiation.** For neural differentiation, the hPSC colonies were mechanically cut into small cell aggregates (Figure 5, step 1) and were directly transferred into the neural differentiation medium (1NDM) containing 1:1 DMEM/F12: Neurobasal supplemented with GlutaMax (2 mM), 1 × B27™, 1 × N2, penicillin/streptomycin (25 U/ml) purchased from Thermo Fisher Scientific (Waltham, MA, USA) and bFGF (20 ng/ml) from Bio-Techne (Minneapolis, MN, USA). After one week in the culture, the cell aggregates formed round, freely floating neurospheres (Figure 5, step 2). During differentiation, one third of the cell culture medium was changed three times per week. The neurosphere diameter was kept at approximately 500 μm by mechanically cutting the neurospheres with a scalpel once a week to ensure an optimal growth factor gradient and diffusion to the cells in the central parts of the neurospheres.

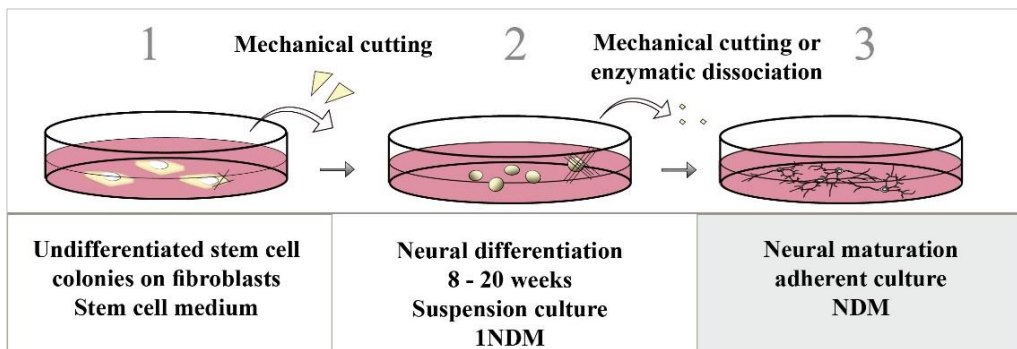


Figure 5. Undifferentiated hPSC colonies (1) were mechanically passaged, and cell aggregates were transferred into neural differentiation media as free-floating neurospheres. Neurospheres were kept within a neural niche for 8–20 weeks (2) and were plated as adherent cultures for the final maturation (3). The cells used in the experiments were all at stage 3. **1NDM** neural differentiation media containing bFGF, **NDM** neural differentiation media without growth factors.

**Neural maturation.** For neural maturation, the neurospheres were mechanically dissected into small cell aggregates (3,000–7,000 cells/aggregate) or were enzymatically dissociated into a single cell suspension using 1× TrypLE Select (Gibco). Cells were then plated as an adherent culture on laminin-coated cell culture plastic or glass (coating solution: 10 mg/ml mouse laminin in Dulbecco's Phosphate-Buffered Saline (DPBS), Sigma-Aldrich, St. Louis, MO, USA), on top of the



hydrogel surface, or encapsulated within the hydrogel (Figure 5, step 3). In the beginning of the maturation phase, bFGF was withdrawn from the NDM in order to induce maturation. In Studies III and IV, NDM containing 5 ng/ml bFGF and 4 ng/ml brain-derived neurotrophic factor (BDNF, Prospec Bio, Germany) was used after one week of bFGF withdrawal in order to support neural cell survival. Half of the medium was changed three times per week during the adherent culturing phase.

#### 4.1.3 Quality control and ethical permission (Studies I, II, III and IV)

All cell lines used in this study were under frequent quality control. Both in the undifferentiated stage and during the differentiation, the cultures were mycoplasma-free and the cells had a normal karyotype. In an undifferentiated state, the cells expressed pluripotency-related genes and proteins and were able to spontaneously differentiate into cell types from all three germ layers.

BioMediTech (formerly Regea) has ethical approval to derive, culture, and differentiate hESC lines (Regea- cell lines, Skottman, Pirkanmaa Hospital District, R05116) and iPSC lines (UTA.04511.WTS- cell line, Aalto-Setälä, Pirkanmaa Hospital District, R08070). BioMediTech also has approval to perform stem cell research (National Authority for Medicolegal Affairs in Finland, 1426/32/300/05) and to use hPSC lines for neural research (Pirkanmaa Hospital District, R14023). Biomedicum Stem Cells Center Helsinki has approval for iPSC line generation (cell lines A116 and HEL24.3, Coordinating Ethics Committee of the Helsinki and Uusimaa Hospital District, Nro 423/13/03/00/08).

#### 4.2 Hydrogels (Studies II and III)

The hydrogels used in this study were commercial PuraMatrix® (Study II, BD Bioscience, Sparks, MD, USA) and an in-house designed gellan gum polysaccharide hydrogel crosslinked with spermidine (SPD; Study III). Reagents for the gellan gum-based gels were kindly produced by Janne Koivisto, MSc. and Jenny Parraga, Ph.D. from Minna Kellomäki's group at Tampere University of Technology, Finland.

Briefly, PuraMatrix® was used in concentration 0.05, 0.10, 0.15 and 0.25 wt%. PuraMatrix® was gelled according to the manufacturer's instructions (No 2007) using a cell culture medium.

The gellan gum hydrogels were prepared from gellan gum (Gelzan™ CM, low acyl, #G1910) and SPD both from Sigma-Aldrich (Finland). Gellan gum based hydrogels all contained 5 mg/ml of gellan gum while the concentration of SPD cross-linker was varied 1.25 wt%, 1.50 wt% and 3.00 wt%.

#### 4.2.1 Hydrogel components and gelation

In all the hydrogel studies, three culturing methods were utilized. Briefly, the cells were plated:

1. Under the hydrogel.
2. On top of the hydrogel.
3. Encapsulated within the hydrogel.

The prepared hydrogels were macroscopic in size, with a gel height ranging from 0.5 mm to 1 mm and a volume of 50 to 250  $\mu$ l per sample.

**Cells under the hydrogel.** By casting a hydrogel layer on top of the neural cell culture, the effects of the gelation on cells and nutrient diffusion through the gel were studied. The gelation was performed directly on pre-cultured healthy neural network growing on laminin protein coating.

PuraMatrix® was gelled according to the manufacturer's instructions (No 2007) using a cell culture medium. For gelation directly on top of the cultured cells, the PuraMatrix® was diluted into 20 wt% sucrose in sterile water in order to reduce osmotic shock. This diluted liquid PuraMatrix® precursor was pipetted on top of the cells, and the medium was added on top to induce the gelation.

In the case of the gellan gum hydrogel, the cell culture medium was removed and SPD cross-linker was pipetted onto the cells. Immediately after that, the gellan gum solution was pipetted on the wells and mixture was allowed to crosslink. No additional stirring was performed to avoid disturbing the cells. After 20 minutes of gelation cell culture medium was added to wells.

**Cells on top of the hydrogel surface.** By plating the cells on top of the pre-cast hydrogel surface, cell attachment to and migration along the hydrogel surface were studied.

When making PuraMatrix® hydrogel surfaces for the cell culture, the stock solution was diluted to the final concentration using sterile water and was transferred to the cell culture wells; hydrogel formation was initiated by adding cell culture

medium on top. After gelation, media was changed once and cells were plated on top of the hydrogel surface.

Gellan gum hydrogel surfaces were prepared by first pipetting the cross-linker into the cell culture well, and the gellan gum stock solution was then added on top while the mixture was stirred. Solution was allowed to crosslink 20 minutes and after that cell culture medium was added to wells and cells were plated on top of hydrogel surface.

**Cells encapsulated within the hydrogel.** By mixing the cells with a liquid gel precursor prior to gelation, the cellular response to gelation, survival after gelation, and attachment to the formed hydrogel were studied.

To prepare the encapsulated cultures in PuraMatrix®, the cells were centrifuged and the cell culture medium was removed. The cells were suspended in 10 wt% sucrose in water to a 2× final cell density. The PuraMatrix® was diluted into the 2× final concentration with 20 wt% sucrose in water. Finally, these solutions were mixed 1:1 in order to obtain the intended PuraMatrix® dilution and cell concentration in the final gel. After pipetting this mixture into the culture platform, the gelation was induced by slowly adding the cell culture medium on top of the liquid mixture.

With the gellan gum hydrogels, the cells were mixed into the gellan gum stock solution before gelation. Otherwise, the gelation was performed similarly as described above for preparing hydrogel surface for plating cells on top. To enhance cell attachment to the gellan gum hydrogel, prior to gelation mouse laminin was mixed with gellan gum solution as a physical mixture. Laminin was used at 1 vol%, 5 vol% or 10 vol% of the gellan gum component.

#### 4.2.2 Mechanical testing

Compression testing was performed using a BOSE Electroforce Biodynamic 5100 machine equipped with a 225 N load sensor and Wintest 4.1 software (Bose Corporation, Eden Prairie, Minnesota, USA) at Tampere University of Technology. Unconfined compression was performed with a constant 10 mm/min strain rate, and the samples were compressed until 65% strain was reached from the original height. For elastic materials Hooke's law describes the stress-strain relationship in the linearly elastic range. The compression data was analyzed with MS Excel according to Hooke's law:

$$\sigma = E * \epsilon$$

In the formula the  $\sigma$  is stress, E is the Young's modulus (stiffness of the material), and  $\epsilon$  is strain (a measure of the deformation). The compressive modulus was calculated from the stress-strain curve as the slope of the elastic region. Hydrogel samples and brain tissue samples containing the midbrain, cerebellum, or cortex of New Zealand white rabbits were processed into similarly shaped samples and were analyzed in a similar manner. The rabbits, from which the post mortem brain samples were collected (Study III), were under the ethical approval of the Medical School of the University of Tampere.

### 4.3 Rigid tubular microstructures (Study IV)

The tubular cell culture microstructures were fabricated using photopolymerization. The polymerization was performed on top of 9-mm coverslips using a custom-built 2 photon-direct laser writing (2PP-DLW) setup that is based on previously described system (Käpylä *et al.* 2011). The material used in this study was commercial photocurable polymer-ceramic hybrid Ormocomp<sup>®</sup> (Micro Resist Technology GmbH, Germany) with photoinitiator 2 wt% Irgacure<sup>®</sup> 127 (Ciba Specialty Chemicals, Switzerland). The fabricated microtowers had the following dimensions: ~150  $\mu\text{m}$  in height and an inner diameter of ~75  $\mu\text{m}$ . Microtowers were kindly fabricated by Sanna Turunen, MSc., from Minna Kellomäki's group at Tampere University of Technology, Finland.

Three different tower designs were used (Figure 6): Tower I (openings and intraluminal structures, A), Tower II (openings, B) and Tower III (plain cylinder, C). Before cell culture, the cover slips containing the towers were disinfected with ethanol and were coated with laminin, similar to the earlier description (4.1.2. Neural maturation). Pre-differentiated neural cells were plated as a single-cell solution on the laminin-coated scaffold surface at a density of ~35 000 cells per  $\text{cm}^2$ .

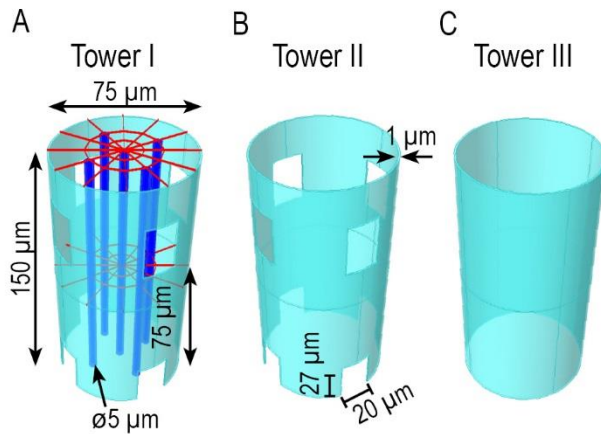


Figure 6. CAD-models of the microtower designs used in Study IV. Design with openings and intraluminal structures (webs and pillars, Tower I, A), design with openings but without intraluminal structures (Tower II, B), and plain cylinder design (Tower III, C). Tower height is 150  $\mu\text{m}$  and inner diameter is 75  $\mu\text{m}$ . Upper openings start at a height of 75  $\mu\text{m}$ . Also, the lower webs are located at a height of 75  $\mu\text{m}$ . All openings are 27  $\mu\text{m}$  in height and 20  $\mu\text{m}$  wide. The pillars in Tower I are 5  $\mu\text{m}$  in diameter, and the wall thickness in all towers is 1  $\mu\text{m}$ .

## 4.4 Fluorescent labeling and imaging

### 4.4.1 Cell viability analysis (Studies I, II, III and IV)

A Viability/Cytotoxicity Kit for mammalian cells (Molecular Probes/Invitrogen, Finland) was used to study cell viability (Althouse & Hopkins 1995). In brief, the method is based on two fluorescent dyes: cell-permeable Calcein-AM (0.1  $\mu\text{M}$ ,  $\lambda$  emission = 488 nm) accumulates in the cytoplasm of intact cells, and cell impermeable ethidium homodimer-1 (0.4  $\mu\text{M}$ ,  $\lambda$  excitation = 568 nm) binds to the nuclei of cells without an intact cell membrane. These dyes were diluted in fresh culture medium to the final concentrations of Calcein-AM 0.1 M and EthD-1 0.5 M, and the solution was added to the cells. After 30 min (2D cultures) or 1 h (3D cultures) of incubation, the cultures were imaged with a fluorescence microscope. Analysis was performed by manually counting the number of labeled cells in the images.

#### 4.4.2 Live cell-accumulating fluorescent labels, DiD and CT (Study I)

The label stock solution was diluted to the cell culture media and was incubated with the cells at +37°C in 5% CO<sub>2</sub> in a humidified atmosphere (the parameters are listed in Table 2). After incubation, the labeling medium was replaced with fresh culture medium. When needed, the pre-labeled cell populations were detached using enzymatic dissociation. Dissociated labeled cells were re-plated, for example, to prepare co-cultures (the method is shown in Figure 7).

#### 4.4.3 Immunocytochemistry (Studies I, II, III and IV)

Cells were fixed with 4 wt% paraformaldehyde (Fluka, Italy). Non-specific staining was blocked with 10 vol% normal donkey serum (NDS) and 1 wt% bovine serum albumin (BSA) in DPBS, abbreviated as blocking solution (all reagents from Sigma-Aldrich). Primary antibodies were diluted to 1 vol% NDS and 1 wt% BSA in DPBS, abbreviated as 1° antibody / 1° wash solution (antibodies in Table 2).

A

| Abbreviation           | DiD                                                                             | CT                                                                      |
|------------------------|---------------------------------------------------------------------------------|-------------------------------------------------------------------------|
| Product                | DiD, D-307, (Molecular Probes®, Life Technologies)                              | Cell-Tracker Green CMFDA, C2925, (Molecular Probes®, Life Technologies) |
| Full name              | Carbocyanine 1,1-dioctadecyl-3,3,3,3-tetramethylindodicarbo-cyanine perchlorate | Carboxymethylfluorescein diacetate                                      |
| Type                   | Incorporates into the cell membranes                                            | Cell membrane permeable, accumulates in cytoplasm of living cells       |
| Labeling concentration | 0.2, 0.5, 1, 5, 10, 20, or 50 $\mu\text{M}$                                     | 0.5, 2, 4, 5, 8, 10, 16, 20, 30, 40, or 60 $\mu\text{M}$                |
| Incubation times       | 2, 10, 30, or 60 min or 2, 4, 8, 16, or 24 h                                    | 15, 30, or 60 min or 2, 4, 24, 48, or 72 h                              |

B

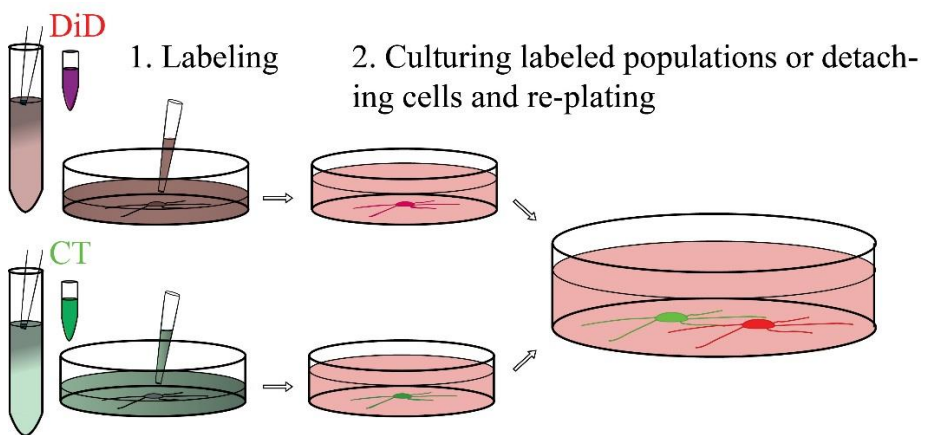


Figure 7. Two fluorescent live cell-accumulating labels were used as a cell population tracking tool. The commercial labels and labeling parameters tested for long-term, live-cell visualization (A). Diagram outlining the labeling protocol and preparation of pre-labeled neural co-cultures (B).

**Table 2** Primary antibodies used in this thesis.

| Abbreviation | Protein full name and target                                                                | Animal, dilution, and manufacturer                                | Study          |
|--------------|---------------------------------------------------------------------------------------------|-------------------------------------------------------------------|----------------|
| <b>b-Tub</b> | $\beta$ -tubulin isotype III Immature neuronal cell bodies and neurites, mature axons       | Mouse monoclonal, 1:1250 (Sigma-Aldrich),                         | I, II, III, IV |
|              |                                                                                             | Rabbit, 1:1000, A01627 (GenScript, Piscataway, NJ, USA)           |                |
| <b>GFAP</b>  | Glial fibrillary acidic protein, astrocytic cytoskeleton                                    | Sheep, 1:800, af2594 (R&D Systems)                                | I, II          |
| <b>MAP-2</b> | Microtubule-associated protein Immature neuronal cell bodies and neurites, mature dendrites | Rabbit, 1:400–1:800, AB5622 (Merck Millipore, Darmstadt, Germany) | I, II, III, IV |
| <b>NF200</b> | Neurofilament 200 KDa, neuronal cytoskeleton and axons                                      | Mouse, 1:500, N5389 (Sigma-Aldrich)                               | I              |

The excess primary antibodies were removed by washing with 1° antibody / 1° wash solution. Next, the secondary antibodies were added in 1 wt% BSA in DPBS, abbreviated as 2° antibody / 2° wash solution. AlexaFluor-488, -568, or -680 conjugates of anti-chicken, anti-rabbit, anti-mouse, or anti-sheep secondary antibodies produced in either in goat or donkey (1:600 or 1:400, Molecular Probes Invitrogen) were used. The excess secondary antibodies were removed by washing with DPBS. Final washes were performed using phosphate buffer without saline (PB) or DPBS (Table 3). Solutions without permeabilization or with permeabilization agent, either 0.1 vol% Triton-X 100 or 0.1 wt% Saponin, both from Sigma-Aldrich were used (Table 3). Triton-X 100 was added to blocking and 1° antibody / 1° wash solutions and saponin was added to blocking and both 1° antibody / 1° wash and 2° antibody / 2° wash. The incubation times for different protocols are listed in Table 3. For nuclear staining and mounting, Vectashield with 4,6-diamidino-2-phenylindole (DAPI, H1200, Vector Laboratories, Peterborough, UK) was utilized (studies I-III). Instead of Vectashield in Study IV, TDE Mounting media (Abberior GmbH, Germany), which is 2,2'-thiodiethanol-based embedding media, was used due to better optical properties (refractive index of 1.518).



**Table 3** Incubation times used in immunocytochemical protocols.

|                                                                         | <b>Fixation</b> | <b>Blocking</b> | <b>1° antibody</b> | <b>1° wash</b>    | <b>2° antibody</b> | <b>2° wash</b>    | <b>PB wash</b> |
|-------------------------------------------------------------------------|-----------------|-----------------|--------------------|-------------------|--------------------|-------------------|----------------|
| <b>2D cultures without hydrogel (Study I)</b>                           | 15 min RT       | 45 min          | ON +4°C            | 3 * 5 min         | 1 h RT             | 5 min * 2         | 5 min * 3      |
| <b>3D optimized for PuraMatrix® (Study II)</b>                          | 30 min RT       | 60 min          | ON +4°C            | 3 * 30 min        | 4–5 h RT           | 3 * 30 min        | 2 * 30 min     |
| <b>3D optimized for gellan gum (Study III) and microstructures (IV)</b> | 30 min 37°C     | 60 min          | 3 days +4°C        | 1* brief + 2 *1 h | ON +4°C            | 1* brief + 2 *1 h | -              |

Solutions used:

Fixation: 4 wt% paraformaldehyde in DPBS

Blocking solution: 10 vol% normal donkey serum (NDS) and 1 wt% bovine serum albumin (BSA) with or without permeabilizations

1° antibody /1° wash: 1 vol% NDS and 1 wt% BSA in DPBS with or without permeabilization agents

2° antibody / 2° wash: 1 wt% BSA in DPBS with or without permeabilization agents

No permeabilization: no permeabilization agent added to any solutions

Saponin permeabilization: 0.1 wt% saponin was present in blocking, 1° antibody /1° wash, and 2° antibody / 2° wash solutions

Triton-X permeabilization: 0.1 vol% Triton-X 100 was present in blocking and 1° antibody /1° wash solutions

**PB**, phosphate buffer without saline, **RT**, room temperature, **ON**, overnight

#### 4.4.4 Wide field imaging and image processing (Studies I, II, III and IV)

During cell culture, samples were monitored using phase contrast microscopes: a Zeiss AxioVert.A1 microscope with an AxioCam ERc 5s camera system or a Nikon Eclipse TE 2000-S microscope with a Nikon Digital Sight DS-Fi1 camera system. For fluorescent sample imaging, an Olympus IX51 inverted microscope and an Olympus DP30BW digital camera were used. The obtained gray scale images were post-processed using Adobe Photoshop CS4 (version 11.0, Adobe Systems, Inc., CA, USA). Channels from the fluorescent images were pseudo-colored and combined. All image panels were created with Adobe InDesign CS4 (version 6.0, Adobe Systems, Inc.).

#### 4.4.5 Confocal imaging and image processing (Studies I, II, III and IV)

Confocal scanning of the samples was performed with a Zeiss LSM 780 mounted onto an inverted Cell Observer microscope (Carl Zeiss, Jena, Germany). The confocal data were visualized as projections or 3D rendered images with ZEN Black 2012 (Carl Zeiss) or ImageJ (Version 1.39, U.S. National Institutes of Health, Bethesda, Maryland, USA) software.

To analyze nuclei distribution in the microtowers, the confocal image stacks were converted into substacks with a height of 15  $\mu\text{m}$  (principle is shown in Figure 8). These substacks were further converted into maximal intensity projections and were used as a data series for cell counting. All cell nuclei inside and outside of the tower were manually calculated using an ImageJ cell counter plugin.

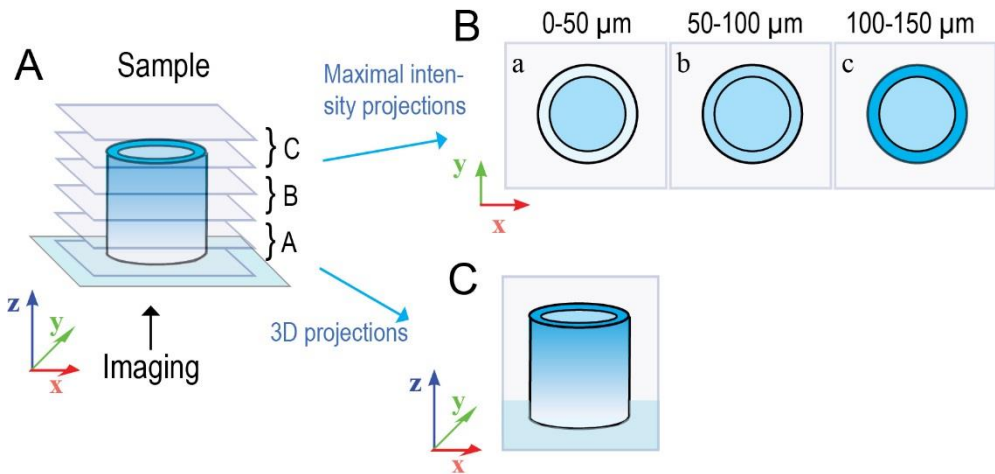


Figure 8. Confocal imaging and image processing. Confocal image stacks (A) were visualized as maximal intensity projections (B) or 3D projections (3D rendering, C). To count cells in the total height of the sample, the confocal stack was divided into substacks and was further processed into maximal intensity projections (in the example, the height of each substack is 50  $\mu\text{m}$ )

#### 4.5 Sample preparation for SEM and imaging (Study IV)

For SEM imaging, the samples were fixed with 5 vol% glutaraldehyde in DPBS (Sigma-Aldrich) for 1 h at RT and were washed with ion exchanged water (15 min). After fixing, the samples were dehydrated by an ascending series of ethanol (10 vol%, 20 vol%, 40 vol%, 60 vol%, 80 vol%, 99.5 vol%, ethanol/water) for 10 min each and were air dried, followed by storage under vacuum. After complete drying, the samples were sputter coated with gold in argon atmosphere (S 150 Sputter Coater) to a coating thickness of approximately 75 nm. Finally, the samples were imaged with an SEM microscope, Philips XL-30 (Philips Electron Optics, the Netherlands).

#### 4.6 Microelectrode array (MEA), (Studies I, and II)

The electrical activity of the neuronal networks was measured with a MEA system (Multi Channel Systems, MCS, Reutlingen, Germany). Cells were plated on top of standard MEA plates containing 59 measurement electrodes (30 mm diameter, 200 mm inter-electrode distance).

During the measurements, the MEA plates were kept at 37°C with an external heater unit (TC02, MCS). Signals were pre-amplified with MEA1060-Inv-BC (gain 53, MCS) and were pre-filtered with FA60SBC (gain 20, MCS), producing a signal with a gain of 1100 and a bandwidth of 1 Hz–8 kHz. The data were recorded with MC\_Rack software (MCS). Continuous extracellular field potential data were collected at a 20-kHz sampling rate and were post-acquisition filtered with a 200 Hz high-pass filter. The spike counts and time stamps on each electrode were extracted with NeuroExplorer (Nex Technologies, Littleton, MA, USA) software, collected into Excel files, and combined into raster plots.

#### 4.7 Statistical analysis (Studies I, II, III and IV)

Statistical analysis was performed with the IBM® SPSS (version 19) statistical software package. Due to the non-Gaussian distribution of the data, the nonparametric Kruskal–Wallis test and Mann–Whitney  $U$  test were used. A  $p$ -value of less than 0.05 was considered significant. When more than two groups were compared, the resulting  $p$ -values were multiplied by the number of comparisons performed (Bonferroni correction).

## 5 RESULTS

### 5.1 Fluorescent probes as a live cell visualization tool (Study I)

To create a cell visualization tool, the neural cells were labeled using fluorescent probes that accumulate in living cells. The criteria for this tool were that it would enable long-term cell population tracking in co-cultures and be capable of enhancing cell visibility inside opaque biomaterials. A wide range of different labeling parameters, dye concentrations, and incubation times were tested for two commercial probes: DiD and CT. The best results were obtained with 10  $\mu\text{M}$  DiD with 2 h incubation and 10  $\mu\text{M}$  CT with 72 h incubation (Figure 9A). With these parameters, the labels were cytocompatible and the labeling was visible for up to 4 weeks, which was considered a reasonable end point for the long-term experiments.

**Parameter optimization.** The effects of labeling were studied using viability analysis and cell proliferation, and durability of labeling was also monitored. The labeling parameters needed to be optimized for both probes in order to find a safe but effective parameter range for DiD and to enhance the durability of CT labeling. DiD was found to be toxic in high concentrations; even a short-term exposure to 50  $\mu\text{M}$  DiD (30 min) caused cell death. In addition, 5, 10, and 40  $\mu\text{M}$  DiD caused cell death if the exposure was 16 h or more (Figure 9B). With optimized parameters (10  $\mu\text{M}$  and an incubation time of 2 h), no toxicity was detected, but DiD still slightly inhibited cell proliferation in the long-term culture. With CT, none of the tested concentrations had an effect on viability or proliferation. It was found that CT incubation times of less than three days caused visible labeling only for up to 2 weeks. When the incubation time was increased to three days, the cell population had a stable fluorescence for up to four weeks. The neuronal phenotype of labeled cells was ensured using immunocytochemical staining (Figure 9A).

To study these probes in cell population tracking, the DiD and CT pre-labeled populations were detached and were further mixed into the co-cultures. Both dyes were preserved during enzymatic dissociation into single cell suspension and after re-plating. The lack of double-stained cells in the co-cultures confirmed that these

dyes did not leak from one cell population to the other, even though the labeled population formed close contacts. In the co-culture, DiD and CT pre-labeled cells formed neural cultures with a homogenous cell distribution (Figure 9C).

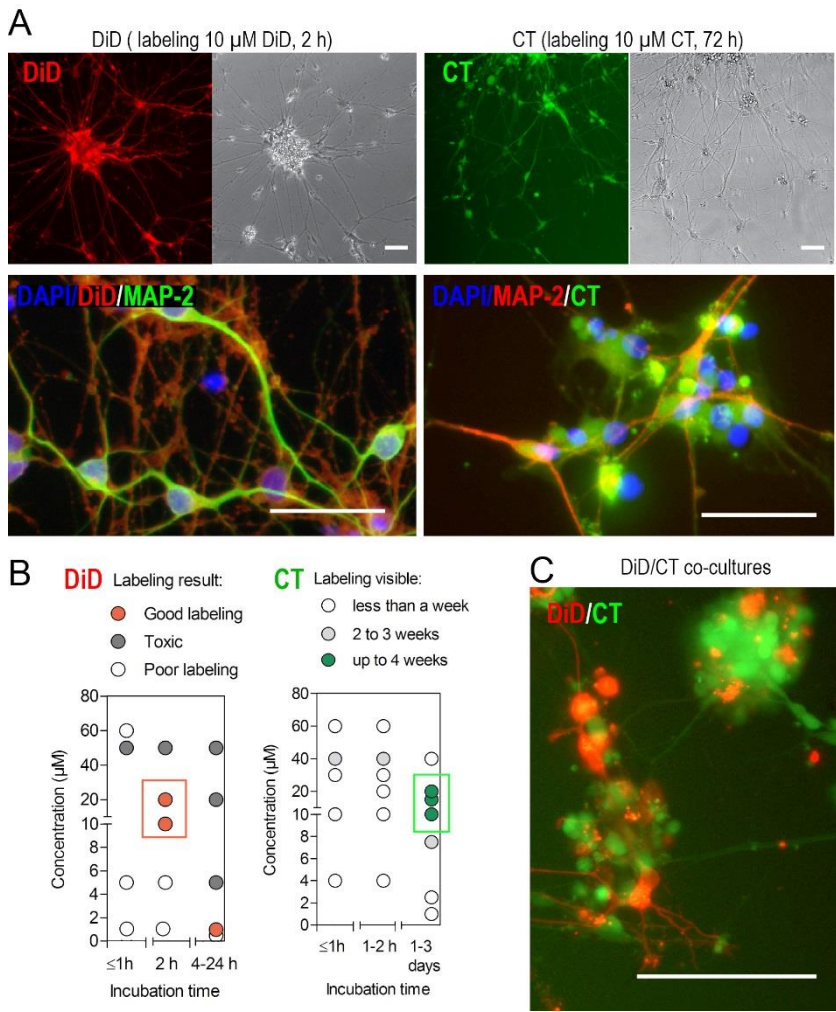


Figure 9. Fluorescence and phase contrast images of living neural cell cultures labeled with DiD (10  $\mu$ M/2 h) and CT (10  $\mu$ M/72 h) (A). Both fluorescent probes label the whole cell morphology in a clear and easily distinguishable way. Neural cultures pre-labeled using DiD or CT, followed by immunocytochemical labeling against neuronal marker MAP-2 (A, bottom row). Effects of the dye concentration and incubation time on the cell population and labeling result for both DiD and CT (B). Living co-culture of cell populations pre-labeled with DiD and CT (C). All scale bars are 100  $\mu$ m. Each dot in figure B presents the labeling parameters tested and the color of the dot describes the result based on visual inspection. Data in figure B is from at least two experiments and at least two parallel samples per experiment.

## 5.2 Analyzing neuronal growth on top of the hydrogels (Studies II and III)

Two different hydrogels were studied as an artificial ECM scaffold for human neural cells:

- 1) A synthetic PuraMatrix®, RADA-peptide hydrogel (Study II), and
- 2) A natural gellan gum polysaccharide-based hydrogel (Study III).

The gel density was optimized for both studied hydrogels. First, the hydrogels were studied as pre-cross-linked surfaces that the cells were cultured on.

**PuraMatrix® hydrogel (Study II):** PuraMatrix® dilutions from 0.05 wt% to 0.25 wt% were tested. The softest hydrogels were found to be the most favorable for human neural cells. The hydrogels with the lowest peptide concentrations, 0.05 wt% and 0.1 wt%, had more neurons compared to other cell types (Figure 10A). The softest composition with 0.05 wt% peptide had a high percentage of neurons, but a dramatically low total cell amount compared to the other dilutions (Figure 10A). This indicates that for some reason, cells were lost during culture or sample analysis, but most of the remaining cells were neurons. The 0.1 wt% PuraMatrix® dilution had a remarkably high amount of neurons without a decrease in total cell quantity. Due to this result, 0.1 wt% PuraMatrix® was chosen as the most suitable option for future studies. Representative images of neurons growing on top of soft PuraMatrix® hydrogels with peptide concentration of 0.1 wt% and 0.15 wt% are shown in Figure 10B.

**Gellan gum hydrogel (Study III):** With the gellan gum hydrogel, the effect of the hydrogel mechanical properties on neuronal cells was studied. The hydrogel softness was tuned by altering the cross-linker concentration. The cross-linker, SPD, was studied at concentrations of 3.00, 1.50, and 1.25 wt%. The modulus of the gellan gum with a cross-linker concentration of 1.25 wt% was the most similar to the rabbit brain sample (no statistically significant difference), whereas the hydrogel with 3.00 wt% SPD was significantly stiffer than all other cases (Figure 10C). However, all tested gellan gum hydrogel compositions had a modulus that was typical for soft tissue. Interestingly, the stiffest hydrogel was the best for the neuronal cells, as the cross-linker amount in the hydrogel increased, the neurite length also increased (Figure 10D).

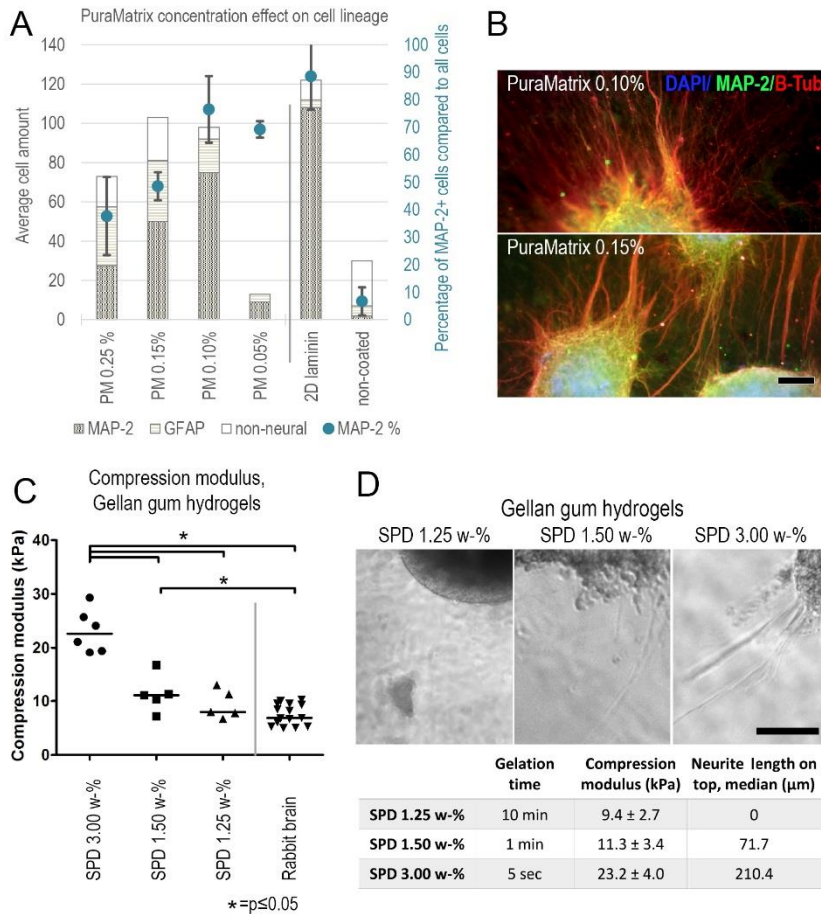


Figure 10. Effect of hydrogel concentration on the cell lineage of human PSC-derived neural cells cultured on top of 0.25–0.05 wt% PuraMatrix® hydrogels (A). Average cell number of MAP-2 (neuronal), GFAP (astrocytic) or non-stained (non-neural) cells on samples are shown as bar shading on the primary axis, and the percentage of MAP-2 positive cells from all cells is presented as dots on the secondary axis with whiskers showing the standard deviation (A). Representative images after immunocytochemical staining of neuronal cells growing on top of 0.10 wt% and 0.15 wt% PuraMatrix® (B). The mechanical properties (compression modulus) of gellan gum hydrogels with 1.25–3.00 wt% SPD cross-linker compared to rabbit brain samples (C). Phase contrast images of neural cells growing on top of gellan gum hydrogel, and a table describing the effects of increasing cross-linker concentration in the hydrogel (D). Scale bars are 100 μm (B) and 50 μm (D). Blue: DAPI, green: MAP-2 and red: B-tub. Data in figure A is from one experiment with at least five analyzed images per condition, in figure C from one experiment, and in figure D from at least two experiments and at least three analyzed images per experiment. **PM** PuraMatrix®, **SPD** Spermidine



On top of the softest gellan gum, hydrogel cells formed spheres, but no neurite outgrowth was observed (Figure 10D). This finding was the complete opposite of the result for PuraMatrix®. Due to the low amount of neurite outgrowth, the gellan gum hydrogel itself was found to be too inert. Adding laminin as a physical mixture to the gellan gum hydrogel was found to enhance neuronal outgrowth.

### 5.3 Neuronal cells under, on top of, or encapsulated within the hydrogel (Studies II and III)

Cell culture experiments were performed using three different experimental designs. Cell growth was analyzed using immunocytochemical analysis as well as a live/dead viability analysis. In all cases, both the PuraMatrix® hydrogel as well as the gellan gum laminin mixture showed good cytocompatibility.

**Cells under the hydrogel (2D).** In the first experimental design, the hydrogel was cast directly over the neural culture, and the cells were cultured under the hydrogel block. The gelation process of both studied hydrogels was found to be non-harmful to the cell cultures, even though the pH of PuraMatrix® is outside the physiological range before gelation occurs (Study II). No neurite withdrawal was seen in the cultures after gelation. In addition to the lack of acute negative effects, both hydrogels also supported long-term cultures (two weeks) under the gel layer (Figure 11A). This indicates that nutrients and waste products were able to flow through the gel layer.

**Cells on the hydrogel surface (2D).** In the second experimental design, the cells were plated on top of the pre-cast hydrogel block. Both PuraMatrix® and gellan gum (+laminin) were able to support neuronal growth on the hydrogel surface (Figure 11B), although slight variation was seen between repetitions. Variation was seen as differences in amount of neurite outgrowth. On PuraMatrix® most of the cell aggregates attached to the hydrogel surface (Study II) whereas on gellan gum (+laminin) hydrogels, in some samples the plated cells remained as free-floating aggregates (Study III). These aggregates contained living cells, but for some reason, they were not able to attach to the hydrogel surface during the two weeks of culturing.

**Cells encapsulated within the hydrogel (3D).** In the third experimental design, the cells were mixed with a liquid gel precursor and were cultured while encapsulated within the hydrogel. Areas with neuronal migration within the hydrogel were found

in both materials (Figure 11C). Cells inside 0.1 wt-% PuraMatrix® extended neurites in all directions to the surrounding hydrogel (Study II). Contrary to the gellan gum (+ laminin) hydrogels, where the cell growth was uneven, and nearly all samples also contained areas without cell migration (Study III). This phenomenon was similar to that detected when the cells were cultured on top of the hydrogel surface. The aggregates were viable, but the hydrogel failed to offer the cells an environment for attachment and migration.

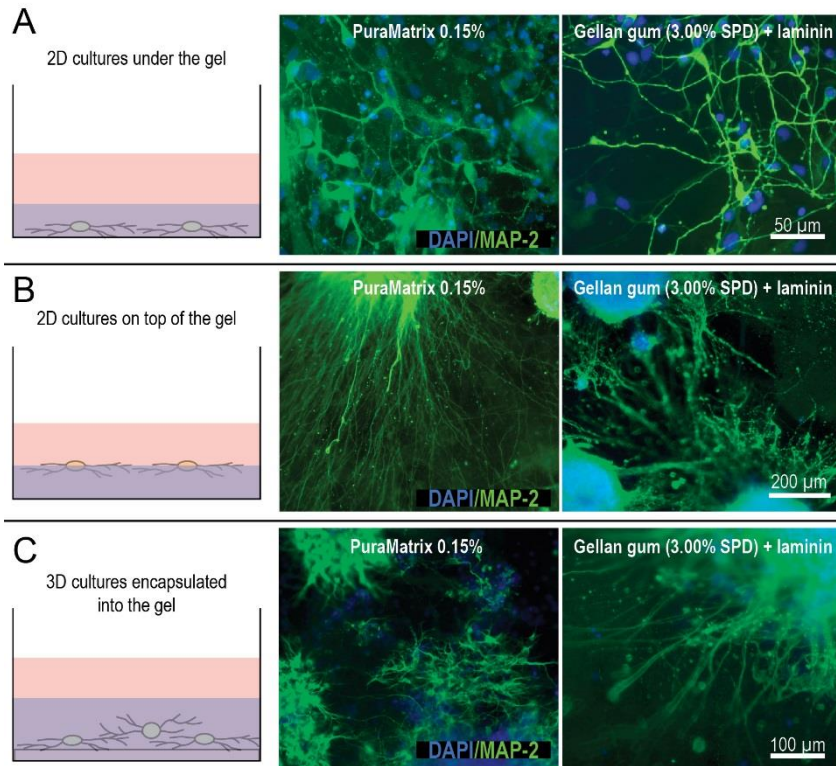


Figure 11. Neural cells cultured under the PuraMatrix® or gellan gum hydrogel block (A), on top of the hydrogel surface (B), or encapsulated within the hydrogel (C). Scale bar is 100 μm. Blue: DAPI (nuclei); green: MAP-2 (neurons). In 2D cultures, the cell morphology is similar for both hydrogels (A, B), but in 3D cultures, there are more differences. Within the PuraMatrix® hydrogel, both cell bodies and neurites spread and migrate into the gel, whereas in gellan gum hydrogel cells, neurites into are sent into the hydrogel, but cell bodies very rarely migrate out of the aggregates (C).

## 5.4 Spontaneous electrical neuronal network activity (Studies I and II)

The spontaneous electrical network activity of the *in vitro* cultured 2D human neural cells was studied using an MEA platform (Study I). With DiD and CT pre-labeled populations, it was found that when these two populations were combined in a co-culture, they formed similar functional networks as cultures from the same origin without labels. Networks matured into train-like activity, but neither the controls nor the co-cultures achieved synchronous bursting activity, which is considered the most mature type of signaling recorded in *in vitro* neuronal networks. The activity was similar in the co-cultures and the control cultures, indicating that labeling had no negative effect on neuronal activity and more importantly, that the cells from the two different populations were able to form one functionally integrated network (Figure 12A).

Similarly, the electrical network activity of 3D neuronal networks cultured within the PuraMatrix<sup>®</sup> hydrogel was studied using MEA (Study II). The 2D cultures on laminin were used as an experimental control. Neuronal networks in the 3D environment within the PuraMatrix<sup>®</sup> hydrogel were able to form spontaneous activity that was similar to 2D cultures at the four-week time point (Figure 12B). The development of activity was slightly slower in 3D. After two weeks on MEA, the first spikes were seen in 3D cultures, whereas in the 2D cultures, the first spikes were detected as soon as after one week on MEA. Nevertheless, neither culture achieved synchronous busting-type activity during this experiment.

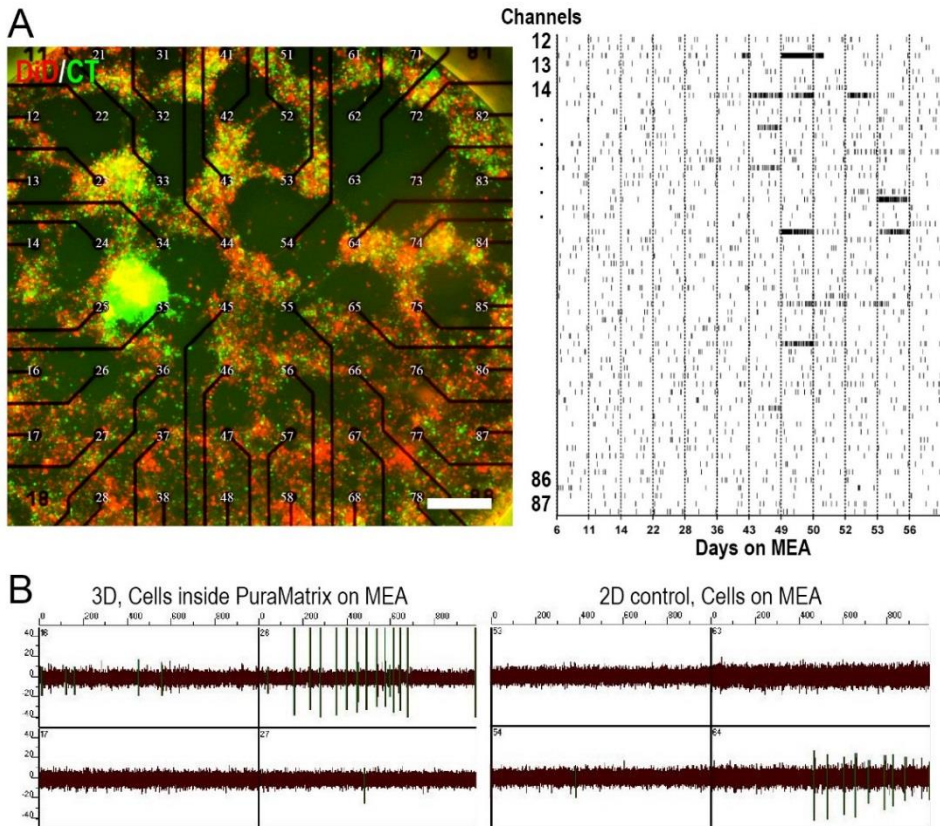


Figure 12. Representative image of neural networks formed from DiD and CT pre-labeled populations growing on top of an MEA plate (A, right-hand side). Red: DiD-labeled cells and green: CT-labeled cells. Scale bar is 200  $\mu\text{m}$ . The development of electrical activity of one fluorescent co-culture for a period of over 56 days on an MEA dish as a raster plot (A, left-hand side). Each vertical line represents spikes detected in the channel during a one-second bin. Each channel on the y-axis represents one electrode on the MEA dish. A close-up view of the MEA signal from 2D and 3D cultures, showing spike amplitude (B).

## 5.5 Microtowers as structural 3D cell culture matrix (Study IV)

Rigid microtowers were used as a 3D culturing scaffold for hESC-derived neuronal cells. Neural cells, which were plated to the microtowers on a cover slip, grew along the outer surface of the microtowers and inside the towers throughout the four-week follow up time (representative images of cell growth in Figure 13). Cells did not only grow along the surfaces, but also formed connections between adjacent towers or between tower walls and the surrounding cover slip surface (see examples in Figure 13, marked with a white arrowhead).

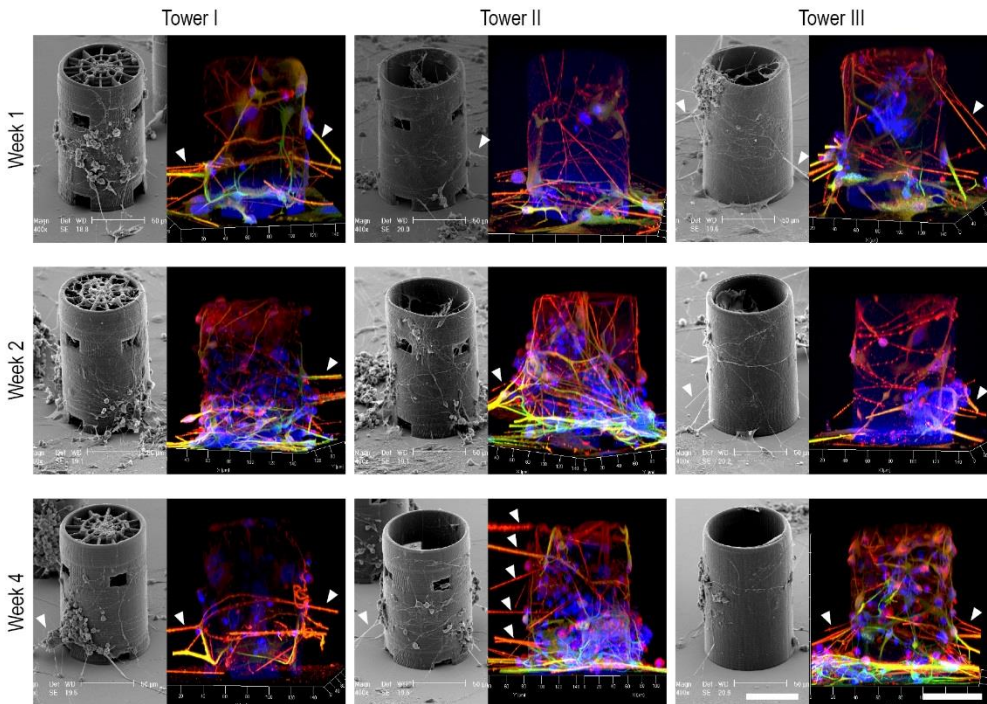


Figure 13. Neural cells were cultured 1 to 4 weeks on the microtowers (A, left-hand side: representative SEM image and right-hand side: representative confocal image. Blue: DAPI, green: MAP-2 and red: b-Tub). Scale bars are 50  $\mu\text{m}$ . White arrow heads: neurites growing between outer wall of the towers and the adjacent tower or cover slip on the bottom surface.

### 5.5.1 Cell distribution in microtowers (Study IV)

The total amount of cells growing along the tower as well as cell localization either outside of the tower or inside the tower was analyzed from confocal stacks (Table 4). At the **one-week time point**, no clear differences could be found in the cell amounts

between the three studied tower designs; the total number of cells in the towers as well as the cell numbers both inside and outside of the tower were quite similar (Table 4).

At the **two-week time point** in tower designs I and II, the cell number increased both inside and outside, whereas in design III the cell amounts stayed similar as in one-week time point (Table 4).

**By week four**, the cell number dropped quite dramatically in designs I and II (Table 4). Although the cell number in design III was slightly lower throughout the experiment, it stayed quite constant during first two weeks in culture, but increased outside the tower by week four. At the same time for tower III at the four-week time point, both the median and maximum values for number of cells outside of had an increasing trend whereas the minimal amount of cells value was very low. This indicates a high variability in cell growth between parallel samples in Tower III at four-week time point.

In all designs, the cell numbers inside the towers were smaller but less variable than the cell numbers outside for all time points, except for the four-week time point in tower I.

**Table 4** Descriptive numbers on the cell distribution outside and inside of the tower designs. Number of analyzed towers, n = 9, except in Tower II, 4 weeks, where n = 8. Within each row the 3-Color scale (green-white-red, high-medium-low) highlights the highest and the lowest values.

| Cell numbers:             | TOWER I |        |        | TOWER II |        |        | TOWER III |        |        |
|---------------------------|---------|--------|--------|----------|--------|--------|-----------|--------|--------|
|                           | Week 1  | Week 2 | Week 4 | Week 1   | Week 2 | Week 4 | Week 1    | Week 2 | Week 4 |
| Inside                    | 377     | 730    | 288    | 441      | 664    | 430    | 336       | 417    | 276    |
| Outside                   | 856     | 1170   | 254    | 1009     | 1792   | 690    | 822       | 735    | 1181   |
| total                     | 1233    | 1900   | 542    | 1450     | 2456   | 1120   | 1158      | 1152   | 1457   |
| Average inside per tower  | 42      | 81     | 32     | 49       | 74     | 61     | 37        | 52     | 31     |
| Average outside per tower | 95      | 130    | 28     | 112      | 199    | 99     | 91        | 92     | 131    |
| Average total per tower   | 137     | 211    | 60     | 161      | 273    | 160    | 129       | 144    | 162    |
| Median inside per tower   | 26      | 77     | 33     | 34       | 74     | 39     | 27        | 48     | 33     |
| Median outside per tower  | 108     | 132    | 31     | 74       | 202    | 85     | 50        | 80     | 142    |
| Median total per tower    | 159     | 222    | 63     | 142      | 304    | 124    | 100       | 121    | 150    |
| MIN inside per tower      | 11      | 15     | 13     | 10       | 42     | 10     | 4         | 5      | 3      |
| MIN outside per tower     | 26      | 47     | 5      | 13       | 85     | 10     | 23        | 26     | 3      |
| MIN total per tower       | 42      | 72     | 18     | 47       | 132    | 24     | 49        | 103    | 9      |
| MAX inside per tower      | 105     | 159    | 45     | 118      | 150    | 145    | 90        | 133    | 58     |
| MAX outside per tower     | 168     | 231    | 56     | 303      | 342    | 243    | 227       | 221    | 355    |
| MAX total per tower       | 184     | 375    | 101    | 333      | 431    | 383    | 248       | 253    | 391    |

MAX Maximum, MIN Minimum

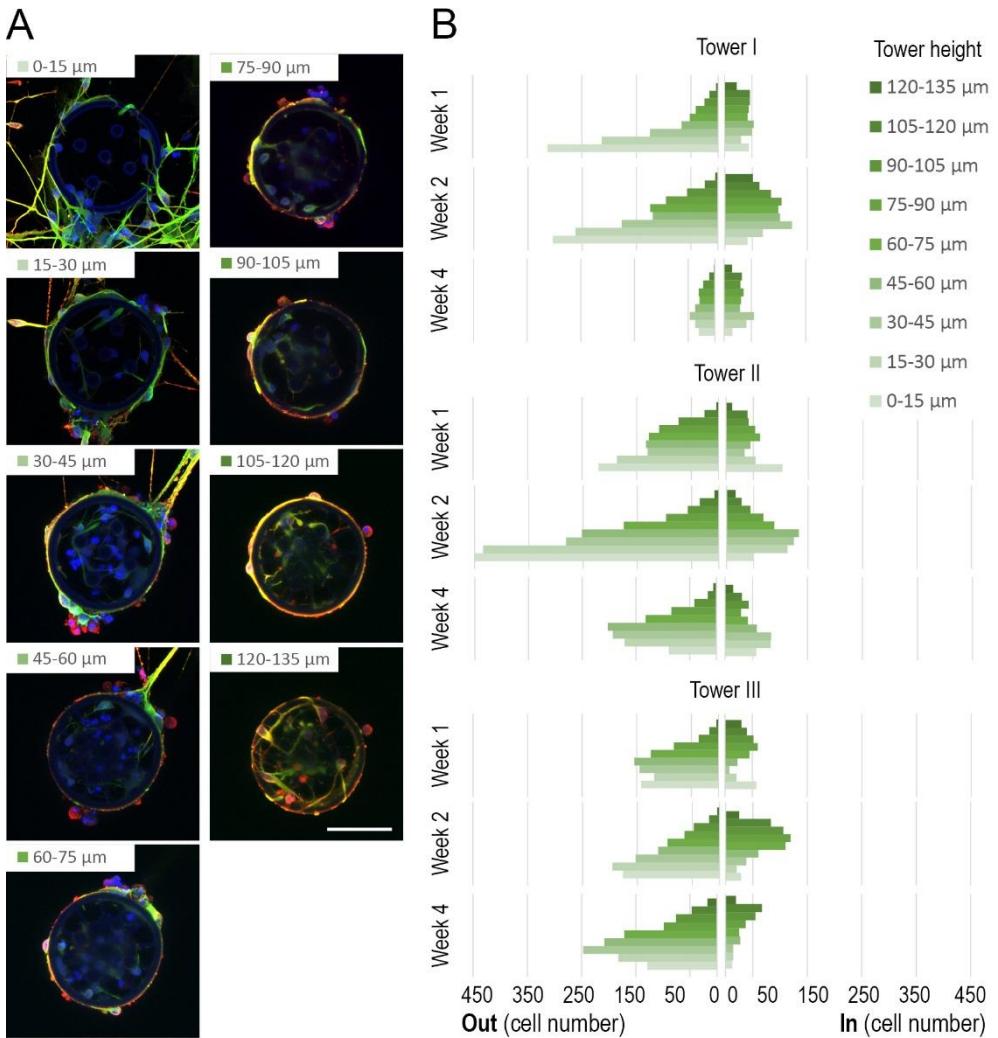


Figure 14. Cell distribution over the height of the tower is represented in 15- $\mu\text{m}$  bins. An example image of Tower I at the two-week time point, showing maximal intensity projections from 15- $\mu\text{m}$  sub-stacks of the confocal images used to calculate the cell distribution (A). A bar chart showing the sum number of nuclei in each height from all samples, describing which locations were attractive to cells during the experiment (B). Left-hand side represents the number of nuclei located outside of the microtower and right-hand side represents the number of nuclei located inside the towers. Blue: DAPI, green: MAP-2 and red: b-Tub. Number of analyzed towers,  $n = 9$ , except in Tower II, 4 weeks, where  $n = 8$ . Scale bar is 50  $\mu\text{m}$ .

The three different microtower designs had different microenvironments for the cells due differences in their internal structures and openings in the tower wall. The effect of the tower design on the distribution of cell nuclei was analyzed more detailed in

different heights of the tower (Figure 14). Cell nuclei were analyzed from the confocal images (example of a confocal image series is shown in Figure 14A). In all studied designs throughout the experiment, the trend in cell distribution outside the tower looked similar (Figure 14B). Most of the cells located in the lower parts of the tower outer wall, and the cell amount constantly decreased from layer to layer in the upper parts of the tower. Contrary to the outside, the cell distributions inside the mictotowers had differences between different designs especially in longer culture times (two and four weeks). In Tower I, the cell distribution inside was constant along the height of the tower in all time points. Tower I had internal polymerized structures that offered surfaces for the cells to grow inside the tower. Inside tower design II, the cell distribution looked similar to that outside of the towers; most of the cells located on the lower part of tower and the cell number decreased in the upper parts. More detailed, cells mainly located between the lower and upper openings of the tower wall (lower opening is located at 0 to 20  $\mu\text{m}$  and the upper opening at 75  $\mu\text{m}$  to 90  $\mu\text{m}$ ). Inside tower design III, the cell distribution was completely opposite, as most of the cells located in the upper parts and the cell number decreased in the lower parts. Tower design III was a plain cylinder without openings or internal structures.



## 6 DISCUSSION

### 6.1 Fluorescent cell-accumulating labels

Fluorescent proteins are widely used in cell biology to visualize cells. In this thesis, fluorescent probes were used as a tool to track living cell populations in co-cultures (Study I). This technique was relatively easy to perform and after optimization, it was very effective for the recognition of cell origins in co-cultures built from two pre-labeled cell populations. Here, the cells were labeled using the fluorescent probes DiD (red) and CT (green), which both accumulate in living cells.

The use of these living cell-accumulating fluorescent probes for visualizing native living cells, as described in this thesis, serves as an alternative to making genetically modified fluorescent cell lines. Three-dimensional cultures (Choi *et al.* 2014), co-cultures (East *et al.* 2010) and animal models (McMahon and McDermott 2006) are few examples of studies where tagging cell populations or tracking them during an experiment is needed. The creation of fluorescent cell lines with transfection is laborious and risky compared to staining with fluorescent labels (McMahon and McDermott 2006). For proof of concept or preliminary experiments, the use of fluorescent probes would be ideal, due to their relatively simple, low-cost protocols.

#### 6.1.1 Method optimization as essential part of experimental design

In this thesis, the optimized CT labeling parameters were found to be relatively safe, as no effect on cell viability, proliferation or electrical behavior were observed. Previously, CT has been reported to alter proliferation when rodent cells were labeled in a single cell suspension (Pettersson *et al.* 2010), whereas in this thesis, no changes in proliferation were seen (Study I). These differences in results can be caused by different degrees of cell maturation, species of origin, and cell handling during the labeling method. In contrast to CT, the DiD label was toxic at high concentrations, and even with optimized parameters, DiD affected hESC-derived neural cell proliferation (Study I). Previously, DiD has been reported to be a safe probe (Honig and Hume 1986), but as described here, others also suggest some degree of toxicity

with DiD (Potter *et al.* 1996). These contradictory findings reveal that it is important to optimize methods and take their restrictions into account when planning experimental setups and analyzing results. Overall, for future experiments, the most important finding regarding the CT and DiD pre-labeled populations was the successful formation of spontaneous neuronal networks. The spontaneous functionality of cultured cells was not altered due to labeling, which indicates that fluorescent probes can be utilized in experimental designs where neuronal functionality is also measured.

For example, in *in vitro* 3D studies, DiD might be more compatible than CT, as CT tends to cause more background staining. The fluorescence of the CT (5-chloromethylfluorescein diacetate) molecule is activated by internal cell esterases, which remove the acetates on the CT molecule, turning it into fluorescent 5-chloromethylfluorescein (Invitrogen 2011). The hydrolysis by esterase also activates a binding site on the CT molecule to thiol-containing biomolecules. In theory, CT is designed to be fluorescent only inside cells, where activating esterase is present. Nevertheless, some amount of fluorescent CT was observed to also accumulate on the laminin-coated cell culture plastic as a background staining after labeling (data not shown). This background staining faded during extended cell culture (Study I, original article: Figure 1B). Due to CT's ability to bind thiols, it can be hypothesized that it might bind to scaffolds containing thiols, causing background staining. The background fluorescence causes a poor signal-to-noise ratio in the samples. Using pre-labeled cells in 3D experiments, rather than labeling *in situ* in the scaffold, might be preferable.

## 6.2 3D cultures, repeatability and variability

The 3D neural cultures are inspired by the complexity of CNS tissue. Three-dimensional culturing is beneficial for obtaining more *in vivo*-like *in vitro* neural models than can be achieved with traditional flat 2D cultures. Cell adaptation to the *in vitro* 2D cell culture might lead to misleading or clinically non-predictive findings (Lee *et al.* 2008, Edmondson *et al.* 2014). The features that researchers want to incorporate into the 3D cultures are mimicking *in vivo*-like cell-ECM contacts, brain-like high cell density and interconnectivity, and cell orientation. Usually, the scaffolds used to obtain these features are based on polymeric hydrogels or solid porous matrices (Pautot *et al.* 2008). In this thesis, three different scaffold materials

were utilized. Each material had its pros and cons. The material used in Studies II and III was a hydrogel, and a rigid composite was used in Study IV.

### 6.2.1 PuraMatrix® is promising material for studying neuronal electrical activity in 3D

The PuraMatrix® hydrogel in was highly supportive for *in vitro* neural network formation, even from single cells (Study II, original article: Figure 3E); however, as a material, the PuraMatrix® solution has a very low pH before gelling (Nagai *et al.* 2012), and as a scaffold, it is very fragile (Zhang *et al.* 2010). Despite these challenges in material handling during long-term culture, it was possible to culture cells up to four weeks when they were encapsulated inside the hydrogel. The most important finding about the 3D networks was their ability to form spontaneous electrical activity inside a PuraMatrix® hydrogel, which requires long culture times (Study II). The development of neuronal signaling and cell growth in general were slower within the hydrogel than in cultures on top of the 2D surface. Similar findings have been published with rodent neurons in an alginate hydrogel (Palazzolo *et al.* 2015). This electrical activity of neural networks is an important feature that shows the natural brain-like functionality of the studied cells (Heikkilä *et al.* 2009, Johnstone *et al.* 2010).

With the PuraMatrix® hydrogel, the neuronal cell morphology was complex and branched (Study II, original article: Figure 3), and it resembled the morphologies seen *in vivo* (Dragunow 2008). Unfortunately, any evidence about increased functional maturity was not observed in the electrophysiological measurements (Study II). Even though the 3D culturing environment is commonly known to affect cell morphology and support the formation of complex cell morphologies, (LaPlaca *et al.* 2010), Sanyal 2014), only in few studies clear *in vivo* mimicking behavior is reported in the *in vitro* model (Hongisto *et al.* 2013, Choi *et al.* 2014).

Seeing some evidence of enhanced maturity in 3D culture might indicate that the 3D cultures indeed can model tissue more precisely than 2D culture, but many current *in vitro* models still need more optimization. One biological difference between 2D and 3D cultures is the localization of cell-ECM attachment sides, which affects cell polarization (Baker and Chen 2012, Murphy *et al.* 2017) and cell behavior via internal signaling routes (Atherton *et al.* 2016). This is suggested to be one of the reasons for bias in the results from 2D cultures *in vitro* (Di Cio and

Gautrot 2016). However, it is worth keeping in mind that all study platforms, *in vitro* systems and animal models have limitations that need to be taken into account when extrapolating results to humans.

### 6.2.2 Neurons in gellan gum-based hydrogels benefit from laminin

The gellan gum hydrogels crosslinked with SPD had mild gelation conditions, formed stiffer gels and were thus easier to handle than the sparse PuraMatrix<sup>®</sup> hydrogel. However, these gellan gum-based hydrogels enabled network formation only between neural cell aggregates in 3D (Study III, original article: Supplementary video 1). The growth of single neural cells in 3D, such as seen with PuraMatrix<sup>®</sup> (Study II), was not observed with gellan gum hydrogels. Similar behaviors and moderate cell growth between aggregates, as seen in Study III, have been reported in bacterial cellulose hydrogels with PC12 cells (Jonsson *et al.* 2015). The lack of neurite outgrowth might be related to the inert nature of gellan gum and thus could be overcome by modification or by adding covalently linked cell adhesion peptides, such as RGD (Silva *et al.* 2012, Lozano *et al.* 2015). Usually, inert materials, such as gellan gum, are used with cell adhesion-enhancing ligands (Lozano *et al.* 2015). In this thesis, utilizing human stem cell derived neuronal cells, ECM protein laminin was used as a physical mixture to enhance bioactivity of the hydrogel (Study III). The addition of laminin was not enough to make the hydrogel supportive for single cell growth when the cells were encapsulated inside the hydrogel, but it enhanced cell migration from the cell aggregates (Study III).

### 6.2.3 Rigid microtower scaffold supports formation of restricted and repeatable 3D culture

As a scaffold, rigid structures, such as microtowers, are very different when compared to ECM-mimicking fibrous hydrogels (Pautot *et al.* 2008, Jgamadze *et al.* 2012). Due to that difference, 3D network formation also occurs differently. When cells are encapsulated within a hydrogel matrix, cell migration and cell localization inside the hydrogel are very random and are partially determined during gel handling and crosslinking. This phenomenon causes variation between samples and repetitions (Lawyer *et al.* 2012). The variability in cell growth inside hydrogel (Study III) might be due to heterogeneous cell distribution in the cell-hydrogel mixture during crosslinking as well as anisotropy in the structure of the hydrogel (Flores-Merino *et*

*al.* 2010). Both of these random processes lead to more or less favorable areas inside the hydrogel, which affect neural network formation. In other words, both the cell and polymer concentrations in the samples vary from one region to another. In the case of the microtowers, a similar phenomenon does not occur. The single cell suspension was plated on the coverslip containing the microtowers, and this method produced quite homogenous samples, which was seen as a low amount of variability at the one-week time point (Study IV, original article: Figure 3). During culture, the 3D networks formed around the towers via cell migration and proliferation. Due to precise and repeatable manufacturing of rigid microstructure scaffolds, the network formation can be controlled via the design (Pautot *et al.* 2008). Nano patterning is one design feature that can be used to guide network formation. Patterned micro pillars supported 3D network formation from hippocampal neurons, whereas smooth pillars produced flat 2D networks (Limongi *et al.* 2013). The surface roughness and patterns caused by polymerization voxels supported 3D network formation, and no additional patterning was needed (Study IV, original article: Figure 2). Microtowers offer a restricted area for 3D neural network formation, whereas the formation of neural networks inside hydrogels, with several hundred microliters of volume, is difficult to control. Due to restricted area, the 3D networks around the microtowers were easier to monitor and analyze.

### 6.3 Neural network formation and response to the mechanical properties of the scaffold

It is thought that a good neural scaffold should have brain-like mechanical properties (Aurand *et al.* 2012). When comparing results, the trend in neural growth compared to the mechanical properties of the hydrogel was completely opposite between Studies II and III. With PuraMatrix® (Study II), more neurons grew on sparser hydrogels, whereas with gellan gum (Study III), the neural growth increased in line with the stiffness. In this thesis, also rigid microtowers with a Young's modulus of 140 MPa were used as a scaffold. The 3D neural network growth was supported by these rigid, micron-scale structures (Study IV), even though the scaffold stiffness was non-physiological. The microtowers were not ECM-like, but they acted as support for 3D network formation.

### 6.3.1 Neurons prefer a sparse PuraMatrix® hydrogel

When cultured on top of the PuraMatrix® hydrogel, the neurons clearly favored sparse hydrogels (0.1 wt% and 0.05 wt% PuraMatrix®; Study II). In these concentrations, PuraMatrix® is mechanically very soft and at a concentration of 0.05 wt%, it is even reported to be below the limit of proper hydrogel formation (Zhao *et al.* 2005). In this thesis, the mechanical properties of PuraMatrix® were not measured in-house. According to the literature, 0.1 wt% PuraMatrix® has a modulus of approximately 1.2 kPa (Leon *et al.* 1998, Yamaoka *et al.* 2006). This is an estimated value for PuraMatrix® stiffness and cannot be directly compared to the measured values with the gellan gum hydrogels (Study III) or other literature due to differences in the measuring setup and analysis. However, it gives an estimate of the softness range of the PuraMatrix® concentration used in this thesis. The hESC-derived neurons clearly preferred the softest PuraMatrix® compositions, whereas astrocytes preferred slightly stiffer compositions (Study II). Even though the exact stiffness values were not measured for 0.05 wt%–0.25 wt% PuraMatrix® (Study II), the results seem to be in line with common knowledge about neural cells. More specifically, low stiffness (0.1–1.0 kPa) is preferred by neurons, whereas glial cells prefer slightly stiffer materials (0.5–10 kPa) (Study II, Aurand *et al.* 2012). These findings are also in line with the widely accepted theory that materials with elasticity or stiffness similar to the target tissue are the best for cells (Engler *et al.* 2006). In other studies, PuraMatrix® was successfully used in higher concentrations with neural cells, from 0.25 wt% to even 1 wt% (Gelain *et al.* 2006, Thonhoff *et al.* 2008). Theoretically, these concentrations produce remarkably stiffer hydrogels than used in this thesis. It has also been found that undiluted 1 wt% PuraMatrix® is toxic to human NPCs, whereas lower concentrations are well tolerated (Thonhoff *et al.* 2008). The differences in the cell maturation stage and cell type could explain why a higher concentration was used earlier (Thonhoff *et al.* 2008). The hydrogel that was best for the neuronal cells, 0.1 wt% PuraMatrix® (Study II), has a very fragile nature, and this might be one reason why more concentrated gels, which are easier to handle, have been studied (Ortinou *et al.* 2010).

### 6.3.2 Neural cells prefer a stiff gellan gum hydrogel

Contrary to the results obtained with PuraMatrix® (Study II), where the softest materials were best, the stiffest gellan gum hydrogel was the most favored by neural cells (Study III). The stiffest studied composition (cross-linker: 3.00 wt% SPD;

Study III) had a compression modulus of approximately 23 kPa. The measurement setup and method of analysis used for evaluating gellan gum hydrogels can lead to slightly higher values than previously published results based on brain sample measurements. However, this fact cannot explain the trend of human neural cells growing better on the stiffer gellan gum than on the softer compositions. This result clearly indicates that the modulus was not the only factor explaining cell behavior. This is not a completely new observation. Although many studies have shown a strong correlation between a brain-like modulus and an excellent neural cell response (Saha *et al.* 2008, Palazzolo *et al.* 2015), concerns were raised by Nisbet and co-workers in 2007. They examined publications and found that not all reports are in line with the common theory of optimal material stiffness for neural cultures. They came to the conclusion that it is possible that some other material property might be more important to cells than stiffness (Nisbet *et al.* 2007). The idea of tissue-like mechanical properties being a leading factor in stem cell response was based on studies made with mesenchymal stem cells: in brain-like soft materials, their behavior becomes neuron-like (Engler *et al.* 2006, Huang *et al.* 2012). After the research made by Engler and coworkers in 2006, many researchers have found similarities, but due to variable material choices, it has been difficult to determine the exact factors that made soft scaffolds favorable for neural cells (Teixeira *et al.* 2009, Aurand *et al.* 2012). More research is therefore needed to find the exact properties that make scaffolds favorable for each neural culture, if the aim is to build a perfect matrix for the cells.

## 6.4 Future perspectives: How to build a perfect model?

Careful selection of the relevant cells and scaffold material, combined with sophisticated methods, are the key issues for successful model or graft development (Figure 15).

### 6.4.1 A relevant cell source for brain tissue models

Rodents and humans are not alike, and the main biological differences worth mentioning in the field of neural TE is a better spontaneous regeneration capacity in mice (Sharif-Alhoseini & Rahimi-Movaghar 2014). There are also differences in brain development (Kelava and Lancaster 2016) and in neural cells, especially astrocytes (Zhang and Barres 2013). These aspects need to be taken into account

when interpreting the findings and forming conclusions. The possibility of using stem cell-derived human cells to gather information specific to humans is important, and it is one of the advantages of *in vitro* stem cell techniques.

One challenge related to all *in vitro* cultures is the heterogeneity of cell populations, the adaptation of cells to the culturing conditions, and batch-to-batch variation. The neural population may contain contaminating cell types or a variation in cell type portions or cell maturity (Lappalainen *et al.* 2010, Toivonen *et al.* 2013). Generally, all stem cell-based cultures are relatively immature (Marx 2016). In developmental models, this does not cause problems, but the situation is very different if the aim is to model diseases that are typical among elderly persons (Choi *et al.* 2014, Kim *et al.* 2015). Transdifferentiation might be able to offer better human neurons for studying CNS diseases typical for elderly patients as the cells are not going through the stem cell stage in that method.

The avoidance of animal components is highly important in clinical applications, but it is also an important aspect to take into account in clinical human *in vitro* models. Exposure to animal components might alter cell behavior (Desai *et al.* 2015). To create human *in vitro* cell models that are as accurate as possible, it is also very desirable to use only xeno-free, defined components, especially in research aimed at clinical translation (Figure 15, 1A).

When building a clinically relevant neural tissue model, it is extremely important to characterize the neuronality of the cultured cells. Characterization is usually performed using gene or protein expression analysis (Figure 15 3A,B). There is a wide pattern of neuronal or glial markers that can be used, and some of the most commonly used markers are microtubulin-associated protein 2 (MAP-2) for neurons and glial fibrillary acidic protein (GFAP) for astrocytes (Cahoy *et al.* 2008). Because the main function of the brain is to process electrical signals, it is ideal to study the electrical functionality of the cultured cells (Heikkilä *et al.* 2009, Johnstone *et al.* 2010). Functionality can be studied using imaging or electrophysiological measurements. In imaging, the functionality of neurons or glia is mainly studied using calcium fluxes inside the cell (Lancaster *et al.* 2013, Palazzolo *et al.* 2015). This is analyzed using fluorescent dyes that indicate the intracellular calcium concentration. Electrophysiological analysis can be performed cell-by-cell using the patch clamp technique (Shi *et al.* 2012) or at the cell population level using a MEA (Wagenaar *et al.* 2004, Illes *et al.* 2007, Heikkilä *et al.* 2009).



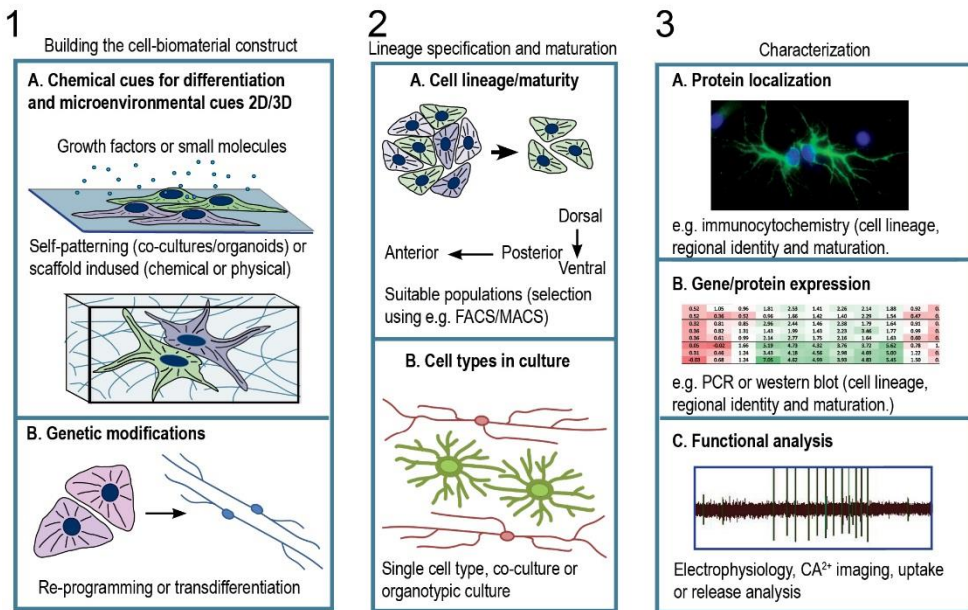


Figure 15. Three key aspects of the production of clinically relevant cell-biomaterial models from stem cells.

**1)** Building the cell-biomaterial construct. Neural populations can be obtained from differentiation using chemical cues (e.g., growth factors; 1A), microenvironmental cues (e.g., co-cultures or directing culture materials; 1A), genetic modification (1B), or using a combination of these methods. The biomaterial scaffold (1A) can be part of the neural niche or can be later combined as a structural component to the model (artificial ECM).

**2)** Lineage specification and maturation degree of the cells affect to the experimental design of the model. Stem cells can be directly differentiated toward region/cell type specific populations or cultures can be purified to obtain more homogenous populations (2A). Cultures can contain single cell type (simplified model) or several cell types (complex more *in vivo* mimicking model, 2B). Both of these model types can be either 2D or 3D (artificial ECM, 1A) models.

**3)** Characterization of the obtained cultures is an important part of evaluating the efficiency of the culturing methods. Characterization can be performed using morphology and protein localization (3A), expression profiling (3B), and functional analysis (3C). For neural cultures, electrical functionality analysis is preferable because it can reveal if the cells in model are truly mimicking a functional brain. **ECM** Extra cellular matrix, **FACS** Fluorescent-activated cell sorting, **MACS** Magnetic-activated cell sorting. Figure modified from (Tabar and Studer 2014).

## 6.4.2 Choosing an optimal biomaterial as a scaffold for a 3D culture

Both *in vitro* and *in vivo* applications of biomaterials need similar biocompatibility, but the requirements for gelation and user-friendliness may differ. Researchers are

interested in materials that are easy to use and produce repeatable samples with low variability and good stability during experiments. For clinicians, the term “user-friendliness” can mean different things. One example of a useful property *in vitro* is the optically clear formulation of gellan gum (Study III). Clear formula enables observation of the cells during *in vitro* culturing; however, this is not an important feature *in vivo*. Furthermore, while many researchers may tolerate protocols with multiple steps for sample preparation and mixing the cells into the material, in the clinical setting this is not possible.

The possibility for *in situ* gelation is thought of as a clinical advantage of hydrogel materials. Hydrogels can be used as injectable scaffolds or as a delivery vector for cells or drugs. It is often discussed that injecting would be the optimal grafting route to the CNS due to the low invasiveness for the patient compared to traditional surgery (Kretlow *et al.* 2007). However, one challenge that arises from the technique itself is the delivery of cells as a vulnerable single suspension. The cells must be suspended in the solution before grafting, making it impossible to deliver *in vitro* pre-made neural networks via injection. It is also worth noting that if the aim is purely an *in vitro* model, there is no need to take injectability into account.

Numerous materials have been published in neural TE, but it seems that none of them is highly superior compared to the others (Nisbet *et al.* 2007, LaPlaca *et al.* 2010). The next generation of scaffolds for some applications might need to be composites, combining the beneficial properties of different materials, such as an IPN hydrogel composite or a hydrogel-rigid particle combination. However, it also might be unrealistic or even unnecessary to engineer a material that has very good performance both *in vivo* and *in vitro*, even though there is a need for *in vitro* experiments in the development of a clinical scaffold. It is preferable to perform preliminary material testing *in vitro* to reduce the use of laboratory animals. However, for preliminary testing, e.g., toxicology or cytocompatibility testing, there is no need to optimize the material for *in vitro* use. Also, for material use *in vitro*, different study questions have very different requirements. For example, a matrix for supporting organoid cultures needs to inhibit migration in order keep cells in aggregates, whereas a matrix for supporting 3D neural networks needs to support cell attachment. The best results are obtained when focusing only on the requirements of the selected application.

Developing a relevant cell based *in vitro* model starts from a clinical need. Theoretically, the perfect workflow for model development consists of the following steps:

1. Hypothesis and aim to guide the workflow
2. Biomaterial that is optimal for requirements of the application and enables studying the experimental question
3. Cells that are able to relevantly model the biological phenomenon related to study question
4. Reliable analysis methods and responsible interpretation and extrapolation of the results



# CONCLUSIONS

The main conclusions of this thesis are as follows:

I Fluorescently pre-labeled neural cell cultures were successfully combined in co-cultures. The electrical activity of the networks combined from two labeled populations had a similar activity development as the control cultures. It was possible to create a functional network using cells originating from two different populations.

II Neuronal cells grown within the sparse PuraMatrix® showed morphologies with *in vivo*-mimicking complexity. In addition, the cultures within the hydrogel displayed spontaneous neuronal network activity.

III It was not possible to predict scaffold suitability for neural cells based on the mechanical properties of the hydrogel. Inert gellan gum hydrogels, offering physical support without cell adhesion sites, are not supportive enough for studying human neural cell 3D network formation.

IV Neuronal cells formed repeatable small networks around cylindrical rigid microtower scaffolds. Cylindrical shape with or without openings and intraluminal structures in the towers had a guiding effect on network formation. The design of a rigid scaffold can be used as a tool to guide cell growth or migration thus affecting neural network architecture.

Careful selection of the relevant cells and scaffold material, combined with sophisticated methods, are the key issues for successful *in vitro* neural models. In summary, none of the studied biomaterials could alone form a perfect all-purpose scaffold for human neural cells. Instead of concentrating on seeking the best material for neural field, it would be beneficial to see materials as part of experimental set up. Each study question has specific needs for material properties and recognizing the potential of different materials and scaffolds as tools would be beneficial for the neural TE field.

# ACKNOWLEDGEMENTS

The research for this thesis has been carried out in NeuroGroup, Institute of Biosciences and Medical technology (BioMediTech) former Regea – Institute for Regenerative Medicine, Faculty of Medicine and Life Sciences, University of Tampere during years 2013-2017.

Former head of Regea Professor Riitta Seppänen, former dean of BioMediTech Hannu Hanhijärvi and director of BioMediTech Minna Kellomäki are warmly thanked for providing excellent research facilities during these years. They are also thanked for enabling the cross-collaboration between researchers and research groups from UTA and TUT and thus creating innovative and fruitful research cluster. Hannu Hanhijärvi is especially acknowledged for warm and supporting attitude towards researchers working on personal grants in the institute.

I would also like to express my gratitude to all financial supporters of this thesis work. Their support has made possible to perform the research and write this thesis. During these years my work has been funded by TEKES (the Finnish Funding Agency for Technology and Innovation), the Academy of Finland, the Finnish Cultural Foundation, the Competitive Research Funding of the Tampere University Hospital, the European Union's Seventh Framework Programme (Future and Emerging Technologies), the Paulo Foundation, the City of Tampere, and Tampere Graduate Program in Biomedicine and Biotechnology (TGPBB).

I would like to express my deepest gratitude to my supervisor and NeuroGroup leader Susanna Narkilahti. Dear Sussu, thank you for accepting me as an undergraduate student to your group at autumn 2008 and ever since supporting my growth as a scientist and as a person. During these years, a lot has happened and I want to thank you for each and every day of this scientific journey. Thank you also for believing in me in those times I myself did not. It has been a privilege to work under your supervision. I also want to emphasize my gratefulness to my other supervisors Mervi Ristola and Laura Ylä-Outinen. I owe my sincere gratitude to you for your support during my PhD studies and especially your guidance in writing the thesis.

Members of my follow-up group Dosent Teemu Ihalainen, Professor Marjo Yliperttula, and Riikka Äänismaa are warmly acknowledged for their scientific

support and valuable discussions. Teemu, I want to express my gratitude for teaching me imaging, and sharing your knowledge and enthusiasm on science, despite of your hectic schedules.

External reviewers Docent Varpu Marjomäki and Associate Professor Ana Pégó are thanked for their effort and valuable comments on my thesis. I would also like to thank all co-authors; Meeri Mäkinen, Laura Ylä-Outinen, Heli Skottman, Susanna Narkilahti, Riikka Äänismaa, Mari Varjola, Janne Koivisto, Jenny Parraga, Rami Pääkkönen, Laura Salonen, Ilari Jönkkäri, Marja Peltola, Teemu Ihalainen, Maiju Hiltunen, Sanna Turunen and Minna Kellomäki for sharing their knowledge and expertise in our joined research. Especially Minna Kellomäki, Sanna Turunen and Janne Koivisto are acknowledged for making our collaboration flourish.

I would also like to thank all personnel of BioMediTech institute and former Regea for helping me during these years and creating warm and encouraging working environment. Especially I want to thank Jennika Karvinen, Kaisa Vuornos and Laura Koivusalo.

Beloved past and present members of NeuroGroup, thank you for the great group spirit during these years! Without you, this research would not have been possible. I want to thank you for all the adventures we have been accompanying, the scientific ones as well as the beyond scientific ones. Thank you all for your friendship, it means a world to me. Especially, Anssi Pelkonen, Sanna Hagman, Marja Peltola and fellow PhD students Meeri Mäkinen, Anu Hyysalo and Tanja Paavilainen are warmly thanked. Hanna Mäkelä, Maarit Patrikainen, Eija Hannuksela, Outi Paloheimo and Juha Heikkilä are acknowledged also for their technical assistance.

My family and friends are thanked for supporting me in my scientific career as well as reminding me that life is much more than neuroscience. I especially wish to express my deepest gratitude to my parents, Auli and Urho. Thank you for your encouraging attitude towards learning, without your support, I would not have been able to aim having PhD degree. My parents-in-law, Anne and Timo, are acknowledged for their effort during difficult times. Finally, I would like to thank my significant other, Janne. Thanks for keeping the wheels turning - in our life and in the garage.

Tampere, September 2017

A handwritten signature in black ink that reads "Tiina Joki". The script is cursive and fluid, with the first letter 'T' being particularly large and stylized.





## REFERENCES

E.A. Appel, X.J. Loh, S.T. Jones, F. Biedermann, C.A. Dreiss, and O.A. Scherman, **2012**. Ultrahigh-Water-Content Supramolecular Hydrogels Exhibiting Multistimuli Responsiveness. *Journal of the American Chemical Society*, 134 (28), 11767–11773.

A. Astashkina, B. Mann, and D.W. Grainger, **2012**. A critical evaluation of in vitro cell culture models for high-throughput drug screening and toxicity. *Pharmacology & Therapeutics*, 134 (1), 82–106.

P. Atherton, B. Stutchbury, D. Jethwa, and C. Ballestrem, **2016**. Mechanosensitive components of integrin adhesions: Role of vinculin. *Experimental Cell Research*, 343 (1), 21–27.

E.R. Aurand, K.J. Lampe, and K.B. Bjugstad, **2012**. Defining and designing polymers and hydrogels for neural tissue engineering. *Neuroscience Research*, 72 (3), 199–213.

S. Avasthi, R.N. Srivastava, A. Singh, and M. Srivastava, **2008**. Stem Cell: Past, Present and Future- A Review Article. *Internet Journal of Medical Update*, 3 (1), 22–30.

B.M. Baker and C.S. Chen, **2012**. Deconstructing the third dimension – how 3D culture microenvironments alter cellular cues. *Journal of Cell Science*, 125 (13), 3015–3024.

E.J. Berns, Z. Álvarez, J.E. Goldberger, J. Boekhoven, J.A. Kessler, H.G. Kuhn, and S.I. Stupp, **2016**. A tenascin-C mimetic peptide amphiphile nanofiber gel promotes neurite outgrowth and cell migration of neurosphere-derived cells. *Acta Biomaterialia*, 37, 50–58.

S.J. Bidarra, C.C. Barrias, and P.L. Granja, **2014**. Injectable alginate hydrogels for cell delivery in tissue engineering. *Acta Biomaterialia*, 10 (4), 1646–1662.

- K.K. Bokara, J.Y. Kim, Y. Il Lee, K. Yun, T.J. Webster, and J.E. Lee, **2013**. Biocompatibility of carbon nanotubes with stem cells to treat CNS injuries. *Anatomy & Cell Biology*, 46 (2), 85–92.
- F. Brandl, F. Sommer, and A. Goepferich, **2007**. Rational design of hydrogels for tissue engineering: Impact of physical factors on cell behavior. *Biomaterials*, 28 (2), 134–146.
- N. Broguiere, L. Isenmann, and M. Zenobi-Wong, **2016**. Novel enzymatically cross-linked hyaluronan hydrogels support the formation of 3D neuronal networks. *Biomaterials*, 99, 47–55.
- S. Budday, R. Nay, R. de Rooij, P. Steinmann, T. Wyrobek, T.C. Ovaert, and E. Kuhl, **2015**. Mechanical properties of gray and white matter brain tissue by indentation. *Journal of the Mechanical Behavior of Biomedical Materials*, 46 (10), 318–330.
- J.D. Cahoy, B. Emery, A. Kaushal, L.C. Foo, J.L. Zamanian, K.S. Christopherson, Y. Xing, J.L. Lubischer, P. a Krieg, S. a Krupenko, W.J. Thompson, and B. a Barres, **2008**. A Transcriptome Database for Astrocytes, Neurons, and Oligodendrocytes: A New Resource for Understanding Brain Development and Function. *Journal of Neuroscience*, 28 (1), 264–278.
- A.L. Carlson, N.K. Bennett, N.L. Francis, A. Halikere, S. Clarke, J.C. Moore, R.P. Hart, K. Paradiso, M. Wernig, J. Kohn, Z.P. Pang, and P. V Moghe, **2016**. Generation and transplantation of reprogrammed human neurons in the brain using 3D microtopographic scaffolds. *Nature Communications*, 7, 10862. <https://www.nature.com/articles/ncomms10862>
- M.K. Carpenter, M.S. Inokuma, J. Denham, T. Mujtaba, C.-P. Chiu, and M.S. Rao, **2001**. Enrichment of Neurons and Neural Precursors from Human Embryonic Stem Cells. *Experimental Neurology*, 172 (2), 383–397.
- S.M. Chambers, C. Fasano, E.P. Papapetrou, M. Tomishima, M. Sadelain, and L. Studer, **2009**. Highly efficient neural conversion of human ES and iPS cells by dual inhibition of SMAD signaling. *Nature Biotechnology*, 27 (3), 275–280.
- B.P. Chan and K.W. Leong, **2008**. Scaffolding in tissue engineering: general approaches and tissue-specific considerations. *European Spine Journal*, 17 (S4), 467–479.

- S.H. Choi, Y.H. Kim, M. Hebisch, C. Sliwinski, S. Lee, C. D'Avanzo, H. Chen, B. Hooli, C. Asselin, J. Muffat, J.B. Klee, C. Zhang, B.J. Wainger, M. Peitz, D.M. Kovacs, C.J. Woolf, S.L. Wagner, R.E. Tanzi, and D.Y. Kim, **2014**. A three-dimensional human neural cell culture model of Alzheimer's disease. *Nature*, 515 (7526), 274–278.
- S. Di Cio and J.E. Gautrot, **2016**. Cell sensing of physical properties at the nanoscale: Mechanisms and control of cell adhesion and phenotype. *Acta Biomaterialia*, 30, 26–48.
- H. Clevers, **2016**. Modeling Development and Disease with Organoids. *Cell*, 165 (7), 1586–1597.
- J.M. Cyphert, C.S. Trempus, and S. Garantziotis, **2015**. Size Matters: Molecular Weight Specificity of Hyaluronan Effects in Cell Biology. *International Journal of Cell Biology*, 2015, 1–8. <https://www.hindawi.com/journals/ijcb/2015/563818/>
- X. Dai and Y.-C. Huang, **2013**. Pluripotent Stem Cell Derived Neural Lineage Cells and Biomaterials for Neuroscience and Neuroengineering. *Journal of Neuroscience and Neuroengineering*, 2 (2), 119–140.
- N. Desai, P. Rambhia, and A. Gishto, **2015**. Human embryonic stem cell cultivation: historical perspective and evolution of xeno-free culture systems. *Reproductive Biology and Endocrinology*, 13 (1), 9. <https://rbej.biomedcentral.com/articles/10.1186/s12958-015-0005-4>
- S.K. Dhara and S.L. Stice, **2008**. Neural differentiation of human embryonic stem cells. *Journal of Cellular Biochemistry*, 105 (3), 633–640.
- A.D. Doyle and K.M. Yamada, **2016**. Mechanosensing via cell-matrix adhesions in 3D microenvironments. *Experimental Cell Research*, 343 (1), 60–66.
- M. Dragunow, **2008**. High-content analysis in neuroscience. *Nature Reviews Neuroscience*, 9 (10), 779–788.
- J.L. Drury and D.J. Mooney, **2003**. Hydrogels for tissue engineering: scaffold design variables and applications. *Biomaterials*, 24 (24), 4337–4351.
- E. East, J.P. Golding, and J.B. Phillips, **2012**. Engineering an Integrated Cellular Interface in Three-Dimensional Hydrogel Cultures Permits Monitoring of

Reciprocal Astrocyte and Neuronal Responses. *Tissue Engineering Part C: Methods*, 18 (7), 526–536.

E. East, D.B. de Oliveira, J.P. Golding, and J.B. Phillips, 2010. Alignment of Astrocytes Increases Neuronal Growth in Three-Dimensional Collagen Gels and Is Maintained Following Plastic Compression to Form a Spinal Cord Repair Conduit. *Tissue Engineering Part A*, 16 (10), 3173–3184.

R. Edmondson, J.J. Broglie, A.F. Adcock, and L. Yang, 2014. Three-Dimensional Cell Culture Systems and Their Applications in Drug Discovery and Cell-Based Biosensors. *ASSAY and Drug Development Technologies*, 12 (4), 207–218.

A.J. Engler, S. Sen, H.L. Sweeney, and D.E. Discher, 2006. Matrix Elasticity Directs Stem Cell Lineage Specification. *Cell*, 126 (4), 677–689.

E.A. Eugenin, J.E. Clements, M.C. Zink, and J.W. Berman, 2011. Human Immunodeficiency Virus Infection of Human Astrocytes Disrupts Blood-Brain Barrier Integrity by a Gap Junction-Dependent Mechanism. *Journal of Neuroscience*, 31 (26), 9456–9465.

M. Evans, 2011. Discovering pluripotency: 30 years of mouse embryonic stem cells. *Nature Reviews Molecular Cell Biology*, 12 (10), 680–686.

L.J. Fisher, 1997. Neural Precursor Cells: Applications for the Study and Repair of the Central Nervous System. *Neurobiology of Disease*, 4 (1), 1–22.

M. V. Flores-Merino, S. Chirasatitsin, C. LoPresti, G.C. Reilly, G. Battaglia, and A.J. Engler, 2010. Nanoscopic mechanical anisotropy in hydrogel surfaces. *Soft Matter*, 6 (18), 4466–4470

M. Frega, M. Tedesco, P. Massobrio, M. Pesce, and S. Martinoia, 2015. Network dynamics of 3D engineered neuronal cultures: a new experimental model for in-vitro electrophysiology. *Scientific Reports*, 4 (1), 5489. <https://www.nature.com/articles/srep05489>

S. Gascón, E. Murenu, G. Masserdotti, F. Ortega, G.L. Russo, D. Petrik, A. Deshpande, C. Heinrich, M. Karow, S.P. Robertson, T. Schroeder, J. Beckers, M. Irmeler, C. Berndt, J.P.F. Angeli, M. Conrad, B. Berninger, and M. Götz, 2016. Identification and Successful Negotiation of a Metabolic Checkpoint in Direct Neuronal Reprogramming. *Cell Stem Cell*, 18 (3), 396–409.

- F. Gelain, D. Bottai, A. Vescovi, and S. Zhang, **2006**. Designer Self-Assembling Peptide Nanofiber Scaffolds for Adult Mouse Neural Stem Cell 3-Dimensional Cultures. *PLoS ONE*, 1 (1), e119. <http://journals.plos.org/plosone/article?id=10.1371/journal.pone.0000119>
- X. Gu, F. Ding, and D.F. Williams, **2014**. Neural tissue engineering options for peripheral nerve regeneration. *Biomaterials*, 35 (24), 6143–6156.
- X. Guo, S. Spradling, M. Stancescu, S. Lambert, and J.J. Hickman, **2013**. Derivation of sensory neurons and neural crest stem cells from human neural progenitor hNP1. *Biomaterials*, 34 (18), 4418–4427.
- J.B. Gurdon, **1962**. The developmental capacity of nuclei taken from intestinal epithelium cells of feeding tadpoles. *Journal of embryology and experimental morphology*, 10 (4), 622–640.
- D. Han and K.C. Cheung, **2011**. Biodegradable Cell-Seeded Nanofiber Scaffolds for Neural Repair. *Polymers*, 3 (4), 1684–1733.
- J. a Harrill, T.M. Freudenrich, D.W. Machacek, S.L. Stice, and W.R. Mundy, **2010**. Quantitative assessment of neurite outgrowth in human embryonic stem cell-derived hN2<sup>TM</sup> cells using automated high-content image analysis. *NeuroToxicology*, 31 (3), 277–290.
- J.S. Harunaga and K.M. Yamada, **2011**. Cell-matrix adhesions in 3D. *Matrix Biology*, 30 (7–8), 363–368.
- T.J. Heikkilä, L. Ylä-Outinen, J.M.A. Tanskanen, R.S. Lappalainen, H. Skottman, R. Suuronen, J.E. Mikkonen, J.A.. Hyttinen, and S. Narkilahti, **2009**. Human embryonic stem cell-derived neuronal cells form spontaneously active neuronal networks in vitro. *Experimental Neurology*, 218 (1), 109–116.
- C. Heinrich, F.M. Spagnoli, and B. Berninger, **2015**. In vivo reprogramming for tissue repair. *Nature Cell Biology*, 17 (3), 204–211.
- L. Heinrich, A.-M. Freyria, M. Melin, Y. Tourneur, R. Maksoud, J.-C. Bernengo, and D.J. Hartmann, **2007**. Confocal laser scanning microscopy using dialkylcarbocyanine dyes for cell tracing in hard and soft biomaterials. *Journal of Biomedical Materials Research Part B: Applied Biomaterials*, 81B (1), 153–161.

V. Hongisto, S. Jernström, V. Fey, J. Mpindi, K.K. Sahlberg, O. Kallioniemi, and M. Perälä, **2013**. High-Throughput 3D Screening Reveals Differences in Drug Sensitivities between Culture Models of JIMT1 Breast Cancer Cells. *PLoS ONE*, 8 (10). <http://journals.plos.org/plosone/article?id=10.1371/journal.pone.0077232>

M.G. Honig and R.I. Hume, **1986**. Fluorescent carbocyanine dyes allow living neurons of identified origin to be studied in long-term cultures. *Journal of Cell Biology*, 103 (1), 171–187.

G. Huang, L. Wang, S. Wang, Y. Han, J. Wu, Q. Zhang, F. Xu, and T.J. Lu, **2012**. Engineering three-dimensional cell mechanical microenvironment with hydrogels. *Biofabrication*, 4 (4), 42001. <http://iopscience.iop.org/article/10.1088/1758-5082/4/4/042001/meta>

S. Illes, W. Fleischer, M. Siebler, H. Hartung, and M. Dihné, **2007**. Development and pharmacological modulation of embryonic stem cell-derived neuronal network activity. *Experimental Neurology*, 207 (1), 171–176.

Invitrogen, **2011**. CHAPTER 14 Fluorophores and Fluorescent Tracers Their Amine-Reactive of Cell Morphology Derivatives and Fluid Flow Molecular. *In: The Molecular Probes handbook. A guide to fluorescent probes and labeling technologies*. 589–648.

D. Jgamadze, J. Bergen, D. Stone, J.-H. Jang, D. V. Schaffer, E.Y. Isacoff, and S. Pautot, **2012**. Colloids as Mobile Substrates for the Implantation and Integration of Differentiated Neurons into the Mammalian Brain. *PLoS ONE*, 7 (1), e30293. <http://journals.plos.org/plosone/article?id=10.1371/journal.pone.0030293>

A.F.M. Johnstone, G.W. Gross, D.G. Weiss, O.H.-U. Schroeder, A. Gramowski, and T.J. Shafer, **2010**. Microelectrode arrays: A physiologically based neurotoxicity testing platform for the 21st century☆. *NeuroToxicology*, 31 (4), 331–350.

M. Jonsson, C. Brackmann, M. Puchades, K. Brattås, A. Ewing, P. Gatenholm, and A. Enejder, **2015**. Neuronal Networks on Nanocellulose Scaffolds. *Tissue Engineering Part C: Methods*, 21 (11), 1162–1170.

C. Jopling, S. Boue, and J.C.I. Belmonte, **2011**. Dedifferentiation, transdifferentiation and reprogramming: three routes to regeneration. *Nature Reviews Molecular Cell Biology*, 12 (2), 79–89.

- T. Kadoshima, H. Sakaguchi, T. Nakano, M. Soen, S. Ando, M. Eiraku, and Y. Sasai, **2013**. Self-organization of axial polarity, inside-out layer pattern, and species-specific progenitor dynamics in human ES cell-derived neocortex. *Proceedings of the National Academy of Sciences*, 110 (50), 20284–20289.
- I. Kelava and M.A. Lancaster, **2016**. Stem Cell Models of Human Brain Development. *Cell Stem Cell*, 18 (6), 736–748.
- M. Kim and D. Evans, **2005**. Tissue Engineering: The Future of Stem Cells. *In: Topics in Tissue Engineering*. 1–22.
- Y.H. Kim, S.H. Choi, C. D’Avanzo, M. Hebisch, C. Sliwinski, E. Bylykbashi, K.J. Washicosky, J.B. Klee, O. Brüstle, R.E. Tanzi, and D.Y. Kim, **2015**. A 3D human neural cell culture system for modeling Alzheimer’s disease. *Nature Protocols*, 10 (7), 985–1006.
- P. Koch, **2015**. Direct Conversion Provides Old Neurons from Aged Donor’s Skin. *Cell Stem Cell*, 17 (6), 637–638.
- J.D. Kretlow, L. Klouda, and A.G. Mikos, **2007**. Injectable matrices and scaffolds for drug delivery in tissue engineering. *Advanced Drug Delivery Reviews*, 59 (4–5), 263–273.
- E. Käpylä, S. Turunen, J. Pelto, J. Viitanen, and M. Kellomäki, **2011**. Investigation of the optimal processing parameters for picosecond laser-induced microfabrication of a polymer–ceramic hybrid material. *Journal of Micromechanics and Microengineering*, 21 (6), 65033. <http://iopscience.iop.org/article/10.1088/0960-1317/21/6/065033/meta>
- M. Lancaster, M. Renner, C.-A. Martin, D. Wenzel, L.S. Bicknell, M.E. Hurles, T. Homfray, J.M. Penninger, A.P. Jackson, and J. a Knoblich, **2013**. Cerebral organoids model human brain development and microcephaly. *Nature*, 501 (7467), 373–379.
- M. Lancaster and J. Knoblich, **2014**. Generation of cerebral organoids from human pluripotent stem cells. *Nature Protocols*, 9 (10), 2329–2340.
- M.C. LaPlaca, V.N. Vernekar, J.T. Shoemaker, and D.K. Cullen, **2010**. Three-Dimensional Neuronal Cultures. *Methods in Bioengineering: 3D Tissue Engineering*, 187–204.

- R.S. Lappalainen, M. Salomäki, L. Ylä-Outinen, T.J. Heikkilä, J.A.K. Hyttinen, H. Pihlajamäki, R. Suuronen, H. Skottman, and S. Narkilahti, **2010**. Similarly derived and cultured hESC lines show variation in their developmental potential towards neuronal cells in long-term culture. *Regenerative medicine*, 5 (5), 749–762.
- L.W. Lau, R. Cua, M.B. Keough, S. Haylock-Jacobs, and V.W. Yong, **2013**. Pathophysiology of the brain extracellular matrix: a new target for remyelination. *Nature Reviews Neuroscience*, 14 (10), 722–729.
- T. Lawyer, K. McIntosh, C. Clavijo, L. Potekhina, and B.K. Mann, **2012**. Formulation Changes Affect Material Properties and Cell Behavior in HA-Based Hydrogels. *International Journal of Cell Biology*, 2012, 1–9. <https://www.hindawi.com/journals/ijcb/2012/737421/>
- J. Lee, M.J. Cuddihy, and N. a Kotov, **2008**. Three-Dimensional Cell Culture Matrices: State of the Art. *Tissue Engineering Part B: Reviews*, 14 (1), 61–86.
- J.Y. Lee, C.A. Bashur, N. Gomez, A.S. Goldstein, and C.E. Schmidt, **2010**. Enhanced polarization of embryonic hippocampal neurons on micron scale electrospun fibers. *Journal of Biomedical Materials Research Part A*, 92 (4), 1398–1406.
- E.J. Leon, N. Verma, S. Zhang, D.A. Lauffenburger, and R.D. Kamm, **1998**. Mechanical properties of a self-assembling oligopeptide matrix. *Journal of biomaterials science. Polymer edition*, 9 (3), 297–312.
- H. Li, A. Wijekoon, and N.D. Leipzig, **2012**. 3D Differentiation of Neural Stem Cells in Macroporous Photopolymerizable Hydrogel Scaffolds. *PLoS ONE*, 7 (11), e48824. <https://www.ncbi.nlm.nih.gov/pmc/articles/PMC3492243/pdf/pone.0048824.pdf>
- N. Li, Q. Zhang, S. Gao, Q. Song, R. Huang, L. Wang, L. Liu, J. Dai, M. Tang, and G. Cheng, **2013**. Three-dimensional graphene foam as a biocompatible and conductive scaffold for neural stem cells. *Scientific Reports*, 3 (1), 1604. <https://www.nature.com/articles/srep01604>
- T. Limongi, F. Cesca, F. Gentile, R. Marotta, R. Ruffilli, A. Barberis, M. Dal Maschio, E.M. Petrini, S. Santoriello, F. Benfenati, and E. Di Fabrizio, **2013**. Nanostructured Superhydrophobic Substrates Trigger the Development of 3D Neuronal Networks. *Small*, 9 (3), 402–412.



- E.S. Lippmann, S.M. Azarin, J.E. Kay, R.A. Nessler, H.K. Wilson, A. Al-Ahmad, S.P. Palecek, and E. V Shusta, **2012**. Derivation of Blood-Brain Barrier Endothelial Cells from Human Pluripotent Stem Cells. *Nat. Biotechnol.*, 30 (8), 783–791.
- Y. Loo, M. Goktas, A.B. Tekinay, M.O. Guler, C.E. Hauser, and A. Mitraki, **2015**. Self-Assembled Proteins and Peptides as Scaffolds for Tissue Regeneration. *Advanced Healthcare Materials*, 4 (16), 2557–2586.
- Y. Loo, S. Zhang, and C.A.E. Hauser, **2012**. From short peptides to nanofibers to macromolecular assemblies in biomedicine. *Biotechnology Advances*, 30 (3), 593–603.
- R. Lozano, L. Stevens, B.C. Thompson, K.J. Gilmore, R. Gorkin, E.M. Stewart, M. in het Panhuis, M. Romero-Ortega, and G.G. Wallace, **2015**. 3D printing of layered brain-like structures using peptide modified gellan gum substrates. *Biomaterials*, 67, 264–273.
- S. Malchenko, J. Xie, M. de Fatima Bonaldo, E.F. Vanin, B.J. Bhattacharyya, A. Belmadani, G. Xi, V. Galat, W. Goossens, R.E.B. Seftor, T. Tomita, J. Crispino, R.J. Miller, M.C. Bohn, M.J.C. Hendrix, and M.B. Soares, **2014**. Onset of rosette formation during spontaneous neural differentiation of hESC and hiPSC colonies. *Gene*, 534 (2), 400–407.
- V. Marx, **2016**. Stem cells: a dish of neurons. *Nature Methods*, 13 (8), 617–622.
- P. Matricardi, C. Di Meo, T. Coviello, W.E. Hennink, and F. Alhaique, **2013**. Interpenetrating Polymer Networks polysaccharide hydrogels for drug delivery and tissue engineering. *Advanced Drug Delivery Reviews*, 65 (9), 1172–1187.
- S.S. McMahon and K.W. McDermott, **2006**. A comparison of cell transplantation and retroviral gene transfection as tools to study lineage and differentiation in the rat spinal cord. *Journal of Neuroscience Methods*, 152 (1–2), 243–249.
- V. Melissinaki, A. Gill, I. Ortega, M. Vamvakaki, A. Ranella, J.W. Haycock, C. Fotakis, M. Farsari, and F. Claeysens, **2011**. Direct laser writing of 3D scaffolds for neural tissue engineering applications. *Biofabrication*, 3 (4), 45005. <http://iopscience.iop.org/article/10.1088/1758-5082/3/4/045005/meta;jsessionid=910BD98CB4F826BEABDD8E7BD06F8A6F.ip-10-40-2-120>

- J. Mertens, M.C. Marchetto, C. Bardy, and F.H. Gage, **2016**. Evaluating cell reprogramming, differentiation and conversion technologies in neuroscience. *Nature Reviews Neuroscience*, 17 (7), 424–437.
- E.R. Morris, K. Nishinari, and M. Rinaudo, **2012**. Gelation of gellan – A review. *Food Hydrocolloids*, 28 (2), 373–411.
- A.R. Murphy, A. Laslett, C.M. O'Brien, and N.R. Cameron, **2017**. Scaffolds for 3D in vitro culture of neural lineage cells. *Acta Biomaterialia*, 54, 1–20.
- Y. Nagai, H. Yokoi, K. Kaihara, and K. Naruse, **2012**. The mechanical stimulation of cells in 3D culture within a self-assembling peptide hydrogel. *Biomaterials*, 33 (4), 1044–1051.
- R. Nat, M. Nilbratt, S. Narkilahti, B. Winblad, O. Hovatta, and A. Nordberg, **2007**. Neurogenic neuroepithelial and radial glial cells generated from six human embryonic stem cell lines in serum-free suspension and adherent cultures. *Glia*, 55 (4), 385–399.
- D.R. Nisbet, K.E. Crompton, M.K. Horne, D.I. Finkelstein, and J.S. Forsythe, **2007**. Neural tissue engineering of the CNS using hydrogels. *Journal of Biomedical Materials Research - Part B Applied Biomaterials*, 87 (1), 251–263.
- C. No, **2007**. BD™ PuraMatrix™ Peptide Hydrogel Guidelines, (354250), 1–16. [http://puramatrix.com/publications/PuraMatrix\\_Guidelines.pdf](http://puramatrix.com/publications/PuraMatrix_Guidelines.pdf)
- M. Ojala, C. Prajapati, R.-P. Pölönen, K. Rajala, M. Pekkanen-Mattila, J. Rasku, K. Larsson, and K. Aalto-Setälä, **2016**. Mutation-Specific Phenotypes in hiPSC-Derived Cardiomyocytes Carrying Either Myosin-Binding Protein C Or  $\alpha$ -Tropomyosin Mutation for Hypertrophic Cardiomyopathy. *Stem Cells International*, 2016, 1–16.
- S. Ortinau, J. Schmich, S. Block, A. Liedmann, L. Jonas, D.G. Weiss, C. a Helm, A. Rolfs, and M.J. Frech, **2010**. Effect of 3D-scaffold formation on differentiation and survival in human neural progenitor cells. *BioMedical Engineering OnLine*, 9 (1), 70. <https://biomedical-engineering-online.biomedcentral.com/articles/10.1186/1475-925X-9-70>
- M.L. Oyen, **2014**. Mechanical characterisation of hydrogel materials. *International Materials Reviews*, 59 (1), 44–59.

- G. Palazzolo, N. Broguiere, O. Cenciarelli, H. Dermutz, and M. Zenobi-Wong, **2015**. Ultrasoft Alginate Hydrogels Support Long-Term Three-Dimensional Functional Neuronal Networks. *Tissue Engineering Part A*, 21 (15–16), 2177–2185.
- A.M. Paşca, S.A. Sloan, L.E. Clarke, Y. Tian, C.D. Makinson, N. Huber, C.H. Kim, J.-Y. Park, N.A. O'Rourke, K.D. Nguyen, S.J. Smith, J.R. Huguenard, D.H. Geschwind, B.A. Barres, and S.P. Paşca, **2015**. Functional cortical neurons and astrocytes from human pluripotent stem cells in 3D culture. *Nature Methods*, 12 (7), 671–678.
- S. Pautot, C. Wyart, and E.Y. Isacoff, **2008**. Colloid-guided assembly of oriented 3D neuronal networks. *Nature Methods*, 5 (8), 735–740.
- J. Pettersson, S. Lobov, and L.N. Novikova, **2010**. Labeling of olfactory ensheathing glial cells with fluorescent tracers for neurotransplantation. *Brain Research Bulletin*, 81 (1), 125–132.
- S.M. Potter, J. Pine, and S.E. Fraser, **1996**. Neural transplant staining with DiI and vital imaging by 2-photon laser-scanning microscopy. *Scanning microscopy. Supplme*, 10 (3), 189–199.
- D.X. Qian, H.T. Zhang, X. Ma, X.D. Jiang, and R.X. Xu, **2010**. Comparison of the efficiencies of three neural induction protocols in human adipose stromal cells. *Neurochemical Research*, 35 (4), 572–579.
- K. Rajala, H. Hakala, S. Panula, S. Aivio, H. Pihlajamaki, R. Suuronen, O. Hovatta, and H. Skottman, **2007**. Testing of nine different xeno-free culture media for human embryonic stem cell cultures. *Human Reproduction*, 22 (5), 1231–1238.
- K. Rajala, B. Lindroos, S.M. Hussein, R.S. Lappalainen, M. Pekkanen-Mattila, J. Inzunza, B. Rozell, S. Miettinen, S. Narkilahti, E. Kerkelä, K. Aalto-Setälä, T. Otonkoski, R. Suuronen, O. Hovatta, and H. Skottman, **2010**. A Defined and Xeno-Free Culture Method Enabling the Establishment of Clinical-Grade Human Embryonic, Induced Pluripotent and Adipose Stem Cells. *PLoS ONE*, 5 (4), e10246. <http://journals.plos.org/plosone/article/comments?id=10.1371/journal.pone.0010246>
- M. Ravi, V. Paramesh, S.R. Kaviya, E. Anuradha, and F.D.P. Solomon, **2015**. 3D Cell Culture Systems: Advantages and Applications. *Journal of Cellular Physiology*, 230 (1), 16–26.

- K. Safford and H. Rice, 2005. Stem Cell Therapy for Neurologic Disorders: Therapeutic Potential of Adipose-Derived Stem Cells. *Current Drug Targets*, 6 (1), 57–62.
- K. Saha, A.J. Keung, E.F. Irwin, Y. Li, L. Little, D. V. Schaffer, and K.E. Healy, 2008. Substrate Modulus Directs Neural Stem Cell Behavior. *Biophysical Journal*, 95 (9), 4426–4438.
- S. Sanyal, 2014. Culture and Assay Systems Used for 3D Cell Culture. *Corning*. [http://csmedia2.corning.com/LifeSciences/media/pdf/an\\_245\\_culture\\_and\\_assay\\_systems\\_used\\_for\\_3D\\_cell\\_culture.pdf](http://csmedia2.corning.com/LifeSciences/media/pdf/an_245_culture_and_assay_systems_used_for_3D_cell_culture.pdf)
- J.M. Saul and D.F. Williams, 2013. Hydrogels in Regenerative Medicine. *Handbook of Polymer Applications in Medicine and Medical Devices*, 279–302.
- C.A. Schevon, S.A. Weiss, G. McKhann, R.R. Goodman, R. Yuste, R.G. Emerson, and A.J. Trevelyan, 2012. Evidence of an inhibitory restraint of seizure activity in humans. *Nature Communications*, 3, 1060. <https://www.nature.com/articles/ncomms2056.pdf>
- M. Sharif-Alhoseini and V. Rahimi-Movaghar, 2014. Animal Models in Traumatic Spinal Cord Injury. *In: Topics in Paraplegia*. InTech, 209–228.
- F. Sharifi, B.B. Patel, A.K. Dzuilko, R. Montazami, D.S. Sakaguchi, and N. Hashemi, 2016. Polycaprolactone Microfibrous Scaffolds to Navigate Neural Stem Cells. *Biomacromolecules*, 17 (10), 3287–3297.
- Y. Shi, P. Kirwan, J. Smith, H.P.C. Robinson, and F.J. Livesey, 2012. Human cerebral cortex development from pluripotent stem cells to functional excitatory synapses. *Nature Neuroscience*, 15 (3), 477–486.
- N. Silva, M.J. Cooke, R.Y. Tam, N. Sousa, A.J. Salgado, R.L. Reis, and M.S. Shoichet, 2012. The effects of peptide modified gellan gum and olfactory ensheathing glia cells on neural stem/progenitor cell fate. *Biomaterials*, 33 (27), 6345–6354.
- H. Skottman, 2010. Derivation and characterization of three new human embryonic stem cell lines in Finland. *In Vitro Cellular & Developmental Biology - Animal*, 46 (3–4), 206–209.

G.M. Smith, Y. Liu, and J.W. Hong, **2013**. *Neuronal Cell Culture*. Methods in Molecular Biology. Totowa, NJ: Humana Press. 1078, 153-161

A.E. Sorkio, E.P. Vuorimaa-Laukkanen, H.M. Hakola, H. Liang, T.A. Ujula, J.J. Valle-Delgado, M. Österberg, M.L. Yliperttula, and H. Skottman, **2015**. Biomimetic collagen I and IV double layer Langmuir–Schaefer films as microenvironment for human pluripotent stem cell derived retinal pigment epithelial cells. *Biomaterials*, 51, 257–269.

M.M. Stevens, **2005**. Exploring and Engineering the Cell Surface Interface. *Science*, 310 (5751), 1135–1138.

A. Subramanian, U. Krishnan, and S. Sethuraman, **2009**. Development of biomaterial scaffold for nerve tissue engineering: Biomaterial mediated neural regeneration. *Journal of Biomedical Science*, 16 (1), 108. <https://www.ncbi.nlm.nih.gov/pmc/articles/PMC2790452/pdf/1423-0127-16-108.pdf>

S. Suri and C.E. Schmidt, **2010**. Cell-Laden Hydrogel Constructs of Hyaluronic Acid, Collagen, and Laminin for Neural Tissue Engineering. *Tissue Engineering Part A*, 16 (5), 1703–1716.

V. Tabar and L. Studer, **2014**. Pluripotent stem cells in regenerative medicine: challenges and recent progress. *Nature Reviews Genetics*, 15 (2), 82–92.

K. Takahashi and S. Yamanaka, **2006**. Induction of Pluripotent Stem Cells from Mouse Embryonic and Adult Fibroblast Cultures by Defined Factors. *Cell*, 126 (4), 663–676.

A.I. Teixeira, S. Ilkhanizadeh, J. Wiggenius, J.K. Duckworth, O. Inganäs, and O. Hermanson, **2009**. The promotion of neuronal maturation on soft substrates. *Biomaterials*, 30 (27), 4567–4572.

J. Thomson, **1998**. Embryonic Stem Cell Lines Derived from Human Blastocysts. *Science*, 282 (5391), 1145–1147.

J.R. Thonhoff, D.I. Lou, P.M. Jordan, X. Zhao, and P. Wu, **2008**. Compatibility of human fetal neural stem cells with hydrogel biomaterials in vitro. *Brain Research*, 1187 (1), 42–51.

V. Tieng, L. Stoppini, S. Villy, M. Fathi, M. Dubois-Dauphin, and K.-H. Krause, **2014**. Engineering of Midbrain Organoids Containing Long-Lived Dopaminergic Neurons. *Stem Cells and Development*, 23 (13), 1535–1547.

S. Toivonen, M. Ojala, A. Hyysalo, T. Ilmarinen, K. Rajala, M. Pekkanen-Mattila, R. Äänismaa, K. Lundin, J. Palgi, J. Weltner, R. Trokovic, O. Silvennoinen, H. Skottman, S. Narkilahti, K. Aalto-Setälä, and T. Otonkoski, **2013**. Comparative Analysis of Targeted Differentiation of Human Induced Pluripotent Stem Cells (hiPSCs) and Human Embryonic Stem Cells Reveals Variability Associated With Incomplete Transgene Silencing in Retrovirally Derived hiPSC Lines. *STEM CELLS Translational Medicine*, 2 (2), 83–93.

R. Trokovic, J. Weltner, and T. Otonkoski, **2015**. Generation of iPSC line HEL24.3 from human neonatal foreskin fibroblasts. *Stem Cell Research*, 15 (1), 266–268.

W.T. Truong, Y. Su, J.T. Meijer, P. Thordarson, and F. Braet, **2011**. Self-Assembled Gels for Biomedical Applications. *Chemistry - An Asian Journal*, 6 (1), 30–42.

Y.-H. Tsou, J. Khoneisser, P.-C. Huang, and X. Xu, **2016**. Hydrogel as a bioactive material to regulate stem cell fate. *Bioactive Materials*, 1 (1), 39–55.

M.B. Victor, M. Richner, T.O. Hermanstynne, J.L. Ransdell, C. Sobieski, P.-Y. Deng, V.A. Klyachko, J.M. Nerbonne, and A.S. Yoo, **2014**. Generation of Human Striatal Neurons by MicroRNA-Dependent Direct Conversion of Fibroblasts. *Neuron*, 84 (2), 311–323.

D. Wagenaar, J. Pine, and S.M. Potter, **2004**. Effective parameters for stimulation of dissociated cultures using multi-electrode arrays. *Journal of Neuroscience Methods*, 138 (1–2), 27–37.

N.J. Walters and E. Gentleman, **2015**. Evolving insights in cell-matrix interactions: Elucidating how non-soluble properties of the extracellular niche direct stem cell fate. *Acta Biomaterialia*, 11 (1), 3–16.

B. Weng, J. Diao, Q. Xu, Y. Liu, C. Li, A. Ding, and J. Chen, **2015**. Bio-Interface of Conducting Polymer-Based Materials for Neuroregeneration. *Advanced Materials Interfaces*, 2 (8), 1500059.

- E.C. Williams, X. Zhong, A. Mohamed, R. Li, Y. Liu, Q. Dong, G.E. Ananiev, J.C.C. Mok, B.R. Lin, J. Lu, C. Chiao, R. Cherney, H. Li, S.-C. Zhang, and Q. Chang, **2014**. Mutant astrocytes differentiated from Rett syndrome patients-specific iPSCs have adverse effects on wild-type neurons. *Human Molecular Genetics*, 23 (11), 2968–2980.
- H. Yamaoka, H. Asato, T. Ogasawara, S. Nishizawa, T. Takahashi, T. Nakatsuka, I. Koshima, K. Nakamura, H. Kawaguchi, U. Chung, T. Takato, and K. Hoshi, **2006**. Cartilage tissue engineering using human auricular chondrocytes embedded in different hydrogel materials. *Journal of Biomedical Materials Research Part A*, 78A (1), 1–11.
- L. Yla-Outinen, C. Mariani, H. Skottman, R. Suuronen, A. Harlin, and S. Narkilahti, **2010**. Electrospun Poly(L,D-lactide) Scaffolds Support the Growth of Human Embryonic Stem Cell-derived Neuronal Cells. *The Open Tissue Engineering and Regenerative Medicine Journal*, 3 (1), 1–9.
- S.J. Yoo, J. Kim, C.-S. Lee, and Y. Nam, **2011**. Simple and Novel Three Dimensional Neuronal Cell Culture Using a Micro Mesh Scaffold. *Experimental Neurobiology*, 20 (2), 110.
- S. Zhang, F. Gelain, and X. Zhao, **2005**. Designer self-assembling peptide nanofiber scaffolds for 3D tissue cell cultures. *Seminars in Cancer Biology*, 15 (5 SPEC. ISS.), 413–420.
- Y. Zhang and B. Barres, **2013**. A smarter mouse with human astrocytes. *BioEssays*, 35 (10), n/a-n/a.
- Y. Zhang, P. Heher, J. Hilborn, H. Redl, and D. Ossipov, **2016**. Hyaluronic acid-fibrin interpenetrating double network hydrogel prepared in situ by orthogonal disulfide cross-linking reaction for biomedical applications. *Acta Biomaterialia*, 38, 23–32.
- Z.X. Zhang, Q.X. Zheng, Y.C. Wu, and D.J. Hao, **2010**. Compatibility of neural stem cells with functionalized self-assembling peptide scaffold in vitro. *Biotechnology and Bioprocess Engineering*, 15 (4), 545–551.
- X. Zhao, S. Zhang, and L. Spirio, **2005**. PuraMatrix. *In: Scaffolding In Tissue Engineering*. CRC Press, 217–238.

J. Zhu and R.E. Marchant, 2011. Design properties of hydrogel tissue-engineering scaffolds. *Expert Review of Medical Devices*, 8 (5), 607–626.





## Basic Neuroscience

## Fluorescent probes as a tool for cell population tracking in spontaneously active neural networks derived from human pluripotent stem cells

M. Mäkinen<sup>a,1</sup>, T. Joki<sup>a,1</sup>, L. Ylä-Outinen<sup>a</sup>, H. Skottman<sup>b</sup>, S. Narkilahti<sup>a,c</sup>, R. Äänismaa<sup>a,\*</sup><sup>a</sup> NeuroGroup, Institute of Biomedical Technology/BioMediTech, Biokatu 12, FI-33014 University of Tampere, Finland<sup>b</sup> Ophthalmology Group, Institute of Biomedical Technology/BioMediTech, Biokatu 12, FI-33014 University of Tampere, Finland<sup>c</sup> The Science Center of Pirkanmaa Hospital District, Tampere, Finland

## H I G H L I G H T S

- Fluorescent labels CT and DiD can be utilized with human stem cell-derived neurons.
- Labels do not affect the cell viability and minimally affect the cell proliferation.
- Labeled cells can be successfully followed for at least 4 weeks.
- Labeled cell populations form spontaneously active neural networks.

## A R T I C L E I N F O

## Article history:

Received 27 November 2012

Received in revised form 25 February 2013

Accepted 27 February 2013

## Keywords:

CellTracker

DiD

Co-culture

Fluorescent probe

Labeling

Human stem cell derived neural cells

Long term

## A B S T R A C T

Applications such as 3D cultures and tissue modelling require cell tracking with non-invasive methods. In this work, the suitability of two fluorescent probes, CellTracker, CT, and long chain carbocyanine dye, DiD, was investigated for long-term culturing of labeled human pluripotent stem cell-derived neural cells. We found that these dyes did not affect the cell viability. However, proliferation was decreased in DiD labeled cell population. With both dyes the labeling was stable up to 4 weeks. CT and DiD labeled cells could be co-cultured and, importantly, these mixed populations had their normal ability to form spontaneous electrical network activity. In conclusion, human neural cells can be successfully labeled with these two fluorescent probes without significantly affecting the cell characteristics. These labeled cells could be utilized further in e.g. building controlled neuronal networks for neurotoxicity screening platforms, combining cells with biomaterials for 3D studies, and graft development.

© 2013 Elsevier B.V. All rights reserved.

## 1. Introduction

For the development of *in vitro* cell and tissue models it is often desirable to distinguish different cell populations within co-cultures in real time. This can be performed on the basis of differences in the cell morphology. However, morphological differences can vary even within the same cell type and become difficult to observe in a three dimensional culture environment. Fluorescent probes are an alternative to morphology-based identification. These probes have been tested with animal-derived cell cultures

(Honig and Hume, 1989) but only one study has earlier described the use of fluorescent probes in human-derived neural cell cultures (Rizvanov et al., 2010). Furthermore, the possible cytotoxic effects should be assessed separately for human or primate cells due to species differences in neurotoxicity (Boyce et al., 1984).

The objective of this research was to find suitable fluorescent probes for the long term labeling of human embryonic stem cell (hESC)-derived neural cell co-cultures. The suitability of two widely used dyes, CellTracker (CT, also known as chloromethylfluorescein diacetate, CMFDA) and long chain carbocyanine dye 1,1'-dioctadecyl-3,3',3'-tetramethylindodicarbocyanine perchlorate (DiD or DiI18(5)) were investigated. CT has been widely used to label living cells (Redelman et al., 1988), and has been utilized in tracking both animal (Silverman et al., 2000) and human derived (Jablonska et al., 2010) cell transplants. Lipophilic long chain dicarbocyanine dyes belong to large family of cyanine dyes (for review see Mishra et al., 2000). DiD and its analogs have been used for cell visualization both in tissue slices and cell cultures (Honig and Hume, 1986, 1989). The impact of these dyes on human-derived

\* Corresponding author at: NeuroGroup, Institute of Biomedical Technology/BioMediTech, University of Tampere, Biokatu 12, 6th floor, 33520 Tampere, Finland. Tel.: +358 40 1782942; fax: +358 3 35518498.

E-mail addresses: [meeri.makinen@uta.fi](mailto:meeri.makinen@uta.fi) (M. Mäkinen), [tiina.joki@uta.fi](mailto:tiina.joki@uta.fi) (T. Joki), [laura.yla-outinen@uta.fi](mailto:laura.yla-outinen@uta.fi) (L. Ylä-Outinen), [heli.skottman@uta.fi](mailto:heli.skottman@uta.fi) (H. Skottman), [susanna.narkilahti@uta.fi](mailto:susanna.narkilahti@uta.fi) (S. Narkilahti), [riikka.aanismaa@uta.fi](mailto:riikka.aanismaa@uta.fi) (R. Äänismaa).

<sup>1</sup> These authors contributed equally to this work.

neural cells has not been previously studied although they have been used in cell cultures from both animal and human origin (Packard et al., 1984; Honig and Hume, 1986; Jablonska et al., 2010; Markiewicz et al., 2011).

The optimum labeling parameters and the characteristics of cell population labeled with each of these dyes were defined. Furthermore, the effect of labeling on the proliferation and viability was studied. The behavior of CT and DiD during immunocytochemistry as well as in co-cultures was also studied. Finally, the ability of CT- and DiD-labeled hESC-derived co-cultures to form functional neural networks was investigated.

## 2. Materials and methods

### 2.1. Cells

#### 2.1.1. HESC line derivation and maintenance

A number of hESC lines (Regea 08/056, 06/040, 08/023) were used in this study. The Regea lines were derived at Institute of Biomedical Technology (IBT), University of Tampere, Finland. IBT holds an approval from the Ethics Committee of Pirkanmaa Hospital District for derivation, characterization, and differentiation of hESC-lines (R05051, R05116) as well as an approval of Valvira, the Finnish National Supervisory Authority for Welfare and Health, for research on human embryos (1426/32/300/05). The derivation and characterization of Regea lines has been described previously (Rajala et al., 2010; Skottman, 2010). The maintenance of hESC lines was done as described earlier (Rajala et al., 2007). The hESC lines were quality controlled with frequent gene and protein expression analysis, karyotype, and mycoplasma assays.

#### 2.1.2. Derivation of neural cultures

The neural differentiation of hESCs was performed as described by Lappalainen et al. (2010). Basic fibroblast growth factor (bFGF) was used in 20 ng/ml concentration during the neurosphere culturing step. For the final neural maturation, the neurospheres were mechanically dissected and plated onto 24- or 48-well plates coated (overnight in +4 °C or two hours in +37 °C) with laminin (10 µg/ml, mouse or human, Sigma–Aldrich, St. Louis, MO). The bFGF was withdrawn at the beginning of adherent culture. Half of the medium was replaced 2–3 times a week. For co-culturing, the adherent fluorescent labeled cultures were dissected enzymatically (TrypLe Select™, Gibco).

### 2.2. Fluorescent dyes

Fluorescent probe 5-chloromethylfluorescein diacetate (Cell-Tracker Green CMFDA, CT, C2925, Molecular Probes®, Life Technologies, UK) was prepared by dissolving it to DMSO (10 mM stock). Lipophilic carbocyanine 1,1'-dioctadecyl-3,3,3',3'-tetramethylindodicarbocyanine perchlorate (DiD, D-307, Molecular Probes®, Life Technologies) was prepared by dissolving it to 99.8% ethanol (20 mM stock). On the day of use, a labeling medium was prepared by diluting stock solution to fresh culture medium. The final concentrations recommended by the manufacturer, Molecular Probes®, were 0.5–25 µM for CT and 25 µM for DiD. However, during the experiments we came to test a wider range for CT (0.5, 2, 4, 5, 8, 10, 16, 20, 30, 40 or 60 µM). Based on the literature (Honig and Hume, 1986, 1989; Potter et al., 1996) we decided to test a larger range for DiD as well (0.2, 0.5, 1, 5, 10, 20 or 50 µM). The culture medium on the cells was replaced with the labeling medium and incubated (CT: 15, 30 or 60 min or 2, 4, 24, 48, or 72 h; DiD: 2, 10, 30 or 60 min or 2, 4, 8, 16 or 24 h) at +37 °C, 5% CO<sub>2</sub>, humidified atmosphere. After incubation, the labeling medium was replaced with fresh culture medium and the cells were imaged at varying periods after labeling. Every parameter set

was tested at least once with 2 parallel samples for both probes and the optimal parameters were tested at least 8 times with 2–20 parallel samples.

### 2.3. Cell viability

The LIVE/DEAD® Viability/Cytotoxicity Kit (L-3224, Molecular Probes®, Life Technologies) or the components of the kit purchased individually (Calcein AM; C1430, EthD-1; E1169, Molecular Probes®, Life Technologies) were used to assess the cell viability (Althouse and Hopkins, 1995). Briefly, Calcein AM and EthD-1 were diluted to culture medium to the final concentrations of 0.1 µM and 0.5 µM, respectively. After 30 min of dark incubation, the cells were imaged with a fluorescence microscope. Analysis was performed by manually counting the number of Calcein AM and EthD-1 labeled cells from the images.

### 2.4. Immunocytochemistry

Cells were fixed with cold 4% paraformaldehyde for 15 min in room temperature. To prevent unspecific binding of antibodies, cells were permeabilized with 0.1% Triton X-100 (Sigma) or 0.1% saponin (Sigma–Aldrich) and blocked with 10% normal donkey serum (NDS, Millipore) in 1% bovine serum albumin (BSA, Sigma) in DPBS. Primary antibodies were diluted to 1% NDS, 1% BSA in DPBS with 0.1% Triton X-100 or 0.1% saponin. The primary antibody solution was kept on cells overnight at +4 °C. The excess primary antibodies were removed by washing with 1% BSA in DPBS without or with 0.1% saponin. Next, the secondary antibodies were added in 1% BSA in DPBS without or with 0.1% saponin. Secondary antibodies were incubated at room temperature for one hour. Immunocytochemical staining protocol was also performed with no permeabilization. The excess secondary antibodies were removed by washing with PBS and phosphate buffer without saline. For nuclear staining and mounting, Vectashield with 4,6-diamidino-2-phenylindole (DAPI, H1200, Vector laboratories, Peterborough, UK) was utilized. Primary antibodies anti-MAP-2 (rabbit, 1:600, AB5622, Millipore, Billerica, MA, USA) for detecting neuronal cells as well as their processes, anti-GFAP (sheep, 1:600, AF2594, R&D Systems, Minneapolis, MN, USA) for detecting astrocytes and anti-Ki-67 (rabbit, 1:800, AB9260, Millipore) for detecting proliferating cells were used. AlexaFluor-488, -568 or -680 conjugates of anti-rabbit or anti-sheep secondary antibodies (1:600, Molecular Probes Invitrogen) were used. In order to quantify proliferation, DAPI and Ki-67 positive cell nuclei were counted from the microscope images.

### 2.5. Imaging system

Cells were visualized and imaged with a fluorescent microscope set (Olympus IX51 inverted microscope, PlanFLN 4×, 10×, 20×, and 40× objectives, Olympus DP30BW CCD camera). The light was filtered with U-MNU2 (excitation filter 360–370; emission filter 420; dichromatic filter 400), U-MNB2 (excitation filter 470–490; emission filter 520; dichromatic filter 500), U-MWG2 (excitation filter 550–510; emission filter 590; dichromatic filter 570), or U-N41023 (excitation filter 625–675; emission filter 710; dichromatic filter 680) filter cube. The images were processed with Adobe Photoshop. Briefly, the grayscale images were converted to an RGB format and the output levels were adjusted to zero, except for the channel corresponding to the color of the fluorescent light.

### 2.6. Microelectrode array system

The electrical activity of the neural networks were measured by culturing cells on microelectrode array (MEA)-dishes (Multi

Channel Systems, MCS, Reutlingen, Germany) ( $n=9$ ). The electrodes on bottom of the MEA-dish detect extracellular local field potential changes produced by the electrical activity of the overlying neurons. Thus, MEA is a non-invasive method and can be used for long term neuronal network activity follow up studies (Wagenaar et al., 2006). The microelectrodes in the dishes used had 30  $\mu\text{m}$  diameter and 200  $\mu\text{m}$  inter-electrode distance. The microelectrode measurements were performed using MEA-dishes sealed with 70% ethanol cleaned semi-permeable membrane (ALA MEA-MEM, ALA Scientific Instruments Inc., Westbury, NY). MEA-dishes were placed into a faraday cage protected amplifier (MEA-1060BC, MCS) and kept warm with an external heater unit (TC02, MCS) set to  $+38^\circ\text{C}$ . After placing the MEA-dish into the amplifier, the system was allowed to settle for one minute after which the recording was started. The measured signals were preamplified with MEA1060-Inv-BC (gain 53, MCS) and prefiltered with FA60SBC (gain 20, MCS) producing signal with 1100 gain and 1 Hz–8 kHz bandwidth. Analog to digital conversion was performed with MC\_card (MCS) with 20 kHz sampling frequency. The data acquisition card was controlled via MC\_Rack software (MCS). The digitized recordings were further processed by removing power line noise (50 Hz band reject) and baseline fluctuations (200 Hz high pass) with 2nd order Butterworth filter. Spike detection was performed online with MC\_Rack software. Threshold based detection (5 times standard deviation of noise level) was used. Both, the electrode raw data and detected spikes were saved for analysis. Signals were recorded for 5 min 1–3 times a week for each MEA. The spike counts and time stamps on each electrode were extracted with NeuroExplorer (Nex Technologies, Littleton, MA, USA) software, collected to Excel files, and combined to raster plots.

### 2.7. Statistical analysis

Statistical analysis were performed with IBM® SPSS (version 19) statistical software package. The data gained from manual cell counting from LIVE/DEAD- or Ki-67-stained cells were analyzed with nonparametric Kruskal-Wallis test followed by a Mann-Whitney U-test (*post hoc* test). A  $p$ -value less than 0.05 was considered significant. If more than two groups were analyzed the resulting  $p$  values were multiplied by the number of comparisons performed (Bonferroni correction).

## 3. Results

### 3.1. Optimizing labeling

A group of different labeling parameters were studied to obtain long time dye retention. A CT concentration of 0.5, 2, 4, 5, 8, 10, 16, 20, 30, 40, or 60  $\mu\text{M}$  was incubated for 15 or 30 min, 1, 2, 4, 12, 24, 48, or 72 h (Fig. 1A). Properly observable labeling of the cells up to 4 weeks was obtained by incubating 10, 16, and 20  $\mu\text{M}$  CT dilutions for 72 h. These labeling parameters enabled the labeling of both cell bodies and processes (Fig. 1B). Based on the comparison between fluorescent and transmission light images, CT seemed to label the whole cell population (Fig. 1B). At the end of the experiment, 4 weeks after labeling, CT labeled cells were fixed and stained with DAPI. The percentage of CT labeled cells from DAPI identified nuclei was 94% (604 cells, 6 imaged areas from 2 parallel wells). Hence, it can be argued that CT labels virtually all cells of the differentiated population. The labeling did not have effect on cell viability based on visual inspection. The cell viability was studied in more detail only in optimal concentration (Section 3.2).

DiD concentrations of 0.2, 0.5, 1, 5, 10, 20, and 50  $\mu\text{M}$  were tested with 10 min, 30 min, 1, 2, 16, or 24 h incubation times (Fig. 1C). A high DiD concentration (50  $\mu\text{M}$ ) or a long incubation time (16 h)

with over 5  $\mu\text{M}$  DiD concentration had clearly adverse effect on cell viability and were not further studied. Optimal labeling was observed with 10 or 20  $\mu\text{M}$  DiD concentration and 1 or 2 h incubation time (Fig. 1D). During the first week of 5 weeks follow up time, the labeling was bright and cellular processes were clearly visible. After the second week, some of the labeled processes were no longer visible. During the third week, the probe concentrated into cell somas. After 4 weeks, the probe accumulated into somatic granules (data not shown).

### 3.2. Effect on viability and proliferation

The cytochemical effects of both CT and DiD were studied by assessing cell viability and proliferation. For these experiments, the CT labeling was performed for 72 h with 10  $\mu\text{M}$  concentration and the DiD labeling was performed for 2 h with 10  $\mu\text{M}$  concentration. For CT labeled cells, LIVE/DEAD staining was performed 4 or 15 days after labeling to study the acute labeling effect and long term dye retaining effect on cell viability. No clear difference was observed between labeled cells and control cells on the 4 days time point (>1000 cells from 5 parallel images from 2 parallel wells, Fig. 2A). However, at 15 days time point, there were slightly more dead cells in CT labeled cultures compared to control cultures. No significant differences were found between control and CT labeled cells in the time points studied. For studying the effect on proliferation, the CT labeled cells were fixed 6–7 or 11–13 days after labeling and immunocytochemistry was performed against Ki-67, a marker of dividing cell nucleus. The cells were counted after imaging the stained cells (>450 cells, 2 parallel wells 3 figures each, Fig. 2B) and no significant differences between control and CT labeled cells were found in either time point.

For DiD labeled cells the viability was analyzed 5 days after the labeling. A triple labeled population (Calcein-AM, DiD, ethidium homodimer) was imaged using the U-N41023 filter cube in order to distinguish DiD. This was required due to the ability of DiD to also pass the U-MWG2 filter cube used for ethidium homodimer. The ethidium homodimer was, in turn, distinguished from DiD by having clearly brighter emission. Furthermore, ethidium homodimer labeled dead cell nuclei had a distinct round morphology whereas living cells labeled with DiD had more complex morphology with somas and neurites. No difference in viability was seen between the DiD labeled and the control cells (>6900 cells counted from 3 parallel wells, Fig. 2C). Proliferation was analyzed 3 weeks after cell plating. For acute effects, the adherent cultures were labeled with DiD and fixed 2 days later. For long term effects, the adherent cultures were labeled with DiD and fixed 2 weeks after labeling. The control group was cultured adherent for 3 weeks. The population that was labeled 2 days before analysis had slight decrease in proliferation but the difference was not significant. As a long term effect (2 weeks after labeling), DiD was observed to reduce cell proliferation as the amount of Ki-67 positive cells was significantly lower in labeled population when compared to the control cells (>1500 cells counted from 2 parallel wells, Fig. 2D) ( $p < 0.05$ ).

### 3.3. Optimizing immunocytochemistry

Fluorescent probes integrating to cell membranes, such as DiD, can be sensitive to reagents used to increase cell membrane permeability. Permeabilization, however, is required in order to perform immunocytochemistry against intracellular epitopes. We compared immunocytochemical stainings performed without permeabilization, with a common permeabilizer Triton X-100 or with a milder permeabilizer saponin. With DAPI there were no differences (Fig. 3A–C). The immunocytochemistry was performed against intracellular proteins MAP-2 and GFAP. Without permeabilization, the immunocytochemistry produced an uneven labeling and the

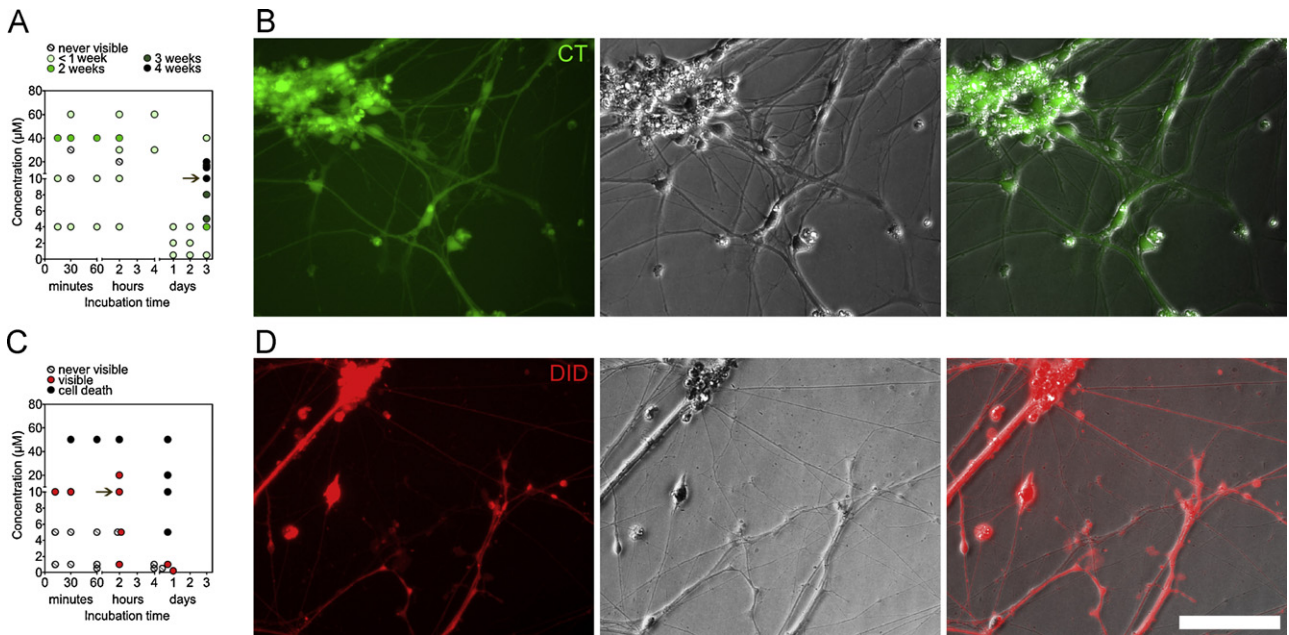


**Fig. 1.** Live-labeling of cells with fluorescent probes CT (A, B) and DiD (C, D). In pictures A and C, circles with slash present the labeling parameters when no labeling with CT or DiD was observed. In picture A, the CT label retention time in the cultures is presented with colored dots (from light green to dark green = from less than a week up to 3 weeks, black = up to 4 weeks). Thus, with 10  $\mu\text{M}$  and 3 days incubation, CT labeling was traceable up to 4 weeks and these parameters were considered optimal (marked with arrow). Picture B shows cells labeled using the optimal parameters. In picture C, red dots shows labeling parameters for good labeling whereas black dots shows parameters that caused cell death. The dye retention was followed at least 2 weeks for each labeling parameter set. Thus, the optimal parameters for DiD were 10  $\mu\text{M}$  and 2 h incubation (marked with arrow). Picture D shows cells labeled using the optimal parameters. In pictures B and D, the rightmost image is an overlay between the fluorescent and wide field image. In pictures A and C, the x-axis is scaled to minutes (0–60), hours (1–4), and to days (1–3) in order to show all the times in same axis. Scale bar is 100  $\mu\text{m}$ .

cell morphologies were difficult to perceive (Fig. 3D). With Triton X-100 and saponin the labeling was bright and clear (Fig. 3E and F). Without permeabilization or with saponin permeabilization the DiD probe was well retained and remained clearly visible (Fig. 3G and I). However, with Triton X-100 DiD was dissolved from the membranes causing faint labeling and red background fluorescence (Fig. 3H). None of the permeabilizers used disturbed the retainment or fluorescence of CT (Fig. 3J–L). An example of immunocytochemistry with saponin permeabilization performed against MAP-2 or GFAP with CT or DiD labeled cells is presented in Fig. 4.

### 3.4. Co-culturing

To further assess the suitability of CT and DiD for mixed cell cultures, the effect of dissociating and replating previously labeled cells was studied. CT was retained during dissociation and no clear difference in the intensity of the dye was observed between the control and the replated CT labeled cells during one week follow

up time (data not shown). Furthermore, it was observed that the background fluorescence of CT was diminished during replating. DiD was also found to be suitable for enzymatic cell detachment and replating. After the effect of cell dissociation was studied, mixed cell cultures of CT and DiD labeled cells were produced. The cells originating from different adherent cultures labeled with different fluorescent dyes did not avoid each other and grew as a mixed network (Fig. 5A–C). Initially, the dyes were retained in different cells. However, during the long term co-culturing the dyes became partially co-localized and granular (Fig. 5D–F).

The effect of CT and DiD labeling on the formation of the neural network activity was studied with planar MEAs (Fig. 6). Adherent hESC-derived neural cultures were labeled either with CT or DiD and dissociated to single cell suspensions. Cells from both suspensions were replated onto MEA plates ( $n = 9$ ). The development of the network activity was followed by weekly measurements (Fig. 6B). During the follow up period, the co-cultures first developed single spikes and later semi synchronous trains (Fig. 6C). From these

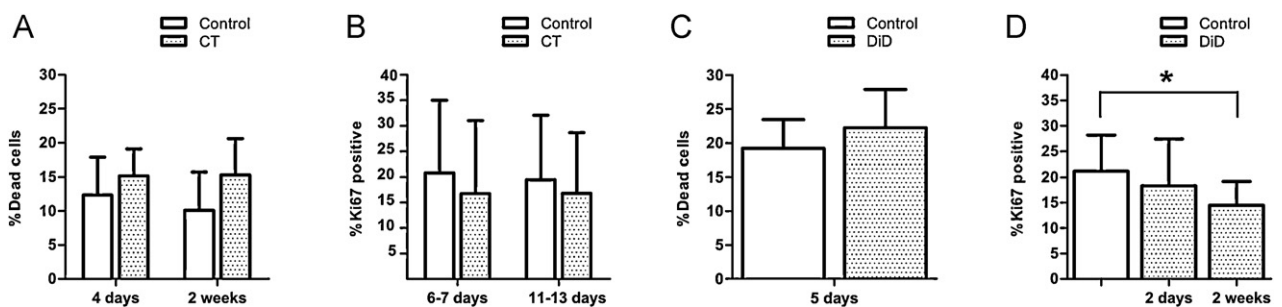


**Fig. 2.** Viability and proliferation studied with labeled and unlabeled populations. (A) In LIVE/DEAD analysis CT labeling slightly increased the amount the dead cells in the cultures. (B) Similarly, the amount of the Ki-67 positive proliferative cells was slightly lower in CT labeled cell populations when compared to unlabeled control cells. Similarly, DiD labeling slightly increased the amount of the dead cells (C) while decreasing the amount of proliferative Ki-67 positive cells. The decrease was significant after long term culturing (D). \* represents a  $p$ -value less than 0.05.

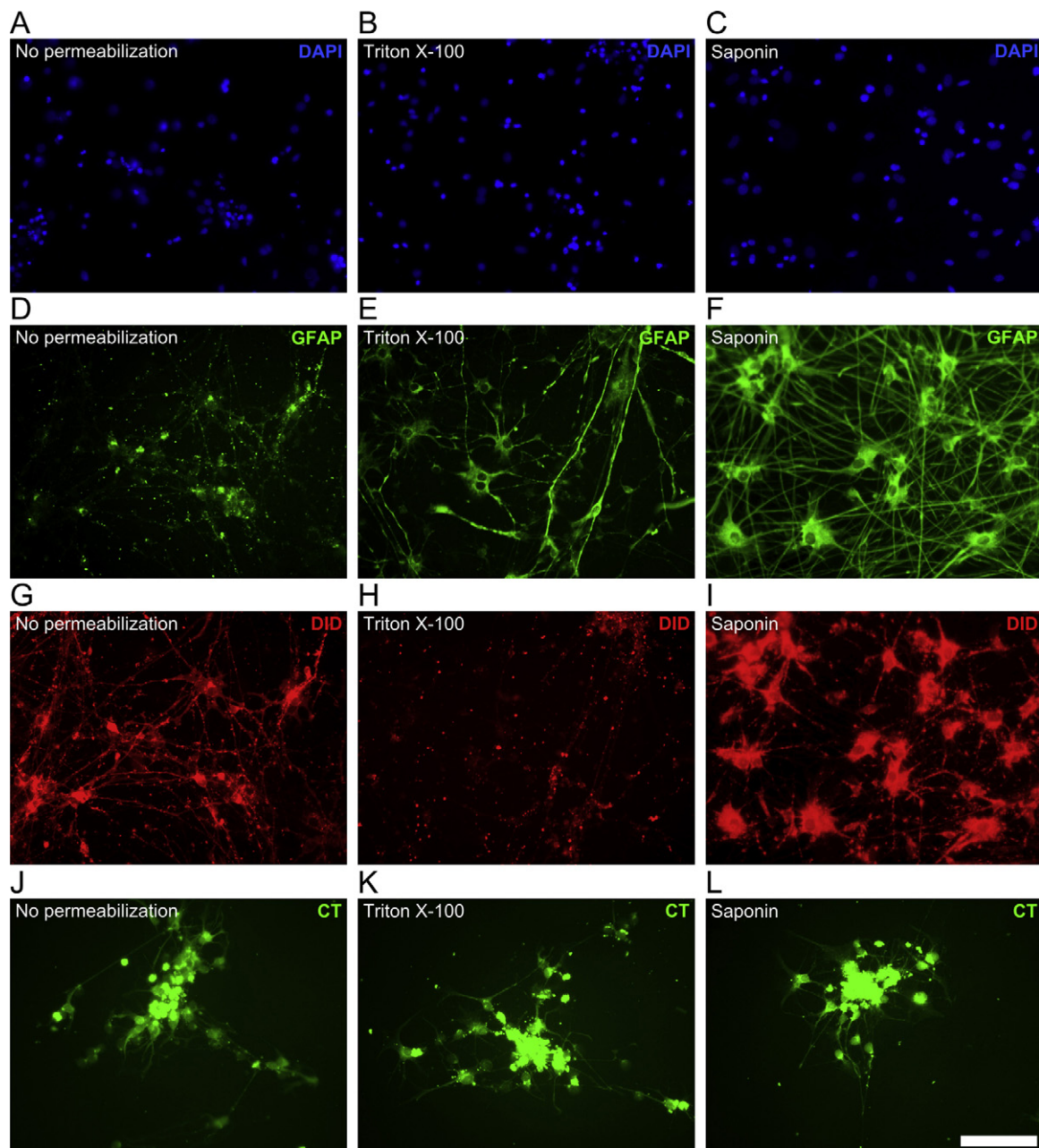


**Fig. 3.** Dye retention with different immunocytochemical permeabilization approaches. (A–C) DAPI stained all the nuclei regardless of the permeabilization. (D) GFAP, an antibody against intracellular protein could not be used without permeabilization whereas with either (E) Triton-X or (F) saponin the GFAP staining was successfully detected. DiD staining could be detected without permeabilization (G) and with saponin (I) whereas (H) with Triton-X DiD was extracted. CT staining was not affected by any of the permeabilization approaches (J–L). Scale bar 100  $\mu\text{m}$ .

observations, it was deduced that the labeling with CT and DiD, as well as co-culturing in a mixed form, does not prevent the formation of network connections between the hESC-derived neurons.

#### 4. Discussion

The objective of this research was to find and study the effects of fluorescent probes suitable for long term labeling of hESC-derived neural cell co-cultures. The suitability of two dyes, CT and DiD were investigated. Our results indicated that CT and DiD can be used for studying co-cultures of hESC-derived neural cells without adverse cytotoxic or functional effects.

CT at a concentration of 10  $\mu\text{M}$  in cell culture medium with 72 h incubation time enabled cell visualization at least up to 4 weeks.

Labeling concentration of CT used in previous experiments with neural lineage cell cultures tend to follow those recommended by the Molecular Probes (0.5–25  $\mu\text{M}$ ), e.g. 20  $\mu\text{M}$  for 30 min (McMahon and McDermott, 2006), 5  $\mu\text{M}$  for 60 min (Pettersson et al., 2010), and 10  $\mu\text{M}$  for 30 min (Markiewicz et al., 2011). The observations about the CT retention varied as CT labeled radial glial cells were reported to be observable up to 20 days (McMahon and McDermott, 2006) while CT labeled olfactory ensheathing glial cells lost their fluorescence in under 14 days (Pettersson et al., 2010). However, the parameters used by Pettersson et al. (2010), McMahon and McDermott (2006), and Markiewicz et al. (2011) were not reported to be optimized for the cell type used. We discovered that with short incubation times (15 min–4 h) the labeling was detectable less than 2 weeks whereas with longer incubation times (toward 72 h) the

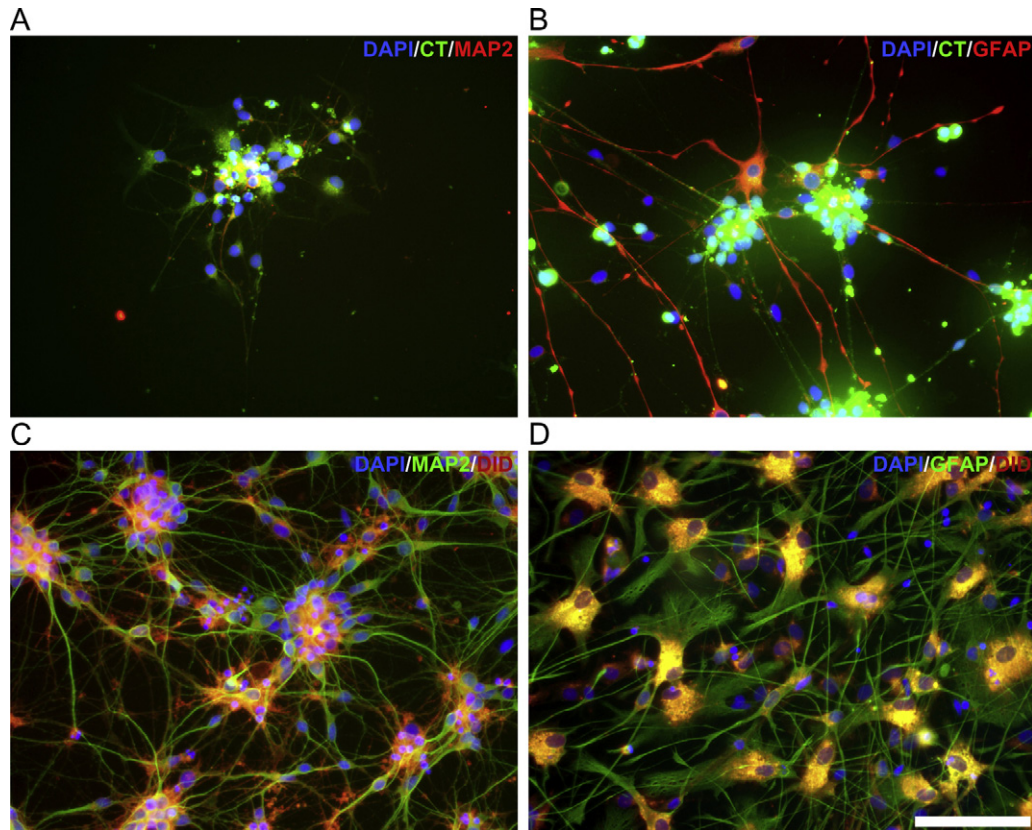


**Fig. 4.** Immunocytochemical staining combined with CT and DiD labeling. CT labeled cells stained positive (A) with MAP-2 and (B) with GFAP. Similarly, DiD label co-localized (C) with MAP-2 and (D) with GFAP. Scale bar 100  $\mu\text{m}$ .

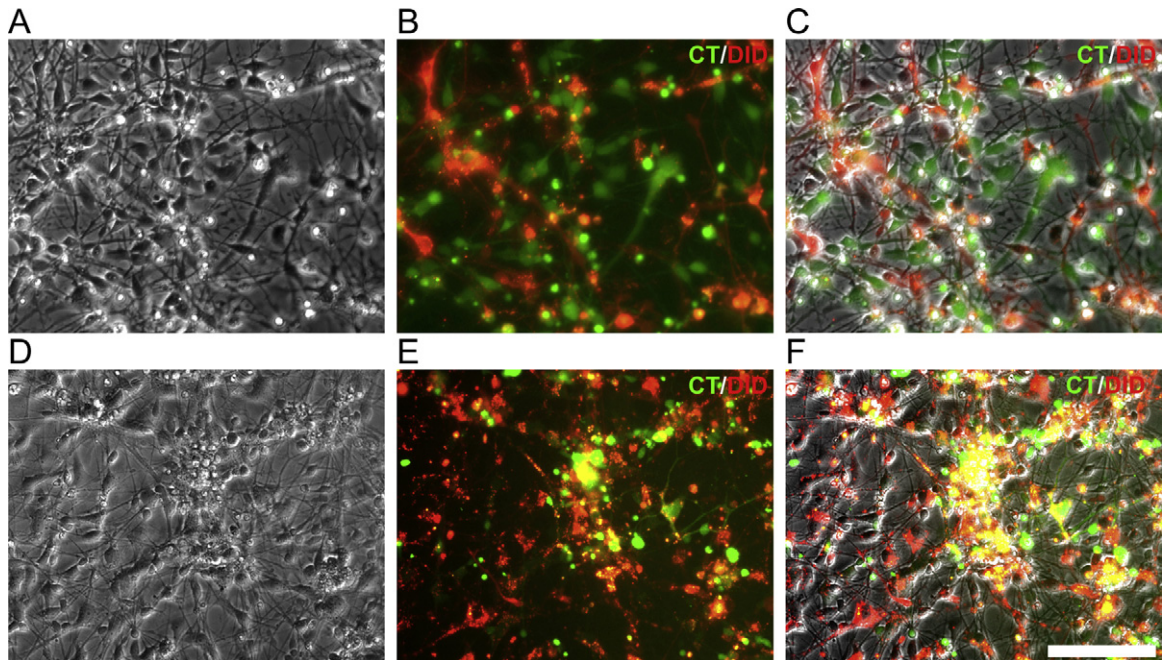


**Fig. 5.** Combined co-cultures of cells pre-labeled with CT (green) or DiD (red). (A–C) Four days after combining, the separately labeled cell populations could be easily detected. (A) A wide field image of the co-culture, (B) a corresponding fluorescent image from two channels, and (C) an overlay of the wide field and fluorescent images. (D–F) 17 days after combining the separate populations could still be detected. (D) A wide field image of the co-culture, (E) a corresponding fluorescent image from two channels, (F) an overlay of the wide field and fluorescent images. Scale bar 100  $\mu\text{m}$ .

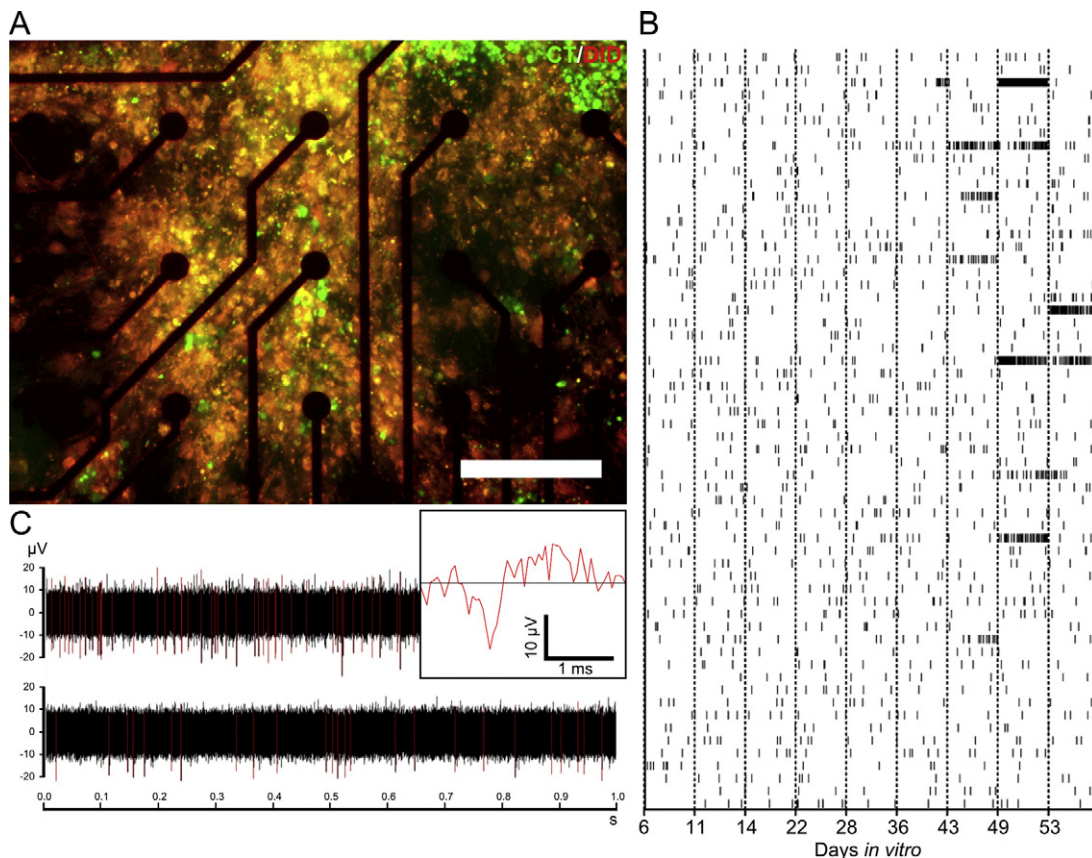


**Fig. 6.** Functionality of the neural network formed by mixed pre-labeled neural populations. (A) A dense network from cells stained with CT or DiD grew over microelectrode array. (B) Development of network activity from single spikes to spike trains during the culturing period of over 53 days. Each vertical tic represents a spike while each row represents activity from a single microelectrode. Measurement days are on the x-axis. (C) A close-up view of training from two adjacent electrodes. The red lines represent spikes. The shape of one spike is presented in larger time scale in the box in (C). The horizontal black line is 0 mV level. Scale bar in (A) is 100 μm.

probe became detectable for at least 4 weeks. Thus, at least with CT, it seems that the labeling parameters should be optimized according to the cell type. In their experiments [McMahon and McDermott \(2006\)](#), transplanted CT labeled radial glial cells and reported them to be traceable up to 20 days *in vivo*. Based on this, CT could also be feasible for *in vivo* studies.

With DiD, the 20 μM (19.2 μg/ml) working solution with 2 h incubation time was most suitable for hESC-derived neuronal cultures. Previously with neural applications, the probe concentration in working solution has typically been between 10 and 40 μg/ml and incubation times between 15 min and 2 h ([Honig and Hume, 1986, 1989](#); [Potter et al., 1996](#)). In this study, DiD probe was detectable for 4 weeks in hESC-derived neuronal cultures. The detectability of DiD fluorescence was quite similar to DiO and DiI as described earlier with embryonic chick neurons which were visible for three and half weeks *in vitro* ([Honig and Hume, 1986](#)). Previously, carbocyanine dyes (DiI, DiO, DiD, DiR and analogs) have been used to study neuronal architecture in animal derived fixed or living tissue ([Honig and Hume, 1986, 1989](#); [Matsubayashi et al., 2008](#)). In addition, DiI has been used to label rat neural cells for *ex vivo* transplantation studies ([Potter et al., 1996](#)) and to label human bone marrow fibroblasts crafted into mice or rat *in vivo* ([Ferrari et al., 2001](#)). The human fibroblast labeled with DiI (20 μM) were detectable in the craft after one month ([Ferrari et al., 2001](#)). This indicates that carbocyanine dyes are also suitable for *in vivo* applications.

The viability of hESC-derived neural cells was not changed few days after CT labeling with the optimal parameters. However, after longer period from CT labeling (>2 weeks) the proportion of dead

cells was larger even though no statistical differences were found. Based on this observation, CT might induce a decrease in the cell viability after several weeks. No literature assessing the viability effect of CT was found. CT did not affect the proliferation of hESC-derived neural cells as during experiments no trend with respect to post labeling period length was observed. Contradictory, CT labeling has previously been described to reduce the proliferation rate of rat olfactory ensheathing cells ([Pettersson et al., 2010](#)). The labeling performed by [Pettersson et al. \(2010\)](#) was performed with a lower CT concentration and shorter incubation time compared to our study. Because these gentler labeling parameters affected proliferation, it is possible that such effects are cell type dependent. Previously, CT has been described to label human cord blood stem cell-derived neurons, astrocytes, oligodendrocytes, and microglia ([Markiewicz et al., 2011](#)). In this study the percentage of CT labeled cells was observed not to reach 100%. This is most likely due to the easier visualization of DAPI stained nuclei compared to CT stained cell bodies from groups of tightly packed cells.

With the optimal labeling parameters DiD labeling did not affect the cell viability. In the literature, the carbocyanine dyes are also commonly described as non-harmful to different animal-derived cell cultures ([Honig and Hume, 1986](#); [Ferrari et al., 2001](#)). In this study some cytotoxic effects were seen when the cells were exposed to a high probe concentration, but this was not analyzed any further. In line, [Potter et al. \(1996\)](#) have also reported cytotoxic effects with neuronal cultures when exposed to high (40 μg/ml) probe concentrations for over 30 min. One previous study described that no differences in cell behavior was found between labeled and unlabeled chicken neural cell populations ([Honig and Hume,](#)

1986). In contrast, we found that the proliferation of the hESC-derived neural cells was decreased during long term culture after DiD labeling. The difference of observations might be due to different analysis method or differences in neural cell characteristics between two different species. Furthermore, when using these dyes with hESC-derived neurons the decrease in proliferation during long term culture needs to be taken into account.

All studied permeabilizations and primary antibody incubation times allowed the retention of CT and clear immunolabeling. CT was localized around virtually all DAPI stained nuclei. DiD was lost if permeabilization was performed with Triton-X. However, 0.1% Saponin permeabilization allowed DiD retention. Both MAP-2 positive neurons and GFAP positive astrocytes were found to be labeled by DiD. Thus, both probes labeled all cell types present in hESC-derived neural cultures. Previously, both probes used in this study or their analogs have been shown to label several cell types (Redelman et al., 1988; Ferrari et al., 2001; Heinrich et al., 2007; Matsubayashi et al., 2008; Markiewicz et al., 2011).

Dissociation of labeled adherent cultures did not cause visible intensity changes in CT or DiD labeling. Co-cultures of CT and DiD labeled cells grew as mixed cell networks. Hence, no obvious signs of self-organization caused by labeling with CT and DiD were observed. CT can be argued to be suitable for replating due to the observed retention of the dye in cells after replating. The effect of replating on the maximal visualization time, however, was not studied. Some of the co-cultured cells had both dyes in them after long term co-culturing. However, cells which were originally labeled with CT or DiD could be separated by visual inspection from cells which had taken up either of the dyes. Previous publications about carbocyanine dyes have not reported transfer from labeled population to unlabeled cells (Honig and Hume, 1986) although some dye transfer has been reported to take place *via* labeled cell debris in cultures (Potter et al., 1996). The co-localization of CT and DiD to same cells could be due to cells engulfing cell debris or parts of each other during close cell-cell interactions. To the best of our knowledge, no one else has studied the usage of dual fluorescent dye labeled neural cells in long term co-cultures *i.e.* during several weeks. One dual labeled co-culture system utilizing human cells has been described (Rizvanov et al., 2010). However, this work did not address the effects of dyes on cells and the culturing time was not mentioned (Rizvanov et al., 2010). Studying long term suitability of dyes for co-cultures is important, because it is desirable to visualize cells during long term culturing required for studying slow tissue formation processes as well as to be able to distinguish the cell populations after fixing the cultures for immunocytochemical characterization.

Co-cultures of CT and DiD labeled cells were able to develop network activity. Thus, the ability of hESC derived neurons to form functional neural networks is not compromised by CT and DiD labeling. Earlier Honig and Hume have reported that carbocyanine labeling does not affect the electrical properties of single chicken neurons (Honig and Hume, 1986). This is in line with our findings. To the best of our knowledge, our study is the first one to study the electrical functionality of fluorescent probe labeled human derived neuronal cell networks. The aspect of functionality is extremely important to consider when utilizing neural cells and aiming toward applications such as *in vitro* models, neurotoxicity studies or graft development. Thus, it is of high importance to note that labeling living cells with studied probes did not affect the formation of functional neural networks from hESC-derived neurons described earlier (Heikkilä et al., 2009). In functional neural tissue the signal is transmitted along cells *via* action potentials, and between cells *via* synaptic connections. MEAs can be used to make recordings of the action potentials in the network scale (Whitson et al., 2006). Subsequent network scale recordings allow the study of development of signal transmission in neural cultures (Wagenaar

et al., 2006). Thus, the network activity measured by MEA can be argued to demonstrate that separately CT and DiD labeled co-cultured neural cells are able fire action potentials and are able to form a functional network. However, the MEA methodology does not enable the direct study of synapses or detailed electrophysiological features of single cells (Whitson et al., 2006). Hence, nothing can be concluded about the formation of synapses between the two differently labeled cell populations or about subtle effects of these dyes on the electrophysiological properties of single cells. These aspects could be studied in the future by utilizing patch clamp or calcium imaging methods, and immunocytochemical staining against synaptic structures.

Here, we have shown that human pluripotent stem cell-derived neuronal cells can be labeled with two fluorescent probes, CT and DiD, without affecting the cells' viability (and with CT, proliferation), and most importantly their electrical functionality at network level. This study clearly shows, that live-labeling is possible and can be potentially helpful in many important applicative fields such as neuronal network formation studies for building *e.g.* neurotoxicity testing platforms or actual graft development. Presumably this method can also be used when studying these cells in biomaterials, however, the reactivity of CT chloromethyl moieties with protein thiols should be taken into account when staining cell cultures in biomaterials containing thiol groups.

## Acknowledgements

The personnel of IBT Stem cell unit is acknowledged for the support in stem cell research. This study was funded by Competitive Research funding of the Tampere University Hospital (Grant 9M064) and SpareBrain project, Academy of Finland (139345). These organizations were not involved in study design, execution, and manuscript preparation.

## References

- Althouse GC, Hopkins SM. Assessment of boar sperm viability using a combination of two fluorophores. *Theriogenology* 1995;43:595–603.
- Boyce S, Kelly E, Reavill C, Jenner P, Marsden C. Repeated administration of N-methyl-4-phenyl 1,2,5,6-tetrahydropyridine to rats is not toxic to striatal dopamine neurones. *Biochem Pharmacol* 1984;1:1747–52.
- Ferrari A, Hannouche D, Oudina K, Bourguignon M, Meunier A, Sedel L, et al. In vivo tracking of bone marrow fibroblasts with fluorescent carbocyanine dye. *J Biomed Mater Res* 2001;56:361–7.
- Heikkilä TJ, Ylä-Outinen L, Tanskanen JMa, Lappalainen RS, Skottman H, Suuronen R, et al. Human embryonic stem cell-derived neuronal cells form spontaneously active neuronal networks in vitro. *Exp Neurol* 2009;218:109–16.
- Heinrich L, Freyria A, Melin M, Tourneur Y, Maksoud R, Bernengo J, et al. Confocal laser scanning microscopy using dialkylcarbocyanine dyes for cell tracing in hard and soft biomaterials. *J Biomed Mater Res* 2007;81:153–61.
- Honig MG, Hume RI. Fluorescent carbocyanine dyes allow living neurons of identified origin to be studied in long-term cultures. *J Cell Biol* 1986;103:171–87.
- Honig MG, Hume RI. Dil and diO: versatile fluorescent dyes for neuronal labelling and pathway tracing. *Trends Neurosci* 1989;12:333–41.
- Jablonska A, Kozłowska H, Markiewicz I, Domanska-Janik K, Lukomska B. Transplantation of neural stem cells derived from human cord blood to the brain of adult and neonatal rats. *Acta Neurobiol* 2010;70:337–50.
- Lappalainen RS, Salomaki M, Ylä-Outinen L, Heikkilä TJ, Hyttinen JA, Pihlajamäki H, et al. Similarly derived and cultured hESC lines show variation in their developmental potential towards neuronal cells in long-term culture. *Regen Med* 2010;5:749–62.
- Markiewicz I, Sypecka J, Domanska-Janik K, Wyszomirski T, Lukomska B. Cellular environment directs differentiation of human umbilical cord blood-derived neural stem cells in vitro. *J Histochem Cytochem* 2011;59:289–301.
- Matsubayashi Y, Iwai L, Kawasaki H. Fluorescent double-labeling with carbocyanine neuronal tracing and immunohistochemistry using a cholesterol-specific detergent digitonin. *J Neurosci Methods* 2008;174:71–81.
- McMahon SS, McDermott KW. A comparison of cell transplantation and retroviral gene transfection as tools to study lineage and differentiation in the rat spinal cord. *J Neurosci Methods* 2006;152:243–9.
- Mishra A, Behera RK, Behera PK, Mishra BK, Behera GB. Cyanines during the 1990: a review. *Chem Rev* 2000;100:1973–2012.
- Packard BS, Karukstis KK, Klein MP. Intracellular dye heterogeneity determined by fluorescence lifetimes. *BBA Biomembr* 1984;769:201–8.



- Pettersson J, Lobov S, Novikova LN. Labeling of olfactory ensheathing glial cells with fluorescent tracers for neurotransplantation. *Brain Res Bull* 2010;81:125–32.
- Potter SM, Pine J, Fraser SE. Neural transplant staining with Dil and vital imaging by 2-photon laser-scanning microscopy. *Scanning Microsc Suppl* 1996;10:189–99.
- Rajala K, Hakala H, Panula S, Aivio S, Pihlajamäki H, Suuronen R, et al. Testing of nine different xeno-free culture media for human embryonic stem cell cultures. *Hum Reprod* 2007;22:1231–8.
- Rajala K, Lindroos B, Hussein SM, Lappalainen RS, Pekkanen-Mattila M, Inzunza J, et al. A defined and xeno-free culture method enabling the establishment of clinical-grade human embryonic, induced pluripotent and adipose stem cells. *PLoS ONE* 2010;5:e10246.
- Redelman D, Butler S, Robison J, Garner D. Identification of inflammatory cells in bovine milk by flow cytometry. *Cytometry* 1988;9:463–8.
- Rizvanov AA, Yalvaç ME, Shafigullina AK, Salafutdinov II, Blatt NL, Sahin F, et al. Interaction and self-organization of human mesenchymal stem cells and neuro-blastoma SH-SY5Y cells under co-culture conditions: a novel system for modeling cancer cell micro-environment. *Eur J Pharm Biopharm* 2010;76:253–9.
- Silverman AJ, Sutherland AK, Wilhelm M, Silver R. Mast cells migrate from blood to brain. *J Neurosci* 2000;20:401–8.
- Skottman H. Derivation and characterization of three new human embryonic stem cell lines in Finland. *In Vitro Cell Dev Biol* 2010;46:206–9.
- Wagenaar DA, Pine J, Potter SM. An extremely rich repertoire of bursting patterns during the development of cortical cultures. *BMC Neurosci* 2006;7:11.
- Whitson J, Kubota D, Shimono K, Jia Y. Multi-electrode arrays enhancing traditional methods and enabling network physiology. In: *Advances in Network Electrophysiology*. 2006 ed. Signapore: Springer; 2006:38–68.

# Three-dimensional growth matrix for human embryonic stem cell-derived neuronal cells

Laura Ylä-Outinen<sup>1,2,3</sup>, Tiina Joki<sup>1,2,3</sup>, Mari Varjola<sup>1,2</sup>, Heli Skottman<sup>1,2</sup> and Susanna Narkilahti<sup>1,2,3\*</sup>

<sup>1</sup>NeuroGroup, Institute of Biomedical Technology, University of Tampere, Tampere, Finland

<sup>2</sup>BioMediTech, Tampere, Finland

<sup>3</sup>The Science Center of Pirkanmaa Hospital District, Tampere University Hospital, Tampere, Finland

## Abstract

The future of tissue engineering applications for neuronal cells will require a supportive 3D matrix. This particular matrix should be soft, elastic and supportive for cell growth. In this study, we characterized the suitability of a 3D synthetic hydrogel matrix, PuraMatrix™, as a growth platform for human embryonic stem cell (hESC)-derived neural cells. The viability of the cells grown on top of, inside and under the hydrogel was monitored. The maturation and electrical activity of the neuronal networks inside the hydrogel were further characterized. We showed that cells stayed viable on the top of the PuraMatrix™ surface and growth of the neural cells and neural processes was good. Further, hESC-derived neurons, astrocytes and oligodendrocytes all grew, matured and migrated when cultured inside the hydrogel. Importantly, neuronal cells were able to form electrically active connections that were verified using microelectrode array. Thus, PuraMatrix is a good supportive growth matrix for human neural cells and may serve as a matrix for neuronal scaffolds in neural tissue engineering. Copyright © 2012 John Wiley & Sons, Ltd.

Received 17 May 2011; Revised 30 January 2012; Accepted 4 February 2012

**Keywords** astrocytes; encapsulation; hydrogel; neural tissue engineering; neuronal network activity; oligodendrocytes; PuraMatrix

## 1. Introduction

Currently, there is much hope in the field of cell therapy for central nervous system (CNS) deficits. Specifically, stem cells are seen as a potential source for new regenerative therapies. Human embryonic stem cells (hESC) are considered to have significant potential in transplantation therapies; they have been successfully differentiated into neuronal cells, astrocytes and oligodendrocytes (Lappalainen *et al.*, 2010; Sundberg *et al.*, 2010). In addition to transplantation therapies, these cells can be used for *in vitro* toxicity and drug testing as well as developmental studies (Johnstone *et al.*, 2010; Ylä-Outinen *et al.*, 2010a, b; Zeng *et al.*, 2006). Another potential cell source for neural applications are human induced pluripotent stem (hiPS) cells. These cells are pluripotent (similar to hESCs) and are derived/created directly from the patient's own somatic cells (Hu *et al.*, 2010; Takahashi *et al.*, 2007). hiPS cells

are seen as a potential for patient specific drug screening platforms as well as for future treatments (Hu *et al.*, 2010). These cells have been successfully differentiated into neuronal cells that can form spontaneously active neuronal networks and thus resemble their hESC-derived counterparts (Hu *et al.*, 2010; Äänismaa *et al.*, 2011). As a result, neural cells *in vitro* should be studied in more tissue-like environments (such as in 3D) to mimic native cell behaviour as much as possible.

*In vivo* experiments have shown that cell transplantations alone are insufficient to support regeneration in the host tissue. After transplantation, the viability of the cells is often poor (Hicks *et al.*, 2009; Oizumi *et al.*, 2008). Typically after severe CNS trauma, the cavity at the injury site does not support the viability of transplanted cells and is slowly filled with glial scar preventing regeneration of the functional tissue (Hejcl *et al.*, 2008; Nisbet *et al.*, 2008; Zhong and Bellamkonda, 2008). Therefore, the presence of a structural support preventing scar formation on the injury site is important and has been shown to be achievable with biomaterials (Hejcl *et al.*, 2008; Nisbet *et al.*, 2008). In addition, in cases of allogeneous cell grafts, the transplantation is associated with graft

\*Correspondence to: Susanna Narkilahti, Institute of Biomedical Technology, University of Tampere, Biokatu 12, 33520 Tampere, Finland. Tel: + 358 40 708 5113, Fax: + 358 3 3551 8498. E-mail: susanna.narkilahti@uta.fi

rejection, which is currently counteracted with high doses of immunosuppressive medications that can cause harmful side-effects (Li and Zhong, 2009). Thus, more sophisticated tissue-engineering designs combining both cells and supportive biomaterial scaffold could offer solutions to overcome most of the challenges seen in current cell transplantation methods.

Biomaterials for neural tissue engineering should be non-toxic, three dimensional, support the growth of the desired cell type and allow nutrition flux (Holmes *et al.*, 2000; Thonhoff *et al.*, 2008). Materials should also allow cell migration and interaction with the host tissue. Material scaffolds could also be engineered to release cell supportive substances such as growth factors or allow the local release of immunosuppressant (Lindvall and Kokaia, 2010; Zhong and Bellamkonda, 2008) Hydrogels are potential materials for CNS deficits because they are highly porous, can form 3D structures *in vitro* and/or *in vivo* and can fill the cavity and thus prevent the formation of glial scars (Hejcl *et al.*, 2008). Only a few 3D hydrogels have been studied in combination with neuronal cells: Matrigel (Thonhoff *et al.*, 2008), PuraMatrix™ (PM) (Gelain *et al.*, 2006; Thonhoff *et al.*, 2008), hyaluronic acid (Brännvall *et al.*, 2007), polyethylene glycolide) derivatives (Freudenberg *et al.*, 2009) and chitosan (Leipzig *et al.*, 2010). Although these materials have been shown to support growth of neuronal cells, not all are suitable for clinical use such as Matrigel which is of mouse origin and not is a defined natural product.

As for hyaluronic acid and chitosan, they have only been tested with animal-derived neural cells and not with human neural cells (Brännvall *et al.*, 2007; Leipzig *et al.*, 2010). PM and Matrigel, on the other hand, have been shown to be biocompatible with human fetal stem cell-derived neuronal cells (Thonhoff *et al.*, 2008). PM is a synthetic peptide nanofibrous hydrogel whose composition is fully known and controlled (Zhang *et al.*, 2005). It consists of peptide sequence RADA16 and its modification with functional groups has been studied (Zhang, 2002). Nevertheless, whether PM actually supports long-term survival of encapsulated human neuronal cells and whether those cells are able to mature into functional neurons has not been addressed. The aim of the current study was to determine whether hESC-derived neurons, astrocytes and oligodendrocytes could survive on top, encapsulated in, or under PM for prolonged periods. We also examined whether these cells could mature into spontaneously active neurons/neuronal networks inside the 3D structure. Results showed adequate cell survival and functionality using PM hydrogel.

## 2. Materials and methods

### 2.1. hESC and neural differentiation

Two hESC lines derived at the Regea-Institute for Regenerative Medicine, Regea 06/040 and Regea 08/023,

were used in this study. Regea, current IBT, has ethical approval by the Pirkanmaa Hospital District to derive, culture and differentiate hESCs (Skottman, R05116) and permission was obtained from the National Authority for Medicolegal Affairs (Valvira, 1426/32/300/05) to conduct human stem cell research.

hESCs grown as colonies were mechanically cut into smaller pieces and placed into suspension culture in differentiation media, and neuronal and astrocytic differentiation was performed as described previously (Lappalainen *et al.*, 2010). Neural differentiation medium (NMD) was used containing 1:1 DMEMedium/F12 (Gibco®, Invitrogen, Finland) and neurobasal medium supplemented with 2 mM GlutaMax™, 1 x B27, 1 x N2 (all from Gibco), 20 ng/ml fibroblast growth factor (bFGF, R&D Systems, Minneapolis, MN, USA) and 25 U/ml penicillin/streptomycin (Cambrex, Belgium). The small cell aggregates formed neurospheres in suspension culture as previously described (Lappalainen *et al.*, 2010). The medium was changed three times per week and the spheres were mechanically dissected once a week. Neurospheres were cultured for eight weeks to gain pure neuronal population and for 20 weeks to gain astrocytic population. During these differentiation periods, cell populations differentiated into neuronal or astrocytic lineages (Lappalainen *et al.*, 2010; Sundberg *et al.*, 2009). Moreover, additional hESC colony pieces were cultured as suspension culture in oligodendrocyte precursor cell (OPC) differentiation medium (OPCDM). The OPC differentiation procedure has been described (Sundberg *et al.*, 2010). Briefly, OPC differentiation was initiated in suspension culture in N2 medium [DMEM/F-12 medium with 1 x N2, 2 mM GlutaMax, 0.6% glucose, 5 mM HEPES, 2 µg/ml heparin (all from Sigma-Aldrich)] as well as 25 U/ml penicillin and streptomycin supplemented with 10 ng/ml human ciliary neurotrophic factor (CNTF), 20 ng/ml human epithelial growth factor (EGF) and 20 ng/ml bFGF (R&D Systems Europe) for four weeks. Next, for the following three weeks, cells were cultured in N2 medium containing 10 ng/ml CNTF, 20 ng/ml EGF, 10 ng/ml bFGF, 100 ng/ml insulin-like growth factor-1 (Sigma-Aldrich), 20 ng/ml platelet-derived growth factor-AA (Peprotech Inc.) and 1 µg/ml laminin (Sigma-Aldrich). Then, cells were encapsulated to the PM scaffold and finally, OPCDM [N2 medium supplemented with 200 µM L-ascorbic acid 2-phosphate (Sigma-Aldrich), 10 ng/ml CNTF and 40 ng/ml 3,3',5-triiodo-L-thyronine (Sigma-Aldrich)] was used as the culture medium for OPCs.

### 2.2. Preparation of the hydrogels and cell culture setups

Synthetic self-assembled PM (BD Bioscience, Sparks, MD, USA) was used as hydrogel scaffold. The hydrogel was used in concentrations of 0.05%, 0.10%, 0.15% and 0.25%. Cells were seeded either 1) on top of the gelled material, 2) encapsulated into the hydrogel or 3) under the hydrogel (hydrogel added on top of the cells first grown on top of the laminin for one week). Results from

### 3D culturing matrix for human neuronal cells

the 3D cultures were compared to 2D control in which cells were cultured on the laminin (10 µg/ml, Sigma-Aldrich) surface, a standard culture matrix (Lappalainen *et al.*, 2010). A non-coated cell culture polystyrene (CCPS) was used as a negative control. After differentiation periods, cells were either dissociated into single cell suspension with Trypsin (Sigma-Aldrich) or mechanically cut into smaller cell aggregates ( $\varnothing \sim 100 \mu\text{m}$ ). For single cell suspension, 1 x Trypsin was added on top of the neurospheres and incubated for 5 min. Trypsin was inactivated with 5% human serum (Sigma-Aldrich) and the single cell suspension was washed with NDM or OPCDM. Cell aggregates were cut with a scalpel and placed in NDM or OPCDM.

#### 2.2.1. Preparation of the hydrogel surfaces

The PM was gelled according to manufacturer instructions. Briefly, the stock solutions were diluted into concentrations of 0.05%, 0.10%, 0.15% or 0.25% with sterile water and added to the cell culture wells (140 µl/cm<sup>2</sup>). Cell culture medium was gently added on top and the solution was left to form a gel at 37 °C for 30 min. During that period, cell culture medium was changed three times. After gelation, the single cell suspension and cell aggregates were plated onto hydrogel surfaces for 2D culture on top of the hydrogel.

#### 2.2.2. Preparation of encapsulated cells

For encapsulation, cells were mixed with PM resulting in a final cell density of 1 x 10<sup>6</sup> cells in 1 ml 0.10% hydrogel. First, the cells were mixed with 10% sucrose. This solution was mixed in 1:1 ratio with PM that was first diluted to 0.20% solution in 20% sucrose. Then, the cell culture medium was pipetted on top of the cell/PM solution to initiate the gelation process. The spontaneously formed gels had non-uniform layer height ranging from 500 µm (centre of the well) to 1000 µm (edges of the well).

#### 2.2.3. Preparation of cells embedded with hydrogel

First, cells were plated onto a 10 µg/ml laminin-coated CCPS in small cell aggregates and cultured in NDM for three days. During that time, neuronal outgrowth was prominent. The hydrogel solution was prepared as above in sterile water before adding it on top of the cells. Gelation was initiated by gently adding NDM. In addition, cells were seeded onto laminin- (10 µg/ml) coated CCPS wells, which served as a positive growth matrix control. Cells seeded on non-treated wells were used as a negative growth matrix control. Cells were cultured as described for four weeks.

### 2.3. Time-lapse monitoring

For time-lapse imaging, the well-plate was transferred into a Cell-IQ<sup>®</sup> imaging system (Chip-man Technologies Ltd., Tampere, Finland), which allowed for continuous

monitoring of selected cells as described previously (Narkilahti *et al.*, 2007). The sealed culture well-plate was placed in a chamber (36.5 °C) with 5% CO<sub>2</sub> and imaged continuously except during medium changing periods (< 15 min, three times/week). Cells grown on top of, in, or under the hydrogel were monitored for up to two weeks using this system.

### 2.4. Cytotoxicity analysis

After seven days of culture, the cells on the top or under the hydrogels and the 2D controls were stained using the LIVE/DEAD<sup>®</sup> Viability/Cytotoxicity Kit for mammalian cells (Molecular Probes/Invitrogen, Finland). Briefly, the kit stained live cells with green fluorescence dye calcein-AM (emission at 488 nm) and dead cells with red fluorescence dye ethidium homodimer-1 (emission at 568 nm). Cells were incubated with calcein-AM (0.1 µM) and ethidium homodimer-1 (0.5 µM) for 30 min and immediately imaged with an Olympus IX51 inverted microscope and an Olympus DB71 digital camera (Olympus, Finland).

### 2.5. Immunostaining

For immunocytochemistry, cells were fixed with 4% paraformaldehyde (Fluka, Italy) after four weeks of culture and stained with neural markers. Briefly, unspecific staining was blocked with 10% normal donkey serum (NDS), 0.1% Triton-X 100 and 1% bovine serum albumin (BSA) (all from Sigma-Aldrich) for 45 min at room temperature. Cells were then washed once with 1% NDS, 0.1% Triton-X and 1% BSA. Thereafter, the following primary antibodies were incubated with cells at 4 °C overnight: rabbit anti-microtubule associated protein MAP-2 1:800 (Chemicon International, Millipore, Massachusetts, MA, USA); mouse anti-neurofilament 200 kD (Sigma-Aldrich); monoclonal mouse anti-β-tubulin isotype III (β-tub, 1:1250 Sigma-Aldrich) or sheep anti-human glial fibrillary acidic protein antibody (GFAP, 1:800 R&D systems); chondroitin sulfate proteoglycan (NG-2, 1:200, Chemicon, protocol without Triton-X); and galactocerebroside (GalC, 1:400 Chemicon, protocol without Triton-X) in 1% NDS, 0.1% Triton-X and 1% BSA. The following day, cells were washed three times with 1% BSA and the following secondary antibodies were added for 1 h at room temperature: Alexa Fluor<sup>®</sup> 488 (Invitrogen) conjugated to anti-rabbit, anti-mouse or anti-sheep (1:400, Molecular Probes) in 1% BSA. Finally, cells were washed three times with PBS and twice with phosphate buffer and mounted with VECTASHIELD<sup>®</sup> containing 4',6-diamidino-2-phenylindole (DAPI, Vector Laboratories, England).

### 2.6. Confocal imaging

The encapsulated cells were cultured four weeks prior to confocal imaging. Confocal images were taken with an LSM 700 confocal microscope (Carl Zeiss, Jena, Germany)

using a 40x air objective. Stack images were taken in 1  $\mu\text{m}$  range for a total 70  $\mu\text{m}$  thickness. The visualization of confocal data was performed with a Zen2009 (Carl Zeiss) or BioImageXD (www.bioimagexd.net).

## 2.7. Electrophysiological measurements

In addition, differentiated neuronal cells encapsulated into the hydrogel matrix were plated onto microelectrode array (MEA) plates (Multi Channel Systems, MCS, Reutlingen, Germany). Extracellular field potentials from electrically active neural cells can be measured with MEA. MEA is non-invasive and suitable for prolonged and continuous measurements, and allows measurements at neuronal network level. Thus, MEAs provide activity information of the neural cell population both in spatial and temporal levels (Potter and DeMarse, 2001; Wagenaar *et al.*, 2006).

Each standard MEA plate contained 59 titanium nitride measurement electrodes (30- $\mu\text{m}$  diameter, 200- $\mu\text{m}$  inter-electrode distance). For liquid container and cell seeding areas, electrode areas were separated with in-house polydimethylsiloxane (PDMS) structures designed and manufactured by J. Kreutzer and P. Kallio, Tampere University of Technology, Department of Automation Science and Engineering, Finland. Control MEA plates were coated with a two-step coating procedure: overnight incubation with

polyethyleneimine (PEI, Sigma-Aldrich, 0.05% w/v, incubation 4°C) followed by washing with sterile water, and overnight incubation with mouse laminin (Sigma-Aldrich, 20  $\mu\text{g}/\text{ml}$ , incubation 4°C). Thereafter, neuronal cells were plated as aggregates onto laminin-coated MEA plates for 2D standard control. The cell culture medium was changed three times/week and MEAs were measured with a MEA1060-Inv-BC amplifier (MCS). To keep the temperature at 37°C during measurements, a TC02 temperature controller (MCS) was integrated into the system. Data were recorded with MC\_Rack software (MCS). Continuous extracellular field potential data were collected at a 20 kHz sampling rate and post-acquisition filtered with a 200 Hz high-pass filter. MEA data showed electrical activity of neuronal cells at the network level as well as spatially. Spatio-temporal field potential data were post-recording processed with MC Datatool (MCS) and MATLAB (MathWorks, Natick, MA, USA).

## 2.8. Statistical analysis

For statistical analysis, cells were calculated from at least three parallel samples with at least five images/sample, and at least 50 cells were counted/figure, except for the non-coated CCPS where the cell amount was extremely small. Data were analysed with SPSS 19

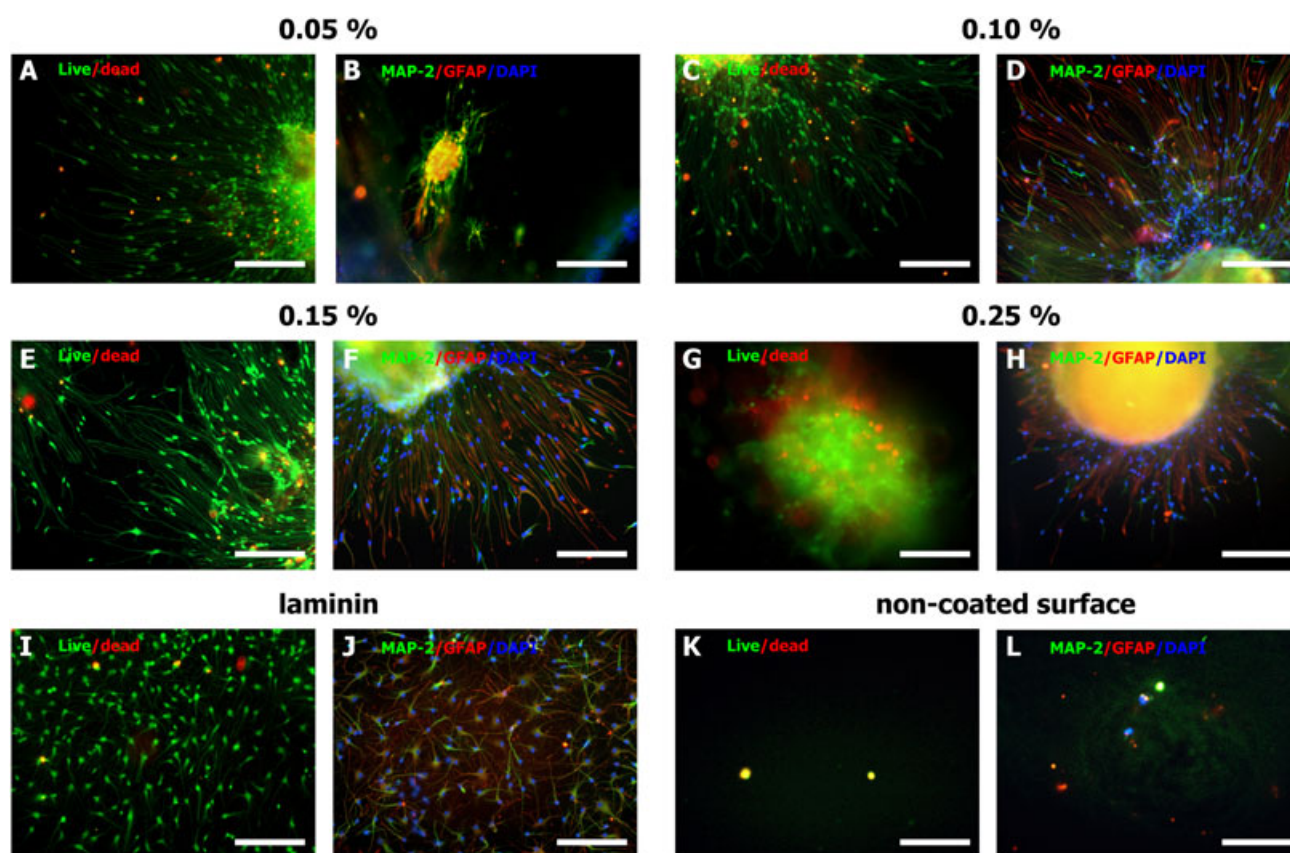


Figure 1. Effect of hydrogel concentrations on cell viability and differentiation. Neuronal cells cultured on top of the PuraMatrix™-hydrogel at concentrations 0.05% (A-B), 0.10% (C-D), 0.15% (E-F) and 0.25% (G-H). Cells cultured on top of laminin coating (I-J) and non-coated cell culture plastic (K-L) were used as reference. In each condition, LIVE/DEAD-analysis (A,C,E,G,I,K) and immunostaining (B,D,F,H,J,L) were performed. Immunostaining: MAP-2 = green, GFAP = red, and DAPI = blue. The scalebar is 100  $\mu\text{m}$

### 3D culturing matrix for human neuronal cells

software (SPSS Inc., Chicago, USA) using the Kruskal-Wallis non-parametric test followed by *post-hoc* comparison by Mann-Whitney U-test. A *p*-value (corrected with alpha spending function) of  $< 0.05$  was considered significant.

## 3. Results

### 3.1. Cells cultured in different hydrogel concentrations

To optimize the hydrogel concentration to support the hESC-derived neuronal and astroglial cells, four different hydrogel concentrations were used: 0.05%, 0.10%, 0.15% and 0.25% (Figures 1A-B, C-D, E-F and G-H, respectively). Moreover, cells were cultured on a laminin surface (Figure 1I, J) and non-coated CCPS (Figures 1K, L). Cells were cultured for two weeks on the top of the hydrogel and then either stained with LIVE/DEAD kit or immunostained against MAP-2 and GFAP. Viability of the cells was good on the top of the hydrogel (Figures 1A, C, E, G,) compared to the laminin surface (Figure 1I). On the non-coated CCPS, the cells did not attach and thus there were only few dead cells left (Figure 1K). Statistical analysis showed significant differences in cell survival between non-coated CCPS and all other conditions (gels in densities of 0.05%, 0.10%, 0.15% or 0.25%, or 2D laminin surface) (Figure 2A). Cell survival was, however, equally good in all conditions when compared to the 2D laminin control (Figure 2A). According to Figures 1G and H, it can be observed that the 0.25% density did not support neuronal migration as prominently as the lower concentrations. The best outgrowth was observed on 0.10% hydrogel (Figures 1C, D).

For more detailed characterization, cells were seeded on top of the gels at the same densities and were allowed to grow and differentiate for two weeks. Thereafter, cells were stained against MAP-2 for neuronal cells and GFAP for glial cells, and percentages of neurons vs. glial cells in the gels were calculated. The best neuronal cell ratio and cell survival was found in the 0.10% gel structure (Figure 2B). In addition, 0.05% and 0.10% gels supported neuronal cell maturation significantly better than astrocytic maturation (Figure 2C). Based on these results, 0.10% PM was chosen for the next experiments.

### 3.2. Viability of cells under the hydrogel

The viability of the neuronal cells under the hydrogel was evaluated by LIVE/DEAD assay. Cells were plated on laminin-coated cell culture wells and cultured for one week, during which time the cells were viable and neuronal outgrowth was prominent in all the wells. Next, the 0.10% PM hydrogel was added on top of the cells and cells were stained after one week. According to cell viability analysis, cell survival was poorer under the hydrogel (Figure 3A) compared to the 2D culture control on

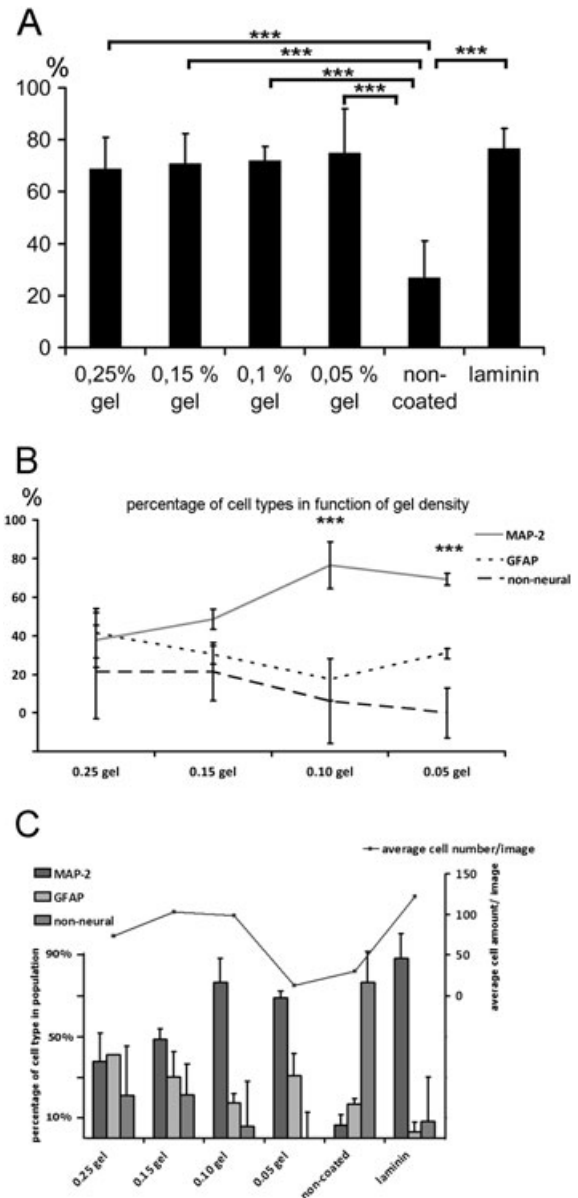


**Figure 2.** Viability and phenotype of the cells inside the PuraMatrix hydrogel and control conditions. LIVE/DEAD analysis shows the proportions of the viable cells from each population (A). Significant difference was detected between negative control (un-treated polystyrene surface) and other conditions (different gel concentrations and laminin treated surface). Total amount of attached cells and percentages of different neural cell types are illustrated according to gel concentration (0.25%, 0.15%, 0.10% and 0.05%) or control conditions (non-coated well-plate surface and laminin-treated surface) (B). Percentages of different cell types in correlation to cell density (C). Significant differences detected between MAP-2 positive cells and GFAP and non-neural cell types in densities 0.10% and 0.05%. Bars are average values and error bars represent standard deviation for all illustrations. Significance:  $***: p < 0.05$

laminin (Figure 3B). However, the neuronal neurites did not withdraw under the gel compared to those without gel (Figure 3C vs. D). Moreover, live cells spread from the cell aggregates and grew long neurites under the hydrogel.

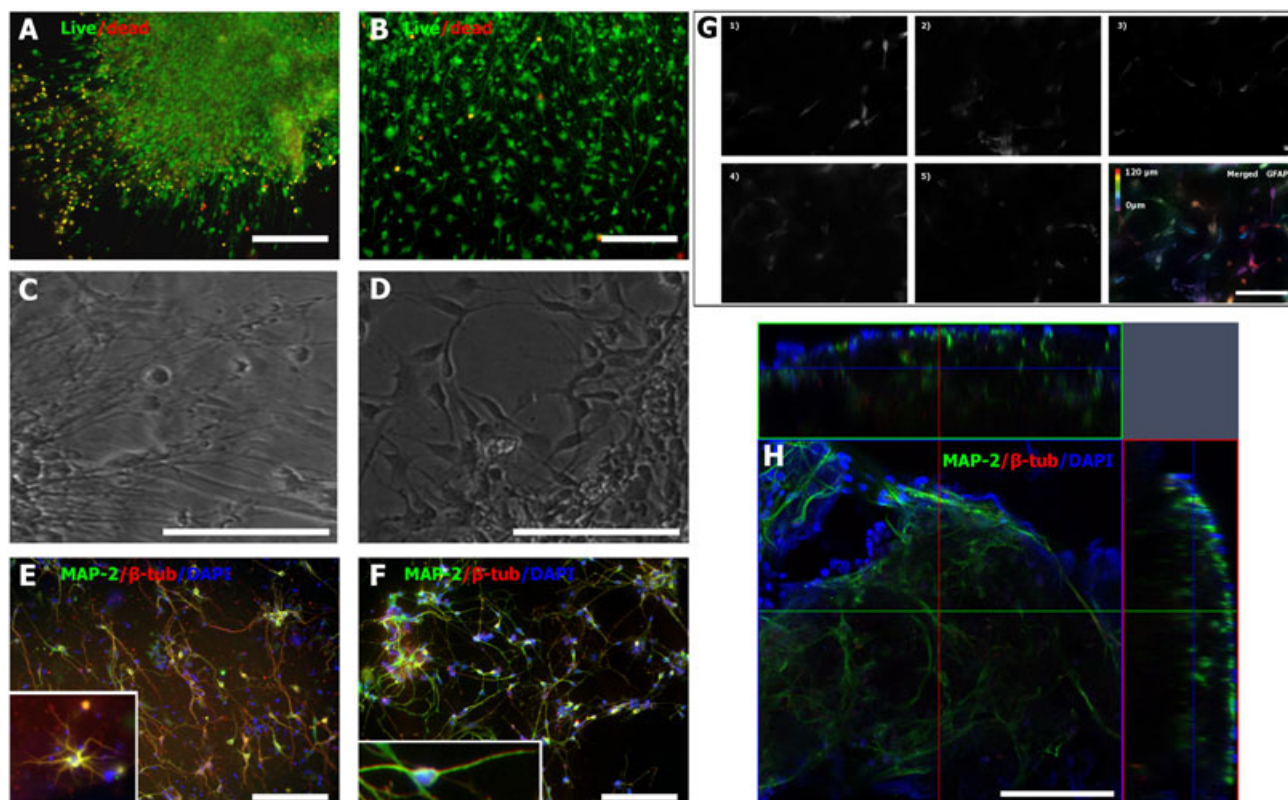


Figure 3. Cell survival under the hydrogel and maturation inside the hydrogel. Cells that were cultured first on the top of laminin (1 week), then covered by PuraMatrix™ after 7 days (C) and stained with LIVE/DEAD assay (A). Laminin cultured cells as a control in Live/Dead analysis (B) and after 2 weeks of culture (D). Network formation and morphology of the 4-week cultured cells inside the hydrogel (E) and on top of the laminin coating (F). Layer-by-layer reconstruction from MAP-2 positive cells shows cells growing in different z-levels (G) inside the gel. Confocal imaging analysis by orthogonal sectioning from 4-week cultured neuronal cells (H). Confocal image: stack with 1  $\mu\text{m}$  intervals, total of 70  $\mu\text{m}$  thickness of hydrogel scaffold structure. Scalebars = 100  $\mu\text{m}$

### 3.3. 3D growth and maturation of encapsulated cells

In 3D culture, cells were fully surrounded by hydrogel material, thus providing a more *in vivo*-like environment for the cells. This affected the migration of the cells as well as the probability for cell-cell interactions and therefore the neuronal network forming capacity. We evaluated the maturation of the cells inside the hydrogel with fluorescence and confocal microscopy. The neurons seemed to have more *in vivo*-like phenotype, including more branched and thicker dendritic processes inside the hydrogel (Figure 3E) compared to laminin surface-grown cells (Figure 3F). Cells were spread over the entire hydrogel. Figure 3G shows layer-by-layer reconstruction of stack images that illustrate the cells in various z-levels. Moreover, rendered confocal z-stack images in orthogonal sections (Figure 3H) show that during prolonged culture time in 3D, the neuronal somas translocated close to the surface of the PM scaffold, while an intensive MAP-2 positive neuronal process network was visible over the entire hydrogel structure.

### 3.4. Suitability of the hydrogel matrix for glial cell types

The different glial cell types of hESC-origin as well as astrocytes and oligodendrocytes were cultured inside the

PM hydrogel. Even though there was significant cell death observed in the long-term 3D cultures (total of four weeks), both cell types remained alive inside the hydrogel (Figures 4 A, B). More detailed phenotypical analysis of astroglial and oligodendrocyte precursor markers showed that cells kept their phenotype in gel (Figures 4C, D).

### 3.5. Neuronal network-forming capability inside the 3D hydrogel

We evaluated the neuronal network-forming capability inside the PM gel on the MEA platform. The action potentials of the cells were detected with 59 small electrodes on the bottom of the cell culture dish (Figure 5A). The neurons inside the gel were able to form active spontaneously firing networks (Figure 5B) similarly to 2D cultures (Figure 5C). The forming of spontaneous network activity inside the gel took  $\sim 4$  weeks to develop into spike train-like activity whereas in the control, this activity level was achieved in two weeks. None of the cultures monitored, however, developed into synchronous bursting level activity, considered as the final maturation stage of *in vitro* cultured neuronal networks. Both cultures showed training-like electrical activity (Heikkilä *et al.*, 2009) after four weeks culture in MEA plates (Figures 5B, C).

### 3D culturing matrix for human neuronal cells

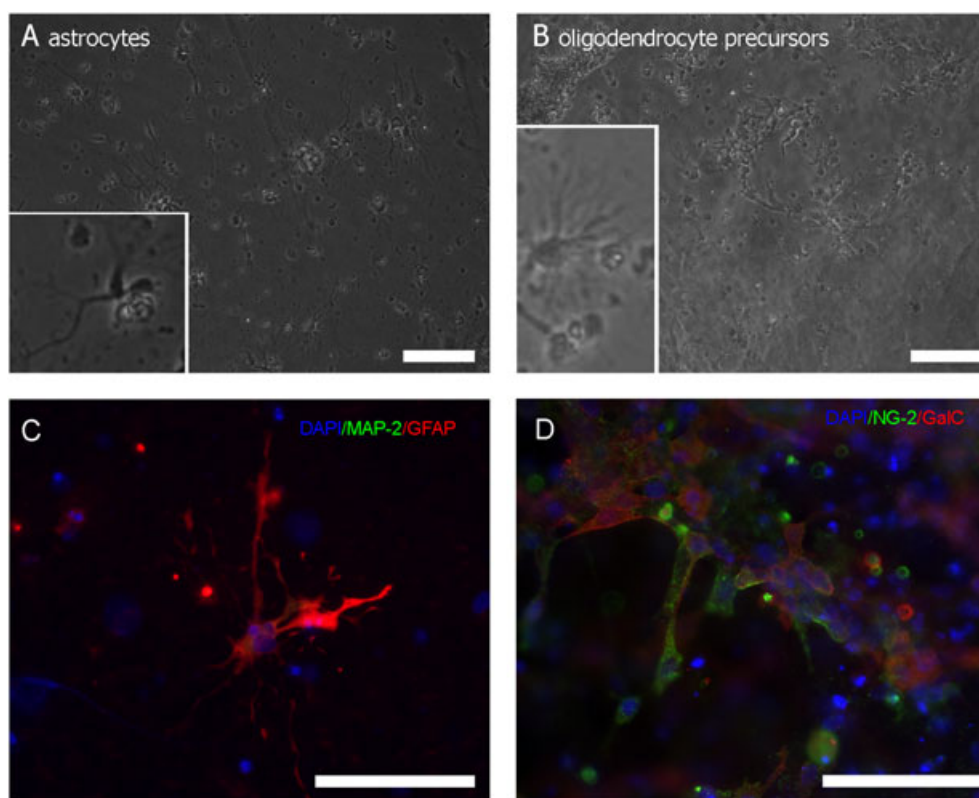


Figure 4. Glial cell culture inside the hydrogel. Astrocytes (A) and oligodendrocyte precursor cells (B) cultured inside the PuraMatrix™-hydrogel. Both cell types retain their typical morphology (enlarged images) in the hydrogel. (C) Immunocytochemical characterization of astroglial cells with MAP-2 (for neuronal cells) and GFAP (for astrocytic cells) inside the gel. (D) Immunocytochemical characterization of oligodendroglial cells with NG-2 and GalC inside the gel. Scalebars for background images are 100  $\mu\text{m}$

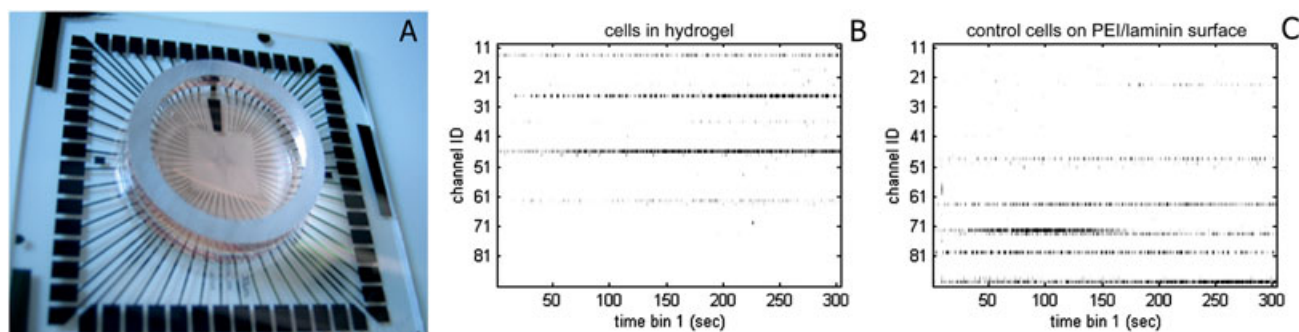


Figure 5. Microelectrode array dish (A). Microelectrode array dish is a cell culture well containing substrate-embedded tiny electrodes on the bottom. Cells encapsulated to hydrogel were added on top of the electrodes and cultured for several weeks. Array wide raster plot is shown from the cells inside the gel (B) and from the laminin surface cultured cells (C). In raster plot, each recorded channel is represented in y-axis and time (300 s) in x-axis. Each raster shows the detected spike. Both networks in raster plots (B, C) show typical training-like activity in several channels

## 4. Discussion

In this study, we showed for the first time the functionality of human-derived neuronal cells in a 3D *in vitro* environment. We evaluated the viability, growth, maturation and electrical activity of clinically relevant human neural cell types in prolonged 3D cultures. We showed that neural cells, i.e. neurons, astrocytes and oligodendrocytes, were viable under the PM hydrogel. In a 3D environment, neuronal cells developed more branched neurite structures compared to 2D culture and thus appeared to better

resemble their *in vivo* counterparts. Moreover, 3D cultured neurons were able to form spontaneously functional networks inside the 3D matrix.

Recently, 3D cultures have been developed for *in vitro* models and for studies related to transplantation therapies. Interconnected neuronal networks in 3D better mimic the *in vivo* environment compared to 2D cultures (Pautot *et al.*, 2008). Thus, they can be used in developmental brain research, in the development of tissue-based biosensors, or neurotoxicological and pharmacological *in vitro* models (Preynat-Seauve *et al.*, 2009; Xu *et al.*, 2009). The brain is composed mainly of relatively soft



tissue with elastic modulus of  $\sim 500$  Pascal (PA) (Lu *et al.*, 2006); it has already been shown that a 3D matrix should have similar characteristics for supporting neural growth and differentiation (Saha *et al.*, 2008; Teixeira *et al.*, 2009). Furthermore, hydrogels offer good options for reconstructing 3D environments suitable for neuronal cells (Brännvall *et al.*, 2007; Gelain *et al.*, 2006) and it has been shown that animal-derived neuronal cells remain viable, grow and mature in a 3D hydrogel environment (Brännvall *et al.*, 2007; Freudenberg *et al.*, 2009; Leipzig *et al.*, 2010). We tested PM in concentration ratios from 0.05% to 0.25% to determine the optimal 3D culture parameters. It has been shown that 0.25% PM supports neuronal differentiation of human fetal stem cells (Thonhoff *et al.*, 2008) whereas for hESC-derived neuronal cells, the optimal concentration seems to be to 0.10% according to our results. This concentration relates approximately to the elastic modulus of 1200 Pa according to earlier studies (Leon *et al.*, 1998; Yamaoka *et al.*, 2006). However we were unable to obtain a better culture in a 3D environment similar to that for 2D, as suggested in a recent study using the same materials and immortalized human fetal stem cells (Ortinou *et al.*, 2011). This might be explained by the much longer follow-up period in our study and also by the composition of the cell population, which in our case, contained mainly neurons vs. glial cells, which is contradictory to a study by Ortinau and colleagues (2011).

Previous studies have shown that neural 3D cultures using hydrogels were prepared by growing cells under, inside, or on top of the hydrogel (Gelain *et al.*, 2006; Thonhoff *et al.*, 2008). In the current study, we showed that hESC-derived neuronal cells not only can be grown but were viable under, inside, and on top of a 0.10% PM hydrogel. In contrast to a recent study (Ortinou *et al.*, 2011), we did not observe any benefits to functionalization of the hydrogel with laminin (data not shown). This is similar to the lack of benefits of functionalization of polylactide meshes for hESC-derived neuronal cultures (Ylä-Outinen *et al.* 2010b). This suggests that a thin nanoscale mesh-like structure is sufficient to support growth and maturation of hESC-derived neuronal cells. Culturing cells encapsulated inside hydrogel is important when designing products for transplantation since the graft should be injectable to enable simple surgical procedures to the CNS tissue (Zhong and Bellamkonda, 2008). The 0.10% PM in the current study also supported growth of encapsulated glial cells (astrocytes and oligodendrocytes), which is beneficial for developing multiple cell type 3D *in vitro* models or cell grafts (Park *et al.*, 2009; Taylor *et al.*, 2005).

There have been few studies comparing the differences between 2D and 3D cultures in genotype (Li *et al.*, 2007) and morphological and phenotypical levels (Crompton *et al.*, 2007; Ortinau *et al.*, 2011; Thonhoff *et al.*, 2008), and very few describing the functional properties of 3D cultured neurons (Mahoney and Anseth, 2006; Xu *et al.*, 2009). Unfortunately, it is difficult to estimate differences between 2D and 3D cultures when the control 2D cells have been cultured in plain polystyrene and not on

laminin or other coated surfaces that favour neuronal attachment and growth. In addition, 3D culture times have been relative short, which does not favour neuronal maturation (Ortinou *et al.*, 2011); thus, longer follow-up periods are clearly needed (Pautot *et al.*, 2008). In our study, we followed the formation of neuronal networks inside the PM gel for up to four weeks. Importantly, the neurons remained alive and were able to form networks that were spontaneously active inside the gel, as described in 2D (Heikkilä *et al.*, 2009). Confocal imaging revealed that neurons did re-organize themselves during the four weeks as the somas aligned near the upper surface close to the medium, whereas neurites formed intensive networks inside the gel. Moreover, most of the encapsulated cells differentiated into neurons. This further suggests that hESC-derived neuronal cells grown in 3D PM could be a suitable source for transplantation, which could result in reconstruction of lost neuronal circuits.

Development of an optimal and as close to a tissue-like environment as possible for neuronal cell regeneration therapies is highly needed. Matrigel, used in some studies, consists of the basal membrane proteins of mouse cells (Uemura *et al.*, 2010). It contains a variety of extracellular proteins and thus supports the growth of many cell types, including neuronal cells (Thonhoff *et al.*, 2008). It is, however, of animal origin and its composition is not defined and thus not appropriate for transplantation therapies in humans. PM, on the other hand, has a potential to be used for clinical applications since there are Good Manufacturing Practice (GMP) level products available ([www.puramatrix.com](http://www.puramatrix.com)). Neuronal cells have also been cultured with other 3D hydrogels such as hyaluronic acid (Brännvall *et al.*, 2007) and chitosan (Leipzig *et al.*, 2010). The suitability of those hydrogels as matrixes for clinically relevant human neural cells has not been studied. In addition to our study, two papers (Ortinou *et al.*, 2011; Thonhoff *et al.*, 2008) have described the suitability of PM as a growth matrix for human-derived neural cells, suggesting that this material should be further studied. There still remains challenges related to the combination of material and cells such as drastic pH changes during gelation and developing this process into injectable GMP-level form.

In conclusion, the cell-biomaterial matrix created in this study can be used for drug screening purposes, toxicological studies on non-invasive repetitive functionality analysis of 3D cultured cells, as well as for providing new information for tissue engineering and stem cell research.

## Acknowledgements

This study was financially supported by the Academy of Finland (Grant 123233), the Competitive Research Funding of the Tampere University Hospital, the Finnish Cultural Foundation/ Pirkanmaa Regional Fund and the Finnish Funding Agency for Technology and Innovation (StemInClin-project). The MEA system was founded by BioNext Tampere. Authors wish to thank personnel at IBT for their support in stem cell research and particularly, Riikka Äänismaa, PhD and Maria Sundberg, PhD are acknowledged.

## References

- Äänismaa R, Ylä-Outinen L, Mikkonen JE *et al.* 2011; Human pluripotent stem cell-derived neuronal networks: their electrical functionality and usability for modelling and toxicology. In *Methodological Advances in the Culture, Manipulation and Utilization of Embryonic Stem Cells for Basic and Practical Applications*, Prof. Craig Atwood (ed). InTech. Available from: <http://www.intechopen.com/books/methodological-advances-in-the-culture-manipulation-and-utilization-of-embryonic-stem-cells-for-basic-and-practical-applications/human-pluripotent-stem-cell-derived-neuronal-networks-their-electrical-functionality-and-usability-f>
- Brännvall K, Bergman K, Wallenquist U *et al.* 2007; Enhanced neuronal differentiation in a three-dimensional collagen-hyaluronan matrix. *J Neurosci Res* **85**: 2138–2146.
- Crompton KE, Goud JD, Bellamkonda RV *et al.* 2007; Polylysine-functionalised thermoresponsive chitosan hydrogel for neural tissue engineering. *Biomaterials* **28**: 441–449.
- Freudenberg U, Hermann A, Welzel PB *et al.* 2009; A star-PEG-heparin hydrogel platform to aid cell replacement therapies for neurodegenerative diseases. *Biomaterials* **30**: 5049–5060.
- Gelain F, Bottai D, Vescovi A *et al.* 2006; Designer self-assembling peptide nanofiber scaffolds for adult mouse neural stem cell 3-dimensional cultures. *PLoS One* **1**: e119.
- Heikkilä TJ, Ylä-Outinen L, Tanskanen JM *et al.* 2009; Human embryonic stem cell-derived neuronal cells form spontaneously active neuronal networks *in vitro*. *Exp Neurol* **218**: 109–116.
- Hejcl A, Lesny P, Pradny M *et al.* 2008; Biocompatible hydrogels in spinal cord injury repair. *Physiol Res* **57**(Suppl 3): S121–132.
- Hicks AU, Lappalainen RS, Narkilahti S *et al.* 2009; Transplantation of human embryonic stem cell-derived neural precursor cells and enriched environment after cortical stroke in rats: cell survival and functional recovery. *Eur J Neurosci* **29**: 562–574.
- Holmes TC, de Lacalle S, Su X *et al.* 2000; Extensive neurite outgrowth and active synapse formation on self-assembling peptide scaffolds. *Proc Natl Acad Sci U S A* **97**: 6728–6733.
- Hu BY, Weick JP, Yu J *et al.* 2010; Neural differentiation of human induced pluripotent stem cells follows developmental principles but with variable potency. *Proc Natl Acad Sci U S A* **107**: 4335–4340.
- Johnstone AF, Gross GW, Weiss DG *et al.* 2010; Microelectrode arrays: a physiologically based neurotoxicity testing platform for the 21st century. *Neurotoxicology* **31**: 331–350.
- Lappalainen RS, Salomaki M, Ylä-Outinen L *et al.* 2010; Similarly derived and cultured hESC lines show variation in their developmental potential towards neuronal cells in long-term culture. *Regen Med* **5**: 749–762.
- Leipzig ND, Wylie RG, Kim H *et al.* 2010; Differentiation of neural stem cells in three-dimensional growth factor-immobilized chitosan hydrogel scaffolds. *Biomaterials* **32**: 57–64.
- Leon EJ, Verma N, Zhang S *et al.* 1998; Mechanical properties of a self-assembling oligopeptide matrix. *J Biomater Sci Polym Ed* **9**: 297–312.
- Li GN, Livi LL, Gourd CM *et al.* 2007; Genomic and morphological changes of neuroblastoma cells in response to three-dimensional matrices. *Tissue Eng* **13**: 1035–1047.
- Li SC, Zhong JF. 2009; Twisting immune responses for allogeneic stem cell therapy. *World J Stem Cells* **1**: 30–35.
- Lindvall O, Kokaia Z. 2010; Stem cells in human neurodegenerative disorders—time for clinical translation? *J Clin Invest* **120**: 29–40.
- Lu YB, Franze K, Seifert G, Steinhauser C *et al.* 2006; Viscoelastic properties of individual glial cells and neurons in the CNS. *Proc Natl Acad Sci U S A* **103**: 17759–17764.
- Mahoney MJ, Anseth KS. 2006; Three-dimensional growth and function of neural tissue in degradable polyethylene glycol hydrogels. *Biomaterials* **27**: 2265–2274.
- Narkilahti S, Rajala K, Pihlajamäki H *et al.* 2007; Monitoring and analysis of dynamic growth of human embryonic stem cells: comparison of automated instrumentation and conventional culturing methods. *Biomed Eng Online* **6**: 11.
- Nisbet DR, Crompton KE, Horne MK *et al.* 2008; Neural tissue engineering of the CNS using hydrogels. *J Biomed Mater Res B Appl Biomater* **87**: 251–263.
- Oizumi H, Hayashita-Kinoh H, Hayakawa H *et al.* 2008; Alteration in the differentiation-related molecular expression in the subventricular zone in a mouse model of Parkinson's disease. *Neurosci Res* **60**: 15–21.
- Ortinou S, Schlich J, Block S *et al.* 2011; Effect of 3D-scaffold formation on differentiation and survival in human neural progenitor cells. *Biomed Eng Online* **9**: 70.
- Park J, Koito H, Li J *et al.* 2009; Microfluidic compartmentalized co-culture platform for CNS axon myelination research. *Biomed Microdevices* **11**: 1145–1153.
- Pautot S, Wyart C, Isacoff EY. 2008; Colloid-guided assembly of oriented 3D neuronal networks. *Nat Methods* **5**: 735–740.
- Potter SM, DeMarse TB. 2001; A new approach to neural cell culture for long-term studies. *J Neurosci Methods* **110**: 17–24.
- Preynat-Seauve O, Suter DM, Tirefort D *et al.* 2009; Development of human nervous tissue upon differentiation of embryonic stem cells in three-dimensional culture. *Stem Cells* **27**: 509–520.
- Saha K, Keung AJ, Irwin EF *et al.* 2008; Substrate modulus directs neural stem cell behavior. *Biophys J* **95**: 4426–4438.
- Sundberg M, Jansson L, Ketolainen J *et al.* 2009; CD marker expression profiles of human embryonic stem cells and their neural derivatives, determined using flow-cytometric analysis, reveal a novel CD marker for exclusion of pluripotent stem cells. *Stem Cell Res* **2**: 113–124.
- Sundberg M, Skottman H, Suuronen R *et al.* 2010; Production and isolation of NG2+ oligodendrocyte precursors from human embryonic stem cells in defined serum-free medium. *Stem Cell Res* **5**: 91–103.
- Takahashi K, Tanabe K, Ohnuki M *et al.* 2007; Induction of pluripotent stem cells from adult human fibroblasts by defined factors. *Cell* **131**: 861–872.
- Taylor AM, Blurton-Jones M, Rhee SW *et al.* 2005; A microfluidic culture platform for CNS axonal injury, regeneration and transport. *Nat Methods* **2**: 599–605.
- Teixeira AI, Ilkhanizadeh S, Wiggen JA *et al.* 2009; The promotion of neuronal maturation on soft substrates. *Biomaterials* **30**: 4567–4572.
- Thonhoff JR, Lou DI, Jordan PM *et al.* 2008; Compatibility of human fetal neural stem cells with hydrogel biomaterials *in vitro*. *Brain Res* **1187**: 42–51.
- Uemura M, Refaat MM, Shinoyama M *et al.* 2010; Matrigel supports survival and neuronal differentiation of grafted embryonic stem cell-derived neural precursor cells. *J Neurosci Res* **88**: 542–551.
- Wagenaar DA, Pine J, Potter SM. 2006; An extremely rich repertoire of bursting patterns during the development of cortical cultures. *BMC Neurosci* **7**: 151–156.
- Xu T, Molnar P, Gregory C, Das M *et al.* 2009; Electrophysiological characterization of embryonic hippocampal neurons cultured in a 3D collagen hydrogel. *Biomaterials* **30**: 4377–4383.
- Yamaoka H, Asato H, Ogasawara T, Nishizawa S *et al.* 2006; Cartilage tissue engineering using human auricular chondrocytes embedded in different hydrogel materials. *J Biomed Mater Res A* **78**: 1–11.
- Ylä-Outinen L, Heikkilä J, Skottman H *et al.* 2010a; Human cell-based micro electrode array platform for studying neurotoxicity. *Front Neuroeng* **3**: 1–9.
- Ylä-Outinen L, Mariani C, Skottman H *et al.* 2010b; Electrospun poly(L,D-lactide) scaffolds support the growth of human embryonic stem cell-derived neuronal cells. *Open Tissue Eng Regen Med J* **3**: 1–9.
- Zeng X, Chen J, Deng X *et al.* 2006; An *in vitro* model of human dopaminergic neurons derived from embryonic stem cells: MPP+ toxicity and GDNF neuroprotection. *Neuro-psychopharmacology* **31**: 2708–2715.
- Zhang S. 2002; Emerging biological materials through molecular self-assembly. *Biotechnol Adv* **20**: 321–339.
- Zhang S, Gelain F, Zhao X. 2005; Designer self-assembling peptide nanofiber scaffolds for 3D tissue cell cultures. *Semin Cancer Biol* **15**: 413–420.
- Zhong Y, Bellamkonda RV. 2008; Biomaterials for the central nervous system. *J R Soc Interface* **5**: 957–975.

# Biomedical Materials



## PAPER

# Bioamine-crosslinked gellan gum hydrogel for neural tissue engineering

RECEIVED  
25 October 2016

REVISED  
17 February 2017

ACCEPTED FOR PUBLICATION  
24 February 2017

PUBLISHED  
24 March 2017

Janne T Koivisto<sup>1,2,4</sup>, Tiina Joki<sup>2,4</sup>, Jenny E Parraga<sup>1</sup>, Rami Pääkkönen<sup>2</sup>, Laura Ylä-Outinen<sup>2</sup>, Laura Salonen<sup>1</sup>, Ilari Jönkkäri<sup>3</sup>, Marja Peltola<sup>2</sup>, Teemu O Ihalainen<sup>2</sup>, Susanna Narkilahti<sup>2,5</sup> and Minna Kellomäki<sup>1,2,5</sup>

<sup>1</sup> BioMediTech Institute and Faculty of Biomedical Sciences and Engineering, Tampere University of Technology, Korkeakoulunkatu 3, FI-33720 Tampere, Finland

<sup>2</sup> BioMediTech Institute and Faculty of Medicine and Life Sciences, University of Tampere, Lääkärintäti 1, FI-33520 Tampere, Finland

<sup>3</sup> Laboratory of Materials Science, Tampere University of Technology, Korkeakoulunkatu 6, FI-33720 Tampere, Finland

<sup>4</sup> Writers contributed equally (researchers).

<sup>5</sup> Writers contributed equally (professors).

E-mail: [janne.t.koivisto@tut.fi](mailto:janne.t.koivisto@tut.fi), [tiina.joki@uta.fi](mailto:tiina.joki@uta.fi), [susanna.narkilahti@uta.fi](mailto:susanna.narkilahti@uta.fi) and [minna.kellomaki@tut.fi](mailto:minna.kellomaki@tut.fi)

**Keywords:** 3D cell culture, gellan gum, human pluripotent stem cells, hydrogel, laminin, neuronal cells

Supplementary material for this article is available [online](#)

## Abstract

Neural tissue engineering and three-dimensional *in vitro* tissue modeling require the development of biomaterials that take into account the specified requirements of human neural cells and tissue. In this study, an alternative method of producing biomimetic hydrogels based on gellan gum (GG) was developed by replacing traditional crosslinking methods with the bioamines spermidine and spermine. These bioamines were proven to function as crosslinkers for GG hydrogel at +37 °C, allowing for the encapsulation of human neurons. We studied the mechanical and rheological properties of the formed hydrogels, which showed biomimicking properties comparable to naïve rabbit brain tissue under physiologically relevant stress and strain. Human pluripotent stem cell-derived neuronal cells demonstrated good cytocompatibility in the GG-based hydrogels. Moreover, functionalization of GG hydrogels with laminin resulted in cell type-specific behavior: neuronal cell maturation and neurite migration.

## 1. Introduction

Tissue engineering (TE) is a field of study that aims to produce tissue-like structures *in vivo* and *in vitro* using a combination of a biomaterial and living cells [1]. Thus, TE has combined advances in cell therapy and biomaterials science to stabilize an injury or defect site and deliver cells and molecules to promote the regeneration of damaged tissues [1, 2]. Neural TE has emerged as a promising strategy for neural regeneration, both for the central nervous system (CNS) and the peripheral nervous system, which suffer from limited regenerative capacity [2–4]. For successful functional neural TE graft, it is important to combine neural tissue mimicking material, for example, a hydrogel, and a clinically relevant human cell type [5]. In addition to therapeutic use in TE, hydrogels as neural scaffolds can also be used for *in vitro* disease

modeling, drug testing and developmental biology studies [5–7].

The main requirement for biomaterials intended for TE is biocompatibility [3, 8, 9], defined by the International Union of Pure and Applied Chemistry as ‘the ability to be in contact with a living system without producing an adverse effect’ [9]. Hydrogel biomaterials can fulfill the biocompatibility (systemic scale) and cytocompatibility (cellular scale) requirements [8], and their tunable physical properties can mimic soft tissues, like those in the CNS [3–5]. Thus, while designing hydrogels for TE, important material characteristics to take into account are, for example, mechanical properties, porosity, permeability and transparency, especially for *in vitro* TE [4, 10–12]. Moreover, hydrogels can be further modified to incorporate extracellular matrix (ECM) molecules (for example, collagen, fibronectin or laminin) and/or

**Table 1.** Hydrogel compositions used in this study and calculated details of bioamine per GG in the specified concentrations.

| Hydrogel nomenclature | Bioamine working solution ( $\mu\text{M}$ ) | Bioamine in hydro-gel (w%) | Bioamine in hydro-gel ( $\mu\text{M}$ ) | Bioamine $\mu\text{moles/}$ GG (g) | Positive charge/ GG (g) |
|-----------------------|---------------------------------------------|----------------------------|-----------------------------------------|------------------------------------|-------------------------|
| GG 1.10%SPM           | 1005                                        | 1.108                      | 138.7                                   | 32.17                              | 128.7                   |
| GG 0.60%SPM           | 502.6                                       | 0.5569                     | 69.43                                   | 16.08                              | 64.33                   |
| GG 0.40%SPM           | 395.0                                       | 0.3984                     | 49.52                                   | 11.49                              | 45.95                   |
| GG 3.00%SPD           | 3927                                        | 3.101                      | 541.7                                   | 125.6                              | 377.0                   |
| GG 1.50%SPD           | 1885                                        | 1.513                      | 260.0                                   | 60.32                              | 180.0                   |
| GG 1.25%SPD           | 1551                                        | 1.248                      | 214.0                                   | 49.64                              | 148.9                   |

peptides to provide anchoring sites for cells and to enhance growth [3, 4, 11].

Gellan gum (GG) is an exopolysaccharide produced by *Sphingomonas elodea* bacteria. This biologically safe polymer has been approved by the Food and Drug Administration (FDA) and the European Medicines Agency (EMA) [13–15], and it has been recently suggested as a material for scaffold development for TE [16, 17]. GG is a deacetylated form of gellan molecule, which has a tetrasaccharide repeating structure of  $\beta$ -D-glucose,  $\beta$ -D-glucuronic acid and  $\alpha$ -L-rhamnose in a 2:1:1 ratio [13]. Like many other polysaccharides, GG is a relatively inert biomaterial [17]. To improve cell attachment, GG-based hydrogels have been functionalized with peptides by covalently binding them into the molecular backbone itself [17, 18]. GG has been studied for bone [16, 19], cartilage [20–22] and spinal cord [23–27] TE applications. In neural applications, GG can support the *in vitro* culture of rodent or human cells (neural stem cells [18, 28], olfactory ensheathing glia cells [18], oligodendrocyte-like cells [23]) and has been shown to be biocompatible *in vivo* in a hemisection rat spinal cord injury model [23].

GG hydrogels produced by physical, ionotropic, crosslinking with metallic cations ( $\text{Ca}^{2+}$ ,  $\text{Mg}^{2+}$ ,  $\text{Na}^+$ ,  $\text{K}^+$ ) are primarily mechanically weak [13, 29]. Another option is chemical crosslinking using methacrylate derivatives, followed by the addition of a photoinitiator and photocrosslinking with UV-light [23, 29]. Disadvantages of these crosslinking methods include cation leakage or exchange, weakening of the mechanical properties of the hydrogel over time [29, 30], phototoxicity of UV-light and chemical reactivity of the photoinitiator [31–33]. Chemical crosslinking is often, in practice, more complicated than ionotropic crosslinking.

Bioamines spermine (SPM) and spermidine (SPD) are small cations that have been demonstrated to interact with anionic polymers such as GG [34–36]. Crosslinking with bioamines is simple, and a wide crosslinker concentration range can be applied to vary the mechanical properties of GG in a controlled way, so they provide an alternative crosslinking method. SPM and SPD are present in all living cells, and they play important roles in many physiological processes, such as protecting DNA by scavenging oxygen radicals

and affecting cell proliferation [37, 38] also in neural cells [39, 40].

In this study, we developed GG bioamine hydrogels, using SPM and SPD as crosslinkers, with mechanical properties that resemble brain tissue. The resulting hydrogels were characterized mechanically and rheologically. The mechanical properties of these hydrogels were compared to naïve rabbit brain tissue by compression testing. Hydrogels with a compressive modulus similar to that of brain tissue were used for the cell studies. Cytocompatibility and cell type-specific behavior were studied *in vitro* using human pluripotent stem cell (hPSC)-derived neuronal cells.

## 2. Materials and methods

### 2.1. Preparation of GG hydrogels

To prepare the hydrogels, GG (Gelzan<sup>TM</sup>, low acyl,  $M_w$  1 kg mol<sup>-1</sup>), SPD (spermidine trihydrochloride), SPM (spermine tetrahydrochloride) and sucrose were acquired from Sigma-Aldrich (Finland) with the highest level of purity available. A 10% (w/w) sucrose solution in deionized water was used as a solvent for the hydrogel components to reduce osmotic pressure on the cells [5]. The GG solution was prepared at 5 mg ml<sup>-1</sup>. We tested two different crosslinkers (SPD and SPM); both with three different concentrations, the names and details are shown in table 1.

All solutions were sterile filtered for mechanical and rheological testing with 0.8/0.2  $\mu\text{m}$  Acrodisc<sup>®</sup> (PALL Corporation, Port Washington, NY, USA) or for cell culture with Whatman FP 30/0.2 CA-s 0.2  $\mu\text{m}$  (Whatman plc, Little Chalfont, UK) syringe filters. The GG solution was heated in a water bath to +60 °C for reduced viscosity prior to sterile filtration. All solutions can be stored for up to one month at +4 °C.

When preparing hydrogels, the solutions were first heated in a water bath to +37 °C. A crosslinker solution of SPM or SPD was mixed with GG at a volume ratio of 4:25 and cast into a suitable mold or directly onto a cell culture plate. When used, laminin (1 mg ml<sup>-1</sup>) was added to the hydrogel just before gelation in the GG solution at 1 v%, 5 v% or 10 v%.

This study follows the ASTM F2900-11 Standard Guide for Characterization of Hydrogels Used in Regenerative Medicine [41]. For initial gelation testing and gelation time estimation, a small glass bottle was

used as the mold. Gelation time was estimated with the tube tilt test, as described by Tanodekaew *et al* [42]. In brief, after mixing the reagents, the bottle was slowly turned upside down at 30 s time intervals, and the flow of gel was observed. If the solution started to move even slightly once tilting started, it was not tilted further to let the gelation continue. Once the solution did not flow, the gelation was considered complete, and the time was recorded.

## 2.2. Mechanical testing

Compression testing was performed using a BOSE Electroforce Biodynamic 5100 machine equipped with a 225 N load sensor and Wintest 4.1 software (Bose Corporation, Eden Prairie, MN, USA). Samples were cast into a self-made cylindrical mold with an approximate height of 6.5 mm and a diameter of 12.2 mm, and stored overnight before compression testing to ensure the complete gelation before each measurement. Each composition was tested in five parallel samples; the exact dimensions of each sample were measured with calipers before testing. To avoid slippage of samples, the compression plates were covered with a piece of wet cellulose paper to increase friction between the hydrogel and the metal plate. The sample was set in between compression plates so that the upper plate touched the sample, but no pre-stress was used. Unconfined compression was performed with a constant 10 mm min<sup>-1</sup> strain rate, and samples were compressed until 65% strain was reached from the original height. The test was performed in wet conditions at room temperature. After compression, the data were analyzed with MS Excel. According to Hooke's law,  $\sigma = E^* \varepsilon$ , the compressive modulus was calculated from the stress-strain curve as the slope of the elastic region [43]. In addition, the fracture strength and fracture strain were recorded as a sudden drop in the stress-strain curve.

To obtain a good reference in terms of the mechanical properties to design hydrogels for neural TE, compression testing was also performed with brain tissue samples. New Zealand white rabbits, age 10 weeks, male, were sacrificed with deep anesthesia, after which the heads were removed and stored in ice for a maximum of 8 h. The brains were removed from the skulls, and samples containing midbrain, cerebellum or cortex were prepared. The samples were cut with a biopsy punch to the same size and shape as the hydrogel compression samples and stored on ice until compression testing. The test parameters used were the same as those described above. The naïve brain tissues were obtained from animal experiments conducted at Tampere University Medical School, University of Tampere.

## 2.3. Rheological testing

Rheological experiments were carried out with a rotational rheometer (Haake RheoStress RS150)

equipped with Rheowizard 4.3 software (Thermo-Haake, Germany). Parallel plate geometry with 20 mm diameter metal plates was used. All the experiments were conducted at room temperature ( $\sim 25^\circ\text{C}$ ) in the oscillatory mode. In the oscillatory mode the sample is subjected to sinusoidal oscillatory shear strain with amplitude  $\gamma_o$ . In the linear viscoelastic region (LVER) with sufficiently small strain amplitudes the resulting stress will also be sinusoidal of the same frequency with amplitude  $\tau_o$  and phase angle  $\delta$ . The complex moduli ( $G^*$ ) represents the rigidity of the sample and in the LVER the following relationship applies:

$$G^* = \frac{\tau_o}{\gamma_o} = \sqrt{(G')^2 + (G'')^2}. \quad (1)$$

The storage modulus ( $G'$ ) is the in-phase and loss modulus ( $G''$ ) the out-of-phase components of the response:

$$G' = \frac{\tau_o}{\gamma_o} \cos \delta, \quad (2)$$

$$G'' = \frac{\tau_o}{\gamma_o} \sin \delta. \quad (3)$$

The  $G'$  represents the elastic and  $G''$  viscous behavior of the sample. The loss factor  $\tan \delta$  is the ratio of the viscous to the elastic portion [44].

The samples for rheological testing were cast in self-made cylindrical molds with height a maximum of 1 and 20 mm cross-section diameter. Prior to each measurement, the hydrogels were stored overnight to ensure the complete gelation. During measurement the gap between plates was set to 0.8 mm. All measurements were done in oscillatory shear deformation mode and both amplitude and frequency sweeps were used for all samples. The strain amplitude range for amplitude sweeps was from 0.01 to 5.00 rad (0.1 rad = 1.6% displacement) with 1 Hz frequency. Six parallel samples were tested with amplitude sweeps and two parallel samples with frequency sweeps. The frequency sweep was done in range from 0.1 to 3.0 Hz, with constant 0.1 rad strain amplitude which is in the LVER for all samples.

## 2.4. Cell culture

hPSCs, both human embryonic stem cells and human-induced pluripotent stem cells were used in this study [45]. The used hESC-lines were Regea 08/023 [46] and Regea 11/013 [47] and the used hiPSC-lines were UTA.04511.WT [48], Hel24.3 and A116 [49] (two kind gifts from Professor Timo Otonkoski, University of Helsinki).

BioMediTech has Pirkanmaa Hospital District's ethical approval to deriviate, culture and differentiate hESCs (Skottman, R05116) and permission from the National Authority for Medicolegal Affairs (FIMEA 1426/32/300/05) to conduct human stem cell research. Additionally, approval has been obtained to use hiPSC lines produced by other laboratories for neuronal research (R14023).

#### 2.4.1. Neuronal differentiation

The culture and neuronal differentiation of hPSCs were performed as described previously [50]. Briefly, undifferentiated stem cell colonies were mechanically cut into small aggregates and placed in a suspension culture on neural differentiation medium (NDM) containing 1:1 DMEM/F12 (Gibco, Thermo Fisher Scientific, Finland) and Neurobasal medium, 2 mM GlutaMax™, 1 × B27, 1 × N2 (all from Gibco), 20 ng ml<sup>-1</sup> basic fibroblast growth factor (bFGF, R&D Systems, Minneapolis, MN, USA) and 25 U ml<sup>-1</sup> penicillin/streptomycin (Cambrex, Belgium). During suspension culture, the cell aggregates formed round, floating neurospheres. Neurospheres were kept small via mechanical cutting once per week, and 1/3 of the medium was changed three times per week. Cells were kept for 8–17 weeks in the differentiation phase prior to the hydrogel experiments. Cells were under constant monitoring for the quality of differentiation. Only experiments in which cells formed good neuronal cultures in 2D control were included in the analysis (representative images of good quality 2D cultures are shown in supplementary figure 1 available online at [stacks.iop.org/BMM/12/025014/mmedia](http://stacks.iop.org/BMM/12/025014/mmedia)).

#### 2.4.2. Hydrogel cell culture experiments

For the biological evaluation of the hydrogels, three approaches were taken to study the cell/biomaterial interactions as shown in figure 1. In every case, control cells were plated on laminin-coated cell culture wells (positive control) and on non-coated cell culture wells (negative control). Cell behavior on the studied materials was always compared to that of the controls. Depending on the well type used, either plastic (Nalge Nunc International, Rochester, NY, USA) or glass bottom (MatTek Corporation, Ashland, MA, USA), the wells were coated either with laminin (10 μg ml<sup>-1</sup> mouse laminin) or poly-L-lysine and laminin (10 μg ml<sup>-1</sup> poly-L-lysine followed by 10 μg ml<sup>-1</sup> mouse laminin), respectively.

Gelation was performed as described in figure 1. A drop of crosslinking agent was added on top of the cell culture, followed by the gentle addition of GG solution, in case of cultures beneath the gel. To avoid disturbing the cells, no additional mixing was performed. For cell encapsulation, the cells were suspended in GG solution with a minimal amount of medium prior to crosslinking. After complete gelation, medium was gently added on top of the gel. In 3D cell encapsulation studies for gels with slow gelation (all except GG 3.00%SPD), a thin bottom layer of gel was cast beforehand to prevent cell aggregates from sedimenting to the well bottom during gelation.

#### 2.4.3. Cell plating

Cells were plated either as mechanically cut small cell aggregates or as enzymatically dissociated single cell suspensions prepared using 1X TrypLE Select (Gibco). For the 2D experiments (controls, cells embedded or

on top), the plating density was 60 000 cells cm<sup>-2</sup> or 7–20 small aggregates/cm<sup>2</sup> (3000–7000 cells/aggregate). The cell density for the 3D experiments (cells encapsulated) was  $\sim 3.5 \times 10^6$  cells ml<sup>-1</sup> of gel, or a corresponding amount of small mechanically cut cell aggregates.

The cells were cultured with the gel for two weeks. NDM without bFGF was used during the first week of the experiments. After one week of culture, NDM containing 5 ng ml<sup>-1</sup> bFGF and 4 ng ml<sup>-1</sup> brain-derived neurotrophic factor (BDNF, Prospec Bio, Germany) was used. Half of the medium was changed three times per week using caution to avoid disrupting the gels.

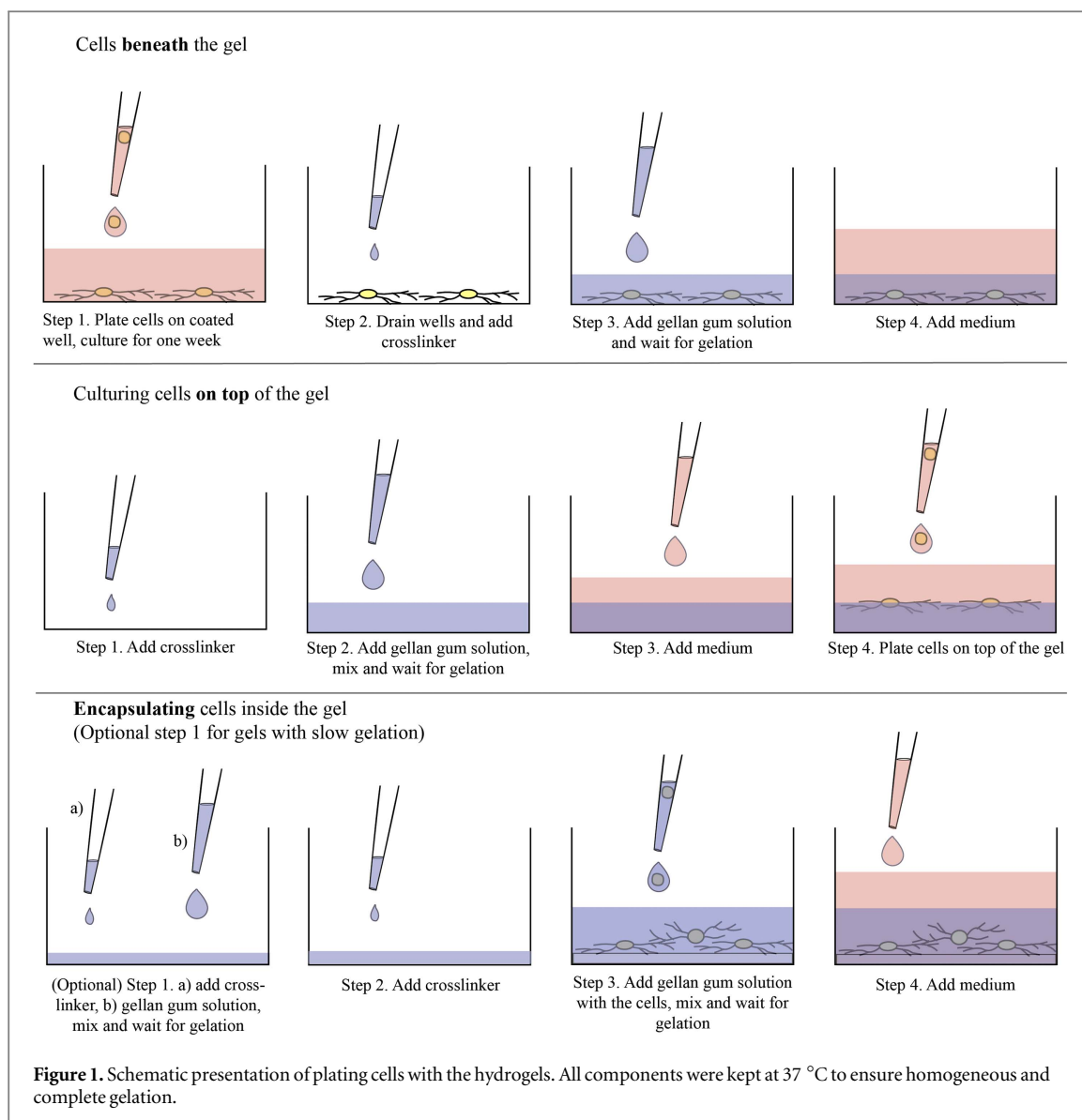
Cells were imaged using a Zeiss AxioVert.A1 microscope and AxioCam ERc 5s camera system or with a Nikon Eclipse TE 2000-S and Nikon Digital Sight DS-Fi1 camera system during the culturing period.

#### 2.5. Live/dead staining

For viability analysis, the cultures were stained using a LIVE/DEAD® viability/cytotoxicity assay (Molecular probes, Thermo Fisher Scientific). In brief, there are two fluorescent dyes in the kit. Calcein-AM (0.1 μM, λ<sup>excitation</sup> = 488 nm) stains intact cells, and ethidium homodimer-1 (0.4 μM, λ<sup>excitation</sup> = 568 nm) stains dead cells. After 1 h of incubation at +37 °C, the cells were imaged with an Olympus IX51 inverted microscope and an Olympus DP30BW digital camera (Olympus, Finland). The numbers of parallel samples varied between 2 and 4.

#### 2.6. Immunostaining

We optimized the parameters for immunostaining cells within macroscopic (60–300 μl) hydrogel blocks. In brief, cultures were fixed with 4% paraformaldehyde preheated to +37 °C for 30 min. After a brief wash in phosphate buffered saline (PBS), non-specific staining was blocked with 10% normal donkey serum (NDS), 0.1% Triton X-100, and 1% bovine serum albumin (BSA) in PBS for 1 h at room temperature, followed by another wash in 1% NDS, 0.1% Triton X-100, and 1% BSA in PBS. Then, the cells were incubated with a combination of primary antibodies at +4 °C for at least 2 d. These antibodies included rabbit anti-microtubule associated protein 2 (MAP-2, 1:400, AB5622, Merck Millipore, Darmstadt, Germany) and rabbit anti-β-tubulin isotype III (β-tub, 1:1000, A01627, GenScript, Piscataway, NJ, USA) in 1% NDS, 0.1% Triton X-100, and 1% BSA in PBS. The samples were washed three times in 1% BSA in PBS (first briefly followed by 2 × 1 h washes) and then incubated overnight at +4 °C with Alexa Fluor 488 conjugated to donkey anti-rabbit antibody (1:400, Life Technologies, A21206) and tetramethylrhodamine isothiocyanate conjugated to phalloidin (TRITC-phalloidin, 0.625 μg ml<sup>-1</sup>, Sigma Aldrich, P1951) in 1% BSA in PBS. The



samples were washed three times (first briefly followed by  $2 \times 1$  h washes) in PBS and then mounted with VECTASHIELD containing 4',6-diamidino-2-phenylindole (DAPI, Vector Laboratories, UK). They were then imaged with an Olympus IX51 inverted microscope and an Olympus DP30BW digital camera. Gray scale images were post-processed (merging and pseudo-coloring) using Adobe Photoshop CS4 (version 11.0, Adobe Systems Inc., CA, USA) and Adobe InDesign CS4 (version 6.0, Adobe Systems Inc.). Confocal scanning of the samples was performed with a Zeiss LSM 780 mounted into inverted Cell Observer microscope (Carl Zeiss, Jena, Germany) using  $10\times$  (NA. 0.45) or  $20\times$  (NA. 0.80) air objectives. The samples were scanned through #1.5 glass bottom well plates (MatTek Corporation, Ashland, MA, USA) or through high performance #1.5 coverslips (Carl Zeiss). The confocal data were visualized with the ZEN Black 2012 software (Carl Zeiss) and ImageJ (Version 1.39, US National Institutes of Health, Bethesda, MD, USA) [51, 52].

## 2.7. Neurite migration

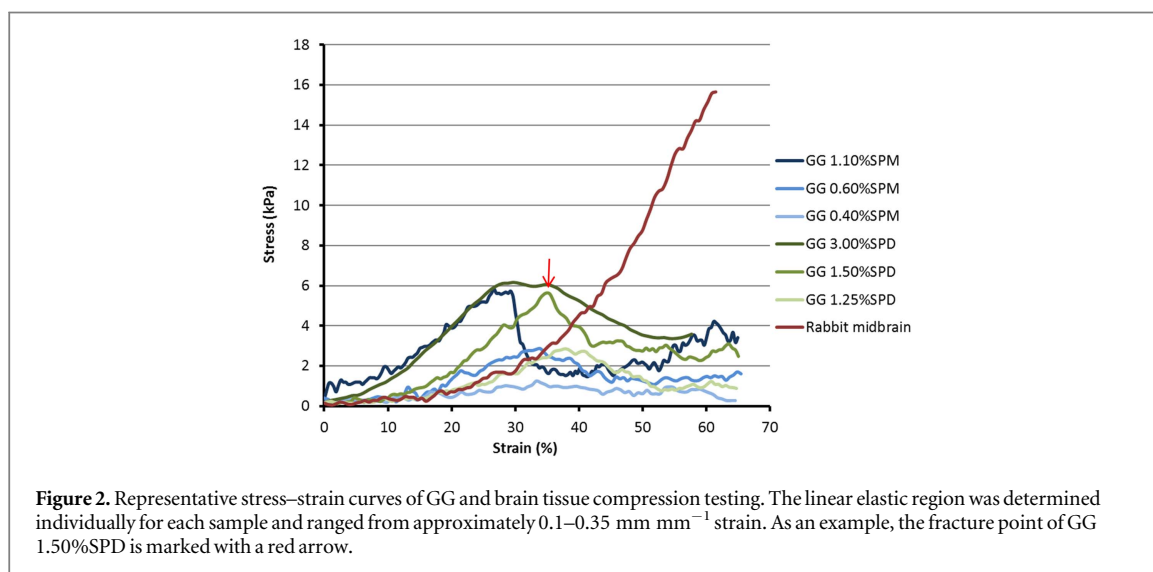
Neurite migration measurements were performed with the ImageJ measure tool. Migration was measured using a straight line from the cell aggregate surface to the visible end of a neuronal process. For each cell aggregate analyzed, the four longest separately distinguishable neurites were measured. Values of less than  $10 \mu\text{m}$  were considered as representing no migration. The analysis was conducted with at least two individual experiments with at least two replicative wells. For each studied group, 7–16 images were analyzed.

## 2.8. Statistical analysis

Due to the non-Gaussian distribution of the data, the nonparametric Kruskal Wallis test and Mann–Whitney U-test were used. A  $p$  value of less than 0.05 was considered significant. If more than two groups were compared, the resulting  $p$  values were multiplied by the number of comparisons performed (Bonferroni correction).

**Table 2.** The gelation times determined by the tube tilt test.

| Gel composition | 1.10%SPM | 0.60%SPM | 0.40%SPM | 3.00%SPD | 1.50%SPD | 1.25%SPD |
|-----------------|----------|----------|----------|----------|----------|----------|
| Gelation time   | 1 min    | 5 min    | 10 min   | 5 s      | 5 min    | 10 min   |



### 3. Results

#### 3.1. Gel forming and gelation time

GG hydrogels were formed with bioamine weight percentage varying from 0.40% to 1.10% for SPM and from 1.25% to 3.00% for SPD. With these concentrations, the hydrogels were transparent and strong enough to hold their own weight and be handled with tweezers. Higher crosslinker concentrations caused partial gelation of the solutions before they could be mixed uniformly, resulting in high anisotropy with non-transparent (cloudy) areas. Lower crosslinker concentrations formed weak gels that could not support their own weight and were not suitable for 3D cell culture, as the encapsulated cells would sediment to the bottom of gel. The 10 v% or lower laminin additions did not affect gelation.

The gelation times approximated with tube tilt test are listed in table 2. As seen, the fastest gelation times were just a few seconds, which could cause difficulties in mixing the reagents evenly and cause anisotropic gels. Gelation times over 10 min were so slow that during plating the cells could sediment to the bottom of the gel before the gelation is completed. From a practical point of view, a gelation time of 1–5 min is optimal, as it is long enough to mix the components uniformly but short enough to keep the cells suspended in the 3D gel and prevent them from sedimenting to the bottom.

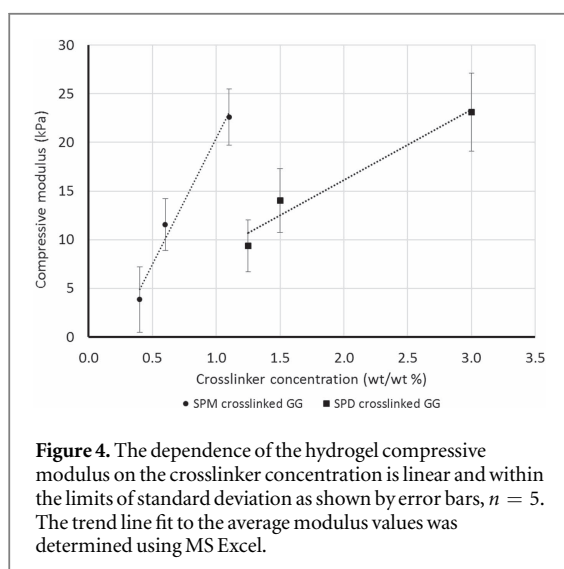
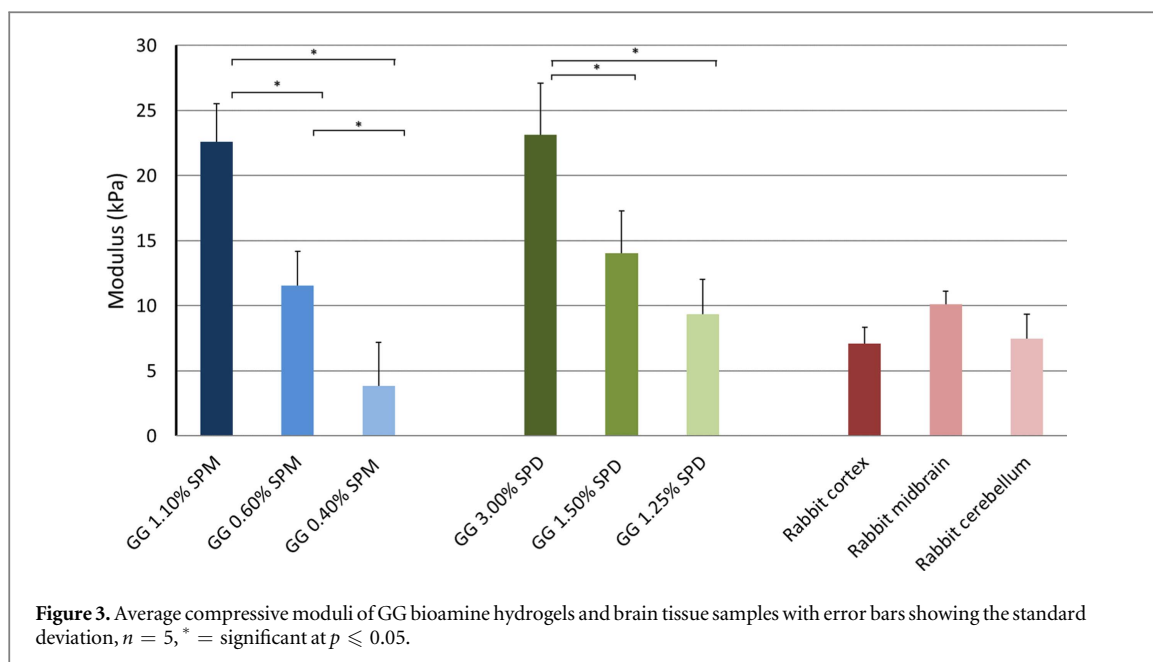
#### 3.2. Compression testing

The main variable influencing the mechanical properties of hydrogels in this study was the crosslinker concentration. The upper and lower limits of crosslinking were tested along with one concentration

between the extremes. The compression testing data were analyzed as stress–strain curves (figure 2), from which the compressive modulus (figure 3) was calculated as the slope of the elastic region. In all GG samples, a distinct fracture point was observed during the test. In contrast, the rabbit brain samples did not have a clear fracture point in the measured displacement but rather a more rubber-like elastic behavior with strong strain stiffening in the end. The GG 0.40% SPM was almost too soft for the load cell, with the force varying during measurement between only 0.01 and 0.12 N.

Based on figure 2, it is clear that brain tissue is more ductile than any of the hydrogel samples as it can endure more plastic deformation without fracture than the GG samples. However, the elastic regions at strain of approximately 0.1–0.35 mm mm<sup>-1</sup> of GG 0.60%SPM and GG 1.25%SPD are very similar to those of the brain stress–strain curve, resulting in both cases in a compressive modulus of approximately 10 kPa. The comparison of calculated compressive moduli is shown in figure 3. The strongest compositions, GG 1.10%SPM and GG 3.00%SPD, both have a ~23 kPa modulus, whereas the weakest composition, GG 0.40%SPM, has only a 3.9 kPa modulus. A significant, linear decrease in the compressive modulus is seen with both crosslinkers when lowering the concentration. The addition of laminin did not affect the compressive modulus (data not shown). The part of the stress–strain curve after the fracture point is negligible. The different parts of the rabbit brain, midbrain, cerebellum and cortex, all behaved very similarly throughout the compression testing, with compressive moduli in the 7–10 kPa range.





The compressive moduli of the hydrogel can be tuned by varying the bioamine concentration, and similar mechanical properties can be achieved with either crosslinker. The compressive moduli of cortex samples were in the same range as the hydrogel moduli with the lowest crosslinker concentrations: GG 0.40% SPM versus GG 1.25%SPD ( $p > 0.05$ ). The standard deviation was approximately 2.5–3.5 kPa in all measurements. This result indicates that the calculated moduli less than 5 kPa are not very accurate, being on the lower limit of the compression testing machine load sensor capability. The dependence of the compressive modulus on the crosslinker concentration is linear and within the limits of the standard deviation, as shown in figure 4. SPM has a tetravalent charge, so the rise of the modulus with increasing crosslinker concentration is steeper than that of trivalent SPD.

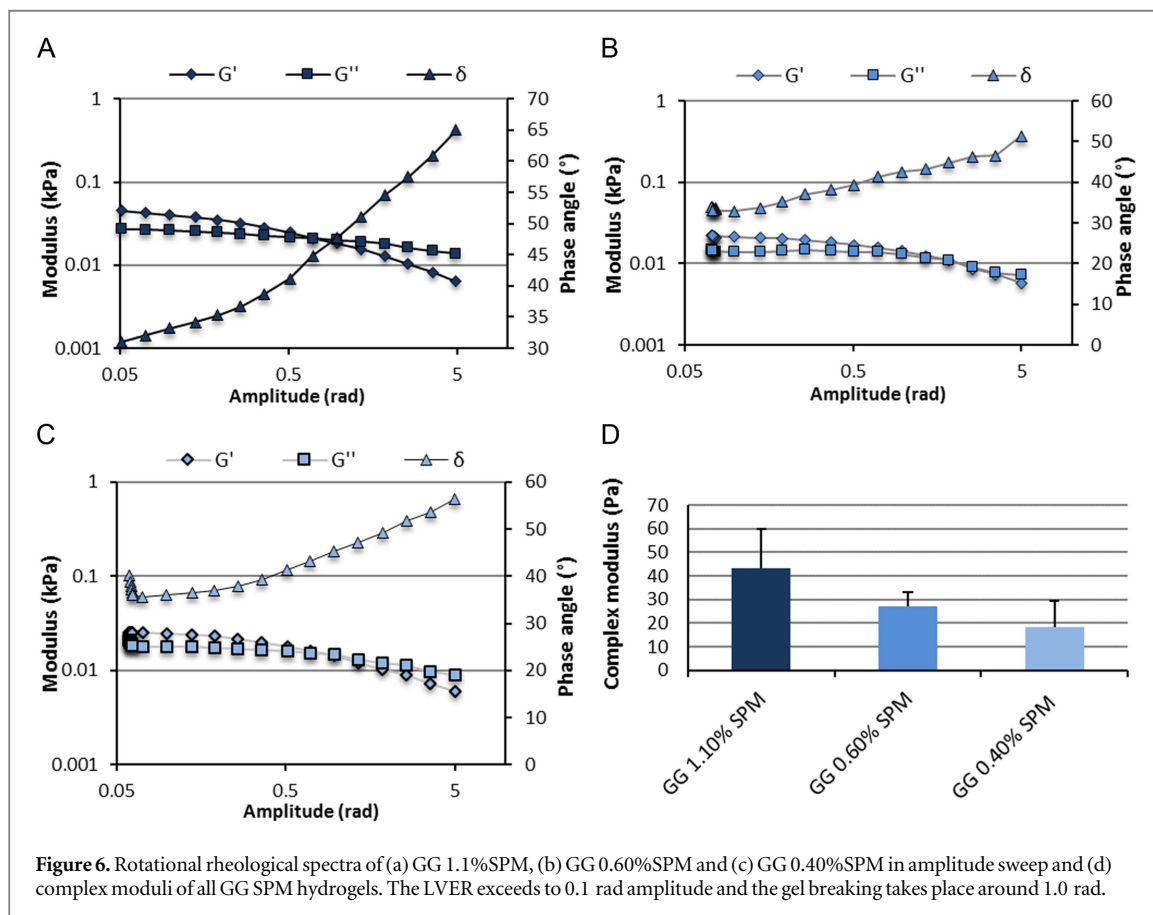
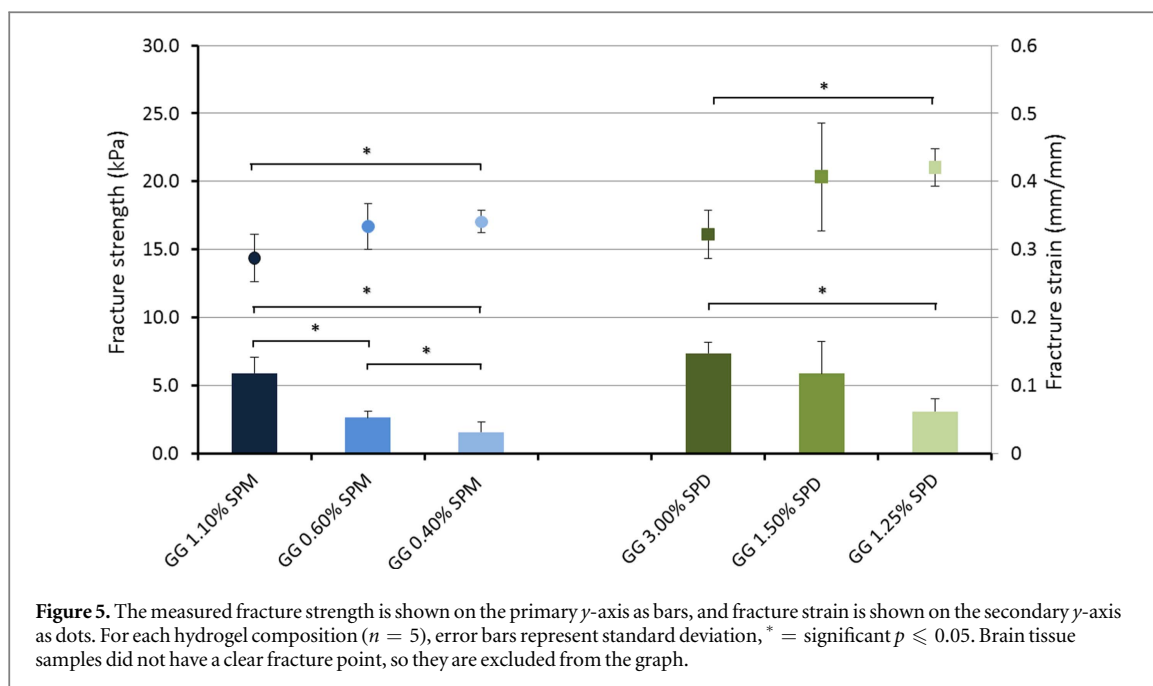
The fracture strength (figure 5) is the ultimate amount of stress a sample can endure, and this value

can be critical for load-bearing TE applications even though a cell's mechanotransduction is likely not affected by it. A significant decrease in fracture strength is seen when the crosslinker concentration is lowered. The fracture strain (figure 5) is an indicator of the brittleness of the sample, and the more crosslinker, the more brittle the hydrogel. The brain tissue samples did not have a visible fracture point when compressed to 65% of the original height, but they had a strong strain hardening effect, as shown in figure 2. However, the strain hardening occurred in the plastic deformation region because the deformation was not recoverable (data not shown).

### 3.3. Rheological testing

The low amplitude strain of the rheological spectrum measured with oscillatory shear amplitude sweep showed a discernible LVER for GG SPM hydrogels, which is used to calculate the complex modulus (figure 6(d)). At higher strain, a decline due to plastic deformation leads to fracture of the sample at the crossover point of the storage and loss modulus as shown in the figure 6 spectra. All the GG SPM hydrogels have a typical gel-like behavior in the LVER with the storage modulus higher than the loss modulus ( $G' > G''$ ), which means that elastic behavior dominates over viscous behavior and that the material is more solid than liquid. As shown in figures 6(a)–(c) by decrease in the phase angle and  $\tan \delta$  value in LVER, when the crosslinker concentration increases, the solid-like behavior increases. And similar to the compressive modulus, the complex modulus decreased upon lowering the crosslinker concentration.

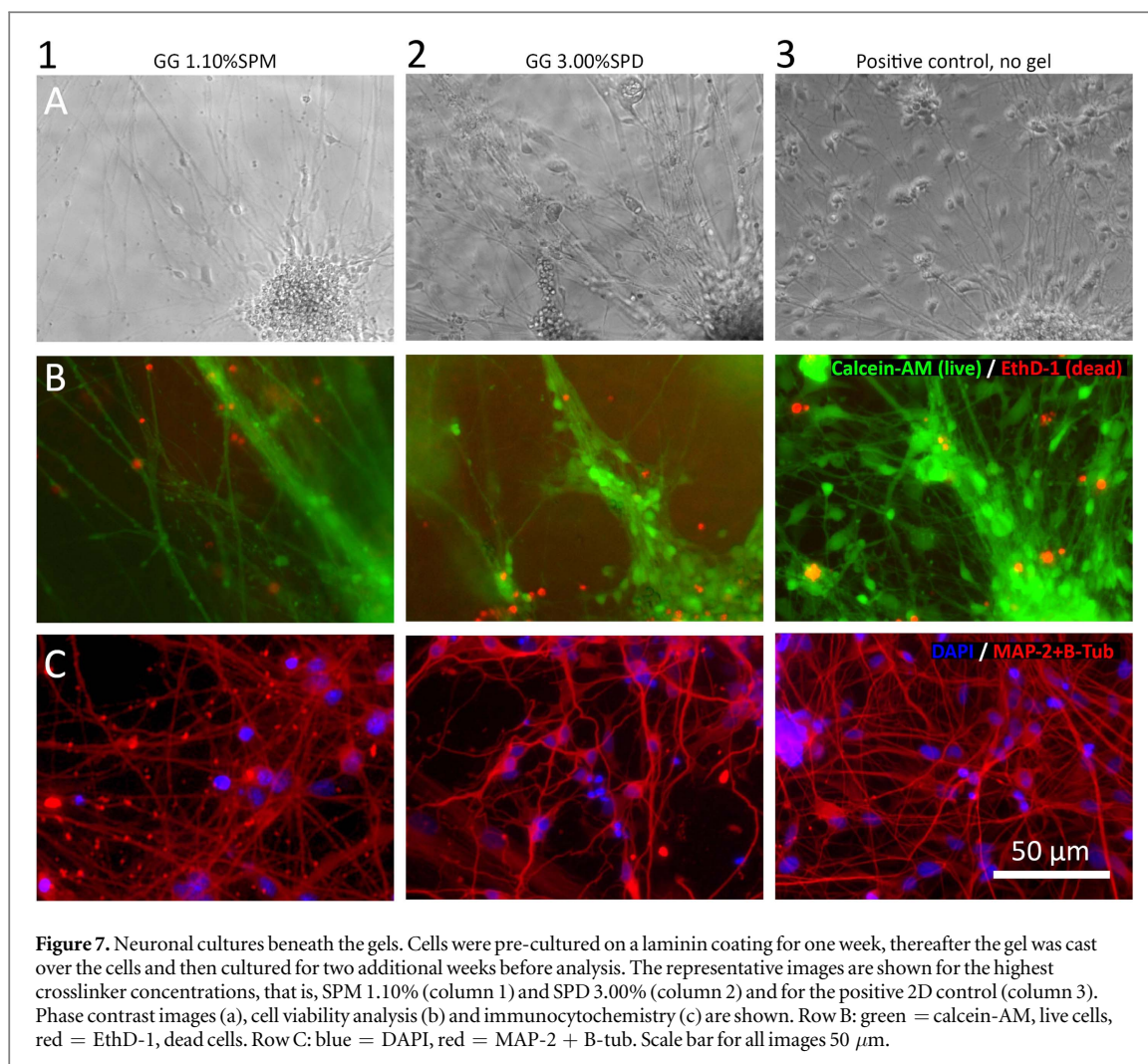
Only SPM crosslinked hydrogels displayed distinctive gel-like behavior related to a stable 3D network structure, which was confirmed by a straight line in the frequency sweep (data not shown). The SPD



crosslinked gels did not have a discernible LVER, likely due to anisotropy or being too solid for rheology, and thus were not possible to measure with this method. The very quick gelation of SPD crosslinked gels can cause nucleation of crosslinking spots. This nucleation leads to anisotropy of gel network structure and density variations, which are not seen in compression testing.

### 3.4. Neuronal cell cultures beneath the hydrogels

Neuronal cells were cultured for one week on the plastic dish before casting gel over the cells. The gelation process on top of cultures did not cause any acute cytotoxic effects. During prolonged culture (up to two weeks) beneath the hydrogel, the neuronal cells remained viable, and neuronal maturation continued similarly as in the positive control cultures without the



GG. Culturing beneath the hydrogel did not cause any morphological changes compared to control 2D cultures (figure 7(a)). In the cell viability analysis, all studied cases had similar degrees of cell viability by visual inspection (figure 7(b)). Neuronal cultures beneath hydrogel also had similar neuronal protein expression according to immunocytochemical analysis as control cultures without hydrogel (figure 7(c)). Figure 7 shows the representative images of cultures beneath hydrogel with highest the crosslinker concentration and a 2D positive control. The results were similar at all studied crosslinker concentrations (SPD 3.00%, 1.50%, and 1.25% or SPM 1.10%, 0.60%, and 0.40%, figure 7, data not shown). Thus, SPD and SPM crosslinkers enable the formation of GG hydrogels that are compatible with culturing human neuronal cells. The hydrogel layers (height 2.2–2.8 mm) on top of the neuronal cultures enabled prolonged culturing, implying that the porosity of the formed hydrogels was high enough for nutrient and metabolite exchange.

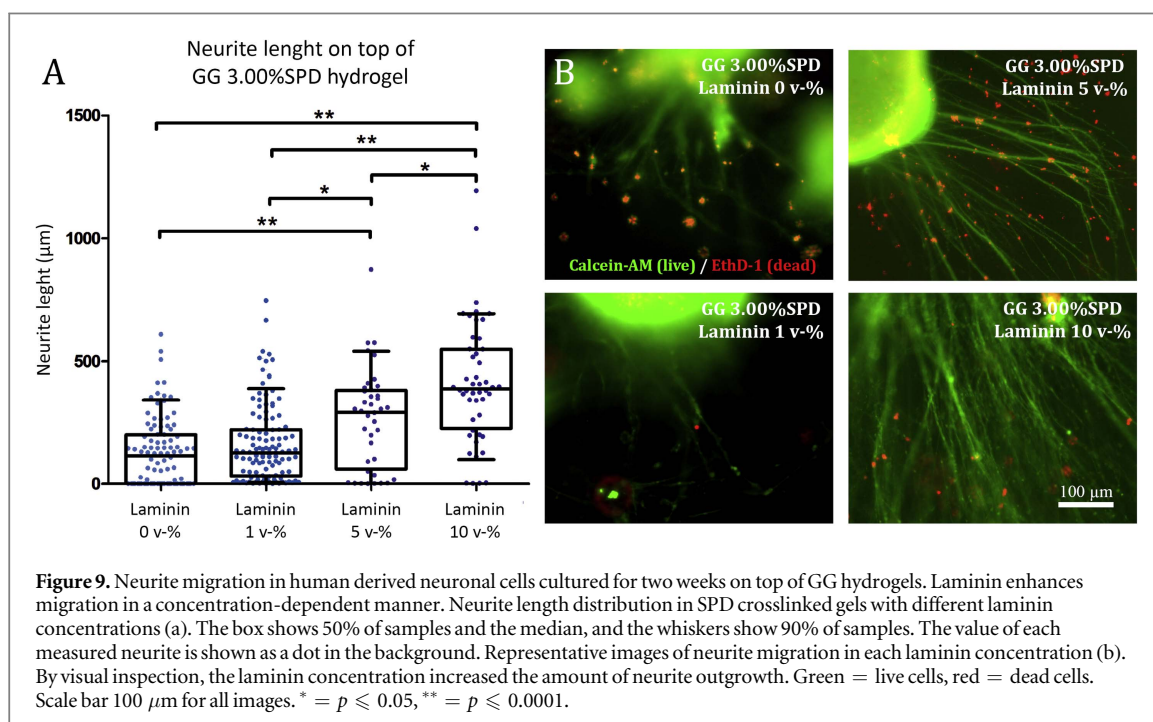
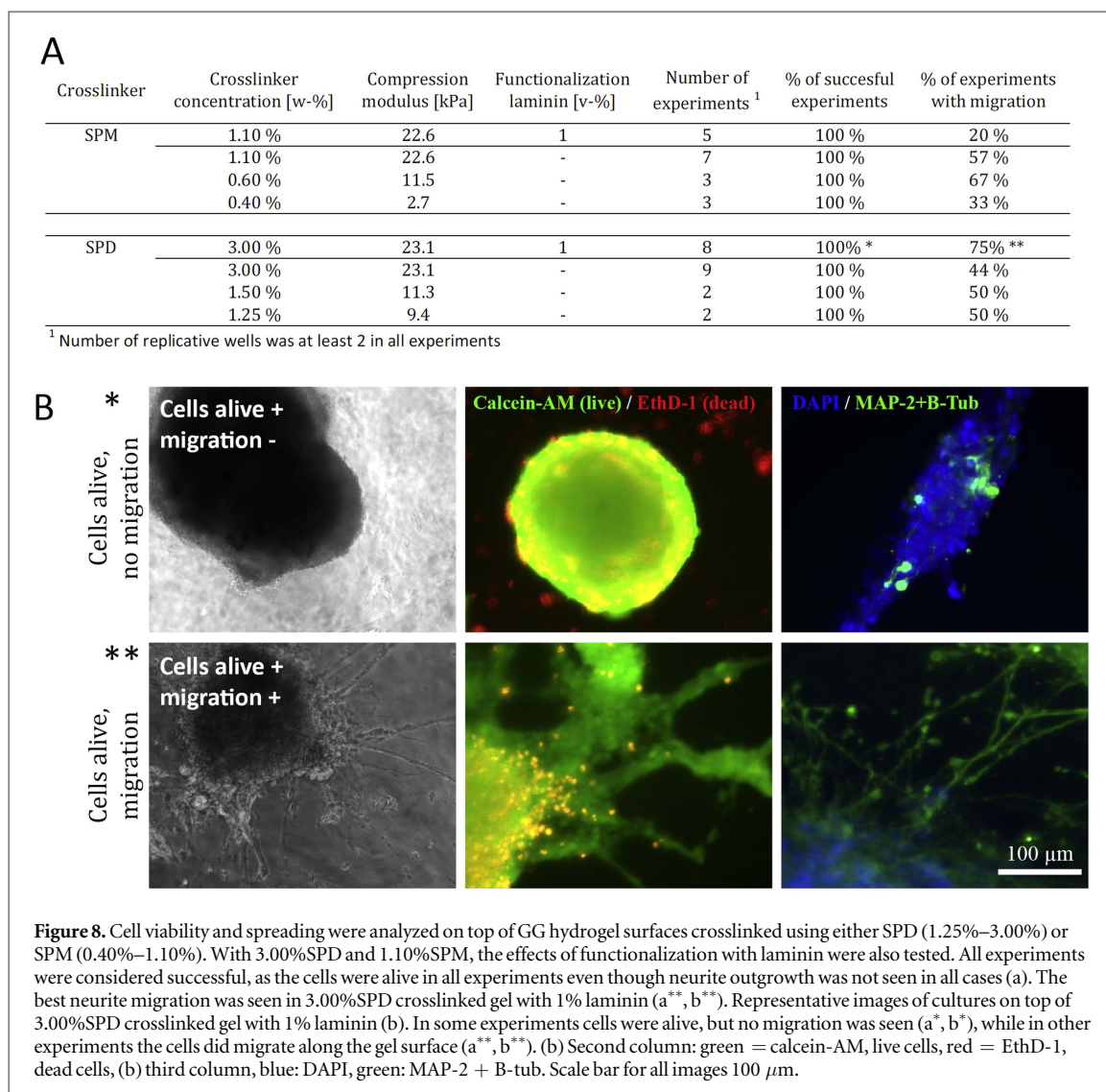
### 3.5. Neuronal cell behavior on top of the hydrogels

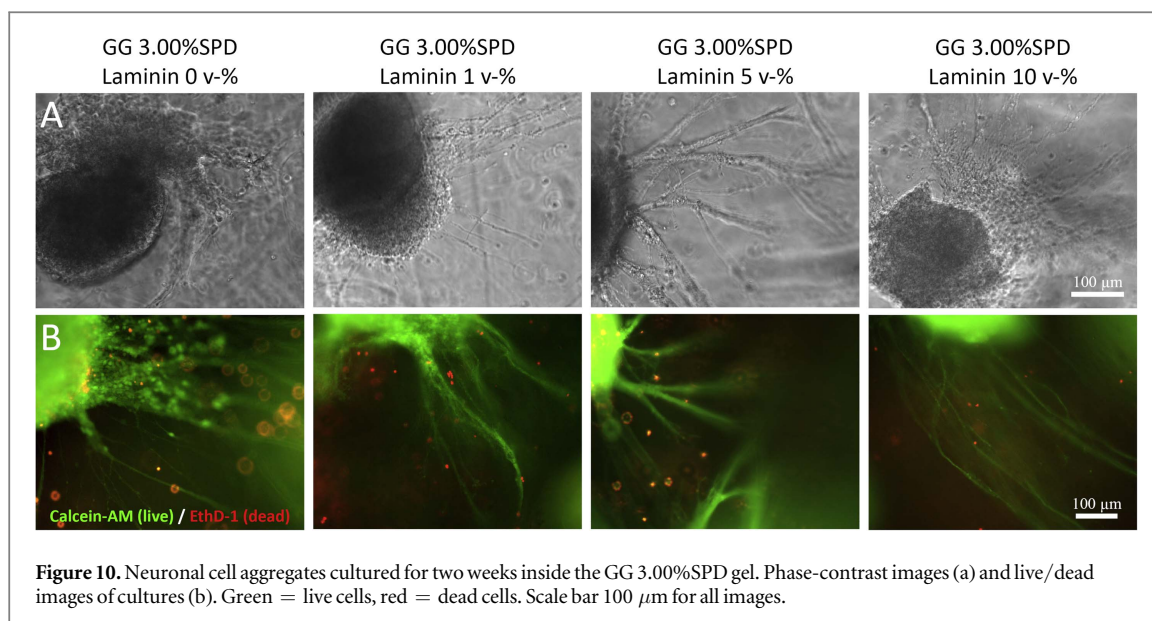
Neuronal cells remained viable during prolonged culturing (two weeks) when plated on top of pre-cast hydrogels (success rate 100%, figure 8). For cell type-specific

behavior, neurite migration was studied in more detail. Although neuronal cells remained alive on top of all the studied hydrogels, their spreading and migration along the hydrogel surfaces varied within and between groups. Figure 8 shows a summary of the results. Without any functionalization with laminin, the GG 1.10%SPM and GG 0.60%SPM were the best compositions for supporting neuronal cell spreading (figure 8(a)). When a low concentration of laminin (1 v%) was added, the performance of the GG 3.00%SPD hydrogel was superior to any other tested gel composition. (figure 8(a)). As GG 3.00%SPD with laminin functionalization gave the best results in neuronal cell spreading and migration, functionalization with higher laminin concentrations was further studied.

### 3.6. Effect of laminin concentration on SPD crosslinked gels

The addition of laminin (5 v% and 10 v%) significantly increased neurite migration on top of gel surfaces during prolonged culturing time (two weeks). Laminin addition increased both the length of the neurites (figure 9(a)) and the number of neurites (figure 9(b)). The most obvious increase in neurite migration was seen on top of GG 3.00%SPD, but a similar trend was





also observed with 1.5%SPD and 1.25%SPD gels (data not shown).

### 3.7. Neuronal cells encapsulated inside the gel

Neuronal cells were cultured as encapsulated in GG hydrogels for two weeks. Cells remained viable inside all the studied GG bioamine compositions (data not shown). Due to promising neurite migration results obtained from cultures on top of the laminin functionalized GG 3.00%SPD hydrogel, this composition was studied further. Neurite migration was observed in cultures inside the GG 3.00%SPD hydrogel both with and without functionalization with laminin (0–10 v%). The amount of neurites migrating from the cell aggregates varied from zero to dense outgrowth from aggregate to aggregate (example images of dense outgrowth are presented in figure 10). Neither neurite amount nor neurite length were affected by laminin concentration of hydrogel. Variation observed was also cell line or cell source independent (supplemental figure 1). The neuronal cells cultured encapsulated inside the GG hydrogel formed 3D neuronal network expressing typical neuronal markers (MAP-2 and  $\beta$ -tubulin<sub>III</sub>) co-labeled with phalloidin, (supplemental video 1).

## 4. Discussion

### 4.1. Bioamine crosslinked GG

GG has been approved by the FDA and EMA for food, cosmetic and pharmaceutical applications as a gelling or emulsion agent [15]. Taking advantage of the wide usage, GG has been applied for TE with promising results [15, 27, 28]. The common method of physical/ionotropic crosslinking of polysaccharides with metallic cations in order to form hydrogels has some inherent problems: controlling the crosslinking process and tuning of properties is challenging [30]. With

this fact in mind, we tested the ability of bioamines for physical crosslinking of GG. The study of alternative ionotropic crosslinking methods using bioamines for anionic polymers in TE is relatively new [34, 35] and those studies focused on the development of multi-component hydrogels for drug delivery applications [35]. On the other hand, we have addressed the GG-based bioamine crosslinked hydrogels specifically as a 3D cell culture scaffold for neural TE applications. Other forms of GG have already been studied in spinal cord injury rodent models [23–27], but not with these alternative crosslinking methods. The small cationic bioamine molecules worked efficiently and in a broad range of concentrations, producing stable hydrogels with tuneable mechanical properties.

The definition of a true gel is a material that responds to high stress by fracturing and is self-supporting, whereas a weak gel is a structured fluid that flows under stress [13]. The hydrogels we produced were macroscopic and strong enough to keep their shape after casting or even being handled with tweezers, thus they are true gels. For SPM, the lowest concentration that still produced a true gel was 0.40 w% and for SPD the limit was 1.25 w%. Lower concentrations produced weak gels that still pass the tube tilt test but flow under stress. When increasing the crosslinker concentration, a non-transparent (cloudy) area is formed inside the gel due to too rapid crosslinking and uneven mixing. This effect corresponds to highly anisotropic hydrogel formation, so the appearance of the cloudy area was considered to indicate the upper limit of the crosslinker concentration. For SPM, this limit was 1.10 w%, and for SPD, it was 3.00 w%. These concentration limitations also limit the mechanical properties of produced hydrogels, as they are directly proportional to the crosslinker concentration, as shown in figure 4. The same bioamine crosslinking method could be used as an alternative to many

hydrogels conventionally formed with ionotropic crosslinking, for example, alginate [30], pectin [13], xanthan gum [13] and other anionic polysaccharides.

#### 4.2. Mechanical and rheological properties of GG bioamine hydrogel

One design basis in current TE scaffold development is to produce biomimicking materials with mechanical properties similar to the corresponding tissue [4, 6, 10–12]. For the applications requiring higher stiffness (compressive or Young's modulus), such as cartilage TE, suitable GG compositions already exist [53]. For lower stiffness applications such as neural TE, however, GG needs to be modified further [17, 18]. The comparison of hydrogel properties with tissue properties would be easier if a higher consensus or standardization of the mechanical testing of biomedical samples existed, as also discussed by others [54, 55]. The lack of standardization and lack of accepted mathematical models causes high variability and difficulties in interpretation of results between different studies. To overcome this challenge, we included rabbit brain tissue samples and tested them with the same parameters as the hydrogels. According to the measurements, GG 0.40%SPM and GG 1.25% SPD gels with 2.7 and 9.4 kPa modulus, respectively, most closely resembled the compression moduli of rabbit cortical brain samples at 6.3 kPa. These values are slightly higher than those often measured for the brain, with previously reported values being 0.5–3 kPa [56, 57].

The hydrogel's fracture strength and strain are not comparable to brain tissue because no clear fracture point was seen on the brain samples, which underwent only a continuous strain hardening effect. In the biologically relevant deformation range of <20% strain, the mechanical behavior is similar between bioamine GG and brain. The compression rate, however, has a direct effect on gel fracture due to the visco-elastic recovery, as elegantly shown for GG already before [58]. Based on their methodology, we chose the compression rate at a relevant range for our application. In general, our results were in line with those of others [58], showing that higher crosslinker concentration or faster compression rate made GG more brittle (data not shown).

Rotational rheometry was used here as a complementary method to compression testing to gain additional insight into viscoelastic properties of the hydrogels. In addition, rheometry is very sensitive to anisotropy of the measured samples; the rheological spectrum is not continuous if the material is not isotropic. This effect makes the measurements more laborious to perform, but it can also be used as a quality control for checking the similarity of parallel samples. The measurements show that all the successfully measured samples had a gel-like response [13, 59]. In the rheological spectra, the gel storage modulus was always higher than the loss modulus, in both

amplitude and frequency sweep, and a fracture was seen under high strain. The rheological spectrum is also in a similar range as previously reported for GG hydrogels [26]. The high precision of rotational rheometry revealed the anisotropic nature of SPD cross-linked gels, causing those measurements to fail, but anisotropy was not discerned in compression testing. However, in cell culture, these anisotropies and nanotopographical variations can actually provide better cell anchoring sites than a totally homogenous hydrogel network [11].

#### 4.3. Suitability of GG as a culturing matrix for human neuronal cells

Cytocompatibility, the cellular scale response, needs to be evaluated with human cells before large-scale systemic biocompatibility testing [8]. In this work, we used hPSC-derived neuronal cells [50] to study both cytocompatibility and cell type-specific behavior in developed GGs. Importantly, when aiming for clinical applications, the development of neural TE products requires the usage of human cells already in the preclinical stage [60].

In this study, we used three steps to evaluate the hydrogel performance: (1) culturing cells beneath, (2) on top of or (3) encapsulated inside the hydrogel. This evaluation protocol gives information of cell survival, cell migration, and 3D network formation, but the different approaches should not be directly compared between each other [5]. First, performing the crosslinking directly on top of a pre-cultured neuronal network can reveal acute cytotoxicity caused by gel components or gelation during the first days in contact with the material [5, 61]. Crosslinking of GG with SPD or SPM did not cause acute (data not shown) or long-term cytotoxicity during two week follow-up. This result is in line with previous cytotoxicity studies for GGs [16, 17, 20, 35]. Importantly, SPD and SPM at the concentrations used for gelation (213–541 and 49.5–138  $\mu\text{M}$ , respectively) do not cause detrimental effects on neuronal cells. Culturing cells beneath hydrogel can also reveal gel-related effect on cell behavior, for example, changes in cell fate as described earlier for Matrigel [61]. With GG hydrogels, no obvious changes in cell fate were observed, as these cultures developed similarly to control cultures. Successful embedding also indicates that the porosity of the developed hydrogels was sufficient for medium diffusion and metabolite exchange through the gel block (height: 2.2–2.8 mm) during two weeks follow up. In conclusion, bioamine crosslinked GG hydrogels provided a suitable growth environment for human neuronal cells.

To study cell type-specific behavior, we cultured human neuronal cells on top of and encapsulated in GGs. GG hydrogels are considered biologically inert materials [17]. According to earlier studies, GG does not *in vitro* support neuronal cell migration on top of

gels or as encapsulated without the addition of cell adhesion cues [18, 28]. Our experiments using cells on top of gels showed similar results, as some neuronal aggregates remained as spheres without neurite migration as previously described for mouse neural cells [18]. Some aggregates, however, had neurite growth along the hydrogel surface. We assume that neurites growing on top of unmodified gel surfaces follow physical cues of the hydrogel. To enhance the cell migration on top of gels, we added the ECM protein laminin by physically mixing it into the GG prior to gelation. This functionalization of GG SPD hydrogels with laminin (5 v%–10 v%) significantly increased neurite migration. A similar positive effect was reported with fibronectin-derived synthetic GRGDS-peptide GG hydrogels [18]. Interestingly, functionalization with laminin was not beneficial with SPM crosslinked gels.

Encapsulated human neuronal cells showed a similar level of neurite migration despite functionalization with laminin. Previous studies using neural cells either on top of hydrogels or encapsulated have contradictory results about the benefits of functionalization on growth and migration. For example, functionalization with RGD, IKVAV or YIGSR peptides has shown both favorable and non-meaningful effects in neural cultures [62, 63]. This discrepancy could reflect the different microenvironments that cells experience in these cases.

The current paradigm of hydrogel development for TE involves making the mechanical properties mimic the tissue of interest [4, 10–12]. For neural cells, a suitable Young's modulus of hydrogel was previously reported between 1–5 kPa [57, 64, 65]. Our study revealed a wider, 2.7–22.6 kPa range in compression moduli, enabling neuronal cell growth. At the same time, our measured compression modulus for the rabbit brain samples ranged from 7.1 to 10.1 kPa. These results strongly suggest that the lack of standardized methods produces high variability in the results, preventing valuable comparisons between studies.

Interestingly, the gels with higher compressive moduli (11.5–22.6 kPa) showed the best cell type-specific response for cells grown on top of these hydrogels; even the compressive moduli brain samples were lower (7.1–10.1 kPa). Thus, there is a clear need to determine the actual threshold limits under which cells sense the mechanical properties of the surrounding scaffold and exhibit cell type-specific behavior [6, 12]. In other words, the true essence of biomimicking is still unknown. To answer this question, more optimal testing patterns need to be designed specifically for each tissue type. For example, the unconfined compression method measures a bulk hydrogel, whereas locally varying modulus and density, which are measurable with atomic force microscopy, are likely more important for cells [11, 12]. Compression testing should be used only to define the correct range of operations and for screening purposes, not to make specific interpretations. Although they are easier to

measure and interpret, the mechanical properties of a bulk hydrogel may not be optimal to predict the cellular level response to the hydrogel.

## 5. Conclusions

We conclude that GG hydrogels crosslinked with either SPM or SPD are cytocompatible and provide a compatible 3D scaffold for human neuronal cells. Metallic cations can be replaced by these small bioamines as ionotropic crosslinking agents. The mechanical properties of the GG bioamine hydrogel show a direct proportionality to crosslinker concentration, increasing the predictability of the properties of a certain composition. Mechanically, the GG bioamine hydrogels closely resemble the naïve rabbit brain. Both SPM and SPD crosslinked hydrogels were supporting the migration of neuronal cultures either on top of the hydrogel or as encapsulated inside the hydrogel and from a practical point of view there was no difference in gel handling between the crosslinkers. Neuronal cells grown on top of the SPD crosslinked GG hydrogels clearly benefit from laminin functionalization of the gel in a concentration dependent manner, suggesting that GG itself is too inert material for consistent neurite outgrowth. Based on our results the GG 3.00%SPD hydrogels were the most supportive for 3D neuronal network formation inside the hydrogel, being the most promising gel composition for further studies.

## Acknowledgments

We thank Outi Paloheimo, MSc from BioMediTech Imaging Core, University of Tampere, for help with microscopy of 3D cell cultures. We also thank Mari Hämäläinen, PhD from Tampere University Medical School for providing the rabbit brain samples. The study was financially supported by the Human Spare Parts program of Tekes—Finnish Funding Agency for Innovation, by the Finnish Cultural Foundation, grant numbers 00140325 and 00150312 and by the Academy of Finland grant number 286990.

## References

- [1] Langer R and Vacanti J 1993 Tissue engineering *Science* **260** 920–6
- [2] Schmidt C E and Leach J B 2003 Neural tissue engineering: strategies for repair and regeneration *Annu. Rev. Biomed. Eng.* **5** 293–347
- [3] Slaughter B V, Khurshid S S, Fisher O Z, Khademhosseini A and Peppas N A 2009 Hydrogels in regenerative medicine *Adv. Mater.* **21** 3307–29
- [4] Nisbet D R, Crompton K E, Horne M K, Finkelstein D I and Forsythe J S 2008 Neural tissue engineering of the CNS using hydrogels *J. Biomed. Mater. Res. B* **87B** 251–63
- [5] Ylä-Outinen L, Joki T, Varjola M, Skottman H and Narkilahti S 2012 Three-dimensional growth matrix for human embryonic stem cell-derived neuronal cells *J. Tissue Eng. Regen. Med.* **8** 186–94

- [6] Asthana A and Kisaalita W S 2013 Biophysical microenvironment and 3D culture physiological relevance *Drug Discov. Today* **18** 533–40
- [7] Annabi N, Tamayol A, Uquillas J A, Akbari M, Bertassoni L E, Cha C, Camci-Unal G, Dokmeci M R, Peppas N A and Khademhosseini A 2014 25th anniversary article: rational design and applications of hydrogels in regenerative medicine *Adv. Mater.* **26** 85–124
- [8] Williams D F 2008 On the mechanisms of biocompatibility *Biomaterials* **29** 2941–53
- [9] Vert M, Doi Y, Hellwich K, Hess M, Hodge P, Kubisa P, Rinaudo M and Schué F 2012 Terminology for biorelated polymers and applications (IUPAC recommendations 2012) *Pure Appl. Chem.* **84** 377–410
- [10] Brandl F, Sommer F and Goepferich A 2007 Rational design of hydrogels for tissue engineering: impact of physical factors on cell behavior *Biomaterials* **28** 134–46
- [11] Walters N J and Gentleman E 2015 Evolving insights in cell–matrix interactions: elucidating how non-soluble properties of the extracellular niche direct stem cell fate *Acta Biomater.* **11** 3–16
- [12] Ihalainen T O, Aires L, Herzog F A, Schwartlander R, Moeller J and Vogel V 2015 Differential basal-to-apical accessibility of lamin A/C epitopes in the nuclear lamina regulated by changes in cytoskeletal tension *Nat. Mater.* **14** 1252–61
- [13] Morris E R, Nishinari K and Rinaudo M 2012 Gelation of gellan—a review *Food Hydrocoll.* **28** 373–411
- [14] CP Kelco. Gellan gum | CP Kelco. 2014 <http://cpkelco.com/products/gellan-gum/> (Accessed: 12 September 2014)
- [15] Fialho A M, Moreira L M, Granja A T, Popescu A O, Hoffmann K and Sá-Correia I 2008 Occurrence, production, and applications of gellan: current state and perspectives *Appl. Microbiol. Biotechnol.* **79** 889–900
- [16] Smith A M, Shelton R M, Perrie Y and Harris J J 2007 An initial evaluation of gellan gum as a material for tissue engineering applications *J. Biomater. Appl.* **22** 241–54
- [17] Ferris C J, Gilmore K J, Wallace G G and in het Panhuis M 2013 Modified gellan gum hydrogels for tissue engineering applications *Soft Matter* **9** 3705–11
- [18] Silva N A, Cooke M J, Tam R Y, Sousa N, Salgado A J, Reis R L and Shoichet M S 2012 The effects of peptide modified gellan gum and olfactory ensheathing glia cells on neural stem/progenitor cell fate *Biomaterials* **33** 6345–54
- [19] Barbani N, Guerra G, Cristallini C, Urciuoli P, Avvisati R, Sala A and Rosellini E 2012 Hydroxyapatite/gelatin/gellan sponges as nanocomposite scaffolds for bone reconstruction *J. Mater. Sci. Mater. Med.* **23** 51–61
- [20] Oliveira J T, Martins L, Picciochi R, Malafaya P B, Sousa R A, Neves N M, Mano J F and Reis R L 2010 Gellan gum: a new biomaterial for cartilage tissue engineering applications *J. Biomed. Mater. Res. A* **93A** 852–63
- [21] Lee H, Fisher S, Kallos M S and Hunter C J 2011 Optimizing gelling parameters of gellan gum for fibrocartilage tissue engineering *J. Biomed. Mater. Res. B* **98B** 238–45
- [22] Shin H, Olsen B D and Khademhosseini A 2012 The mechanical properties and cytotoxicity of cell-laden double-network hydrogels based on photocrosslinkable gelatin and gellan gum biomacromolecules *Biomaterials* **33** 3143–52
- [23] Silva N A et al 2010 Development and characterization of a novel hybrid tissue engineering-based scaffold for spinal cord injury repair *Tissue Eng. A* **16** 45–54
- [24] Pereira D R, Silva-Correia J, Caridade S G, Oliveira J T, Sousa R A, Salgado A J, Oliveira J M, Mano J F, Sousa N and Reis R L 2011 Development of gellan gum-based microparticles/hydrogel matrices for application in the intervertebral disc regeneration *Tissue Eng. C* **17** 961–72
- [25] Silva-Correia J, Oliveira J M, Caridade S G, Oliveira J T, Sousa R A, Mano J F and Reis R L 2011 Gellan gum-based hydrogels for intervertebral disc tissue-engineering applications *J. Tissue Eng. Regen. Med.* **5** e97–107
- [26] Silva-Correia J, Gloria A, Oliveira M B, Mano J F, Oliveira J M, Ambrosio L and Reis R L 2013 Rheological and mechanical properties of acellular and cell-laden methacrylated gellan gum hydrogels *J. Biomed. Mater. Res. A* **101** 3438–46
- [27] Tsaryk R, Silva-Correia J, Oliveira J M, Unger R E, Landes C, Brochhausen C, Ghanaati S, Reis R L and Kirkpatrick C J 2014 Biological performance of cell-encapsulated methacrylated gellan gum-based hydrogels for nucleus pulposus regeneration *J. Tissue Eng. Regen. Med.* (<https://doi.org/10.1002/term.1959>)
- [28] Lozano R, Stevens L, Thompson B C, Gilmore K J, Gorkin R III, Stewart E M, in het Panhuis M, Romero-Ortega M and Wallace G G 2015 3D printing of layered brain-like structures using peptide modified gellan gum substrates *Biomaterials* **67** 264–73
- [29] Coutinho D F, Sant S V, Shin H, Oliveira J T, Gomes M E, Neves N M, Khademhosseini A and Reis R L 2010 Modified gellan gum hydrogels with tunable physical and mechanical properties *Biomaterials* **31** 7494–502
- [30] Lee C, Shin J, Lee J S, Byun E, Ryu J H, Um S H, Kim D, Lee H and Cho S 2013 Bioinspired, calcium-free alginate hydrogels with tunable physical and mechanical properties and improved biocompatibility *Biomacromolecules* **14** 2004–13
- [31] Fedorovich N E, Oudshoorn M H, van Geemen D, Hennink W E, Alblas J and Dhert W J A 2009 The effect of photopolymerization on stem cells embedded in hydrogels *Biomaterials* **30** 344–53
- [32] Hennink W E and van Nostrum C 2002 Novel crosslinking methods to design hydrogels *Adv. Drug. Deliv. Rev.* **54** 13–36
- [33] Ifkovits J L and Burdick J A 2007 Review: photopolymerizable and degradable biomaterials for tissue engineering applications *Tissue Eng.* **13** 2369–85
- [34] Parraga J E, Zorzi G K, Diebold Y, Seijo B and Sanchez A 2014 Nanoparticles based on naturally-occurring biopolymers as versatile delivery platforms for delicate bioactive molecules: an application for ocular gene silencing *Int. J. Pharm.* **477** 12–20
- [35] López-Cebral R, Paolicelli P, Romero-Caamaño V, Seijo B, Casadei M A and Sanchez A 2013 Spermidine-cross-linked hydrogels as novel potential platforms for pharmaceutical applications *J. Pharm. Sci.* **102** 2632–43
- [36] Soto A M, Koivisto J T, Parraga J E, Silva-Correia J, Oliveira J M, Reis R L, Kellomäki M, Hyttinen J and Figueiras E 2016 Optical projection tomography technique for image texture and mass transport studies in hydrogels based on gellan gum *Langmuir* **32** 5173–82
- [37] Khan A U, Mei Y H and Wilson T 1992 A proposed function for spermine and spermidine: protection of replicating DNA against damage by singlet oxygen *Proc. Natl Acad. Sci.* **89** 11426–7
- [38] Ha H C, Sirisoma N S, Kuppasamy P, Zweier J L, Woster P M and Casero R A Jr 1998 The natural polyamine spermine functions directly as a free radical scavenger *Proc. Natl Acad. Sci. USA* **95** 11140–5
- [39] Fujiwara K, Bai G and Kitagawa T 1997 Polyamine-like immunoreactivity in rat neurons *Brain Res.* **767** 166–71
- [40] Laube G, Bernstein H, Wolf G and Veh R W 2002 Differential distribution of spermidine/spermine-like immunoreactivity in neurons of the adult rat brain *J. Comp. Neurol.* **444** 369–86
- [41] ASTM F2900 2011 *Standard Guide for Characterization of Hydrogels used in Regenerative Medicine* (West Conshohocken, PA: ASTM International) pp 1–10
- [42] Tanodekaew S, Godward J, Heatley F and Booth C 1997 Gelation of aqueous solutions of diblock copolymers of ethylene oxide and D,L-lactide *Macromol. Chem. Phys.* **198** 3385–95
- [43] Callister W D 2003 *Materials Science and Engineering: An Introduction* (New York: Wiley) pp 117–20 480–98
- [44] Schramm G 1998 *A Practical Approach to Rheology and Rheometry* (Karlsruhe: Gebrüder HAAKE GmbH) pp 119–33
- [45] Rajala K et al 2010 A defined and xeno-free culture method enabling the establishment of clinical-grade human embryonic, induced pluripotent and adipose stem cells *PLoS One* **5** e10246
- [46] Skottman H 2010 Derivation and characterization of three new human embryonic stem cell lines in Finland *In Vitro Cell. Dev. —Animal* **46** 206–9



- [47] Sorkio A E, Vuorimaa-Laukkanen E P, Hakola H M, Liang H, Ujula T A, Valle-Delgado J J, Österberg M, Yliperttula M L and Skottman H 2015 Biomimetic collagen I and IV double layer Langmuir–Schaefer films as microenvironment for human pluripotent stem cell derived retinal pigment epithelial cells *Biomaterials* **51** 257–69
- [48] Ojala M, Prajapati C, Pölonen R, Rajala K, Pekkanen-Mattila M, Rasku J, Larsson K and Aalto-Setälä K 2016 Mutation-specific phenotypes in hiPSC-derived cardiomyocytes carrying either myosin-binding protein C or  $\alpha$ -tropomyosin mutation for hypertrophic cardiomyopathy *Stem. Cells Int.* **2016** 16
- [49] Toivonen S et al 2013 Comparative analysis of targeted differentiation of human induced pluripotent stem cells (hiPSCs) and human embryonic stem cells reveals variability associated with incomplete transgene silencing in retrovirally derived hiPSC lines *Stem. Cells Transl. Med.* **2** 83–93
- [50] Lappalainen R S, Salomäki M, Ylä-Outinen L, Heikkilä T J, Hyttinen J A K, Pihlajamäki H, Suuronen R, Skottman H and Narkilahti S 2010 Similarly derived and cultured hESC lines show variation in their developmental potential towards neuronal cells in long-term culture *Regener. Med.* **5** 749–62
- [51] Rasband W S ImageJ. 2016 <http://imagej.nih.gov/ij/> (Accessed 11 May 2016)
- [52] Schneider C A, Rasband W S and Eliceiri K W 2012 NIH image to ImageJ: 25 years of image analysis *Nat. Meth.* **9** 671–5
- [53] Oliveira J T, Santos T C, Martins L, Picciochi R, Marques A P, Castro A G, Neves N M, Mano J F and Reis R L 2010 Gellan gum injectable hydrogels for cartilage tissue engineering applications: *In vitro* studies and preliminary *in vivo* evaluation *Tissue Eng. A* **16** 343–53
- [54] Oyen M L 2014 Mechanical characterisation of hydrogel materials *Int. Mater. Rev.* **59** 44–59
- [55] Prevost T P, Balakrishnan A, Suresh S and Socrate S 2011 Biomechanics of brain tissue *Acta Biomater.* **7** 83–95
- [56] Laksari K, Shafieian M and Darvish K 2012 Constitutive model for brain tissue under finite compression *J. Biomech.* **45** 642–6
- [57] Engler A J, Sen S, Sweeney H L and Discher D E 2006 Matrix elasticity directs stem cell lineage specification *Cell* **126** 677–89
- [58] Nakamura K, Shinoda E and Tokita M 2001 The influence of compression velocity on strength and structure for gellan gels *Food Hydrocoll.* **15** 247–52
- [59] Kavanagh G M and Ross-Murphy S B 1998 Rheological characterisation of polymer gels *Prog. Polym. Sci.* **23** 533–62
- [60] Lindvall O and Kokaia Z 2010 Stem cells in human neurodegenerative disorders—time for clinical translation? *J. Clin. Invest.* **120** 29–40
- [61] Thonhoff J R, Lou D I, Jordan P M, Zhao X and Wu P 2008 Compatibility of human fetal neural stem cells with hydrogel biomaterials *in vitro Brain Res.* **1187** 42–51
- [62] Zhang Z et al 2016 Layered hydrogels accelerate iPSC-derived neuronal maturation and reveal migration defects caused by MeCP2 dysfunction *Proc. Natl Acad. Sci.* **113** 3185–90
- [63] Frampton J P, Hynd M R, Shuler M L and Shain W 2011 Fabrication and optimization of alginate hydrogel constructs for use in 3D neural cell culture *Biomed. Mater.* **6** 015002
- [64] Pogoda K, Chin L, Georges P C, Byfield F J, Bucki R, Kim R, Weaver M, Wells R G, Marcinkiewicz C and Janmey P A 2014 Compression stiffening of brain and its effect on mechanosensing by glioma cells *New J. Phys.* **16** 075002
- [65] Palazzolo G, Broguiere N, Cenciarelli O, Dermutz H and Zenobi-Wong M 2015 Ultrasoft alginate hydrogels support long-term three-dimensional functional neuronal networks *Tissue Eng. A* **21** 2177–85

# Direct Laser Writing of Tubular Microtowers for 3D Culture of Human Pluripotent Stem Cell-Derived Neuronal Cells

Sanna Turunen,<sup>\*,†</sup> Tiina Joki,<sup>‡</sup> Maiju L. Hiltunen,<sup>†</sup> Teemu O. Ihalainen,<sup>‡</sup> Susanna Narkilahti,<sup>‡</sup> and Minna Kellomäki<sup>†,§</sup>

<sup>†</sup>Biomaterials and Tissue Engineering Group, BioMediTech and Faculty of Biomedical Sciences and Engineering, Tampere University of Technology, Korkeakoulunkatu 3, 33720 Tampere, Finland

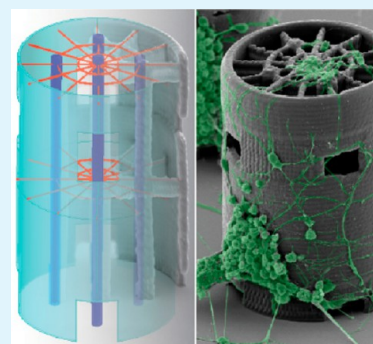
<sup>‡</sup>NeuroGroup, BioMediTech and Faculty of Medicine and Life Sciences, University of Tampere, Lääkärintätkatu 1, 33520 Tampere, Finland

<sup>§</sup>BioMediTech and Faculty of Medicine and Life Sciences, University of Tampere, Lääkärintätkatu 1, 33520 Tampere, Finland

## S Supporting Information

**ABSTRACT:** As the complex structure of nervous tissue cannot be mimicked in two-dimensional (2D) cultures, the development of three-dimensional (3D) neuronal cell culture platforms is a topical issue in the field of neuroscience and neural tissue engineering. Computer-assisted laser-based fabrication techniques such as direct laser writing by two-photon polymerization (2PP-DLW) offer a versatile tool to fabricate 3D cell culture platforms with highly ordered geometries in the size scale of natural 3D cell environments. In this study, we present the design and 2PP-DLW fabrication process of a novel 3D neuronal cell culture platform based on tubular microtowers. The platform facilitates efficient long-term 3D culturing of human neuronal cells and supports neurite orientation and 3D network formation. Microtower designs both with or without intraluminal guidance cues and/or openings in the tower wall are designed and successfully fabricated from Ormocomp. Three of the microtower designs are chosen for the final culture platform: a design with openings in the wall and intraluminal guidance cues (webs and pillars), a design with openings but without intraluminal structures, and a plain cylinder design. The proposed culture platform offers a promising concept for future 3D cultures in the field of neuroscience.

**KEYWORDS:** direct laser writing, two-photon polymerization, microstructures, 3D culture platform, neurons, orientation of neurites



## 1. INTRODUCTION

*In vitro* cell culture platforms are invaluable tools for the study of neural functions in health and disease. However, the planar culture of neuronal cells represents an oversimplification of the structure of the *in vivo* neural system. Moreover, two-dimensional (2D) cultures may lead to uncharacteristic cell–cell and cell–matrix interactions and alter cell behavior.<sup>1</sup> Thus, one of the major strategies in the field of neuroscience and neural tissue engineering (TE) is to develop three-dimensional (3D) cell culture models that more closely mimic the *in vivo*-like microenvironment and organization of neural networks into segregated neuronal nuclei connected by discrete axonal tracts.<sup>2</sup> Various approaches can be used to create a 3D environment such as porous solid scaffolds,<sup>3</sup> hydrogel matrices,<sup>4</sup> microscale tubular guidance conduits,<sup>5</sup> polymer microfibers,<sup>6</sup> or arrays of nano- and microscale structures, e.g., pillars<sup>7</sup> or towers.<sup>2</sup> Axonal alignment is an important goal for neural TE in central nervous system (CNS) and peripheral nervous system (PNS) injuries and deficits. Thus, in recent years, several *in vitro* studies of 3D nerve guidance conduit (NGC) geometries using aligned channels and fibers have been conducted.<sup>8,9</sup> Although NGCs have been mainly used for PNS injury studies,<sup>10</sup> microscale tubular guidance channels may also serve as 3D *in vitro* test platforms for the

investigation of the different factors (mechanical, chemical, or topographical) that influence CNS neuronal survival and axonal directionality. 3D microconduits can be engineered according to specific need by systematically varying several parameters and thus providing a new approach to study the influences of different guidance cues on axonal path finding *in vitro*.<sup>5</sup> For example, the incorporation of an oriented intraluminal framework into the channel lumen to more accurately mimic the tract-like structure present in both CNS and PNS can result in improved cell attachment, migration, and alignment of regenerating axons in comparison with simple hollow tubular structures.<sup>11</sup> The intraluminal topographical cues or fibers promote the growth of neurons because the larger surface area provided by the introduction of an internal architecture significantly increases cell adherence and growth.<sup>12</sup>

The fabrication of multichannel conduits or channels with a regular filament arrangement or intricate intraluminal details is not an easy task. Conventionally, different natural and synthetic polymers have been fabricated into NGCs via injection

Received: April 20, 2017

Accepted: July 11, 2017

Published: July 11, 2017

molding,<sup>13</sup> mandrel coating or dip coating,<sup>14</sup> centrifuge casting,<sup>15</sup> film rolling and sealing,<sup>16</sup> extrusion,<sup>17</sup> electrospinning,<sup>18</sup> and microbraiding of filaments.<sup>19</sup> However, these manufacturing techniques cannot reproduce tubes with precise dimensions or complex microscale internal structures.<sup>20</sup> Hence, several rapid prototyping techniques that enable the production of complicated 3D structures automatically according to computer-aided designs (CADs) have been used. These prototyping techniques that include microstereolithography<sup>21</sup> and inkjet microdispensing<sup>22</sup> have been used to fabricate semicircular trenches and tubular nerve conduits. Usually, the sizes of the scaffold features produced by 3D printing and nozzle-based techniques are in the range of 1 to 6 mm with the width of the printed line limited to a minimum of 200 to 300  $\mu\text{m}$ .<sup>23</sup> However, the highest level of flexibility in structural design is achieved by using a rapid prototyping technique called direct laser writing by two-photon polymerization (2PP-DLW). This technique allows the fabrication of complex features including internal walls, overhangs, or tortuous channels with feature sizes in the  $\mu\text{m}$  and sub- $\mu\text{m}$  range.<sup>23</sup> 2PP-DLW is a sequential fabrication technique in which structures are created by translating either the focal spot of a tightly focused laser beam or the target, according to a predefined scanning path.<sup>24</sup> The two-photon absorption (2PA) of photoinitiator molecules initiates radical chain-growth polymerization that converts small, unsaturated monomer molecules from a liquid state to solid macromolecules.<sup>25</sup> The polymerization is localized within the focal volume of the laser beam enabling the fabrication of isolated structures with <100 nm line widths.<sup>26</sup>

2PP-DLW can process various photosensitive, biocompatible materials. The technique has already been harnessed to construct ordered 3D scaffolds with geometrical details on a cellular scale (10  $\mu\text{m}$ ) for neuronal cell culture purposes.<sup>27</sup> A nonbiodegradable organically modified ceramic, Ormocomp, has been structured by 2PP-DLW into various geometrical shapes for neural applications such as Lego-like blocks,<sup>28</sup> pillars,<sup>29,30</sup> and micro-ridges<sup>31</sup> and has been successfully used for contact guidance of neuroblastoma cells of rat<sup>28,31</sup> and human<sup>29–31</sup> origin. In addition, Zr–Si hybrid material and methacrylated polylactide (PLA) have been structured into hollow cylinder scaffolds and used for culturing rodent neural cells.<sup>32,33</sup> On the basis of these previously reported results, there seems to be an obvious need for studies conducted with human neuronal cells of nonmalignant origin.

In this paper, we describe the optimization of the fabrication process for a novel, detailed, 3D cell culture platform based on direct laser written tubular microtowers and human neuronal cells. Although 2PP-DLW is not an easily upscalable fabrication method such as electrospinning, it enables the repeatable production of platforms with fine details for *in vitro* applications. These easily tunable platforms can be used for studying the effects of the layout and the design (shapes and dimensions) on cell behavior. Thus, the aim of our study was to polymerize different microtower designs including a design with intraluminal longitudinal micropillars that mimic the axonal tracts *in vivo*. In particular, we investigated the ability of the towers to support the adhesion, growth, and orientation of human pluripotent stem cell (hPSC)-derived neuronal cells.

## 2. EXPERIMENTAL SECTION

**2.1. 2PP-DLW Fabrication Setup.** The microtowers were fabricated with a custom-built 2PP-DLW setup, which was an updated version of the system described previously.<sup>34</sup> Briefly, a frequency

doubled femtosecond fiber laser (FP-532-0.2-FS-01, Fianium Ltd., United Kingdom), operating at 532 nm with a pulse duration of 200 fs, repetition rate of 40 MHz, and average output power of 200 mW, was used as an irradiation source. The beam was scanned in the *xy*-direction with a fast steering mirror scanner (FSM-300, Newport Corporation, USA) and in the *z*-direction with a piezoelectric objective lens positioning system (Mipos 250 SGEX, Piezosystem Jena GmbH, Germany). The beam was directed into a 50 $\times$  oil immersion objective (N.A. = 0.90, Meiji Techno, Japan) situated on an upright microscope frame (ECLIPSE ME 600, Nikon, Japan). The objective had an average transmittance of 48%. In order to overfill the back aperture of the objective lens, a combination of two beam expanders, a 10 $\times$  and an adjustable 1–3 $\times$ , was used. The average laser power was adjusted to a suitable polymerization level with a motorized attenuator (Watt Pilot, UAB Altechna, Lithuania). The laser power was measured at the back aperture of the objective with a power meter console (PM100USB, Thorlabs Inc., USA) coupled with a S310C thermal sensor.

**2.2. Materials and Sample Preparation.** A commercial polymer-ceramic hybrid material Ormocomp (Micro Resist Technology GmbH, Germany) was used as a photocurable material in combination with 2 wt % of the photoinitiator Irgacure 127 (Ciba Specialty Chemicals, Switzerland). In order to enhance the adhesion of the microtowers to the glass surface, the coverslips intended for cell culture experiments were pretreated with 3-(trimethoxysilyl) propyl methacrylate (MAPTMS, Sigma-Aldrich Finland Oy, Finland) as described by Käpylä et al.<sup>35</sup> For the polymerization, a drop of Ormocomp was administered on a round coverslip ( $\varnothing = 9$  mm) that was sandwiched between a microscope slide and a coverslip separated by a 250  $\mu\text{m}$  thick stainless steel spacer. After the polymerization, the unexposed part of the resist was dissolved by immersing the coverslip in Ormodev developer (Micro Resist Technology GmbH, Germany) for 15 min and by rinsing with Ormodev and hexamethyldisilazane (HMDS, Sigma-Aldrich Finland Oy, Finland).

**2.3. Determination of Polymerization Window and Feature Size.** In order to define the window of practical operation for the fabrication of the microtowers with good quality, the polymerization windows ( $P_w$ ) were determined for the scanning speeds of 150, 350, and 550  $\mu\text{m s}^{-1}$ . The polymerization window was calculated as the power range between the polymerization ( $P_{th}$ ) and the damage thresholds ( $P_D$ ). For the threshold value determination, the laser focus was positioned inside the resist volume to exclude any interaction with the glass surface, and then, the laser power value was gradually increased while polymerizing simple square patterns. The polymerization threshold was defined as the lowest average laser power that yielded a barely visible polymerized pattern and the damage threshold as the power value where the microexplosions first started to emerge. The average threshold values were calculated from the measurements made from four separate samples. To ensure a large enough margin for the damage-free fabrication without the appearance of microexplosions due to the laser power fluctuation or the inhomogeneity of the resin, the microtowers were fabricated with power values corresponding to 70% of the polymerization window according to the formula  $P = P_w \times x + P_{th}$ , where  $P_w$  is the polymerization window,  $P_{th}$  is the polymerization threshold, and  $x = 0.7$  is the power factor.

In order to determine the optimal slicing distance for the contours, the line width and height were analyzed from suspended lines polymerized between supporting wall structures with scanning speeds of 150, 350, and 550  $\mu\text{m s}^{-1}$ . All the suspended lines were fabricated with the average laser power values corresponding to 70% of the polymerization window determined previously for each scanning speed. Feature dimensions were measured from the top view (0° tilt) and side view (90° tilt) of SEM images with a free software GIMP (version 2.8). The degree of voxel overlap for the chosen contour distances was calculated as the product of voxel displacement in axial and lateral directions according to the following:

$$\delta = \frac{w - dx}{w} \times \frac{h - dz}{h} \quad (1)$$

where  $\delta$  is the degree of the voxel overlap,  $w$  and  $h$  are the width and height of the voxel, and  $dx$  and  $dz$  are the lateral and axial voxel distances, respectively.<sup>36</sup>

**2.4. Microtower Design.** The tubular microtowers were designed using the Rhinoceros CAD program (version 4.0, Robert McNeel & Associates, USA). The outer shell of the towers was a 150.0  $\mu\text{m}$  high cylinder with an outer diameter of 77.0  $\mu\text{m}$  and an inner diameter of 75.0  $\mu\text{m}$ . The cylinder was designed to have openings at the foot of the tower for the cells to enter and in the upper part of the tower to allow the efficient flow of medium also in the lumen of the tower. Two different shapes for the openings, i.e., elliptical and rectangular, were tested to find the one that best retained its shape and size after polymerization. A set of five longitudinal micropillars inspired by the axonal tracts present *in vivo* was placed inside the tower to offer oriented topography for neurites to migrate along through the channel. The diameter of the pillars was set to 5.0  $\mu\text{m}$  to achieve thin but robust enough structures. Spider web-like platforms were inserted on top and halfway down the tower to further increase the surface area for cells to attach to and for neuronal somas to remain stationary. Two different designs for the spider webs were tested: a dense web comprising three concentric polygons with 5.0  $\mu\text{m}$  line spacing (designs I and III) and a sparse web comprising two concentric polygons with 10.0  $\mu\text{m}$  spacing (designs II and IV). As a comparison, hollow microtowers with and without openings were also designed. In total, six different microtower designs were drawn: designs I and II (Figure S2a,b) had elliptical openings with dense or sparse webs, designs III (Figure S2c) and IV (Figure 1a) had rectangular openings with

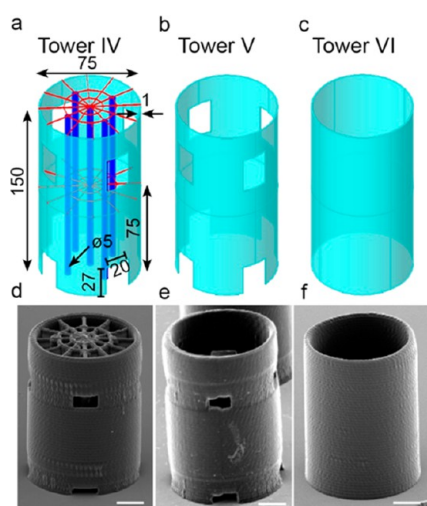


**Figure 1.** CAD and SEM images of the microtowers: (a, d) design IV with rectangular openings and sparse webs, (b, e) design V with rectangular openings, and (c, f) design VI without openings. The dimensions in CAD images are given in micrometers. SEM images are taken from the 60° tilt angle. The top view and the longitudinal cross-section of the design IV tower are presented in Figure S4. The scale bars represent 20  $\mu\text{m}$ .

dense or sparse webs, design V (Figure 1b) was a hollow cylinder with rectangular openings, and design VI (Figure 1c) was a hollow cylinder without any openings.

**2.5. Fabrication of Microtowers.** The microtower designs I–IV were polymerized using the 50 $\times$  objective to find out which version replicated the original CAD model most precisely. The cylinders and pillars were fabricated using the multipath scanning method,<sup>37</sup> in which the cylinder walls were formed by two nested contours separated by a distance of 1  $\mu\text{m}$ , and the micropillars, by three nested contours separated by a distance of 1  $\mu\text{m}$ . Because the spider webs were polymerized as single line scans, a moderate scanning speed of 150  $\mu\text{m s}^{-1}$  had to be used in order to achieve robust and untwisted threads. For the cylinders and pillars, scanning speeds of 350 and 550  $\mu\text{m s}^{-1}$  were tested to optimize the fabrication time versus surface quality of the structures. For each scanning speed, the average laser power corresponding to the

predetermined 70% of the polymerization window was used. In order to explore the intraluminal architecture of the microtowers with SEM imaging, longitudinal cross sections of design II and IV towers were also fabricated with the scanning speeds of 350 and 550  $\mu\text{m s}^{-1}$ .

For the cell culture experiment, six parallel samples per time point with an array of nine microtowers comprising three pieces of each design (IV, V, and VI) were fabricated on MAPTMS-coated round glass coverslips ( $\Phi = 9 \text{ mm}$ ). The distance between individual towers of the same design was  $\sim 90 \mu\text{m}$  and between different tower designs was  $\sim 260 \mu\text{m}$ . The cylinders and pillars were produced with the constant scanning speed of 550  $\mu\text{m s}^{-1}$  and approximately 70% power, and the webs were scanned with the speed of 150  $\mu\text{m s}^{-1}$  and power of 70%.

**2.6. Characterization of Microtowers.** The dimensions of the fabricated suspended line structures and the microtowers were analyzed by SEM imaging with a Philips XL-30 microscope (Philips Electron Optics, The Netherlands). Prior to imaging, the samples were sputter coated with gold in an argon atmosphere either to a nominal thickness of 113 nm (S 150 Sputter Coater, Edwards Ltd., UK) or 60 nm (SCD 050 Sputter Coater, BAL-TEC AG, Liechtenstein). The feature dimensions were measured from top (0° tilt) and side (90° tilt) view SEM images with GIMP software.

Because the cell adhesion can be affected by surface topography, the surface roughness of the microtower cylinder walls was investigated by noncontact mode AFM (XE-100, Park Systems Inc., USA). For the imaging, the coverslip containing the microtowers was mounted in an upright position on the  $xy$ -scanning stage in order to access the surface of the walls of the towers with the AFM cantilever. Measurements were performed using silicon probes (ACTa, Applied NanoStructures Inc., USA) with a nominal resonance frequency of 300 kHz, spring constant of 40  $\text{N m}^{-1}$ , and a tetrahedral pyramidal shaped tip with a face angle of 18°. Images were acquired with a scan rate of 1.0 Hz. Areas of 10  $\mu\text{m} \times 10 \mu\text{m}$  were imaged from the cylindrical walls of each tower design (IV, V, and VI). From the two designs with openings, images were acquired from two different locations of the cylinder: the sections with a smoother surface and the sections located between the openings with a seemingly rougher texture. The roughness of the surface was analyzed from the AFM images with XEI image processing software (version 1.8.0, Park Systems Inc., USA). The curvature resulting from the cylindrical shape of the tower wall was removed from the acquired images by using the flattening tool with second order fitting curve in the  $x$ -direction. As the microtowers appeared to be tilted to some extent in the  $y$ -direction, the slope was eliminated by also flattening the images in a vertical direction with a first order fitting curve. The surface roughness was defined as the areal average surface roughness ( $R_a$ ).

The stiffness of the polymerized structures is mainly expressed by the Young's modulus of the material. Thus, force spectroscopy measurements were performed with AFM to estimate the Young's modulus of Ormocomp. The elastic properties of the sample were investigated with AFM force curves by recording the applied force and the depth of indentation as the tip was pushed against the sample surface.<sup>38</sup> Force–indentation curves were recorded at three points from each tower design by scanning areas of 15  $\mu\text{m} \times 15 \mu\text{m}$  from the upper rim of the cylinder with a scan rate of 0.5 Hz. For comparison, similar sized areas were also recorded from the three UV-cured Ormocomp thin films. The fabrication of the thin films is described in the Supporting Information.

One of the most commonly used models for deriving the elastic modulus from force curve data is the Hertz model<sup>39</sup> that gives the force on a spherical tip as a function of the elastic properties of the material, the radius of the tip, and the indentation depth.<sup>40</sup> The following is a modified Hertz model<sup>41</sup> for a four-sided pyramidal indenter:

$$F = \frac{E}{1 - \nu^2} \frac{\tan \alpha}{\sqrt{2}} \delta^2 \quad (2)$$

where  $F$  is the indentation force applied to the sample,  $E$  is the Young's modulus,  $\nu$  is the Poisson's ratio of the sample (set to 0.35 according to<sup>42</sup>),  $\delta$  is the indentation depth, and  $\alpha$  is the face angle of the pyramidal tip (18° in our case). The cantilever deflection during the indentation was taken into account in XEI by transforming the Force–Z displacement curve to Force–Separation curve via the cantilever's spring constant value ( $k$ ). The spring constant of the cantilever was not

calibrated prior to the analysis. Instead, the nominal value of  $k = 40 \text{ N m}^{-1}$  quoted by the manufacturer was used. Stiffness data was calculated automatically with XEI from the slopes of the force curves after fitting with the Hertz model.

**2.7. Differentiation of Neuronal Cells and Cell Culture.** Human neural cells derived from the hESC line Regea 08/023 (passage 46) were used in cell culture experiments. Stem cell line derivation, culturing, and characterization as well as neuronal differentiation have been previously published.<sup>43,44</sup> The BMT institute has been given ethical permissions to derive hESC lines and to use stem cells for neural research (1426/32/300/05, R05116). The quality control of the used stem cell line was implemented by frequent gene and protein expression analysis for pluripotency in addition to karyotype and mycoplasma assays. Stem cells were predifferentiated for 13 weeks into neural fate before using them for culture experiments. Briefly, undifferentiated colonies were mechanically cut into small cell aggregates and transferred into neural differentiation medium (NDM) on low cell binding culture plates. NDM contains 1:1 DMEM/F12 and Neurobasal supplemented with GlutaMax (2 mM), 1 $\times$  B27, 1 $\times$  N2, and penicillin/streptomycin (25 U mL<sup>-1</sup>), all from Thermo Fisher Scientific Corporation, USA. During differentiation, the medium was supplemented with bFGF (20 ng mL<sup>-1</sup>, R&D Systems Inc., USA). Cell aggregates formed round freely floating neurospheres, which were kept small ( $\varnothing \sim 500 \mu\text{m}$ ) by cutting once a week under a microscope. One third of the medium was changed three times a week.

For cell culture experiments, coverslips containing microtowers were disinfected with 70% (v/v) ethanol for 15 min, immersed in Dulbecco's phosphate buffered saline (DPBS, Lonza Group Ltd., Switzerland) for 2 h at +4 °C, and allowed to air-dry. The PDMS cell restrictors were attached to coverslips, and the samples were placed on 6-well plates. The surfaces were coated using mouse laminin (10  $\mu\text{g mL}^{-1}$ , Sigma-Aldrich). The laminin coating solution was incubated on samples for 72 h at +4 °C.

For the plating of the cells on the microtower samples, neurospheres were enzymatically dissociated into a single cell solution using TrypLE Select 1 $\times$  (Thermo Fischer Scientific) according to the manufacturer's instructions. The cells were plated as a single cell suspension on top of the laminin-coated samples at a density of  $\sim 35\,000 \text{ cells cm}^{-2}$ . For the first week in culture, NDM without growth factors was used, after which NDM was supplemented with bFGF (4 ng mL<sup>-1</sup>) and brain-derived neurotrophic factor (BDNF, 5 ng mL<sup>-1</sup>, ProSpec-Tany TechnoGene Ltd., Israel). During culturing, the cells were monitored and phase contrast images were taken with an inverted microscope (Nikon Eclipse TE 2000-S, Nikon Corporation, Japan) equipped with the Nikon Digital Sight Camera System (DS-5M-L1). Half of the cell culture media was changed three times a week.

**2.8. Viability Assay.** For viability analysis, the cultures were stained using a LIVE/DEAD viability/cytotoxicity assay (Thermo Fisher Scientific). In brief, the assay comprises two fluorescent dyes: Calcein-AM (0.1  $\mu\text{M}$ ,  $\lambda_{\text{excitation}} = 488 \text{ nm}$ ) that stains intact cells and ethidium homodimer-1 (0.4  $\mu\text{M}$ ,  $\lambda_{\text{excitation}} = 568 \text{ nm}$ ) that stains dead cells. After 30 min of incubation at +37 °C, the cells were imaged with an Olympus IX51 inverted microscope and an Olympus DP30BW digital camera (Olympus Corporation, Japan). Three parallel samples were analyzed per time point (1, 2, and 4 weeks).

**2.9. Immunofluorescence and Confocal Imaging.** For immunocytochemical staining, cells were fixed for 30 min using 4% paraformaldehyde (Fluka, Italy) after 1, 2, or 4 weeks of culture and stained with neuronal markers. Unspecific staining was blocked for 30 min at room temperature (RT) with 10% normal donkey serum (NDS), 0.1% saponin, and 1% bovine serum albumin (BSA) in DPBS (all from Sigma-Aldrich). The cells were then washed once with 1% NDS, 0.1% saponin, and 1% BSA in DPBS. Primary antibodies, rabbit antimicrotubule associated protein 2 (MAP-2, 1:400, AB5622, Merck Millipore, Germany), and monoclonal mouse anti- $\beta$ -tubulin III (1:1250, Sigma-Aldrich) were incubated with the cells at +4 °C overnight. Then, the cells were washed three times with 1% BSA in DPBS and incubated with secondary antibodies for 1 h at RT. AlexaFluor-488 or -568 conjugated antirabbit or antimouse secondary antibodies (1:400, Thermo Fischer Scientific) in 1% BSA on DPBS were used. DAPI (0.2  $\mu\text{g mL}^{-1}$ ,

Sigma-Aldrich) in DPBS was added to the samples and incubated for 15 min. Finally, the cells were washed twice with DPBS. The samples were then mounted according to the manufacturer's instructions with TDE Mounting media (Abberior GmbH, Germany), a 2,2'-thiodiethanol-based embedding media with a refractive index of 1.518 matching perfectly with the refractive index of Ormocomp. The embedding media was used to minimize spherical aberration that causes a scattering of light and a blurring of the images.

Confocal images were acquired with a Zeiss LSM 780 mounted into an inverted Cell Observer microscope (Carl Zeiss, Germany) using 63 $\times$  (N.A. = 1.40, Zeiss Plan Apochromat, Carl Zeiss) and 25 $\times$  (N.A. = 0.80, Zeiss LD LCI Plan-Apochromat, Carl Zeiss) objectives. The confocal data was visualized with ZEN Black 2012 SP1 software (version 8.1, Carl Zeiss) and ImageJ (Version 1.39, U.S. National Institutes of Health, USA). For cell number analysis, confocal image stacks were divided into 15  $\mu\text{m}$  thick substacks, and cell nuclei were counted with the Cell Counter ImageJ plugin. The data were further rearranged to represent the proportion of cells attached to smooth and rough surfaces, total cell number in the microtowers, and the proportion and longitudinal distribution of cells inside the towers.

**2.10. Confocal Image Analysis of Neurites.** For analyzing neurite orientation inside the microtowers, orthogonal projections were created from confocal image stacks. To exclude the cells growing on the outer surface of the towers, cropped slices representing only the center part of the towers were analyzed. These slices were projected into 2D via the maximum intensity projection function in ImageJ. The projection represented 50% of the total microtower volume. Orthogonal projections were analyzed with a spectral analysis software tool, CytoSpectre,<sup>45</sup> to quantify the circular variance and mean orientation of the neurites inside the towers. Circular variance is a measure of the uniformity of the orientation distribution. It varies from 0 to 1. The value of 1 describes a situation where the neurites are spread evenly in all angles lacking a dominant direction, whereas a value of 0 signifies a case of perfect alignment along a single orientation angle. In addition, the orientation angles of all neurite segments with a length of  $\geq 5 \mu\text{m}$  were traced and measured manually with ImageJ from the same orthogonal projections. In total,  $\sim 3200$  neurite segments were measured. The angle of each segment was calculated relative to the vertical plane, and all orientation angles across the 0° to 90° spectrum were then binned in 10° sections. This method was adapted from Tuft et al.<sup>46</sup> A lack of neurite alignment would thus be supported by a relatively equal distribution of neurite segment angles across the whole angle spectrum, whereas strong alignment to the longitudinal direction would be evidenced by a high incidence of neurite segments with angles of 20° or less.

**2.11. Preparation of Cell Culture Samples for SEM Imaging.** The 3D morphology and organization of neuronal cells were assessed by SEM imaging. Prior to imaging, samples were fixed with 5% glutaraldehyde (Sigma-Aldrich) in DPBS (pH 7.4) at RT for 1 h. Afterward, the samples were immersed in ion-exchanged water for 15 min. Next, the samples were dehydrated using an ascending series of ethanol concentrations (10%, 20%, 40%, 60%, 80%, 99.5%, v/v) for 10 min each. Finally, the samples were air-dried and stored under vacuum. After drying, the samples were sputter coated with gold in an argon atmosphere (S 150 Sputter Coater) to a coating thickness of approximately 75 nm. Samples were analyzed by SEM imaging with a Philips XL-30.

**2.12. Statistical Analysis.** All statistical tests were performed with IBM SPSS-software (version 23, IBM, USA). Statistical analysis was performed using the nonparametric Mann-Whitney U test or Kruskal-Wallis test followed by Dunn-Bonferroni tests. The  $p$ -values of  $<0.05$  or  $<0.01$  were considered significant.

## 3. RESULTS

**3.1. Polymerization Windows and Feature Dimensions.** In order to fabricate Ormocomp microtowers with good structural quality, i.e., without the emergence of damaging micro-explosions, the applicable average laser power range (i.e., the polymerization window) for polymerization was first determined. The measured values are collated in Table 1. The threshold values

**Table 1. Polymerization ( $P_{th}$ ) and Damage Threshold ( $P_D$ ) Power Values As Well As the Calculated Polymerization Windows ( $P_w$ ) and the Power Values Corresponding to 70% of the Polymerization Window for the Tested Scanning Speeds<sup>a</sup>**

| scanning speed [ $\mu\text{m s}^{-1}$ ] | $P_{th}$ [mW] | $P_D$ [mW] | $P_w$ [mW] | 70% $P_w$ [mW] |
|-----------------------------------------|---------------|------------|------------|----------------|
| 150                                     | 0.3 ± 0.04    | 5.4 ± 0.5  | 5.1 ± 0.5  | 3.8 ± 0.4      |
| 350                                     | 0.3 ± 0.04    | 5.3 ± 0.2  | 5.0 ± 0.2  | 3.9 ± 0.2      |
| 550                                     | 0.3 ± 0.06    | 5.4 ± 0.2  | 5.0 ± 0.2  | 3.9 ± 0.2      |

<sup>a</sup>The measured data represent mean ± standard deviation ( $n = 4$ ).

for the examined scanning speeds were almost identical and resulted in very similar polymerization window ranges.

SEM images of suspended line structures polymerized with scanning speeds of 150, 350, and 550  $\mu\text{m s}^{-1}$  are shown in Figure S1. The measured line widths and heights for the three scanning speeds are summarized in Table 2.

Although the voxel dimensions remained nearly constant, the uniformity of the lines decreased and the surface roughness increased with scanning speed. As the fabrication time can be reduced by taking advantage of the axial height of the voxels and setting the layer distance to match the voxel height, the axial voxel distance of the microtower cylinder was set to 3.0  $\mu\text{m}$  and the micropillars to 4.0  $\mu\text{m}$ . In order to achieve relatively smooth surface roughness, the lateral voxel distance was set to 1.0  $\mu\text{m}$ . The lateral, axial, and overall voxel overlap degrees calculated for the cylinder according to eq 1 are presented in Table 2. The voxel overlap ratios were not determined for the scanning speed 150  $\mu\text{m s}^{-1}$  as it was only used for single line scans when polymerizing the spider webs. According to the results of previous studies, the lateral surface roughness tends to saturate when the voxel overlap ratio is over 0.5 due to the self-smoothing effect.<sup>47,48</sup> For the scanning speeds of 350 and 550  $\mu\text{m s}^{-1}$ , the lateral voxel overlap ratios were over 0.5 suggesting that similar surface roughness would be achieved with both scanning speeds.

**3.2. Microtower Fabrication by 2PP-DLW.** The microtower designs I and II were polymerized with scanning speeds of 350 and 550  $\mu\text{m s}^{-1}$  (Figure S3) to determine the optimal scanning speed for the fabrication and to evaluate whether the elliptically shaped openings would give round openings. However, as the axial contour distance was quite large (i.e., 3.0  $\mu\text{m}$ ), the elliptical shape of the openings was not traced properly, especially with the scanning speed of 550  $\mu\text{m s}^{-1}$ . As predicted by the similar voxel overlap degrees, both scanning speeds resulted in comparable surface quality. The rectangular shape of openings (designs III and IV) was reproduced quite accurately with both scanning speeds (Figure S4).

Figures S3 and S4 show that some of the gaps in the spider webs were enclosed by self-polymerized membranes (designs I and III) that formed in-between the web threads as the scanned lines were packed densely enough. These designs were considered

too closed to allow efficient cell migration. Thus, microtower design IV (Figure 1a,d) together with the reference structure designs V (Figure 1b,e) and VI (Figure 1c,f) were selected as the most optimal models for the cell culture experiments.

The fabrication of a single design IV tower using scanning speeds of 350  $\mu\text{m s}^{-1}$  (the cylinder and pillars) and 150  $\mu\text{m s}^{-1}$  (the webs) took approximately 7 min 32 s. Increasing the scanning speed from 350 to 550  $\mu\text{m s}^{-1}$  reduced the fabrication time by 22 s to 7 min 10 s. As there was no essential difference in the surface quality of the towers, the samples for the cell culture experiments were fabricated with the scanning speed of 550  $\mu\text{m s}^{-1}$ . In addition, the reference microtowers (designs V and VI) were fabricated with the same scanning speed. The fabrication of design V took only 3 min 49 s and design VI took 4 min 30 s. Design VI towers had a smooth uniform surface morphology with surface roughness  $R_a = 11.2 \pm 0.4$  nm (henceforth denoted as “smooth surface”) as the cylinder comprised only closed circular contours. The surface roughness ( $R_a = 30.9 \pm 6.6$  nm, henceforth denoted as “rough surface”) was higher in designs IV and V at the opening layers. The higher surface roughness was caused by the fluctuation of the laser dose due to the acceleration and deceleration of the scanner producing variation in voxel size. Other layers of the design IV and V towers had a smooth surface as in design VI. Figure S5 shows examples of atomic force microscopy (AFM) 3D topography images and the line scan profiles of the smooth and rough parts of the tower walls.

Fabrication accuracy using the 2PP-DLW setup was assessed by measuring the dimensions of the design IV microtowers from SEM images and comparing them with the theoretical dimensions of the CAD model (Table 3). The comparison revealed

**Table 3. Theoretical and Experimental Dimensions of Design IV Microtower<sup>a</sup>**

|                         | CAD dimensions [ $\mu\text{m}$ ] | measured dimensions [ $\mu\text{m}$ ] | deviation [%] |
|-------------------------|----------------------------------|---------------------------------------|---------------|
| cylinder height         | 150.0                            | 119.2 ± 4.5                           | 20.5 ± 3.0    |
| lower opening height    | 27.0                             | 11.9 ± 4.2                            | 55.9 ± 15.6   |
| lower opening width     | 20.0                             | 18.6 ± 0.3                            | 7.2 ± 1.3     |
| upper opening height    | 33.0                             | 10.1 ± 0.4                            | 69.4 ± 1.1    |
| upper opening width     | 20.0                             | 18.1 ± 0.1                            | 9.3 ± 0.7     |
| cylinder inner diameter | 75.0                             | 71.7 ± 0.4                            | 4.3 ± 0.6     |
| pillar diameter         | 5.0                              | 8.5 ± 0.8                             | 70.6 ± 15.9   |

<sup>a</sup>The cylinder and pillar diameters were measured from the top view (0° tilt), and height of the cylinder along with the dimensions of the openings, from the side view (90° tilt) of SEM images. The measured data represent the mean ± standard deviation ( $n = 5$ ).

that the microtowers had shrunk in both  $xy$ - and  $z$ -directions on average 4% and 21%, respectively. The Young's modulus of Ormocomp processed by 2PP-DLW was estimated via force spectroscopy measurements performed with AFM at the upper rim of the microtower cylinder. For comparison, the Young's

**Table 2. Measured Line Widths and Heights for Scanning Speeds of 150, 350, and 550  $\mu\text{m s}^{-1}$  and Calculated Voxel Overlap Ratios<sup>a</sup>**

| scanning speed [ $\mu\text{m s}^{-1}$ ] | line width [ $\mu\text{m}$ ] | line height [ $\mu\text{m}$ ] | lateral voxel distance [ $\mu\text{m}$ ] | lateral voxel overlap | axial voxel distance [ $\mu\text{m}$ ] | axial voxel overlap | overall voxel overlap degree |
|-----------------------------------------|------------------------------|-------------------------------|------------------------------------------|-----------------------|----------------------------------------|---------------------|------------------------------|
| 150                                     | 1.9 ± 0.2                    | 7.5 ± 0.2                     | n.a.                                     | n.a.                  | n.a.                                   | n.a.                | n.a.                         |
| 350                                     | 2.1 ± 0.1                    | 7.4 ± 0.2                     | 1.0                                      | 0.53                  | 3.0                                    | 0.59                | 0.31                         |
| 550                                     | 2.1 ± 0.2                    | 6.8 ± 0.6                     | 1.0                                      | 0.51                  | 3.0                                    | 0.56                | 0.29                         |

<sup>a</sup>The data represent mean ± standard deviation ( $n = 5$ ).

modulus was also measured from UV-polymerized Ormocomp thin films. According to the Hertz model, the average Young's modulus of the microstructures was  $E = 140 \pm 18$  MPa, whereas in the UV-cured Ormocomp thin films it was  $E = 2.4 \pm 0.18$  GPa underlining a significant difference between the two differently cured specimens (two-tailed Mann–Whitney U test,  $p < 0.001$ ,  $n = 9$ ). Examples of the force versus indentation depth plots are shown in Figure S6.

**3.3. Applicability of the Microtower Structures for Cell Culture Purposes.** The applicability of microtowers for cell culture purposes was assessed by cell viability analysis. Cells grew in close vicinity to and inside the towers throughout the four-week experiment (Figure 2a). The viability of the cells was not affected by the microtowers. In addition, cell growth on the outer surface of the towers was studied to further ensure the suitability of the surface texture for cell attachment (Figure 2b,c). The outer surface of the towers at the height of 75 to 90  $\mu\text{m}$  representing either rough ( $R_a = 31$  nm) or smooth ( $R_a = 11$  nm) surface texture was closely examined. Visual inspection showed no differences between the different textures. This was confirmed by also comparing the proportions of cells attached to the analyzed areas. There were no statistically significant differences in cell attachment among surfaces with different roughness. Therefore, microtowers fabricated by 2PP-DLW provided a suitable environment for cells.

**3.4. Neuronal Cell Distribution in Microtowers.** Cell phenotype was confirmed as neuronal via immunocytochemical staining against the neuronal markers MAP-2 and  $\beta$ -tubulin III (Figure 3a). Cell growth inside and outside the microtowers was studied by counting cell nuclei from confocal image stacks. At the one-week time point, the total cell growth in all the studied tower designs was quite similar (Figure 3b). At the two-week time point, the total cell number increased in designs IV and V, whereas the number remained constant in design VI. By week four, the total cell number decreased in designs IV and V but

increased in design VI. Most of the cells, regardless of tower design, were located on the outside walls but there was a high variation in cell number ( $945 \pm 424$  cells), whereas the cell number on the inside was lower but interestingly with less variation ( $440 \pm 158$  cells). As the inside of the tower provided a more stable microenvironment for the cells, we next calculated the relative proportion of cells inside from the total cell number. Despite the dramatic changes in cell number outside of design IV, the proportion of cells inside increased significantly from week one to week four (Figure 3b,c). In addition, the portion of cells inside tower design IV was significantly higher compared with design VI at the four-week time point.

The cell distribution inside the towers was analyzed on the basis of six layers. Each layer represented different regions of design IV: from 0 to 15  $\mu\text{m}$  lower openings, from 15 to 60  $\mu\text{m}$  pillars, from 60 to 75  $\mu\text{m}$  lower web, from 75 to 90  $\mu\text{m}$  upper openings, from 90 to 120  $\mu\text{m}$  pillars, and from 120 to 135  $\mu\text{m}$  upper web. Figure 4a presents examples of confocal z-projections of samples at the two-week time point. In design IV, the cell distribution at the upper half (from 60 to 135  $\mu\text{m}$ ) of the tower remained rather similar throughout the 4 weeks (Figure 4b). Whereas in the lower layers (from 0 to 60  $\mu\text{m}$ ), the cell localization was observed to shift from the lowest layer (from 0 to 15  $\mu\text{m}$ ) to the next layer (from 15 to 60  $\mu\text{m}$ ) over time. However, this movement upward was halted at the layer containing the lower web (from 60 to 75  $\mu\text{m}$ ). In design V, most of the cells were located in the lower half of the tower throughout the study (Figure 4c). In design VI, the cells were quite evenly distributed throughout the height of the tower during the first 2 weeks (Figure 4d). By week four, the majority of the cells had migrated to the upper parts of the tower.

**3.5. Orientation of Neurites along Microtowers.** The orientation of neurites along the microtowers was first analyzed with automated analysis. Then, a more detailed analysis was performed manually to investigate the distribution of neurite

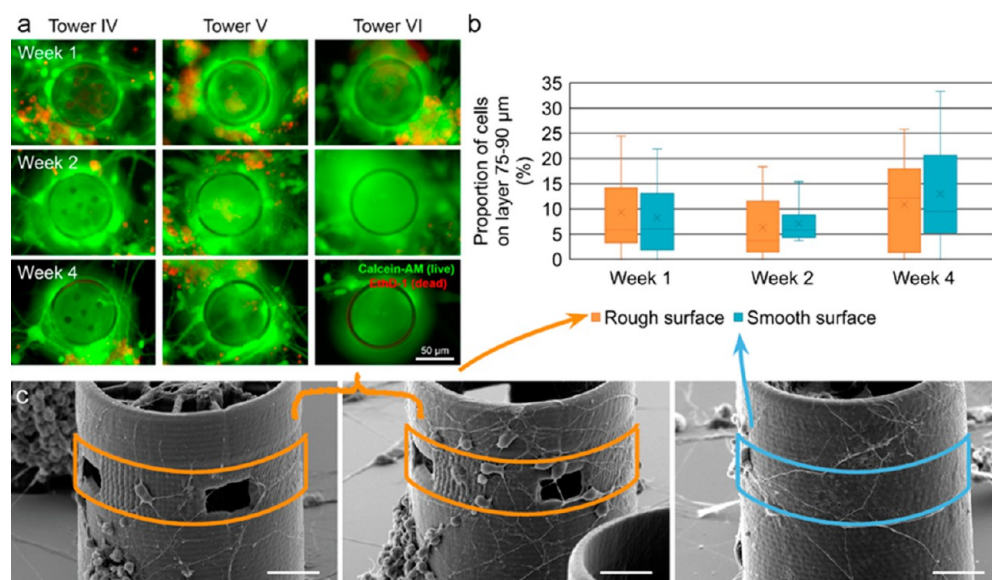


**Figure 2.** Applicability of the direct laser written microtower structures for cell culture purposes: (a) fluorescence images of live/dead stained cells at different time points; (b) proportion of cells attached to the outer surface layer at height 75 to 90  $\mu\text{m}$  representing either rough or smooth surface texture. The cell numbers on the rough surface have been counted by combining the data of tower designs IV and V. The cell numbers on the smooth surface represent the data of tower design VI. There was no statistically significant difference in cell attachment among surfaces with different roughness ( $p > 0.05$ , two-tailed Mann–Whitney U test,  $n = 8–18$ ); (c) SEM images of microtower designs IV, V, and VI from one-week time point illustrating the surface area used for analysis of cell attachment on differently textured surfaces. Scale bars represent 20  $\mu\text{m}$ .

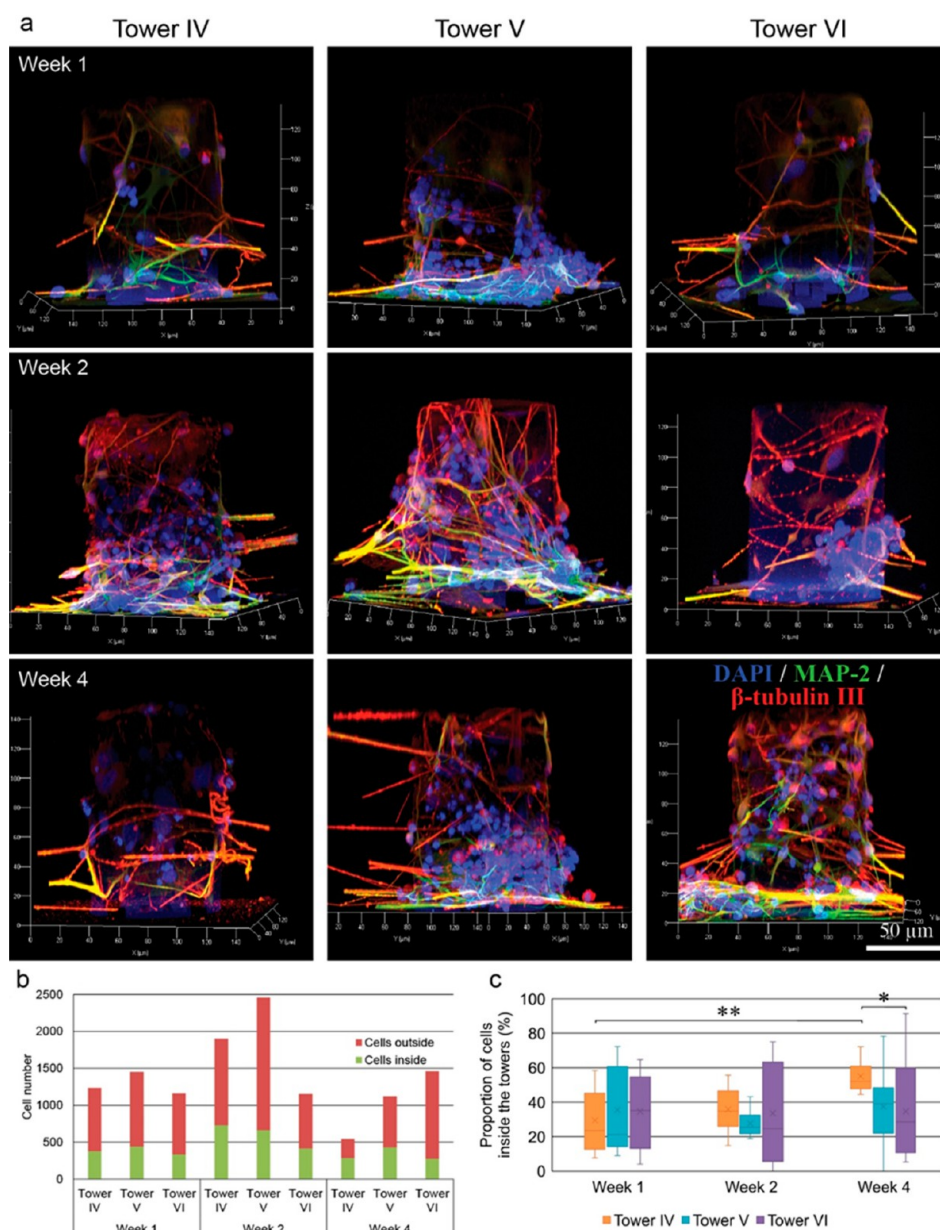


**Figure 3.** Total cell number in microtowers. (a) Representative 3D renderings of confocal image stacks with immunocytochemical staining against neuronal markers MAP-2 (green),  $\beta$ -tubulin III (red), and DAPI (blue) for nuclei. (b) Total cell number in microtowers and (c) proportions of cells inside the towers ( $*p = 0.041 < 0.05$ ,  $**p = 0.007 < 0.01$ ,  $n = 7-9$ , Kruskal-Wallis test followed by posthoc Dunn-Bonferroni tests).

orientation angles. As an example, plots of the neurite orientation distributions from the automated analysis and projections demonstrating manual neurite tracing are shown in Figure 5a–c. According to automated CytoSpectre analysis of circular variances, all tower designs had cases of high orientation (circular variance  $\leq 0.6$ ). However, there was a great variation between parallel samples (Figure 5d). The dominant orientation for each tower design is represented as a box plot of mean orientation angles between  $0^\circ$  and  $180^\circ$  in Figure 5e. The longitudinal axis of the tower is at the angle of  $90^\circ$ , and the neurites following this angle were considered to be perfectly oriented. The majority of the measured mean orientation angles represented  $\pm 10^\circ$  deviation from the longitudinal axis throughout the experiment indicating the presence of longitudinally oriented neurites.

In the manual analysis, the lengths of the traced neurite segments were summed and compared with the total cell number

(Figure 5f). The main finding was that design IV had the highest neurites to cell number ratio at 1 and 4 weeks. Therefore, design IV provided the most promising environment for neurite growth. Figure 5g–i shows the distribution of the manually measured neurite segment angles. During the first week (Figure 5g), all the tower designs demonstrated similar neurite orientation behavior; the highest neurite occurrence was found in the  $10^\circ$  bin. Throughout the experiment, design IV had the highest incidence of neurite segments (41% to 46%) with an alignment angle of  $\leq 20^\circ$  indicating orientation along the longitudinal direction. At the two-week time point (Figure 5h), design V had a fairly equal distribution of neurite segment angles across the bins demonstrating quite random orientation, whereas in design VI, the highest neurite incidence was detected in bins  $10^\circ$ ,  $20^\circ$ , and  $40^\circ$ . All the tower designs had approximately the same number of longitudinally oriented neurites ( $\sim 40\%$ ) at the four-week time



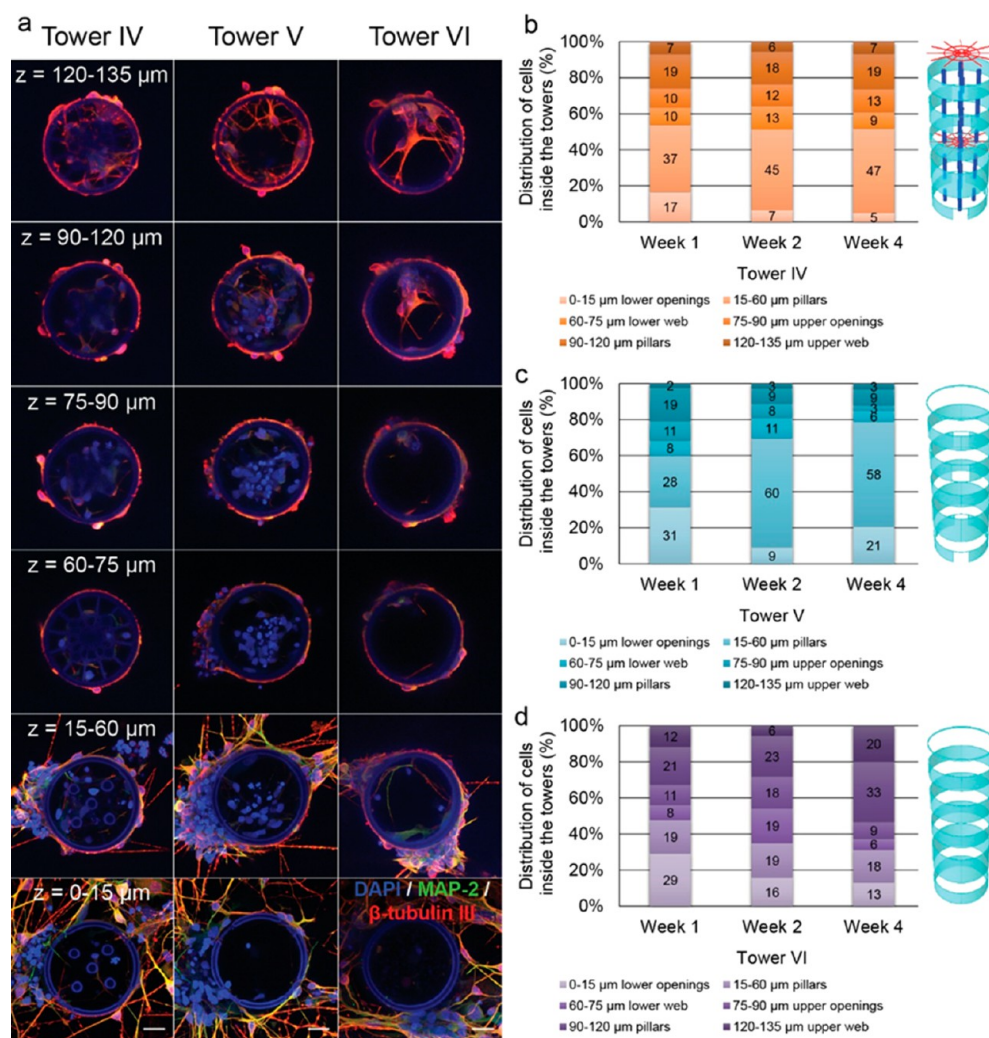


**Figure 4.** Distribution of cells inside the towers. The counted nuclei data were regrouped into six layers representing different regions of interest present in tower design IV. (a) Illustrative projections of confocal microscopy images from immunocytochemically stained samples representing the six layers of interest. Average cell number per layer inside microtower (b) design IV, (c) design V, and (d) design VI. Immunocytochemical markers MAP-2 (green),  $\beta$ -tubulin III (red), and DAPI (blue). Scale bars represent 20  $\mu\text{m}$ .

point, indicating that the cylindrical shape itself enhanced orientation in long-term culture (Figure 5i). Overall, in all the tower designs throughout the experiment, the highest incidence of neurites was located in the  $10^\circ$  to  $20^\circ$  bins indicating good longitudinal orientation.

**3.6. Formation of 3D Networks.** The cell morphology and organization of neuronal networks were assessed by SEM imaging. In all microtower designs, neurons grew in close contact with the 2PP-DLW fabricated towers spreading neurites along the inner and outer surfaces, as shown in Figure 6. On the outer surface of the towers, neurons and neurites extended across the total height of the towers. Neurites as well as neurons migrated between the outer and inner surface through the wall openings in designs IV and V. In addition, similar behavior was seen in all designs at the upper rim of the cylinder, where cells formed connections between outer and inner populations by migrating over the edge (Figure 6, Top view). Interestingly, neurons formed 3D networks with suspended bridges between the adjacent microtowers and between tower walls and bottom surfaces (Figures 3a and 6, Last row). These bridges were mostly formed from several neurites intertwined into bundles. On the basis of the known distance between towers, several suspended

neurite bridges were estimated to be  $\sim 90 \mu\text{m}$  long and the longest bridges found were  $\sim 260 \mu\text{m}$ .

#### 4. DISCUSSION

Computer-assisted laser-based fabrication techniques such as 2PP-DLW offer powerful tools to produce cell culture platforms with highly ordered geometries that recapitulate the structure and size scale of natural 3D cell environments.<sup>49</sup> Here, we present the design, 2PP-DLW fabrication process, and cell culture results of a novel 3D neuronal cell culture platform based on tubular microtowers. In total, six different microtower designs were successfully fabricated from Ormocomp. To study the relevance of the intraluminal infrastructure (design IV) for cell growth, two designs without internal structures (designs V and VI) were used for comparison. The process was optimized by defining the operational polymerization windows for Ormocomp for the tested scanning speeds of 150, 350, and 550  $\mu\text{m s}^{-1}$ .

Microtower designs with dense spider webs (I and III) were excluded from further study because some web threads were agglutinated due to a self-polymerization phenomenon.<sup>50</sup> On the grounds of the preliminary findings, the microtower designs IV, V, and VI were selected as the most optimal models for the cell

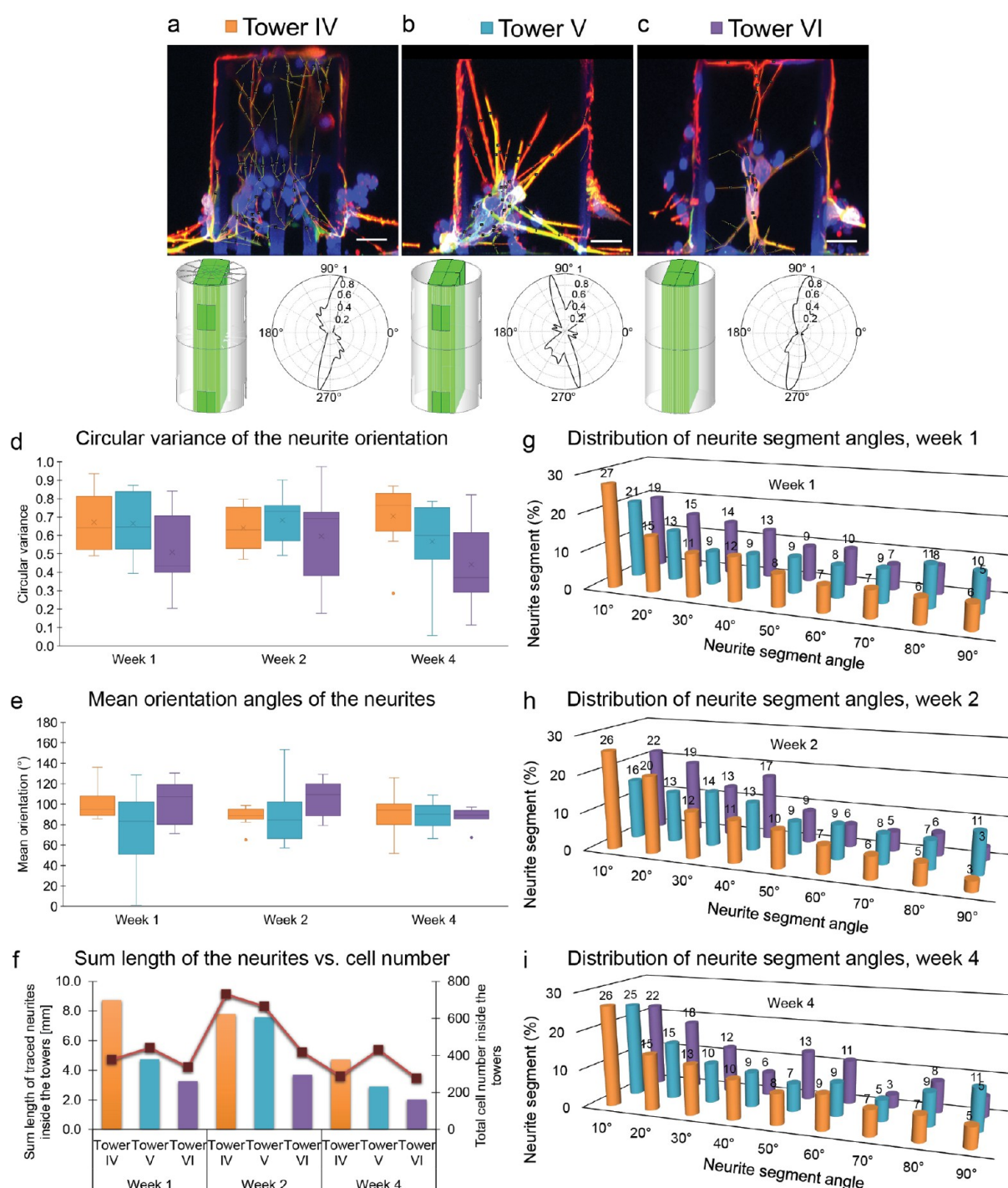


**Figure 5.** Orientation of neurites inside the towers was determined by measuring the angles of neurite segments from the longitudinal projections taken from the confocal microscopy image stacks of the microtowers. Representative projections of confocal micrographs from the two-week time point with traced neurites marked with yellow lines inside the microtower (a) design IV, (b) design V, and (c) design VI. For each design, the CAD model is presented to illustrate the analyzed volume utilized for the neurite angle measurements (marked with green). In addition, plots of orientation distribution created with CytoSpectre software are shown for each case. The distance from the origin represents the relative frequency of the corresponding angle. Value 1 has been designated to the angle with highest incidence. (d) Box plot of the circular variance of the neurite orientation obtained with CytoSpectre. (e) Box plot of the mean orientation angles of neurites (from 0° to 180°, the longitudinal axis of the tower is at 90°) analyzed with CytoSpectre. (f) Sum length of traced neurites inside each microtower design at different time points and the total cell number (marked with red line). (g–i) Distribution of neurite angles relative to the vertical plane measured from all neurite segments with length 5  $\mu\text{m}$  or more. The longitudinal axis is set to 0°, while horizontal axis is denoted as 90°. Scale bars represent 20  $\mu\text{m}$ .

culture experiments. The fabrication accuracy of the 2PP-DLW setup was evaluated by measuring the dimensions of the towers of design IV. The height of the cylinder had shrunk  $\sim 21\%$  because of the low polymerization yield caused by high scanning

speed and relatively large axial contour distance. However, this rather high shrinkage rate is in line with the previous results for Ormocomp with  $\sim 20\%$  to  $24\%$  shrinkage in the  $z$ -direction reported.<sup>51,52</sup> The diameters of the micropillars had broadened

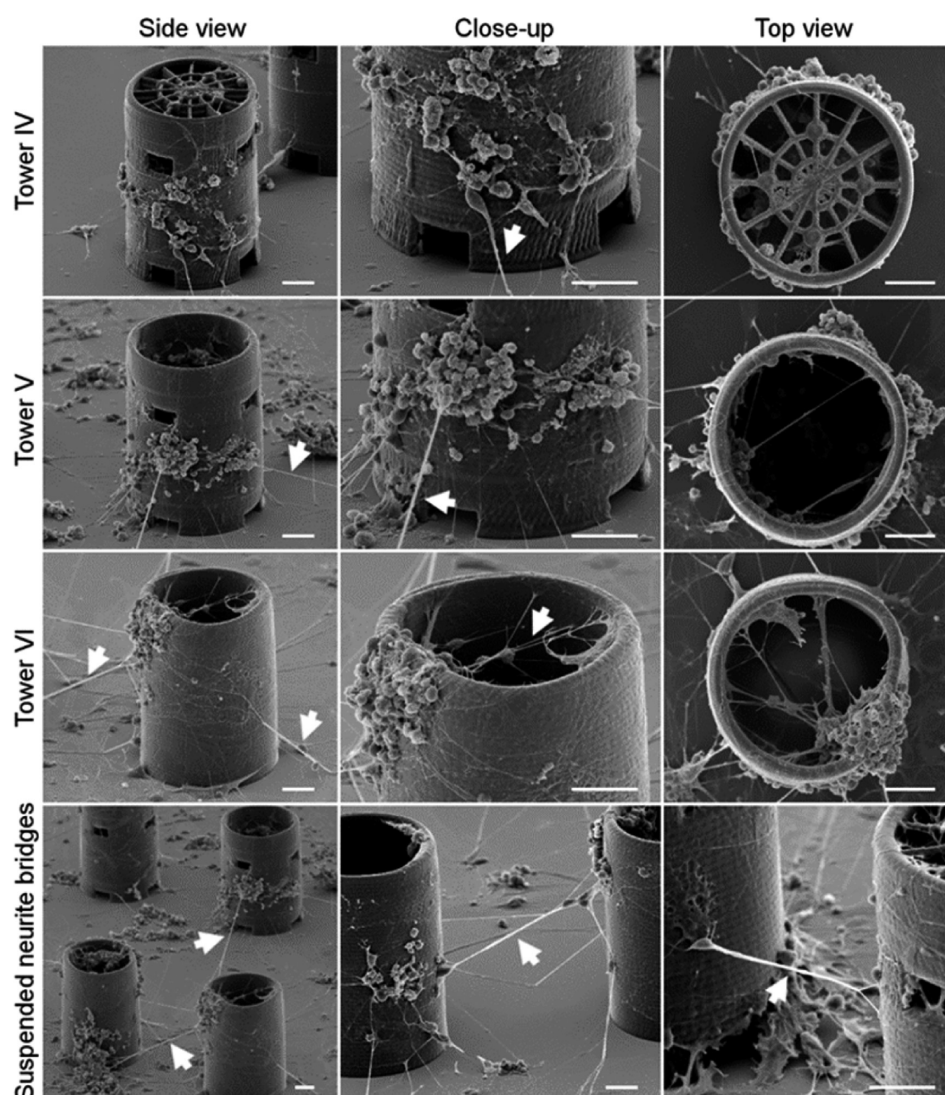


**Figure 6.** SEM images of neuronal cells inside and outside of different microtower designs at the one-week time point. The images of the three upper rows show the towers from the tilt angles of  $60^\circ$  (first and second column) and  $0^\circ$  (third column). The last row illustrates the close-ups of the suspended neurite bridges extending between adjacent towers. Suspended neurite bridges are marked with arrowheads. Scale bars represent  $20\ \mu\text{m}$ .

71% ( $\sim 3.5\ \mu\text{m}$ ), which is more than the width of a voxel ( $\sim 2\ \mu\text{m}$ ). The difference could be explained by the overcuring phenomenon resulting from the multipath scanning with three nested contours separated by a distance of  $1.0\ \mu\text{m}$ . Solid voxels are surrounded by subactivated regions, in which the concentration of active radicals is below the polymerization threshold.<sup>53</sup> However, when two subactivated regions overlap as a consequence of closely situated scanning paths as in the case of the multipath scanning method, the laser-generated radical concentration can exceed the threshold value, which leads to self-assembly of oligomers into features sustaining the postexposure development.<sup>50</sup> According to Uppal and Shiakolas,<sup>54</sup> with a diffraction-limited laser spot having a lateral diameter of  $1\ \mu\text{m}$ , the radius of the subactivated region is approximately  $5\ \mu\text{m}$ . In our case, the lateral diameter of the diffraction-limited laser spot can be estimated as  $d = 1.22\lambda/\text{NA} = 720\ \text{nm}$ , where  $\lambda$  is the wavelength of the laser ( $532\ \text{nm}$ ) and NA is the numerical aperture of the objective lens (0.90). Thus, in our case, the radius of the subactivated region can be estimated to be  $\sim 3.6\ \mu\text{m}$ . The offset between the three nested contours was set to  $1.0\ \mu\text{m}$ , so it can be concluded that the overlap of subactivated regions

occurred and led to broadening of the diameter of the micropillars. The overcuring could be avoided by taking into account the spot size of the laser beam when preparing the CAD designs and carefully selecting optimal offset between the nested contours. The height of the lower openings deviated from the theoretical height considerably (56%) because the glass-photoresist interface, i.e., the initial focal spot height, had to be manually set for each structure. The experimental width of the lower and upper openings corresponded well with the CAD model when taking into account the overcuring caused by the size of the laser beam. The height of the upper openings shrank considerably (69%). This finding cannot be solely explained by the height of the voxel ( $6.8\ \mu\text{m}$ ). Presumably, the shrinkage is a consequence of several phenomena such as material shrinkage and overcuring phenomenon occurring at the lower and upper edges of the openings. The inner diameter of the microtower cylinder deviated from the theoretical value by only 4%. One of the acknowledged limiting factors impairing the fabrication accuracy of 2PP-DLW and other photolithographic fabrication methods is that material shrinkage induces deviations from the CAD model.<sup>55,56</sup> However, from the point of view of our test

arrangement, the shrinkage had no essential effect on the usability for cell culture.

The measured Young's modulus of the UV-cured Ormocomp thin film specimens ( $E = 2.4 \pm 0.18$  GPa) was in the same order as that reported earlier by Schizas and Karalekas<sup>57</sup> and Li et al.,<sup>42</sup> 1.27 and 1.58 GPa, respectively. However, the average Young's modulus of the microtowers ( $E = 140 \pm 18$  MPa) was considerably smaller when compared with the thin film specimens. This finding is the result of the lower cross-linking degree of polymer chains achieved via 2PP-DLW when compared with the UV-curing process.<sup>57,58</sup> The only reported Young's modulus for Ormocomp microstructures fabricated by 2PP-DLW is  $E = 800$  MPa,<sup>59</sup> which is considerably larger than that measured here. The difference can be partially explained by the higher scanning speed ( $550 \mu\text{m s}^{-1}$  vs  $50$  to  $250 \mu\text{m s}^{-1}$ ) and the lower laser power values ( $3.9$  mW vs  $10$  to  $17$  mW) used in our fabrication process. These factors resulted in a reduction in exposure, a decrease of the cross-linking degree of the polymer, and the lower Young's modulus. Nevertheless, the level of stiffness was adequate for the fabricated microtowers to withstand all the handling and cell culture procedures without major shape distortions.

In 2PP-DLW, the laser exposure dose (i.e., the scanning speed and average laser power) determines the resulting voxel size. Voxel size combined with the chosen contour distance for the CAD model define the final surface topography of the structure.<sup>60</sup> Thus, the surface roughness of the microstructures can be tuned by changing these parameters. Depending on the microtower layer, the surface roughness was either  $\sim 11$  or  $\sim 31$  nm due to the fluctuation of the laser dose caused by different contour geometries. The achieved surface roughness is, nevertheless, in line with previous studies; Malinauskas et al. have reported a roughness of  $\sim 30$  nm  $\pm 3$  nm for sol-gel photopolymer SZ2080,<sup>61</sup> and Takada et al. found a roughness of 4 to 11 nm for urethane acrylate resin SCR500.<sup>62</sup> It has been suggested that the higher surface roughness resulting in an increase of the surface area can promote the attachment of glioblastoma cells.<sup>63</sup> In our study, there was no significant difference in cell adhesion between the smooth and the rough areas of the tower wall. This is in accordance with previous results stating that the neurons of substantia nigra can adhere to a surface with  $R_a$  ranging from 20 to 50 nm, whereas on surfaces with  $R_a < 10$  nm or  $> 70$  nm adherence is negatively affected.<sup>64</sup> Contrary to the studies mentioned above utilizing uncoated surfaces,<sup>63,64</sup> we studied surface topographies coated with laminin. As reported previously by Käpylä et al.,<sup>65</sup> protein coating levels off differences in the surface roughness of Ormocomp, which in our case resulted in similar cell behavior on both roughnesses. Furthermore, the surface chemistry of Ormocomp appears to have a stronger effect on cell attachment compared with surface roughness. Consequently, although the surface quality of the structures prepared by the 2PP-DLW technique is very susceptible to any variation in fabrication conditions, small changes in the surface roughness were assumingly compensated by the laminin coating.

Interestingly, surface roughness has been shown to dramatically affect cell behavior by Limongi et al.<sup>7</sup> In their study, nanopatterned micropillar ( $h = 10 \mu\text{m}$ ,  $\varnothing = 10 \mu\text{m}$ ) arrays supported the formation of 3D networks via suspended neurite bridges, whereas smooth pillars promoted only the formation of a flat sparse neuronal network on the bottom surface as well as at the root of the pillars (surface roughness not reported for either case). In our study, however, the smooth surface appeared to be

very attractive for human-derived neuronal cells. Moreover, 3D neuronal networks and suspended bridges were able to form throughout the tower height and along and between the tower walls. To some extent, a similar formation of suspended neurite bridges has also been reported with microfibers<sup>6</sup> and 2PP-DLW fabricated microstructures.<sup>32,33</sup> Thus, it can be concluded that with the 2PP-DLW fabrication method no additional patterning phase is needed to enhance cell growth.

According to the cell behavior, the tower structures seemed to create different microenvironments for the cells: one on the inner and other on the outer surface of the towers. The lumen provided a more stable, enclosed environment, as seen by the relatively constant cell number throughout the experiment. Although the cell number in lumen of all tower designs was similar, the distribution of cells was affected by the microtower design. The openings in the tower wall seemed to have an impact on the extent of cell migration or proliferation inside the towers, whereas the existence of the spider webs did not considerably alter the cell localization. Moreover, cells inside design VI without the openings were more equally distributed throughout the tower height indicating a homogeneous microenvironment.

According to both the automatic and manual analysis of the neurite orientation angles, the microtower structures were able to orient neurites. More detailed manual analysis showed that during the first 2 weeks the longitudinal orientation of the neurites was enhanced by the intraluminal infrastructure, most probably by the micropillars (design IV). By week four, the differences in the degree of orientation leveled off in all tower designs. Overall, the intraluminal structures appeared promising for orientation purposes, but the design clearly needs more optimization. It has been reported that 2PP-DLW fabricated guiding structures ( $\varnothing = 10$ – $20 \mu\text{m}$ ) are able to orient rodent neuroblastoma-glioma cells, although quantitative verification has not been conducted.<sup>66</sup> Fibers ( $\varnothing = 7$ – $8 \mu\text{m}$ ) have been shown to effectively orient rat neural cells as 63% of the cells had a dominant growth direction of  $\leq 10^\circ$  compared with the longitudinal direction of the fibers.<sup>6</sup> Our results suggest a similar kind of behavior even though we analyzed the orientation of all neurite segments instead of measuring only the main angles for single neurons. Thus, micropillar structures can be used effectively as components of scaffolds for orientation purposes.

Similar microtower structures without an intraluminal infrastructure ( $h = 250 \mu\text{m}$ ,  $\varnothing = 200 \mu\text{m}$ ) embedded in hydrogel have been used to study rodent neural cell interactions and distribution at the tower interface in 3D.<sup>2</sup> In that study, cells accumulated to the towers and formed 3D neural networks around and across the towers. Our study showed surprisingly similar results without the support of the hydrogel matrix. We consider this finding to be important as the use of microstructure-supported cell cultures instead of random 3D cultures in a gel matrix could enhance the reproducibility of the experiments *in vitro*.

## 5. CONCLUSIONS

Our study introduced a feasible fabrication method for the creation of a microtower-based 3D cell culture platform with intricate and detailed features. The cell culture platform was proven to be efficient for the long-term 3D culturing of human stem cell-derived neuronal cells. The proposed culturing concept may be used as a substitute for the hydrogel matrix commonly used to mechanically support the 3D growth of cells. The platform is especially suitable for studying cell behavior in a 3D environment, for example, the orientation and migration of

neuronal cells, both of which are important aspects to consider in future studies.

## ■ ASSOCIATED CONTENT

### ● Supporting Information

The Supporting Information is available free of charge on the ACS Publications website at DOI: 10.1021/acsami.7b05536.

Fabrication of Ormocomp thin films; SEM images of suspended lines polymerized on top of supporting walls with different scanning speeds (Figure S1); CAD images of microtower designs I–III (Figure S2); SEM images of microtower designs I and II fabricated with scanning speeds of  $350 \mu\text{m s}^{-1}$  or  $550 \mu\text{m s}^{-1}$  (Figure S3); SEM images of microtower designs III and IV fabricated with scanning speeds of  $350 \mu\text{m s}^{-1}$  or  $550 \mu\text{m s}^{-1}$  (Figure S4); AFM topography images and line scan profiles of the outer surface of the cylindrical tower walls (Figure S5); representative force versus indentation depth plots from the AFM force spectroscopy measurements performed on microtower and Ormocomp thin film samples (Figure S6) (PDF)

## ■ AUTHOR INFORMATION

### Corresponding Author

\*E-mail: [sanna.turunen@tut.fi](mailto:sanna.turunen@tut.fi). Phone: +358 50 301 3375.

### ORCID

Sanna Turunen: 0000-0002-6823-8811

Tiina Joki: 0000-0001-7397-6694

Maiju L. Hiltunen: 0000-0002-8742-2737

Teemu O. Ihalainen: 0000-0003-4351-8697

### Author Contributions

S.T. and T.J. share first authorship. S.N. and M.K. share last authorship. The manuscript was written through contributions of all authors. All authors have given approval to the final version of the manuscript.

### Notes

The authors declare no competing financial interest.

## ■ ACKNOWLEDGMENTS

This research study was supported by the TEKES (the Finnish Funding Agency for Technology and Innovation) Human Spare Parts project, the Finnish Cultural Foundation (Award numbers 00141012, 00140325, and 00150312), Academy of Finland Grant #267471, and the Paulo Foundation. The authors gratefully acknowledge M.S. (Tech.) Taru Karhula for SEM imaging and M.S. Risto-Pekka Pölönen and M.S. Kimmo Kartasalo for guidance with the CytoSpectre software. Hanna Mäkelä and Eija Hannuksela are thanked for technical assistance.

## ■ REFERENCES

- (1) LaPlaca, M. C.; Vernekar, V. N.; Shoemaker, J. T.; Cullen, D. K. Three-Dimensional Neuronal Cultures. In *3D Tissue Engineering*; Berthiaume, F., Morgan, J. R., Eds.; Artech House: Boston, USA, 2010; Chapter 11, pp 187–204.
- (2) Cullen, D. K.; Wolf, J. A.; Vernekar, V. N.; Vukasinovic, J.; LaPlaca, M. C. Neural Tissue Engineering and Biohybridized Microsystems for Neurobiological Investigation in Vitro (Part 1). *Crit. Rev. Bioeng.* **2011**, *39*, 201–240.
- (3) Lai, Y.; Cheng, K.; Kisaalita, W. Three Dimensional Neuronal Cell Cultures More Accurately Model Voltage Gated Calcium Channel Functionality in Freshly Dissected Nerve Tissue. *PLoS One* **2012**, *7*, e45074.

(4) McKinnon, D. D.; Kloxin, A. M.; Anseth, K. S. Synthetic Hydrogel Platform for Three-Dimensional Culture of Embryonic Stem Cell-Derived Motor Neurons. *Biomater. Sci.* **2013**, *1*, 460–469.

(5) Cullen, D. K.; Tang-Schomer, M. D.; Struzyna, L. A.; Patel, A. R.; Johnson, V. E.; Wolf, J. A.; Smith, D. H. Microtissue Engineered Constructs with Living Axons for Targeted Nervous System Reconstruction. *Tissue Eng., Part A* **2012**, *18*, 2280–2289.

(6) Sharifi, F.; Patel, B. B.; Dzuilko, A. K.; Montazami, R.; Sakaguchi, D. S.; Hashemi, N. Polycaprolactone Microfibrous Scaffolds to Navigate Neural Stem Cells. *Biomacromolecules* **2016**, *17*, 3287–3297.

(7) Limongi, T.; Cesca, F.; Gentile, F.; Marotta, R.; Ruffilli, R.; Barberis, A.; Dal Maschio, M.; Petrini, E. M.; Santoriello, S.; Benfenati, F.; Di Fabrizio, E. Nanostructured Superhydrophobic Substrates Trigger the Development of 3D Neuronal Networks. *Small* **2013**, *9*, 402–412.

(8) He, L.; Zhang, Y.; Zeng, C.; Ngiam, M.; Liao, S.; Quan, D.; Zeng, Y.; Lu, J.; Ramakrishna, S. Manufacture of PLGA Multiple-Channel Conduits with Precise Hierarchical Pore Architectures and in Vitro/Vivo Evaluation for Spinal Cord Injury. *Tissue Eng., Part C* **2009**, *15*, 243–255.

(9) Wen, X.; Tresco, P. A. Effect of Filament Diameter and Extracellular Matrix Molecule Precoating on Neurite Outgrowth and Schwann Cell Behavior on Multifilament Entubulation Bridging Device in Vitro. *J. Biomed. Mater. Res., Part A* **2006**, *76A*, 626–637.

(10) Tian, L.; Prabhakaran, M. P.; Ramakrishna, S. Strategies for Regeneration of Components of Nervous System: Scaffolds, Cells and Biomolecules. *Regener. Biomater.* **2015**, *2*, 31–45.

(11) Huang, Y.; Huang, Y. Biomaterials and Strategies for Nerve Regeneration. *Artif. Organs* **2006**, *30*, 514–522.

(12) Hadlock, T.; Elisseeff, J.; Langer, R.; Vacanti, J.; Cheney, M. A Tissue-Engineered Conduit for Peripheral Nerve Repair. *Arch. Otolaryngol., Head Neck Surg.* **1998**, *124*, 1081–1086.

(13) Wang, S.; Yaszemski, M. J.; Knight, A. M.; Gruetzmacher, J. A.; Windebank, A. J.; Lu, L. Photo-Crosslinked Poly( $\epsilon$ -Caprolactone Fumarate) Networks for Guided Peripheral Nerve Regeneration: Material Properties and Preliminary Biological Evaluations. *Acta Biomater.* **2009**, *5*, 1531–1542.

(14) Bender, M. D.; Bennett, J. M.; Waddell, R. L.; Doctor, J. S.; Marra, K. G. Multi-Channeled Biodegradable Polymer/Cultispher Composite Nerve Guides. *Biomaterials* **2004**, *25*, 1269–1278.

(15) Dalton, P. D.; Flynn, L.; Shoichet, M. S. Manufacture of Poly(2-Hydroxyethyl Methacrylate-Co-Methyl Methacrylate) Hydrogel Tubes for use as Nerve Guidance Channels. *Biomaterials* **2002**, *23*, 3843–3851.

(16) Yucel, D.; Kose, G. T.; Hasirci, V. Polyester Based Nerve Guidance Conduit Design. *Biomaterials* **2010**, *31*, 1596–1603.

(17) Widmer, M. S.; Gupta, P. K.; Lu, L.; Meszlenyi, R. K.; Evans, G. R.; Brandt, K.; Savel, T.; Gurlek, A.; Patrick, C. W., Jr; Mikos, A. G. Manufacture of Porous Biodegradable Polymer Conduits by an Extrusion Process for Guided Tissue Regeneration. *Biomaterials* **1998**, *19*, 1945–1955.

(18) Kim, Y.; Haftel, V. K.; Kumar, S.; Bellamkonda, R. V. The Role of Aligned Polymer Fiber-Based Constructs in the Bridging of Long Peripheral Nerve Gaps. *Biomaterials* **2008**, *29*, 3117–3127.

(19) Bini, T. B.; Gao, S.; Xu, X.; Wang, S.; Ramakrishna, S.; Leong, K. W. Peripheral Nerve Regeneration by Microbraided Poly(L-Lactide-Co-Glycolide) Biodegradable Polymer Fibers. *J. Biomed. Mater. Res.* **2004**, *68A*, 286–295.

(20) Wang, S.; Cai, L. Polymers for Fabricating Nerve Conduits. *Int. J. Polym. Sci.* **2010**, *2010*, 138686.

(21) Pateman, C. J.; Harding, A. J.; Glen, A.; Taylor, C. S.; Christmas, C. R.; Robinson, P. P.; Rimmer, S.; Boissonade, F. M.; Claeysens, F.; Haycock, J. W. Nerve Guides Manufactured from Photocurable Polymers to Aid Peripheral Nerve Repair. *Biomaterials* **2015**, *49*, 77–89.

(22) Radulescu, D.; Dhar, S.; Young, C. M.; Taylor, D. W.; Trost, H.; Hayes, D. J.; Evans, G. R. Tissue Engineering Scaffolds for Nerve Regeneration Manufactured by Ink-Jet Technology. *Mater. Sci. Eng., C* **2007**, *27*, 534–539.

- (23) Greiner, A. M.; Richter, B.; Bastmeyer, M. Micro-Engineered 3D Scaffolds for Cell Culture Studies. *Macromol. Biosci.* **2012**, *12*, 1301–1314.
- (24) Juodkakis, S.; Mizeikis, V.; Misawa, H. Three-Dimensional Structuring of Resists and Resins by Direct Laser Writing and Holographic Recording. In *Photoresponsive Polymers I*; Marder, S., Lee, K., Eds.; Springer Berlin Heidelberg: Berlin, Germany, 2008; pp 157–206.
- (25) Sun, H. B.; Kawata, S. Two-Photon Photopolymerization and 3D Lithographic Microfabrication. In *NMR • 3D Analysis • Photopolymerization*; Springer Berlin Heidelberg: Berlin, Germany, 2004; pp 169–273.
- (26) Burmeister, F.; Steenhusen, S.; Houbertz, R.; Zeitner, U. D.; Nolte, S.; Tünnermann, A. Materials and Technologies for Fabrication of Three-Dimensional Microstructures with Sub-100 Nm Feature Sizes by Two-Photon Polymerization. *J. Laser Appl.* **2012**, *24*, 042014.
- (27) Ovsianikov, A.; Mironov, V.; Stampfl, J.; Liska, R. Engineering 3D Cell-Culture Matrices: Multiphoton Processing Technologies for Biological and Tissue Engineering Applications. *Expert Rev. Med. Devices* **2012**, *9*, 613–633.
- (28) Doraiswamy, A.; Jin, C.; Narayan, R. J.; Mageswaran, P.; Mente, P.; Modi, R.; Auyeung, R.; Chrisey, D. B.; Ovsianikov, A.; Chichkov, B. Two Photon Induced Polymerization of Organic-Inorganic Hybrid Biomaterials for Microstructured Medical Devices. *Acta Biomater.* **2006**, *2*, 267–275.
- (29) Ovsianikov, A.; Schlie, S.; Ngezhayo, A.; Haverich, A.; Chichkov, B. N. Two-Photon Polymerization Technique for Microfabrication of CAD-Designed 3D Scaffolds from Commercially Available Photosensitive Materials. *J. Tissue Eng. Regen. Med.* **2007**, *1*, 443–449.
- (30) Schlie, S.; Ngezhayo, A.; Ovsianikov, A.; Fabian, T.; Kolb, H. A.; Haferkamp, H.; Chichkov, B. N. Three-Dimensional Cell Growth on Structures Fabricated from ORMOCER by Two-Photon Polymerization Technique. *J. Biomater. Appl.* **2007**, *22*, 275–287.
- (31) Marino, A.; Ciofani, G.; Filippeschi, C.; Pellegrino, M.; Pellegrini, M.; Orsini, P.; Pasqualetti, M.; Mattoli, V.; Mazzolai, B. Two-Photon Polymerization of Sub-Micrometric Patterned Surfaces: Investigation of Cell-Substrate Interactions and Improved Differentiation of Neuron-Like Cells. *ACS Appl. Mater. Interfaces* **2013**, *5*, 13012–13021.
- (32) Timashev, P. S.; Vedunova, M. V.; Guseva, D.; Ponimaskin, E.; Deiwick, A.; Mishchenko, T. A.; Mitroshina, E. V.; Koroleva, A. V.; Pimashkin, A. S.; Mukhina, I. V.; Panchenko, V. Y.; Chichkov, B. N.; Bagratashvili, V. N. 3D in Vitro Platform Produced by Two-Photon Polymerization for the Analysis of Neural Network Formation and Function. *Biomed. Phys. Eng. Express* **2016**, *2*, 035001.
- (33) Koroleva, A.; Gill, A. A.; Ortega, I.; Haycock, J. W.; Schlie, S.; Gittard, S. D.; Chichkov, B. N.; Claeysens, F. Two-Photon Polymerization-Generated and Micromolding-Replicated 3D Scaffolds for Peripheral Neural Tissue Engineering Applications. *Biofabrication* **2012**, *4*, 025005.
- (34) Käpylä, E.; Turunen, S.; Pelto, J.; Viitanen, J.; Kellomäki, M. Investigation of the Optimal Processing Parameters for Picosecond Laser-Induced Microfabrication of a Polymer-Ceramic Hybrid Material. *J. Micromech. Microeng.* **2011**, *21*, 065033.
- (35) Käpylä, E.; Sedlačík, T.; Aydogan, D. B.; Viitanen, J.; Rypáček, F.; Kellomäki, M. Direct Laser Writing of Synthetic Poly(Amino Acid) Hydrogels and Poly(Ethylene Glycol) Diacrylates by Two-Photon Polymerization. *Mater. Sci. Eng., C* **2014**, *43*, 280–289.
- (36) Žukauskas, A.; Malinauskas, M.; Reinhardt, C.; Chichkov, B. N.; Gadonas, R. Closely Packed Hexagonal Conical Microlens Array Fabricated by Direct Laser Photopolymerization. *Appl. Opt.* **2012**, *51*, 4995–5003.
- (37) Yang, D.; Park, S. H.; Lim, T. W.; Kong, H.; Yi, S. W.; Yang, H. K.; Lee, K. Ultraprecise Microreproduction of a Three-Dimensional Artistic Sculpture by Multipath Scanning Method in Two-Photon Photopolymerization. *Appl. Phys. Lett.* **2007**, *90*, 013113.
- (38) Heinz, W. F.; Hoh, J. H. Spatially Resolved Force Spectroscopy of Biological Surfaces using the Atomic Force Microscope. *Trends Biotechnol.* **1999**, *17*, 143–150.
- (39) Hertz, H. Ueber die Berührung fester elastischer Körper. *J. für die reine und angewandte Mathematik* **1882**, *92*, 156–171.
- (40) Johnson, K. L. *Contact Mechanics*; Cambridge University Press: Cambridge, U.K., 1985.
- (41) Bilodeau, G. G. Regular Pyramid Punch Problem. *J. Appl. Mech.* **1992**, *59*, 519–523.
- (42) Li, Z.; Brand, U.; Ahbe, T. Towards Quantitative Modelling of Surface Deformation of Polymer Micro-Structures Under Tactile Scanning Measurement. *Meas. Sci. Technol.* **2014**, *25*, 044010.
- (43) Lappalainen, R. S.; Salomäki, M.; Ylä-Outinen, L.; Heikkilä, T. J.; Hyttinen, J. A.; Pihlajamäki, H.; Suuronen, R.; Skottman, H.; Narkilahti, S. Similarly Derived and Cultured hESC Lines show Variation in their Developmental Potential Towards Neuronal Cells in Long-Term Culture. *Regener. Med.* **2010**, *5*, 749–762.
- (44) Skottman, H. Derivation and Characterization of Three New Human Embryonic Stem Cell Lines in Finland. *In Vitro Cell. Dev. Biol. Anim.* **2010**, *46*, 206–209.
- (45) Kartasalo, K.; Pölönen, R.; Ojala, M.; Rasku, J.; Leikkala, J.; Aalto-Setälä, K.; Kallio, P. CytoSpectre: A Tool for Spectral Analysis of Oriented Structures on Cellular and Subcellular Levels. *BMC Bioinf.* **2015**, *16*, 344.
- (46) Tuft, B. W.; Xu, L.; White, S. P.; Seline, A. E.; Erwood, A. M.; Hansen, M. R.; Guymon, C. A. Neural Pathfinding on Uni- and Multidirectional Photopolymerized Micropatterns. *ACS Appl. Mater. Interfaces* **2014**, *6*, 11265–11276.
- (47) Liao, C. Product Model Creation and Simulation for Two-photon Polymerization Micro-manufacturing. Ph.D. Thesis, Joseph Fourier University/National Taiwan University, 2008.
- (48) Wu, D.; Wu, S.; Niu, L.; Chen, Q.; Wang, R.; Song, J.; Fang, H.; Sun, H. High Numerical Aperture Microlens Arrays of Close Packing. *Appl. Phys. Lett.* **2010**, *97*, 031109–1–031109–3.
- (49) Greiner, A. M.; Richter, B.; Bastmeyer, M. Micro-Engineered 3D Scaffolds for Cell Culture Studies. *Macromol. Biosci.* **2012**, *12*, 1301–1314.
- (50) Malinauskas, M.; Bičkauskaitė, G.; Rutkauskas, M.; Paipulas, D.; Purlys, V.; Gadonas, R. Self-Polymerization of Nano-Fibres and Nano-Membranes Induced by Two-Photon Absorption. *Lith. J. Phys.* **2010**, *50*, 135–140.
- (51) Käpylä, E.; Aydogan, D. B.; Virjula, S.; Vanhatupa, S.; Miettinen, S.; Hyttinen, J.; Kellomäki, M. Direct Laser Writing and Geometrical Analysis of Scaffolds with Designed Pore Architecture for Three-Dimensional Cell Culturing. *J. Micromech. Microeng.* **2012**, *22*, 115016.
- (52) Turunen, S.; Käpylä, E.; Lähteenmäki, M.; Ylä-Outinen, L.; Narkilahti, S.; Kellomäki, M. Direct Laser Writing of Microstructures for the Growth Guidance of Human Pluripotent Stem Cell Derived Neuronal Cells. *Opt. Laser Eng.* **2014**, *55*, 197–204.
- (53) Jariwala, S.; Venkatakrishnan, K.; Tan, B. Single Step Self-Enclosed Fluidic Channels Via Two Photon Absorption (TPA) Polymerization. *Opt. Express* **2010**, *18*, 1630–1636.
- (54) Uppal, N.; Shiakolas, P. S. Modeling of Temperature-Dependent Diffusion and Polymerization Kinetics and their Effects on Two-Photon Polymerization Dynamics. *J. Micro/Nanolithogr., MEMS, MOEMS* **2008**, *7*, 043002–1–043002–10.
- (55) Koseki, K.; Sakamaki, H.; Jeong, K. M. In Situ Measurement of Shrinkage Behavior of Photopolymers. *J. Photopolym. Sci. Technol.* **2013**, *26*, 567–572.
- (56) Ovsianikov, A.; Viertel, J.; Chichkov, B.; Oubaha, M.; MacCraith, B.; Sakellari, I.; Giakoumaki, A.; Gray, D.; Vamvakaki, M.; Farsari, M.; Fotakis, C. Ultra-Low Shrinkage Hybrid Photosensitive Material for Two-Photon Polymerization Microfabrication. *ACS Nano* **2008**, *2*, 2257–2262.
- (57) Schizas, C.; Karalekas, D. Mechanical Characteristics of an Ormocomp® Biocompatible Hybrid Photopolymer. *J. Mech. Behav. Biomed. Mater.* **2011**, *4*, 99–106.
- (58) Bayindir, Z.; Sun, Y.; Naughton, M. J.; et al. Polymer Microcantilevers Fabricated Via Multiphoton Absorption Polymerization. *Appl. Phys. Lett.* **2005**, *86*, 064105.
- (59) Klein, F.; Striebel, T.; Fischer, J.; Jiang, Z.; Franz, C. M.; von Freymann, G.; Wegener, M.; Bastmeyer, M. Elastic Fully Three-

Dimensional Microstructure Scaffolds for Cell Force Measurements. *Adv. Mater.* **2010**, *22*, 868–871.

(60) Burmeister, F.; Steenhusen, S.; Houbertz, R.; Asche, T. S.; Nickel, J.; Nolte, S.; Tucher, N.; Josten, P.; Obel, K.; Wolter, H.; Fessel, S.; Schneider, A. M.; Gartner, K. H.; Beck, C.; Behrens, P.; Tunnermann, A.; Walles, H. Two-Photon Polymerization of Inorganic-Organic Polymers for Biomedical and Microoptical Applications. In *Optically Induced Nanostructures: Biomedical and Technical Applications*; König, K., Ostendorf, A., Eds.; De Gruyter: Berlin, Germany, 2015; pp 239–266.

(61) Malinauskas, M.; Gilbergs, H.; Zukauskas, A.; Belazaras, K.; Purlys, V.; Rutkauskas, M.; Bickauskaite, G.; Momot, A.; Paipulas, D.; Gadonas, R.; Juodkasis, S.; Piskarskas, A. Femtosecond Laser Fabrication of Hybrid Micro-Optical Elements and their Integration on the Fiber Tip. *Proc. SPIE* **2010**, 7716.

(62) Takada, K.; Sun, H. B.; Kawata, S. Improved Spatial Resolution and Surface Roughness in Photopolymerization- Based Laser Nano-writing. *Appl. Phys. Lett.* **2005**, *86*, 071122.

(63) Zamani, F.; Amani-Tehran, M.; Latifi, M.; Shokrgozar, M. A. The Influence of Surface Nanoroughness of Electrospun PLGA Nanofibrous Scaffold on Nerve Cell Adhesion and Proliferation. *J. Mater. Sci.: Mater. Med.* **2013**, *24*, 1551–1560.

(64) Fan, Y. W.; Cui, F. Z.; Hou, S. P.; Xu, Q. Y.; Chen, L. N.; Lee, I. S. Culture of Neural Cells on Silicon Wafers with Nano-Scale Surface Topography. *J. Neurosci. Methods* **2002**, *120*, 17–23.

(65) Käpylä, E.; Sorkio, A.; Teymouri, S.; Lahtonen, K.; Vuori, L.; Valden, M.; Skottman, H.; Kellomäki, M.; Juuti-Uusitalo, K. Ormocomp-Modified Glass Increases Collagen Binding and Promotes the Adherence and Maturation of Human Embryonic Stem Cell-Derived Retinal Pigment Epithelial Cells. *Langmuir* **2014**, *30*, 14555–14565.

(66) Melissinaki, V.; Gill, A. A.; Ortega, I.; Vamvakaki, M.; Ranella, A.; Haycock, J. W.; Fotakis, C.; Farsari, M.; Claeysens, F. Direct Laser Writing of 3D Scaffolds for Neural Tissue Engineering Applications. *Biofabrication* **2011**, *3*, 045005.